Aus dem Walther-Straub-Institut für Pharmakologie und Toxikologie

Institut der Ludwig-Maximilians-Universität München

Vorstand: Prof. Dr. med. Thomas Gudermann

Therapeutic potential of enhancing mitochondrial Ca^{2+} uptake in experimental cardiac arrhythmia models

Dissertation

zum Erwerb des Doktorgrades der Naturwissenschaften

an der Medizinischen Fakultät

der Ludwig-Maximilians-Universität München

vorgelegt von

Maria Katharina Schweitzer

aus Hof/Saale

2021

Mit Genehmigung der Medizinischen Fakultät

der Universität München

Betreuer: Prof. Dr. Michael Mederos y Schnitzler

Zweitgutachter: Prof. Dr. Alexander Faußner

Dekan: Prof. Dr. med. Thomas Gudermann

Tag der mündlichen Prüfung: 28.04.2022

To my family

Table of Contents

Zusammenfassung

Kardiovaskuläre Erkrankungen (KVEs) stellen heute und voraussichtlich auch in der nahen Zukunft weltweit die Haupttodesursache dar. Dabei steigen insbesondere Todesfälle bedingt durch Arrhythmien weiterhin an. Da gängige Antiarrhythmika gravierende Nebenwirkungen aufweisen und häufig nur begrenzt wirksam sind, besteht besondere Dringlichkeit bei der Entwicklung neuartiger Therapieansätze. Kontraktilität und Rhythmizität des Herzens sind eng mit einer funktionalen Kalzium (Ca^{2+})-Homöostase des Myokards verknüpft und so sind Arrhythmien oftmals mit Störungen des zellulären Ca^{2+}-Haushaltes assoziiert. Mitochondrien spielen hier eine grundlegende, jedoch bislang stark unterschätzte Rolle.

Im vorliegenden Promotionsvorhaben wurde das Potential einer pharmakologischen Aktivierung der mitochondrialen Ca^{2+}-Aufnahme zur Behandlung von Arrhythmien untersucht. Hierbei fand einerseits die neuartige synthetische Substanz Efsevin Einsatz, ein Dihydropyrrolcarboxylester, welcher die Aktivität des *voltage-dependent anion channels* 2 (VDAC2) in der äußeren mitochondrialen Membran verstärkt. Andererseits wurde das Flavonoid Kaempferol als Agonist des mitochondrialen Ca^{2+}-Uniporters (MCU) untersucht. In früheren Arbeiten konnte Efsevin die rhythmische Kontraktion des Herzens in einem Zebrafisch-Arrhythmiemodell wiederherstellen. Der antiarrhythmische Effekt von Efsevin konnte hier direkt auf eine gesteigerte Aktivierung des mitochondrialen Ca^{2+}-Kanals VDAC2 zurückgeführt werden. Hierdurch ergibt sich eine gesteigerte Aufnahme und somit Abpufferung von zytosolischem Ca^{2+} in die Mitochondrien. Zusätzlich resultierte die Applikation von Efsevin in einer Reduktion arrhythmogener Ca^{2+}-Wellen in Wildtyp-Kardiomyozyten der Maus. Trotz dieser vielversprechenden Befunde

existierten bis dato keine Studien zu KVE-Krankheitsmodellen an Säugetieren, was hier durch die Evaluierung der Wirksamkeit von Efsevin in einem Arrhythmie-Modell der Maus sowie zwei humanen Arrhythmie-Modellen adressiert wurde. Wir konnten in dieser Arbeit zeigen, dass Efsevin arrhythmogene Ca^{2+}-Sparks, -Wellen, spontane Aktionspotentiale und sogar systolische arrhythmogene Ca^{2+}- Signale in Kardiomyozyten aus $RyR2^{R4496C/WT}$-Mäusen, einem Modell für katecholaminerge polymorphe ventrikuläre Tachykardie (CPVT) signifikant reduziert. Dieser antiarrhythmische Effekt von Efsevin lässt sich durch eine Blockade von MCU und damit der mitochondrialen Ca^{2+}-Aufnahme aufheben und wird, vergleichbar zu Efsevin, auch durch den MCU-Aktivator Kaempferol erreicht. Zudem führte die Gabe beider *mitochondrial Ca^{2+} uptake enhancers* (MiCUps) bei $RyR2^{R4496C/WT}$-Mäusen *in vivo* zu einer signifikanten Reduktion Stress-induzierter Arrhythmien. Abschließend wurde in einem translationalen Ansatz die Wirksamkeit von Efsevin und Kaempferol in humanen, *induced pluripotent stem cell* (iPSC)-basierten Kardiomyozyten zweier CPVT-Patienten getestet. Auch hier konnte eine Reduktion spontaner Ca^{2+}-Wellen in Kardiomyozyten eines Patienten mit einer etablierten CPVT-Mutation ($RyR2^{S406L/WT}$) sowie an Kardiomyozyten eines Patienten mit bislang nicht identifizierter Mutation ($CPVT^{unknown}$) gezeigt werden. Zusammenfassend präsentieren die hier vorgelegten Daten ein immenses Potential der erhöhten mitochondrialen Ca^{2+}-Aufnahme im Einsatz gegen Ca^{2+}-getriggerte Arrhythmien wie CPVT und etablieren MiCUps als vielversprechende Kandidaten einer neuartigen Generation von möglicherweise nebenwirkungsärmeren KVE-Therapeutika, welche erstmals mitochondriales Ca^{2+} als Angriffspunkt haben.

Summary

Cardiovascular diseases (CVDs) constitute the leading cause of death worldwide and will continue to dominate mortality trends in the future. Despite a general decline of CVD-related deaths, mortality rates attributed to arrhythmia are still on the rise. Common antiarrhythmics display perilous side effects and are often not effective pointing out an urgent need for novel therapeutic approaches. Cardiac contractility and rhythmicity are critically linked to a well-balanced calcium (Ca^{2+}) homeostasis in the myocardium and cardiac arrhythmias are often associated with perturbations in cellular Ca^{2+} handling. Mitochondria play a substantial, yet barely acknowledged, role in cellular Ca^{2+} handling and are associated with CVDs. In previous experiments, the novel dihydropyrrole carboxylic ester efsevin was identified by its ability to restore rhythmic cardiac contractions in a zebrafish cardiac fibrillation model. This was caused by activation of the voltage-dependent anion channel 2 (VDAC2) in the OMM which consecutively increased mitochondrial Ca^{2+} uptake causing enhanced clearance of cytosolic Ca^{2+} and thus a reduction of arrhythmogenic Ca^{2+} waves. Despite these pronounced effects, experiments in mammalian disease models were still lacking. In the current thesis, we investigated the potential of a pharmacological activation of mitochondrial Ca^{2+} uptake for the treatment of cardiac arrhythmia. To this aim, we applied efsevin as well as the flavonoid kaempferol, both enhancing Ca^{2+} uptake into mitochondria in different mammalian models of catecholaminergic polymorphic ventricular tachycardia (CPVT). We could demonstrate the potency of efsevin to reduce the propensity for arrhythmogenic Ca^{2+} sparks, waves, spontaneous action potentials and even for systolic arrhythmogenic Ca^{2+} elevations in cardiomyocytes of the murine $RyR2^{R4496C/WT}$ model of CPVT. The antiarrhythmic effect of

efsevin was abolished by blocking the mitochondrial Ca^{2+} uniporter (MCU) and could likewise be achieved with the MCU activator kaempferol. Further, the administration of both mitochondrial Ca^{2+} uptake enhancers (MiCUps), efsevin and kaempferol, to CPVT mice *in vivo* led to the significant reduction of stress-induced ventricular tachycardia. Moreover, MiCUps drastically reduced arrhythmogenic Ca^{2+} waves in human induced pluripotent stem cell-derived cardiomyocytes from two CPVT patients, one harboring the heterozygous $RyR2^{S406L/WT}$ mutation and the other one a yet unidentified mutation presenting with a aggressive and lethal CPVT phenotype. These results altogether highlight a significant potential of enhanced mitochondrial Ca^{2+} uptake to suppress arrhythmogenic events in Ca^{2+} triggered arrhythmias such as CPVT and establish MiCUps as promising pharmacological tools for a new generation of safer CVD therapeutics targeting mitochondrial Ca^{2+}.

List of figures

List of abbreviations

α	alpha
aa	amino acid
AM ester	acetoxymethyl ester
AMP	adenosine monophosphate
AF	atrial fibrillation
Ao	aorta
AP	action potential
AR	adrenergic receptor
ADP	adenosine diphosphate
ATP	adenosine triphosphate
APD_{50}	duration of triggered action potentials at 50 % repolarization
APD_{90}	duration of triggered action potentials at 90 % repolarization
AV	atrioventricular
β	beta
β-AR	beta-adrenergic receptors
bp	base pair(s)
bpm	beats per minute
BVT	bidirectional ventricular tachycardia
BW	body weight
Ca^{2+}	calcium
$[Ca^{2+}]_c$	concentration of cytosolic free Ca^{2+}
$[Ca^{2+}]_m$	concentration of mitochondrial free Ca^{2+}
$[Ca^{2+}]_{SR}$	concentration of sarcoplasmic reticulum free Ca^{2+}
CaM	calmodulin
CaMKII	Ca^{2+}/CaM-dependent protein kinase II
cAMP	cyclic adenosine monophosphate
Casq	calsequestrin
CICR	Ca^{2+} induced Ca^{2+} release
CPVT	Catecholaminergic polymorphic ventricular tachycardia
CPVT1	CPVT type 1, characterized by autosomal dominant inheritance of RyR2 mutation
$CPVT^{unknown}$	human CPVT-causing mutation in yet unidentified gene
CRU	Ca^{2+} release unit
C-terminal	carboxy-terminal
ctrl	control cardiomyocytes from a healthy human individual
CVD	Cardiovascular disease
$\Delta F/F_0$	amplitude of a Ca^{2+} signaling event
$\Delta\Psi_m$	inner mitochondrial membrane potential

DAD	delayed afterdepolarization
DEPC water	ultrapure diethylpyrocarbonate-treated water
DMSO	dimethyl sulfoxide
EAD	early afterdepolarization
EB media	DMEM-based iPSC differentiation media supplemented with FCS
ECC	Excitation-contraction coupling
ECG	electrocardiogram
EMRE	essential MCU regulator
epi/caff	epinephrine caffeine injection
F/F_0	fluorescence intensity ratio
F_1F_0 H^+-ATPase	ATPase in IMM implicated in oxidative phosphorylation
FCCP	carbonyl-cyanide-4-(trifluoromethoxy)phenylhydrazone; mitochondrial uncoupler
FCS	fetal calf serum
FDHM	full duration at half-maximum
FKBP12.6	FK506 binding protein 12.6 kDa (syn. calstabin)
fluo-4 AM	AM ester of fluo-4 Ca^{2+} indicator
FSK	forskolin
FWHM	full width at half-maximum
H^+	proton
he	heterozygous
HEK293	human embryonic kidney 293 cell line
HeLa	human epithelial cell line "Henrietta Lacks"
hERG	human ether-a-go-go related gene; K^+ channel
HL-1	murine cardiac muscle cell line
HR	heart rate
hz	Hertz
IC_{50}	half-maximal inhibitory concentration
ICD	implantable cardioverter-defibrillator
I_{CaL}	Ca^{2+} current carried by LTCCs
I_{K1}	cardiac inwardly rectifying K^+ current
I_{KR}	rapidly activating delayed rectifier K^+ current
I_{KS}	slowly activating delayed rectifier K^+ current
IMM	inner mitochondrial membrane
IMS	mitochondrial intermembrane space
I_{Na}	Na^+ current
$I_{Na/Ca}$	Na^+/Ca^{2+} exchange current
IP	intraperitoneal injection
iPSC	induced pluripotent stem cell

Iso	isoproterenol hydrochloride (synonym. Isoprenaline)
I_{ti}	transient inward current carried by NCX
$I_{to,f}$	fast transient outward K^+ channel
$I_{to,s}$	slow transient outward K^+ channel
Jct	junctin
JTV-519	Rycal; RyR2 channel blocker (synonym. K201)
K^+	potassium
kDa	kilo Dalton(s)
KN-93	CaMKII-inhibitor
K_V	voltage-gated K^+ channel
KVE	Kardiovaskuläre Erkrankungen (synonym. CVD)
K201	Rycal; RyR2 channel blocker (synonym. JTV-519)
LA	left atrium
LC/MS-MS	liquid chromatography-mass spectrometry/mass spectrometry
LCSD	left cardiac sympathetic denervation
LQTS	long-QT syndrome
LTCC	L-type Ca^{2+} channel (synonym. Ca_V)
LV	left ventricle
MCU	mitochondrial Ca^{2+} uniporter
MCUR	mitochondrial Ca^{2+} uniporter regulator
mERG	murine analog of hERG K^+ channel
Mfn	mitofusin
Mg^{2+}	magnesium
MICU	mitochondrial Ca^{2+} uptake
MICUb	mitochondrial Ca^{2+} uniporter b
MiCUp	mitochondrial Ca^{2+} uptake enhancer
mRNA	micro RNA
MICU1	mitochondrial Ca^{2+} uptake 1
MΩ	mega Ohm
mPTP	mitochondrial permeability transition pore
mV	millivolt(s)
nA	nanoampere
[Na^+]	sodium
NADH	nicotinamidadenindinucleotide
NADPH	nicotinamidadenindinucleotidphosphate
$Na_{V1.5}$	voltage-gated Na^+ channel Nav1.5
NCLX	mitochondrial Na^+/Ca^{2+} exchanger
NCX	plasma membrane Na^+/Ca^{2+} exchanger
N-terminal	amino-terminal

OMM	outer mitochondrial membrane
PEG	polyethylene glycol
pF	picofarad
PKA	protein kinase A
PLN	phospholamban
PR	time interval of conduction of excitation from atria to ventricles as seen on the ECG
PVC	premature ventricular complex
QRS complex	represents the spread of a stimulus through the ventricles as seen on the ECG
QT	time interval from depolarization to repolarization of the ventricles as seen on the ECG
RA	right atrium
RaM	rapid mode of Ca^{2+} uptake
RMP	resting membrane potential
rpm	rounds per minute
ROS	reactive oxygen species
RT	room temperature
RuR	Ruthenium Red
Ru_{360}	Ruthenium 360
RV	right ventricle
RyR2	ryanodine receptor 2
R4496C	murine heterozygous, CPVT-causing arginine to cysteine mutation at aa position 4496 of RyR2
$RyR2^{R4496C/WT}$	CPVT mouse model heterozygous for the RyR2-R4496C mutation
$RyR2^{S406L/WT}$	human CPVT patient heterozygous for the RyR2-S406L mutation
$RyR2^{WT/WT}$	WT mouse
SAN	sinoatrial node
SCD	sudden cardiac death
SEM	standard error of the mean
SERCA	sarcoplasmic reticulum Ca^{2+} ATPase
SOICR	store overload-induced Ca^{2+} release
SR	sarcoplasmic reticulum
SSCE	secondary systolic Ca^{2+} elevation
SUD	sudden unexplained death
SV	stroke volume
S107	Rycal; RyR2-FKBP12.6 interaction stabilizer
S406L	human heterozygous, CPVT-causing serine to leucine mutation at aa position 406 of RyR2

T tubuli	transversale tubuli
tau_{decay}	Ca^{2+} decay
$Tau_{inactivation}$	inactivation constant tau
TdP	Torsades de pointes arrhythmia
Trdn	triadin
ttp	time to peak
VDAC2	voltage-dependent anion channel 2
VF	ventricular fibrillation
VK-II-86	Carvedilol analog
VT	ventricular tachycardia
WT	wildtype
w/v	weight per volume

1. INTRODUCTION

1.1 Cardiac physiology – The heart

Living beings are provided with vitally important O_2 and nutrients via distribution of O_2-enriched blood throughout the body. The heart receives blood low in O_2 containing CO_2 and waste products from all organs of the body. Deoxygenated blood returns to the right atrium via *Venae cavae* and fills the right ventricle (RV). After ejection from the RV into the pulmonary artery, the blood is being enriched with O_2 by passage through the lungs. Thereafter, the blood flows into the left atrium (LA), passes the left ventricle (LV) and exits the heart via the aorta to supply the different organs of the body[1]. The events associated with ventricular contraction and ejection are termed systole. In contrast, diastole refers to the relaxation phase of the cardiac cycle, which includes ventricular relaxation and filling. During diastole, the ventricles are not contracting with passive blood flow occurring from the atria into the ventricles. Diastole then culminates in contraction of both atria, which propels an additional amount of blood into the ventricles.

Excitation is propagated throughout the heart by an electrical wavefront whereby the impulse of excitation is formed by action potentials (APs). These APs can be rapidly progressed via gap junctions between cardiac cells forming a functional syncytium. The physiological source of the excitation is the sinoatrial node (SAN) in the RA which is regulated by the autonomic nervous system and circulating catecholamines[2]. The SAN being the heart's primary pacemaker spontaneously generates pulses with a frequency of 60-80 beats per minute (bpm) at rest that are passed to the atrioventricular (AV) node via internodal pathways. The AV node located in the interatrial septum conducts impulses

with a delay to the bundle of His and the stimulus then diverges to the right and left bundle branches in the interventricular septum. The bundle branches taper off into Purkinje fibres that permeate both ventricles and the electrical signal travels towards the apex of the heart. This leads to an activation of electrically coupled ventricular cardiomyoctyes that trigger a synchronized contraction of the ventricles in order to pump O_2-enriched blood throughout the body. By each heartbeat, a specific volume of blood is ejected by the LV, referred to as the stroke volume (SV)[3]. Muscular contraction of the heart is accompanied by changes in electrical potentials that can be recorded with electrodes attached to the body surface. The recorded potential changes yield a shape of the propagation of conduction through the heart, the electrocardiogram (ECG) (Fig. 1). The contraction of atria is represented by the P wave followed by the QRS complex characterizing ventricular contraction. Whereas the PR interval stands for the conduction of excitation through the AV node and down the bundle of His through the bundle branches to the ventricles, QT characterizes the interval from depolarization to repolarization of the ventricles with the T wave generated by ventricular repolarization.

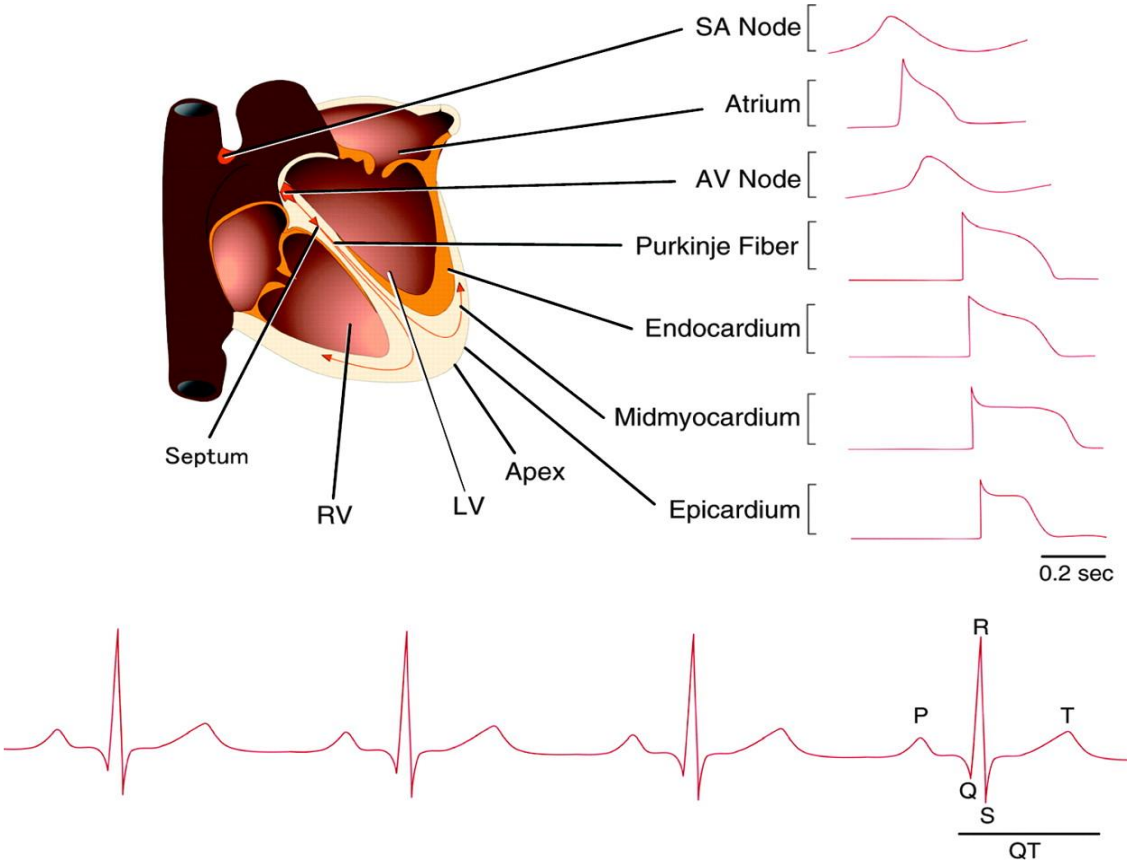

Fig. 1 Conduction of electrical activity in the human heart [from[4]].

The sinoatrial (SA) node as the primary cardiac pacemaker generates pulses that are passed to the atrioventricular (AV) node in the interatrial septum. From there, impulses are conducted to the bundle of His and the stimulus then diverges to the right and left bundle branches in the interventricular septum. The bundle branches taper off into Purkinje fibres that permeate both ventricles and the electrical signal travels towards the apex of the heart where it leads to synchronized ventricular contractions. The propagation of excitation throughout the heart in different cardiac cell types is mediated via action potentials (APs) (right side). The characteristic shapes of these APs from the different cardiac regions altogether form the electrocardiogram (lower section). The P-wave represents contraction of the atria, followed by the QRS-complex characterizing ventricular contraction. QT characterizes the interval from depolarization to repolarization of the ventricles with the T-wave generated by repolarization of the ventricles. Abbreviations: RV = right ventricle; LV = left ventricle.

The propagation of excitation throughout the heart in different cardiac cell types is mediated via APs. Every cardiac cell type is characterized by different expression patterns of Na^+, Ca^{2+} and K^+ channels and thus exhibits a specific AP waveform and these altogether form the characteristic shape of the ECG. The AP of the human ventricular myocardium consists of five distinct phases (Fig. 2): During the upstroke (phase 0), the influx of Na^+ ions causes membrane depolarization. Early repolarization (phase 1) results from K^+ efflux. A subsequent Ca^{2+} influx is counterbalanced by K^+ efflux (phase 2). Final repolarization occurs due to K^+ influx (phase 3) and the cardiomyocyte finally returns to the resting membrane potential (RMP) (phase 4).

Even though some types of K^+ channels are expressed in cardiac tissue of mouse and human, their respective contribution to AP morphology can differ substantially, given the large AP difference between both species. Repolarization in murine cardiac tissue is a very fast process mediated by transient outward K^+ currents with a fast and slow recovery from inactivation ($I_{Kto,f}$ and $I_{Kto,s}$), a slowly inactivating K^+ current ($I_{K,slow1}$ and $I_{K,slow2}$) and a non-inactivating steady-state current (I_{Kss})[5–8]. Human repolarization is predominantly carried by the delayed K^+ currents I_{Kr} and I_{Ks}. Albeit I_{Kr} and I_{Ks} are reported in mouse, their physiological contribution to repolarization if any is negligible[9]. Equivalents of $I_{K,slow}$ and I_{Kss} are not verified in humans and $I_{Kto,f}$ is mainly involved in phase I repolarization[10]. On the contrary, $I_{to,f}$ is crucial for the repolarization of short APs in murine ventricle. The murine AP with a total duration of approx. 50-100 ms[11] is considerably faster than the human one with about 200-300 ms[12] and lacks a prominent plateau during phase 2 of the AP. In contrast, K^+ efflux in human ventricular cardiomyocytes counterbalancing the

Ca^{2+} influx forms a plateau creating time for cardiomyocyte contraction and relaxation in between APs.

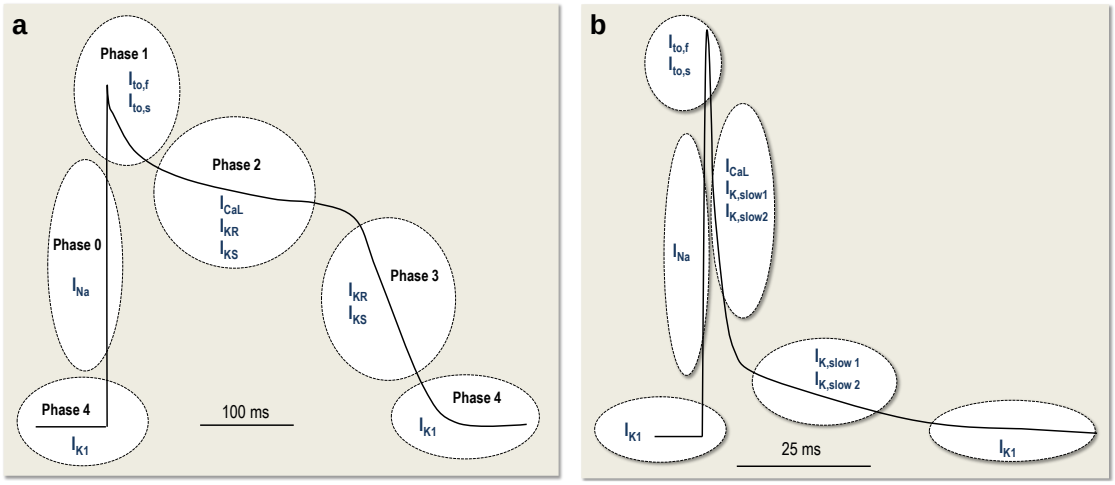

Fig. 2 Membrane currents generating the ventricular AP [modified from[13]].

(a) The human ventricular AP consisting of five distinct phases lasts for approx. 200 ms and starts from a RMP of about 90 mV (Phase 4). During the upstroke (Phase 0), the I_{Na} current carried by Na^+ ions causes membrane depolarization. Early repolarization (Phase 1) results from K^+ extrusion via $I_{to,f}$ and $I_{to,s}$ currents. A subsequent Ca^{2+} influx via I_{CaL} counterbalanced by K^+ efflux through I_{Kr} and I_{Ks} forms a plateau creating time for cardiomyocyte contraction and relaxation in between APs (Phase 2). Final repolarization occurs by the predominant action of I_{Kr} and I_{Ks} (Phase 3). Due to K^+ influx carried by I_{K1} current, the cardiomyocyte finally returns to RMP (Phase 4). (b) In accordance with human ventricular cardiomyocytes, depolarization of the murine ventricular AP is carried by I_{Na} and early repolarization is mediated by $I_{to,f}$ and $I_{to,s}$ currents. However, K^+ extrusion during repolarization to counterbalance Ca^{2+} influx via I_{CaL} results from $I_{K,slow1}$ and $I_{K,slow2}$ in murine ventricular myocardium.

The considerably longer duration of the human AP as compared to the murine one is also reflected in a substantially slower heart rate (HR) in humans. Whereas the human HR under rest amounts to 50-70 bpm[14] (173-188 bpm under stress[15]), the murine heart beats between 500-700[10] times per minute under rest (700-800 bpm under stress) depending on the mouse strain. Comparing the stress-induced HR increase of approx. 100-200 % in humans with that of only up to 50 % in mice[16] clearly demonstrates a much greater ability of the human heart to adapt cardiac output (HR x SV) during exercise. Whereas cardiac output can be increased 5-10-fold in the human body, mice can increase this parameter merely 1.3-2-fold[16]. Owed to these substantial species differences in the physiological and electrophysiological properties of the heart, not all observations made in murine models are directly applicable to the human disease[17]. However, since they can be genetically manipulated easily to carry disease-causing genes and thereby mimic human diseases such as inherited arrhythmia syndromes, mice serve as very valid model organisms in the research of cardiovascular diseases[18].

1.1.1 Excitation-contraction-coupling

In the mammalian myocardium, electrical impulses in the form of APs are converted into contractions in a process called excitation-contraction coupling (ECC) with Ca^{2+} playing the most essential role (Fig. 3). During ECC, an AP causes depolarization of the cell membrane, triggering a small influx of Ca^{2+} (I_{CaL}) through L-type Ca^{2+} channels (LTCCs, synonym. Ca_{V1}). By Ca^{2+} induced Ca^{2+} release (CICR)[19], this small influx causes ryanodine receptors (RyR2) in the sarcoplasmic reticulum (SR) to release a large amount of Ca^{2+} from the organelle which binds to troponin C[20]. This induces a conformational change of

myosin molecules leading to the formation of cross-bridges with actin resulting in contraction of the cardiomyocyte and ejection of blood from the heart[21]. Afterwards, to achieve refilling of the ventricles and diastolic relaxation, Ca^{2+} released from the SR during systole has to be removed from the cytosol. This is accomplished mainly by the Na^{+}/Ca^{2+} exchanger (NCX) in the plasma membrane and via the sarcoplasmic Ca^{2+} ATPase (SERCA) in the SR membrane mediating Ca^{2+} reuptake into the SR. The activity of SERCA is inhibited by phospholamban (PLN)[22]. Upon phosphorylation by PKA and/or CaMKII triggered by β-adrenergic stimulation, PLN dissociates from the ATPase resulting in increased Ca^{2+} uptake. In addition to cytosolic Ca^{2+} removal via NCX and SERCA, approx. 1% of Ca^{2+} [23] released into the cytosol during systole is being taken up by mitochondria.

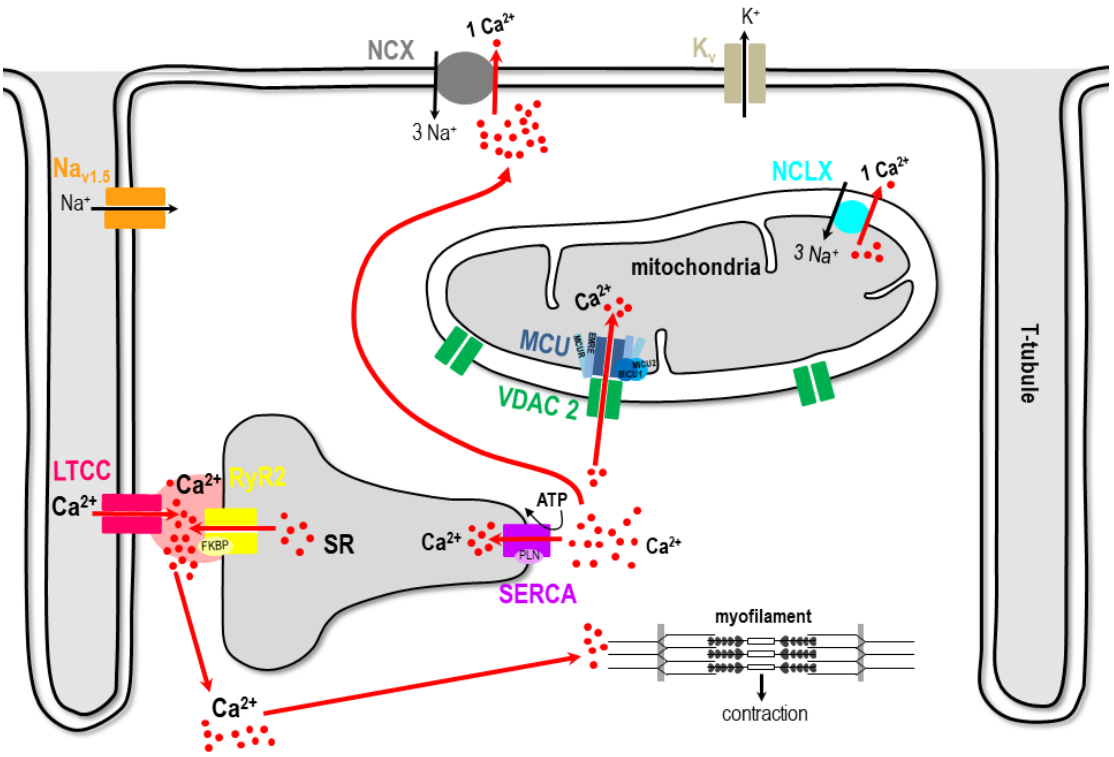

Fig. 3 ECC in the ventricular cardiomyocyte [modified from[24]].

By an oncoming AP, voltage-dependent Na^+ channels ($Na_{V1.5}$) and LTCCs (Ca_{V1}) are activated leading to Ca^{2+} influx into the myocyte. By Ca^{2+} induced Ca^{2+} release, this Ca^{2+} influx causes ryanodine receptors (RyR2) in the sarcoplasmic reticulum (SR) to release a large amount of Ca^{2+} to elicit contraction of the cardiomyocyte by binding of Ca^{2+} to the myofilaments. Voltage-gated K^+ channels (K_V) open leading to a K^+ efflux that favors AP repolarization and establishes conditions required for relaxation. Relaxation occurs via Ca^{2+} reuptake into the SR by SERCA, extrusion from the cardiomyocyte by the Na^+/Ca^{2+} exchanger (NCX) in exchange for Na^+ and uptake into mitochondria via VDAC2 and the mitochondrial Ca^{2+} uniporter (MCU). SR Ca^{2+} extrusion via SERCA is inhibited by phospholamban (PLN). Abbreviations: FKBP12.6 = FK506-binding protein 12.6 kDa; ATP = adenosine triphosphate; T-tubule = transversale tubule; MCUR = MCU regulator; EMRE = essential MCU regulator; MICU = mitochondrial Ca^{2+} uptake; NCLX = mitochondrial Na^+/Ca^{2+} exchanger.

1.2 Ca^{2+} signaling in the heart

1.2.1 Systolic Ca^{2+} release

1.2.1.1 Ryanodine receptor 2

Ca^{2+} has to be released into the cytosol during systole in order to provoke contraction. During CICR, a small amount of Ca^{2+} entering through LTCC binds to RyR2 and thereby activates the channel, which releases a massive amount of Ca^{2+} to the cytosol crucial for every heartbeat. RyR2 is modulated by several ions, small molecules and proteins, e.g. Ca^{2+}, magnesium (Mg^{2+}) and ATP[25]. RyR2, located on the SR membrane, represents the major intracellular Ca^{2+} release channel in cardiac muscle[26]. Ca^{2+} is known to regulate RyR2 on the cytoplasmic as well as on the luminal site. The sensitization of RyR2s to activation by cytosolic Ca^{2+} is mediated at luminal sites[27] and the open probability of the channel is dependent on the Ca^{2+} concentration in the diadic cleft between LTCCs and RyR2s[28]. SR Ca^{2+} release is terminated when luminal Ca^{2+} declines below a threshold level during release, which causes changes in RyR2 gating leading to the deactivation of the receptor and refractoriness until SR Ca^{2+} recovery. These processes are crucial for the rhythmic activity of the heart[27,29].

RyR2 is a large transmembrane protein existing as a macromolecular complex assembled from homotetramers of 565 kDa each. The carboxy (C) terminus spanning from amino acids (aa) 4500 to aa 4967, represents the pore-forming region of the channel formed by six transmembrane segments (Fig. 4)[30–32]. The amino (N) terminal region of RyR2 forms the cytoplasmic domain, involved in regulatory functions. The RyR2 complex is comprised of further proteins on its cytosolic side implicated in the regulation of its gating. The

cytoplasmic domain of RyR2 contains several potential phosphorylation sites and the kinases protein kinase A (PKA) and Ca^{2+}/CaM-dependent protein kinase II (CaMKII) are known to phosphorylate RyR2[33–35]. While contradictory results exist in the literature, phosphorylation by PKA and most likely CaMKII cause dissociation of FK506 binding protein 12.6 kDa (FKBP12.6; synonym. calstabin 2)[25] leading to a destabilization of the complex and enhanced channel activity. Thereby, the open probability of RyR2 is increased and its response to Ca^{2+} dependent activation is augmented[36,37]. To prevent Ca^{2+} leak, the closed state of the channel is stabilized by high-affinity binding of one regulatory FKBP12.6 protein to each RyR2 tetramer[36,37]. Inside the SR, calsequestrin (Casq) monomers interact with the channel via the auxiliary proteins triadin (Trdn) and junctin (Jct)[38].

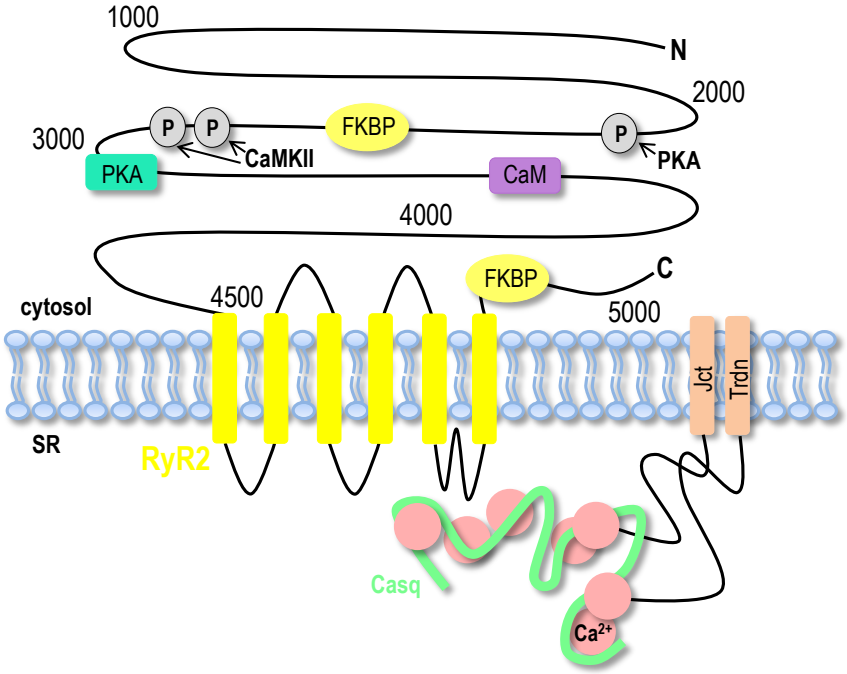

Fig. 4 Structure and organization of the RYR2 macromolecular complex [modified from[30]].

The C-Terminus of RyR2 spanning from aa 4500 to aa 4967 constitutes the pore-forming region formed of 6 transmembrane segments. Inside the SR, calsequestrin monomers interact with the channel via the auxiliary proteins triadin (Trdn) and junctin (Jct). The N-terminal region forms the cytoplasmic domain and is implicated in regulatory functions. To regulate its gating, further proteins interact with the cytosolic side of the channel, namely protein kinase A (PKA) and calmodulin (CaM). Phosphorylation sides of RyR2 are shown (P) where PKA and Ca^{2+}/CaM-dependent protein kinase II (CaMKII) regulate the channel and increase its open probability. The closed state of RyR2 is stabilized by binding of FKBP proteins. Numbers in black indicate the respective aa positions of the channel. Abbreviations: CaM = calmodulin; Casq = calsequestrin.

1.2.1.2 Systolic Ca^{2+} signals in ECC

The systolic release of Ca^{2+} from the SR via a unitary cluster of RyR2s consisting of 30-300 channels[39] is termed a triggered Ca^{2+} spark[40]. In cardiac cells, RyR2s are associated with LTCCs in so-called Ca^{2+} release units (CRU) and each LTCC that opens triggers a synchronous activation of 4–6 RyR2s[41]. Spark initiation thereby results from the increased

dyadic subspace Ca^{2+} followed by elevated SR Ca^{2+} causing increased RyR2 open probability[39]. Sparks occur as local increases in cytosolic Ca^{2+} and are observed in mature ventricular cardiomyocytes of all mammals[40]. Whereas the specific activity of Ca^{2+} channels and transporters involved in spark initiation and termination as well as the contribution of extracellular Ca^{2+} can vary between mice and humans, the basic underlying mechanism is conserved between mammalian species[16]. Ca^{2+} sparks present with a rapid rise (time to peak) and a moderately rapid decay (half-time of decay)[42]. The mechanism of Ca^{2+} spark termination, however, is not fully resolved[43]. Current theories indicate that termination most likely results from a combination[44] of SR Ca^{2+} depletion, an inactivation of RyR2s[45] and stochastic attrition[46]. This means that an increasing number of RyR2s that stochastically close proceeds to augment the number of closed channels causing a decrease of dyadic Ca^{2+} which culminates in the closure of all RyR2 channels and termination[44]. Further, a contribution of luminal Ca^{2+} is quite conceivable.

Depolarization of the cell membrane during systole by an oncoming AP results in Ca^{2+} influx via LTCCs. In CICR, this Ca^{2+} influx results in a concomitant activation of all cellular RyR2s. This triggers synchronous release of Ca^{2+} from numerous CRUs[47], resulting in a temporal and spatial summation of localized triggered Ca^{2+} sparks generating homogeneous, early peaking Ca^{2+} transients[48]. These transients, defined as transitory elevations of cytosolic Ca^{2+} represent the physiological event leading to controlled, systolic Ca^{2+} extrusion from the SR. The Ca^{2+} of the systolic transient binds to troponin C, elicits contraction and is thus responsible for generation of the heart beat[27]. Following a transient, the triggered release of Ca^{2+} becomes refractory[40]. It is of utmost importance for rhythmic ventricular contraction that local Ca^{2+} transients throughout the heart are

synchronized[21]. Any change in the balance between Ca^{2+} influx and efflux in cardiac myocytes can lead to abnormal intracellular Ca^{2+} regulation and arrhythmogenesis. Therefore, coordinated release of Ca^{2+} from the SR through RyR2 is crucial for cardiomyocyte function.

1.2.2 Diastolic Ca^{2+} reuptake

1.2.2.1 Na^{+}- Ca^{2+} exchanger and sarcoplasmic Ca^{2+}-ATPase

For relaxation of the myocyte during diastole, Ca^{2+} has to be removed from the cytosol. The NCX residing in the plasma membrane represents the major Ca^{2+} efflux pathway in ventricular cardiomyocytes thereby playing a crucial role in the regulation of the cytosolic Ca^{2+} concentration ($[Ca^{2+}]_c$)[28,49]. To maintain a cellular Ca^{2+} balance, the NCX extrudes the same amount of Ca^{2+} that entered the cardiomyocyte through LTCCs[28]. The exchanger transports 3 Na^{+} ions from the side with higher Na^{+} concentration ($[Na^{+}]$) in exchange for 1 Ca^{2+} ion, making the pathway electrogenic. Exchange can appear bidirectionally, depending on Na^{+} and Ca^{2+} gradients across the cell membrane as well as on the membrane potential.

Yet, up to 90 % of the termination of Ca^{2+} transients in mammalian ventricular myocytes is arranged by the ATP-dependent ion pump SERCA located in the SR membrane[50–52]. For replenishment of the SR with Ca^{2+}, SERCA couples energy from ATP hydrolysis to active Ca^{2+} transport. A catalytic turnover of SERCA comprises the transport of 2 Ca^{2+} ions and the hydrolyzation of one ATP. Thereby, the ion pump restores the low resting

$[Ca^{2+}]_c$ of approx. 0.1 µM and simultaneously maintains a high luminal sarcoplasmic Ca^{2+} concentration ($[Ca^{2+}]_{SR}$)[53].

1.2.3 β-adrenergic stimulation

To adapt cardiac contraction and energy metabolism and increase cardiac output under stress conditions, sympathetic nerves innervating the heart are activated resulting in release of the catecholamines epinephrine and norepinephrine[1,25]. In cardiac tissue, circulating catecholamines bind to β-adrenergic receptors (β-AR) which couple to stimulatory G proteins in their activated state[54]. The subsequently activated adenylate cyclase converts ATP to cyclic adenosine monophosphate (cAMP)[55]. Enhanced production of cAMP results in activation of PKA that in turn phosphorylates a plethora of substrates including RyR2, PLN and CaMKII[56]. The phosphorylation of RyR2 alters its gating properties to an increased open probability and increases its sensitivity to luminal Ca^{2+} [31]. Phosphorylated PLN releases its inhibitory effect on SERCA stimulating SR Ca^{2+} uptake[27] which renders more Ca^{2+} available for CICR in subsequent heart beats. This in turn causes faster relaxation and augmented SR Ca^{2+} loading[52]. Additionally, β-AR stimulation elevates LTCC activity and leads to larger and faster Ca^{2+} transients[57]. Altogether, the higher SR Ca^{2+} load leading to an increased amplitude of transients results in a stronger force of muscle contraction.

1.3 Cardiac Mitochondria

1.3.1 Mitochondria and Ca^{2+}

During the systolic Ca^{2+} transient, some of the cytosolic Ca^{2+} is buffered into mitochondria[58] with rapid uptake and slow release kinetics[59], large enough to modulate the amplitude and shape of a Ca^{2+} transient. Whereas the role of this fast mitochondrial Ca^{2+} uptake remains largely elusive, it is probably best explained by the existence of a rapid mode of Ca^{2+} uptake (RaM) in combination with mitochondria located close to SR or plasma membrane[60]. The ability of mitochondria to accumulate large amounts of Ca^{2+} has been known for more than 50 years[61,62] when rat cardiac mitochondria were shown to accumulate amounts of Ca^{2+} from suspending media during electron transport exceeding their initial Ca^{2+} content by several hundred times[63]. At rest, the matrix $[Ca^{2+}]_m$ corresponds to that of the cytosol, whereas following stimulation it can reach values up to 100-fold higher than that in the cytoplasm[64].

In general, mitochondrial Ca^{2+} accumulation as a function of extramitochondrial Ca^{2+} can be divided into three phases[65]. Initially, an equilibration between mitochondrial and cytosolic Ca^{2+} adjusts until Ca^{2+} removal from the matrix keeps abreast with the rate of Ca^{2+} uptake. Secondly, in the buffered phase as Ca^{2+} rises above 500 nM, the rate of Ca^{2+} uptake exceeds that of removal from mitochondria and the organelle starts to accumulate Ca^{2+}. The storage of Ca^{2+} in the mitochondrial matrix is ensued in the presence of phosphate in the form of insoluble phosphate salts[66]. This Ca^{2+} accumulation occurs at the cost of oxidative phosphorylation, is driven by the mitochondrial membrane potential[67] and implements several major functions: In addition to controlling the rate of

oxidative phosphorylation, mitochondrial Ca^{2+} uptake adds to the stimulation of oxidative metabolism for cellular energy production in response to an increase in ATP demand[68]. Free mitochondrial Ca^{2+} activates the rate of ATP synthesis by modulating the activity of pyruvate, isocitrate and α-ketoglutarate dehydrogenases of the Krebs cycle[69,70]. These enzymes control the feeding of electrons into the respiratory chain as well as the generation of the H^+ gradient across the IMM which is in turn necessary for Ca^{2+} uptake and ATP production[71]. Mitochondria are able to rapidly accumulate sequential pulses of Ca^{2+} with the extramitochondrial [Ca^{2+}] returning to the same "set point" after each pulse[72]. However, mitochondria do not merely respond to alterations in cytosolic [Ca^{2+}] but preferably take up Ca^{2+} released by the SR. Due to this close connection of both organelles referred to Ca^{2+} signaling, mitochondria can perfectly match ATP production to ATP demand[73]. When extramitochondrial Ca^{2+} rises above the µM level, mitochondria possess the ability to accumulate about 700-1000 nM Ca^{2+} per mg mitochondrial protein[65]. Yet, when Ca^{2+} load exceeds the mitochondrial buffering capacity of the matrix, the third phase of Ca^{2+} accumulation occurs, termed the overload phase where an increase in mitochondrial matrix Ca^{2+} is implicated in the induction of apoptotic cell death via the intrinsic mitochondrial pathway. Here, mitochondria represent both targets of proteins crucial for the regulation of apoptosis and a residence of proteins essentially involved in the execution of apoptosis such as cytochrome C[59]. Apoptotic stimuli lead to an induction of the Ca^{2+} triggered mitochondrial permeability transition pore (mPTP) opening and loss of the mitochondrial membrane potential.

1.3.2 SR-mitochondria Ca^{2+} microdomains

Mitochondria-associated membranes are the site where a multitude of biological functions are regulated, including bioenergetics, autophagy, mitochondrial structure and apoptosis[74]. They constitute a Ca^{2+} signaling hub with intramitochondrial Ca^{2+} signals disseminating in the matrix, after the release from intracellular stores[75]. In cardiomyocytes, mitochondria are closely intertwined with T tubuli and localized in direct proximity to the SR[76,77] with an apposition of both organelles as close as 10-50 nm between terminal cisternae of the SR and mitochondrial membranes[78,79]. A very specific physical coupling between SR and the mitochondrial outer membrane (OMM) has been reported in cardiac cells[80]. SR-mitochondrial Ca^{2+} microdomains were shown to be dependent on physical linkage of both organelles by mitochondrial fusion proteins mitofusin (Mfn) 1 and 2, acting as a molecular tether that links cardiac SR to mitochondria[81–83]. In Ca^{2+} microdomains[84,85] (Fig. 5, light pink circle between both organelles), mitochondria are transiently exposed to local high $[Ca^{2+}]_c$ resulting from SR Ca^{2+} release which exceeds the concentration of the bulk cytosol by about 10 times[86]. SR Ca^{2+} release causes a transient increase in mitochondrial Ca^{2+} [87], resistant to cytosolic Ca^{2+} buffering with BAPTA indicating that Ca^{2+} can reach mitochondria by "tunneling" via microdomains[88]. At this, even Ca^{2+} sparks are sufficient for activation of low affinity Ca^{2+} uptake into adjacent mitochondria[89].

1.3.3 Mitochondrial Ca^{2+} channels

1.3.3.1 Outer mitochondrial membrane - Voltage dependent anion channel 2

For Ca^{2+} transport to occur between cytosol and mitochondria, Ca^{2+} ions need to overcome both the OMM and the mitochondrial inner membrane (IMM). The following section will provide an overview of channels residing on both membranes which are implicated in Ca^{2+} uptake into mitochondria as well as in mitochondrial Ca^{2+} efflux (Fig. 5).

Albeit previously considered to be freely permeable, a role of the OMM as a regulated Ca^{2+} barrier has been recognized not long ago[65]. Flux of Ca^{2+} [90], but also of metabolites such as adenosine diphosphate (ADP), ATP, nicotinamidadenindinucleotide (NADH) or molecules of up to 4-6 kDa across the OMM is conducted by transmembrane voltage-dependent anion channels (VDACs). VDACs represent the most abundant OMM proteins accounting for over 50% of all OMM proteins[91] and play a pivotal role in mitochondrial bioenergetics and cell metabolism with implications in development as well as cell survival. Three isoforms exist which share about 75 % of sequence similarity, yet in mammals VDAC2 exhibits a unique 11-12 aa extension at the N-terminal end pointing to functional versatility of the isoforms. VDACs are formed by β-barrels exhibiting a wide pore diameter of about 2-4 nm[92]. A N-terminal α-helix located inside the pore is seemingly necessary for voltage-gating[93] and presumed to be involved in channel activity for metabolite transfer[94]. When incorporated in artificial membrane systems, VDAC is fully open at potentials between >-30 and <+30 mV and weakly anion-selective, with a high

permeability for metabolites. At higher potentials, it is closed to approx. half of the original conductance referred to as the classical "closed" state with a switch to cation-selectivity leading to increased Ca^{2+} flux across the OMM. The transition between open, gated and closed states, referred to as VDAC gating, is experimentally induced by voltage[95] and different mechanisms of gating were suggested: Intrinsic gating[96] would lead to a change in channel conformation[96] whereas gating by occlusion[96] would lead to protein interaction partners (e.g. tubulin in cardiomyocytes[97]) or metabolites (such as NADH[98]) entering and "corking up" VDACs[91] thereby regulating its conductance. The generation of a potential across the OMM was further suggested as a regulatory mechanism of VDAC gating, with the possibility of a partial application of IMM potential to the OMM occuring at contact sites between both mitochondrial membranes where interactions between proteins residing in IMM and OMM take place[91]. Moreover, Ca^{2+} itself is capable of modulating the gating behavior of VDAC. VDAC was postulated to be a Ca^{2+} activated and regulated Ca^{2+} channel[89,99] since its conductance and transition to full opening were reversibly induced by submicromolar Ca^{2+} in natural OMM[89]. Whereas at resting $[Ca^{2+}]_c$, there is a regulation of VDAC activity and OMM permeation of Ca^{2+} and small molecules in response to an increase of Ca^{2+}, VDAC displayed an immediate shift to large conductances and an eventual transition to full opening after a lag period. During the Ca^{2+} signal, the OMM barrier is seemingly decreased[89]. It remains elusive whether the sensitivity of VDAC to Ca^{2+} is conveyed by a Ca^{2+} sensitive enzyme targeting the channel, by CaM or by a direct effect of the cation on VDAC.

Of particular interest for Ca^{2+} uptake into cardiac mitochondria is the isoform VDAC2[100–102]: A knockdown of VDAC2 attenuated mitochondrial uptake of Ca^{2+} released from the

SR via RyR2 in the cardiac cell line HL-1 which not only supports the pivotal role of VDAC2 for Ca^{2+} signaling but also suggests that a direct coupling of both channels is essential for Ca^{2+} transfer from the SR into cardiac mitochondria[101]. Apart from RyR2, protein interaction partners of VDAC2 include other Ca^{2+} handling proteins such as the mitochondrial Ca^{2+} uniporter (MCU)[103].

1.3.3.2 Inner mitochondrial membrane - Mitochondrial Ca^{2+} uniporter complex

Physiological Ca^{2+} entry into mitochondria mainly occurs by uptake via MCU residing in the IMM. The MCU represents an electrogenic pathway for the rapid transport of Ca^{2+} into the matrix, propelled by the negative charge of the IMM potential ($\Delta\Psi_m$) which is created by the respiratory chain[69,104,105]. The MCU dominates fast uptake at $[Ca^{2+}]_c$ as high as 5-10 µM of free Ca^{2+} [84,85], which are not normally achieved in the cardiomyocyte cytoplasm[79,106]. Due to this low affinity, the MCU would not allow substantial Ca^{2+} uptake under resting (approx. 0.1 µM) or stimulated (1–3 µM at the peak) conditions and significant Ca^{2+} uptake was anticipated to be a unique feature of massive cytoplasmic Ca^{2+} overload[69]. However, the low affinity of MCU for Ca^{2+} is overcome by the close proximity of mitochondria to Ca^{2+} channels such as to RyRs in SR-mitochondria microdomains[76,87,107,108] (Fig. 5). There, the juxtaposition of SR and mitochondria could enhance mitochondrial delivery of SR-derived Ca^{2+} by limiting cytosolic diffusion and the subcellularly restricted high Ca^{2+} of above 10 µM[109] meets the low affinity of the MCU[69]. The MCU exists as a macromolecular complex with a Ca^{2+} permeant pore consisting of

the pore-forming MCU protein, mitochondrial Ca^{2+} uniporter b (MCUb) and the scaffolding essential MCU regulator (EMRE). Further regulatory proteins associated with the MCU are mitochondrial Ca^{2+} uptake (MICU) 1, 2, 3 and mitochondrial Ca^{2+} uniporter regulator 1 (MCUR1)[110].

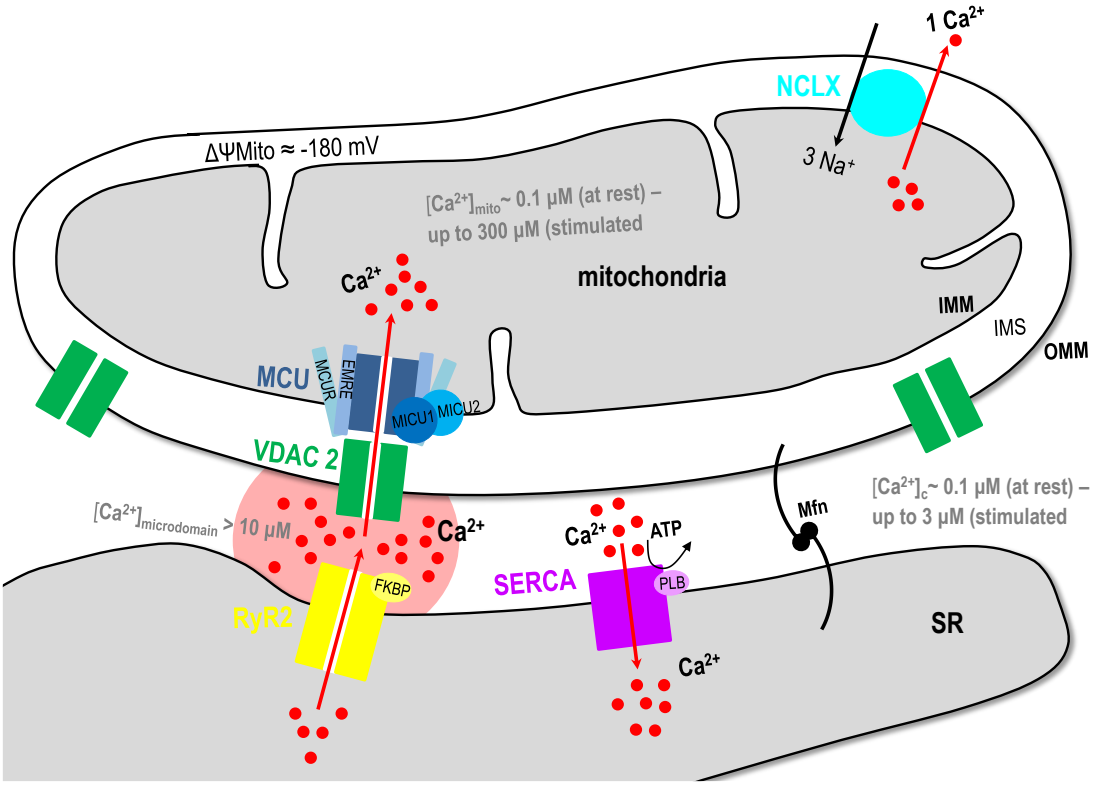

Fig. 5 SR-mitochondria Ca^{2+} microdomains with channels and transporters involved in mitochondrial Ca^{2+} signaling [modified from[111]].

Following release from the SR via RyR2, Ca^{2+} is being taken up from adjacent mitochondria tethered to the SR with Mitofusins (Mfn) acting as molecular tethers. Mfn hold both organelles in place for Ca^{2+} microdomains (indicated by light pink circle) with locally high Ca^{2+} concentrations [Ca^{2+}] to form. Whereas mitochondrial Ca^{2+} import across the OMM is mediated by VDAC, Ca^{2+} enters the mitochondrial matrix though the MCU macromolecular complex located on the IMM. The latter is negatively regulated by mitochondrial Ca^{2+} uptake (MICU) 1 and 2 which possess the ability to prevent Ca^{2+} influx via MCU. Further regulatory proteins associated with the MCU are the scaffolding essential MCU regulator (EMRE) and mitochondrial Ca^{2+} uniporter regulator (MCUR). Mitochondrial Ca^{2+} efflux is governed by Na^+/Ca^{2+} exchanger (NCLX). To prevent SR Ca^{2+} depletion, the ion is transported back into the organelle by the ATP-dependent SERCA. Abbreviations: $\Delta\Psi_m$ = IMM potential.

1.3.3.3 Mitochondrial Ca^{2+} efflux pathways

To prevent Ca^{2+} overload at high $[Ca^{2+}]_c$ and to preserve Ca^{2+} homeostasis and bioenergetics at low $[Ca^{2+}]_c$, mitochondria also possess pathways for Ca^{2+} extrusion with their relative activity determining free $[Ca^{2+}]_m$[67]. Under physiological conditions, Ca^{2+} extrusion from mitochondria is governed by two clearly distinct pathways, referred to as Na^+-dependent and Na^+-independent. In excitable tissues such as the heart with rapid mitochondrial Ca^{2+} release, Ca^{2+} extrusion is primarily governed by the Na^+-dependent mitochondrial Na^+/Ca^{2+}-exchanger (NCLX) located in the IMM[112] (Fig. 5). NCLX exchanges >3 Na^+ for 1 Ca^{2+} [113] and is able to transport Li^+ as a substitute for Na^+ to release Ca^{2+} [114] clearly delineating it from plasma membrane NCX. Further, NCLX is implicated in Ca^{2+} communication between SR and mitochondria in HL-1 cardiomyocytes[115].

1.4 Cardiac pathophysiology – Cardiovascular diseases

1.4.1 The congenital arrhythmia catecholaminergic polymorphic ventricular tachycardia

If the mechanisms of cardiac Ca^{2+} handling and thus ECC are not properly orchestrated, cardiovascular diseases (CVDs) may arise. Until today, CVDs constitute the leading cause of death worldwide and will continue to dominate mortality trends in the future[116]. While in 1990, 14.4 million people died of CVDs globally, this number increased to an estimated 17.9 million people in 2016, accounting for 31 % of all deaths worldwide[117]. Ventricular tachycardia (VT) which is triggered by propagation of ectopic beats leading to fibrillation[118] is the leading cause of sudden cardiac death (SCD)[119,120]. In up to 15 % of sudden unexplained deaths (SUD)[121], patients carried a pathogenic mutation revealed by postmortem genetic testing for catecholaminergic polymorphic VT (CPVT)[122,123]. CPVT has an unknown prevalence, estimated at 1:5000 to 1:10000[124] and it represents a highly malignant cardiac disease characterized by bidirectional or polymorphic VT. Arrhythmias typically arise in relation to adrenergic stimulation or physical exercise[125,126]. It was originally described in 1978[127] and characterized more precisely in 1995[128]. This congenital form of VT is in most cases inherited as an autosomal dominant trait and about 30 % of affected people have a family history of stress-related syncope, seizure and SUD[128]. The underlying reason for SCD in CPVT patients is a degeneration of tachycardia into ventricular fibrillation (VF)[129,130].

1.4.1.1 Manifestation and clinical presentation

The first clinical manifestation of the arrhythmia in over 50 % of patients is syncope, followed by aborted SCD[131]. While patients first show a normal resting ECG and no structural evidence of myocardial abnormalities, the disease manifests with a relatively early onset of clinical symptoms at 7-9 years in average[122]. It accounts for 1.5 % of sudden infant deaths, the mortality rate in untreated children is about 50 %[132]. The rate of occurrence of cardiac events including syncope, aborted cardiac arrest and SCD in untreated individuals amounts to about 58 % and the mortality ranges from 30 to 50 % by the age of 20 to 30 years[20,133]. An estimated 40 % of patients die within 10 years of diagnosis[134] and even in patients receiving medication, the mortality rate can reach up to 13 %[132]. CPVT is termed a VT since in over 50 % of the patients the arrhythmia arises from the ventricles, with the first beat of an arrhythmic episode originating in the ventricular outflow tract[122,134]. Moreover, arrhythmia can develop in the ventricular myocardium[122]. The QT interval is generally normal[133] to borderline prolonged at rest and unchanged during exercise[134]. An increase in exercise workload leads to the progressive worsening of arrhythmias which due to high reproducibility and occurrence at >120 bpm can be considered a hallmark of CPVT (Fig. 6)[122,124]. After premature ventricular complexes (PVCs) arise which can perturb the normal sinus rhythm thereby inducing tachycardia[135], bidirectional (BVT) and/or polymorphic VT are observed. A diagnostic marker, although only present in about 35 % of CPVT patients is the pattern of BVT with a QRS axis rotating 180° on a beat-to-beat basis. The mechanism underlying this alternating QRS axis is not yet fully resolved[131], yet a role of the His-Purkinje system in the genesis of BVT has been demonstrated[136]. Owing to the various characteristic manifestations with different ECG

patterns, CPVT is termed a polymorphic arrhythmia. In the majority of the cases, arrhythmias are non-sustained[134], meaning that after termination of exercise stress testing they gradually dissolve (Fig. 6). Albeit, some patients without the pattern of BVT exhibit rapid polymorphic VT.

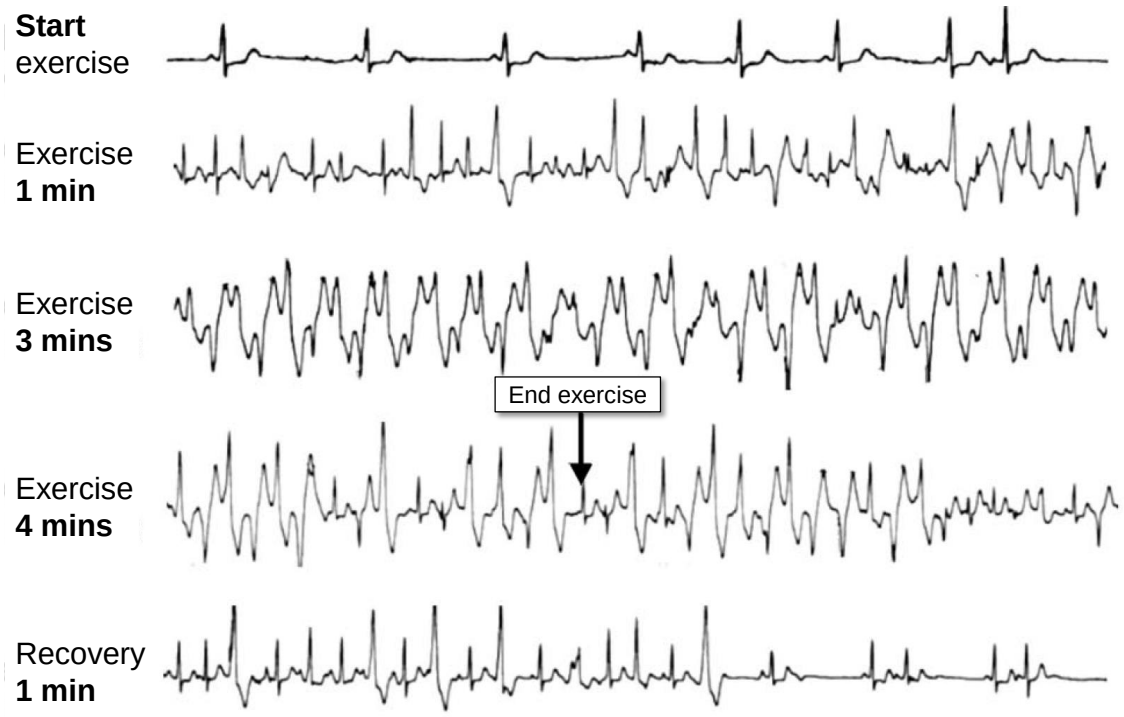

Fig. 6 Representative ECG traces of a CPVT patient carrying a RyR2 mutation during exercise stress testing [modified from[30]].

Whereas before exercise onset, the patient displays a normal resting electrocardiogram, adrenergic stimulation during stress conditions leads to a progressively worsening arrhythmia onset in the form of polymorphic ventricular tachycardia (VT) (exercise 1 minute). An increase in the sinus HR to approx. 120 bpm results in the characteristic bidirectional VT with a QRS axis rotating 180° on a beat-to-beat basis (3-4 min of exercise). Following a recovery period after cessation of stress testing, arrhythmias rapidly recede (Recovery).

1.4.1.2 Mechanisms underlying arrhythmogenesis in CPVT 1 - Aberrant Ca^{2+} handling

As mentioned above, intracellular Ca^{2+} release plays a pivotal role in ECC and needs to be well-orchestrated for cardiac rhythmicity. Any form of disturbance in the regulation of Ca^{2+} uptake and release is associated with CVDs such as CPVT. Mutations in Ca^{2+} handling proteins cause abnormalities in myocardial Ca^{2+} flux, which, in the presence of catecholamines lead to DADs, spontaneous APs and VT[2]. CPVT 1, the autosomal dominant form of the disease is associated with mutations in the cardiac isoform of ryanodine receptor, RyR2[126] accounting for approx. 50-55 % of all cases. Although in the majority of these patients the RyR mutation results in a gain-of-function effect of the channel[137], rare cases of loss-of-function mutations have been reported[138]. Further known mutations causing CPVT exist such as Casq2 in the autosomal recessive form of CPVT 2 in up to 5 % of patients[139], although an autosomal dominant mutation of Casq has recently been identified[140]. The underlying mutation of CPVT 3, a highly malignant autosomal recessive form, has been ascribed to a yet unidentified gene on chromosomal region 7p14-p22[141]. Under 1 % of affected people carry a mutation in CaM1 causative of the arrhythmia in CPVT 4[142], whereas CPVT 5 is caused by mutations in Trdn leading to early severe arrhythmias with sudden death[143,144].

In 2001, Priori et al. identified RyR2 as the gene affected in human CPVT1 patients[129]. To date, 155 different RyR2 mutations causing CPVT 1 are known[145]. Most mutations are single-base pair substitutions resulting in a replacement of highly conserved aa and occur in 4 hot spot clusters of the RYR2 gene[122]. As a consequence of altered properties such as an increased sensitivity of the channel to luminal Ca^{2+} [119], single dysfunctional RyR2s

spontaneously leak Ca^{2+} during diastole. This occurs in the form of spontaneous Ca^{2+} sparks (Fig. 8) originating from brief but frequent openings of single RyR2s[47] in quiescent unstimulated ventricular cardiomyocytes within an individual CRU without an external trigger[123]. Although every cell exhibits frequent single RyR openings (~3000 x $cell^{-1}$ x s^{-1}), these openings are often unable to trigger a spark (~130 x $cell^{-1}$ x s^{-1}) and under physiological conditions, spontaneous sparks remain locally restricted. However, in the setting of cytosolic Ca^{2+} overload apparent in CPVT, RyR2s are sensitized by Ca^{2+} leading to more channels spontaneously leaking Ca^{2+}. Ca^{2+} from one spark can in turn recruit neighboring receptor clusters to form compound sparks and so forth, in a process called spark-induced spark activation. Currently, three hypotheses exist regarding the reason underlying diastolic Ca^{2+} leak in CPVT 1. One explanation is the dissociation of FKBP12.6 from the mutated channel due to a weakened binding affinity resulting in an open state of RyR2[146]. In contrast, the store overload-induced Ca^{2+} release (SOICR) theory states that the threshold for free SR Ca^{2+} is decreased with mutant RyR2 leading to Ca^{2+} spillover from the SR[119,147]. Another possibility are defective intramolecular domain interactions[123]: Central and N-terminal domains of RyR2 are stabilizing the channels closed conformation by interdomain interactions, so-called domain zipping. Mutations in RyR2 possibly involve an unzipping of domains, accounting for diastolic RyR2 leakiness. Taken together, mutated RyR2s with their enhanced Ca^{2+} sensitivity are not alone arrhythmogenic. Rather, the stimulation of SERCA and increased $[Ca^{2+}]_{SR}$ triggered by β-adrenergic stimulation (arrhythmogenic trigger, Fig. 8) lead to the increased propensity of arrhythmic events under stress conditions[148].

1.4.1.3 Diastolic Ca^{2+} waves

As opposed to single Ca^{2+} sparks causing brief changes in local intracellular Ca^{2+} under physiological conditions[149], the rapid rise of the spark rate in CPVT increases $[Ca^{2+}]_c$ which can initiate spontaneous, diastolic Ca^{2+} waves that propagate along myocytes[150] (Fig. 8). Waves either occur as a result of $[Ca^{2+}]_{SR}$ elevated above a threshold or if this threshold is lowered[151]. According to Cheng and Lederer, three relevant features of Ca^{2+} waves exist[40]. Waves are initiated by sparks and their propagation is dependent on sequential activation of Ca^{2+} sparks by locally elevated Ca^{2+} resulting from preceding sparks. The properties of the wave thereby strongly depend on the amount of Ca^{2+} released through a single spark[150]. The increased sensitivity of CICR enables sparks to trigger neighboring sparks leading to a saltatory propagation with the wave occuring as a "fire-diffuse-fire" event with simultaneous release and diffusion of Ca^{2+} throughout the cell[152]. Hereby, an absolute prerequisite for signal propagation is the existence of a sufficiently large population of CRUs that have not already been activated[118]. Since Ca^{2+} waves are not present in ventricular cardiomyocytes under physiological circumstances, they are considered pathological events associated with cellular Ca^{2+} overload[153] causative for ventricular arrhythmias[154] thus regarded a highly recognized feature of CPVT.

1.4.1.4 Delayed afterdepolarizations and spontaneous APs during diastole

Ca^{2+} waves can activate NCX[153] and Ca^{2+} efflux via the exchanger during diastole in turn can generate transient inward currents (I_{ti}). In contrast to various animal species, I_{ti} solely consists of $I_{Na/Ca}$ in human ventricular cardiomyocytes[155]. Yet, in addition to forward-mode NCX generating I_{ti}, there is a possible contribution of further Ca^{2+} sensitive inward currents[118]. I_{ti} can trigger arrhythmias by two different mechanisms. First, it can augment early afterdepolarizations (EADs) (Fig. 8), spontaneous systolic afterdepolarizations occurring during phase 2 or 3 of repolarization[156] (Fig. 7), most probably due to interactions of I_{CaL} and repolarizing K^+ currents[40]. Secondly, I_{ti} has the potential to yield delayed afterdepolarizations (DADs) during diastole (Fig. 8). DADs are pathological low-amplitude voltage oscillations occurring in phase 4 of the cardiac AP after repolarization is complete[157] (Fig. 7). Noteworthy, murine cardiomyocytes are capable of developing DADs *in vitro* despite their short diastolic phase given the fast HR. However, both murine and human healthy cardiomyocytes are not prone to spontaneous DADs without an arrhythmogenic trigger such as intracellular Ca^{2+} overload (i.e. due to a RyR2 mutation), excessive β-AR stimulation and/or an increase in HR[158,159]. In contrast, CPVT cardiomyocytes from $RyR2^{R4496C/WT}$ mice already exhibit DADs under basal conditions with a further increase following β-AR stimulation[158]. If sufficiently large, these DADs may produce aberrant electrical activity in the form of spontaneous APs eventually resulting in arrhythmia[160]. Spontaneous APs represent the most noted mechanism of Ca^{2+} dependent arrhythmogenesis in CPVT.

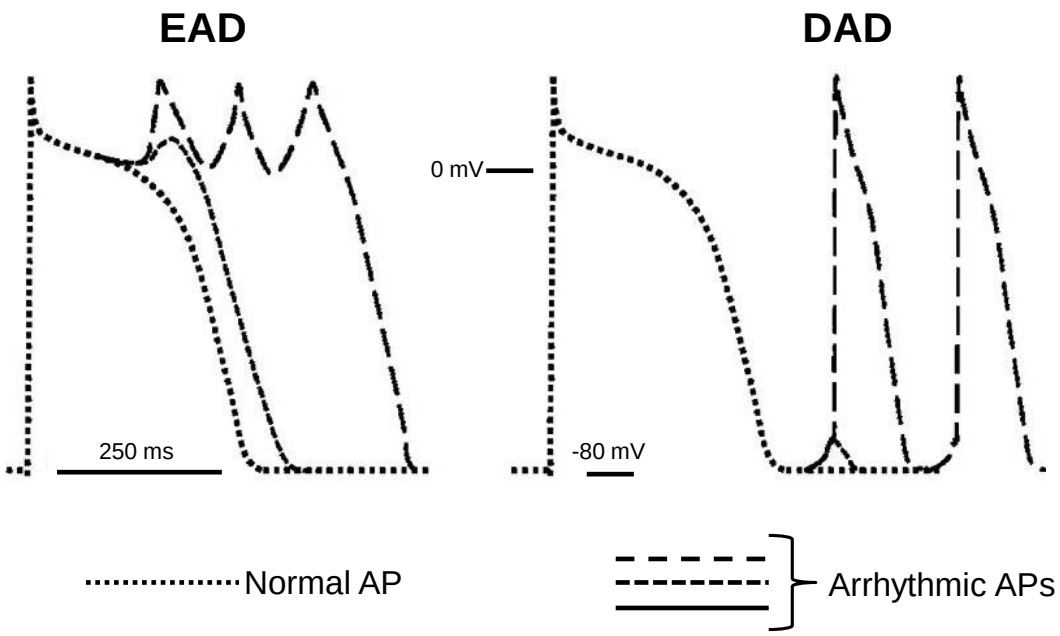

Fig. 7 Mechanisms of Ca^{2+} induced arrhythmogenesis [modified from[161]].

Whereas delayed afterdepolarizations (DADs) are low-amplitude depolarizations occuring after complete repolarization during diastole, early afterdepolarizations (EADs) originate during the cardiac AP before repolarization is complete and lead to AP prolongation. Both types of voltage oscillations may provoke spontaneous APs if they reach the threshold of depolarizing currents. These spontaneous APs can in turn elicit further APs leading to sustained triggered activity eventually resulting in arrhythmia.

1.4.1.5 Overcoming the source-sink mismatch and induction of arrhythmia

Once the membrane potential of an individual cardiomyocyte in the heart deviates from that of surrounding myocytes as in DADs and EADs, electrotonic current flow occurs from adjacent cells to reduce the erratic voltage difference. On average, a ventricular cardiomyocyte (the source) is directly coupled to 11 further myocytes (the sink) which will prevent voltage oscillations from propagating throughout cardiac tissue[162]. Thus, in order to trigger an arrhythmia in the heart (CPVT arrhythmia, Fig. 8), a single cardiomyocyte presenting with DADs or EADs first has to overcome the protective source-sink mismatch with surrounding tissue. A sufficient number of quiescent neighboring cells would have to synchronously evolve an afterdepolarization. Yet, in genetic channelopathies such as in CPVT, the cardiac tissue is not considered normal due to electrical remodelling leading to a weaker sink which drastically decreases the number of adjacent cardiomyocytes necessary to trigger a PVC[162]. In CPVT, the leaky RyR2 causes drastic overload conditions resulting in an increased amplitude, frequency and synchrony of Ca^{2+} waves[163]. Taken together, these factors augment the probability that neighboring Ca^{2+} overloaded myocytes likewise carrying the disease-causing mutation will exhibit SR Ca^{2+} release in relative synchrony. In the presence of β-AR stimulation RyR2 leakiness is further aggravated, additionally promoting DADs and the development of focal arrhythmias.

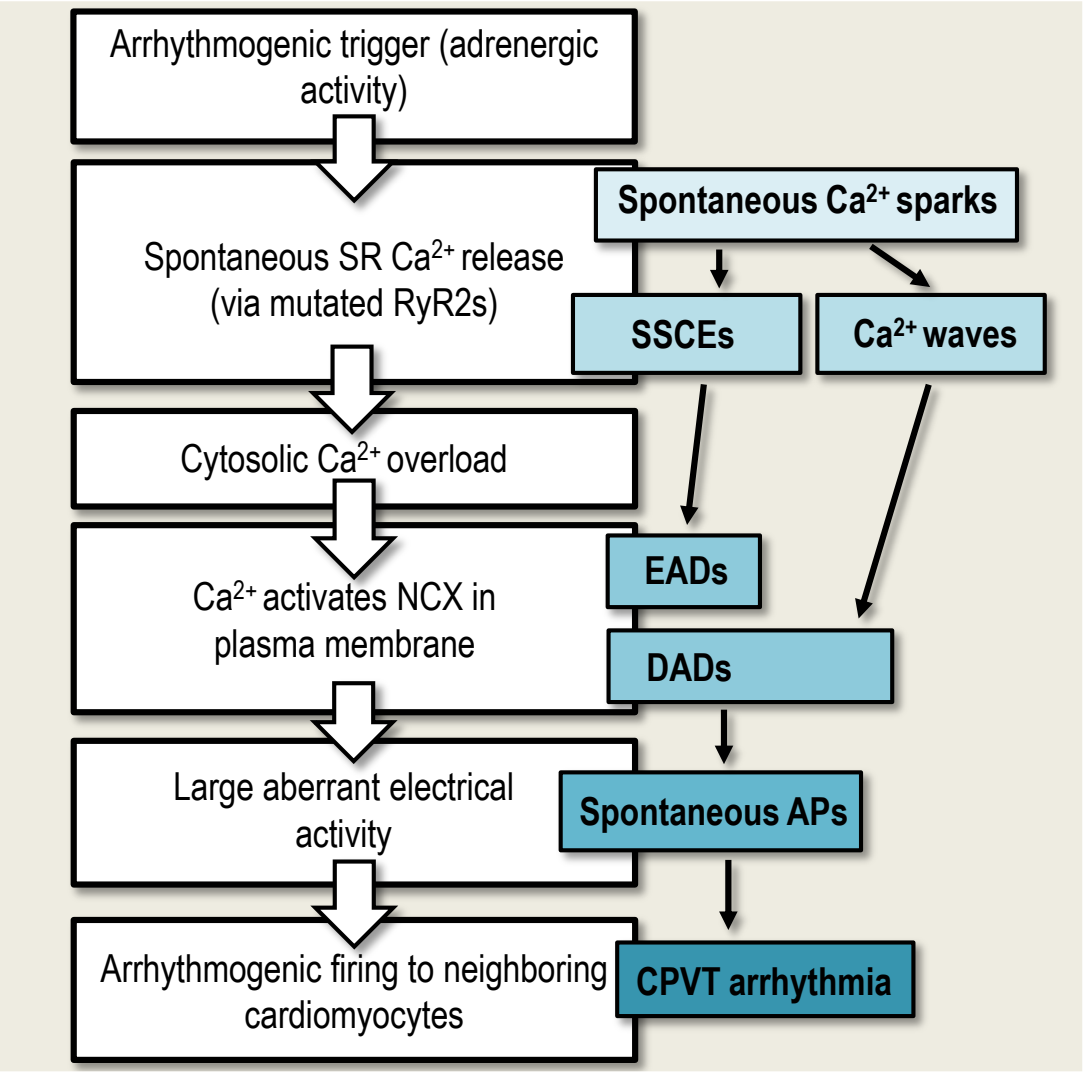

Fig. 8 The steps of CPVT pathogenesis.

In the setting of CPVT (e.g. RyR mutation), an arrhythmogenic trigger (adrenergic activity triggered by physical, emotional or catecholaminergic stress) leads to spontaneous Ca^{2+} release from the SR in the form of spontaneous, untriggered Ca^{2+} sparks. Depending on the time of their occurrence, these sparks can trigger secondary systolic Ca^{2+} elevations (SSCEs) (systole) or Ca^{2+} waves (diastole) which lead to cytosolic Ca^{2+} overload. This Ca^{2+} can in turn activate the NCX carrying transient inward current I_{ti}. which can augment both EADs (systole) and DADs (diastole). Once a single arrhythmic cardiomyocyte becomes capable of transmitting its aberrant stimuli to adjacent cardiac tissue thereby overcoming the source-sink-mismatch of the cardiac syncytium, CPVT arrhythmia occurs.

1.4.1.6 Murine model of CPVT 1

In 2005, the group of Silvia G. Priori published the generation of the conditional knock-in $RyR2^{R4496C/WT}$ mouse model phenotypically resembling a severe form of human CPVT caused by a mutation in RyR2[125]. In 2001, the associated R4497C mutation had been identified as a cause underlying an extremely lethal form of human CPVT[129] with more than 50 % of patients manifesting with cardiac arrest. Akin to the absence of structural heart defects in human patients, R4496C mice do not exhibit macroscopic cardiac alterations such as tissue abnormalities or signs of inflammation[125]. Yet, the presence of the R4496C mutation predisposes the murine heart to the development of BVT, polymorphic VT and VF. The polymorphic pattern of *in vivo* arrhythmia recapitulates the human CPVT phenotype with mice developing sustained and non-sustained VT and also VF[125]. VT in $RyR2^{R4496C/WT}$ mice revealed the typical bidirectional morphology that is considered a hallmark of human CPVT[125]. Also precisely reflecting the cause of disease in human patients, tachycardia in $RyR2^{R4496C/WT}$ animals was shown to be caused by alterations in Ca^{2+} handling with augmented spontaneous SR Ca^{2+} release through the defective RyR2 channels. Due to the high propensity for diastolic waves in cardiomyocytes from CPVT mice, they are prone to the development of spontaneous APs upon adrenergic stimulation[126]. In addition to the remarkable similarities demonstrated in murine and human CPVT mutation carriers in regard to disease morphology and severity, $RyR2^{R4496C/WT}$ mice also manifest an incomplete response to β-blockers[125].

1.4.1.7 Common therapeutic interventions in CPVT

To date, there is no pharmacological therapy with proven effectiveness available for CPVT patients harboring a RyR2 mutation and only 38 % of patients are controlled by drug treatment[134]. The causal association between stress and arrhythmic symptoms make exercise restriction and β-blockers the first-line therapy[128,130]. Although the highest tolerable dose is being prescribed to maximize control of arrhythmias, β-blockers fail to prevent from arrhythmias in 30 % of patients and do not completely prevent from SCD[122]. In addition to drug intolerance occurring in some patients[164], the quality of life can be severely limited since cardiac performance is tempered and physical work load is limited[165]. This represents a significant restriction especially in predominantly very young and active patients oftentimes leading to non-compliance[165]. Various other types of medications belonging to the group of antiarrhythmics are used in the treatment of CPVT with varying degrees of success. Verapamil, a Ca^{2+} channel blocker and class IV antiarrhythmic drug, significantly reduced ventricular arrhythmias without a complete suppression of CPVT[134,166] but also showed an inhibitory effect on K^+ currents. Generally, Ca^{2+} channel blockers are to a large part deprived from CPVT patients since they commonly cause cardiac arrest in infants[134]. Another approach is the treatment with Na^+ channel blockers. Flecainide was shown to improve ventricular arrhythmias in 74 % of genotype-positive[167] and in 92 % of genotype-negative[168] individuals in the absence of structural heart disease. Other promising examples of Na^+ channel blocker therapy for patients bearing a RyR2 mutation include propafenone[169], mexiletine and disopyramide[134], yet only a small number of individuals were being treated to date. Further, the Na^+ channel blocker Ranolazine decreases abnormally high $[Ca^{2+}]_c$ and

prohibits Ca^{2+} overload[170]. Yet, Ranolazine additionally targets I_{Kr}, leading to a prolonged AP duration (APD) with corresponding QT interval prolongation and its antiarrhythmic activity is incomplete. In conclusion, treatment ended fatally in 75 % of patients after either β-blockade was substituted by the Na^+ channel blocker or β-blockers were continued. Thus, a more recent approach is a combined therapy of antiarrhythmics and β-blockers, which proved more effective than monotherapy with β-blockers alone[171]. In this context, a combined therapy with flecainide is by now successfully incorporated into CPVT treatment[169] and current guidelines recommend the use of the Na^+ channel blocker in individuals with recurrent syncope while on β-blockers[172,173]. Despite these promising outcomes, flecainide is still contraindicated for patients with suspicion of structural heart defects and coronary artery disease. Thus, in CPVT patients with preexisting conduction abnormalities such as a QRS interval prolongation by ≥25 %, treatment with Na^+ channel blockers should be discontinued[169,174]. Patients devoid of controlled optimal therapy[131] or those who have experienced cardiac arrest are recommended to carry an inducible cardioverter-defibrillator (ICD) implanted to terminate VT[175]. In addition to clinical problems associated with ICD implantation in children such as infections, only 50 % of patients implanted with an ICD received an appropriate shock following arrhythmia. But in addition to these life-saving interventions, ICD devices often cause inappropriate shocks and electrical storms that may result in lethal events. This led to a frequent application of high dose β-blocker treatment in addition to ICD implantation. As an experimental therapy applicable in high-risk patients with uncontrollable arrhythmia that receive frequent ICD shocks despite β-blockade, left sympathetic denervation (LCSD)[131,176] seems to hold potential by drastically reducing arrhythmic storms[122,177]. By

preventing cardiac release of norepinephrine, LCSD exerts long-lasting effects without impairing myocardial contractility and thereby is especially effective in patients not compliant to β-blockers[176]. The procedure was shown to be an effective antifibrillary intervention in CPVT patients, either as a single therapy or in combination with β-blockers[178]. Since LCSD can significantly reduce the number of ICD shocks and narrow the amount of patients experiencing electrical storms post-procedure[178], it adds to the recommended treatment options for CPVT[172]. A further minimally-invasive approach seemingly effective in some CPVT patients presenting with atrial fibrillation (AF)[124] is catheter ablation, where arrhythmic tissue surrounding the pulmonary veins is freezed leading to the formation of small scars that prevent abnormal electrical signals from propagating throughout the heart. As can be seen from the different aforementioned approaches, fully satisfying treatment options for CPVT are still scarce pointing to an urgent need for new, non-invasive therapeutic strategies that do not intervene in systolic APs thereby causing proarrhythmogenic effects.

1.4.2 The synthetic VDAC2 agonist efsevin exerts antiarrhythmic properties in zebrafish embryos

Cardiac rhythmicity is critically dependent on a well-orchestrated cardiomyocyte Ca^{2+} handling. Prevalent CVDs such as cardiac arrhythmias are causally linked to aberrant Ca^{2+} handling and a disturbed cellular Ca^{2+} homeostasis make intracellular Ca^{2+} transporters lead candidate structures for novel and safer antiarrhythmic therapies.

However, not a single one of today's common cardiac therapeutics directly acts on intracellular Ca^{2+}. Mitochondria are known to regulate cardiac rhythmicity[179,180]. Our lab proposed the pharmacological activation of mitochondrial Ca^{2+} uptake as such a novel intracellular target structure. In a small molecule suppressor screen designed to identify novel regulators of cardiac rhythmicity and chemical modulators thereof, the dihydropyrrole carboxylic ester efsevin (Fig. 9a) was identified by its potent ability to suppress cardiac fibrillation in *tremblor* (*tre*) zebrafish[181,182]. Due to a mutation causing the lack of cardiac NCX, homozygous *tre* embryos are unable to efficiently remove Ca^{2+} from the cytoplasm and display only unsynchronized cardiac contractions resembling cardiac fibrillation. *Tre* embryos treated with the synthetic compound efsevin, however displayed robust rhythmic contractions (Fig. 9c) with fractional shortening comparable to wildtype (WT) and a HR of approx. 40 % of that observed in WT siblings. Efsevin was demonstrated to directly bind to VDAC2 in the OMM and overexpression of the channel likewise restored rhythmic cardiac contractions while VDAC2 knockdown abolished the efsevin-mediated effects indicating that efsevin potentiates VDAC2 activity. Indeed, an enhanced mitochondrial Ca^{2+} uptake was observable upon treatment of HeLa cells with efsevin (Fig. 9b). By potentiating mitochondrial Ca^{2+} uptake, efsevin significantly enhances the removal of cytosolic Ca^{2+} in adult murine cardiomyocytes. This leads to a spatial and temporal restriction of Ca^{2+} sparks causing a significant reduction of Ca^{2+} waves in cardiomyocytes from WT mice challenged by high extracellular Ca^{2+}. These findings point to a great potential of efsevin for future therapeutic use in CVDs such as CPVT where propagating Ca^{2+} waves induce arrhythmias. With the emergence of the substantial role of mitochondria in CVDs, VDAC2 becomes an interesting drug target and

efsevin might serve as a lead candidate drug to target the mitochondrial Ca^{2+} uptake pathway.

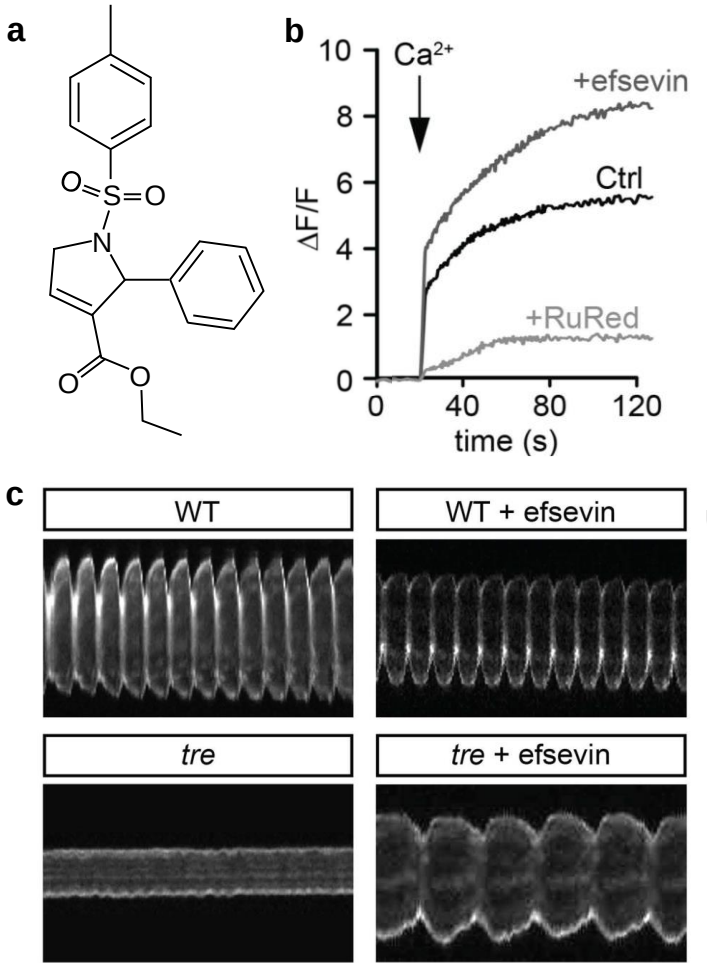

Fig. 9 The dihydropyrrole carboxylic ester efsevin restores rhythmic cardiac contractions in NCX-mutated zebrafish embryos and increases mitochondrial Ca^{2+} uptake in HeLa cells by targeting VDAC2 [compiled from[181]].

(a) Chemical structure of efsevin. (b) The antiarrhythmic effect of efsevin was ascribed to enhanced mitochondrial Ca^{2+} uptake via an interaction with the OMM channel VDAC2 by treatment of HeLa cells with efsevin (dark gray trace). Inhibition of mitochondrial Ca^{2+} uptake with ruthenium red (RuR) (light gray trace) clearly demonstrates the mitochondrial specificity of the signal. (c) Whereas wildtype (WT) zebrafish exhibit robust rhythmic contractions as shown by cross sections through GFP-tagged hearts (left side), mutated *tremblor* (*tre*) fish display only unsynchronized contractions resembling cardiac fibrillation. However, efsevin could recover rhythmic cardiac contractions to approx. 40 % of that observed in WT whithout any adverse effects on WT hearts.

1.4.3 Aim of the thesis: Enhancing mitochondrial Ca^{2+} uptake as a novel treatment strategy in CVDs

Despite the pronounced effects of enhanced mitochondrial Ca^{2+} uptake via efsevin to restore cardiac rhythmicity seen in zebrafish mutants and WT murine cardiomyocyte, experiments in mammalian disease models were still lacking. Interestingly, the observed rescuing effect in *tre* embryos was not limited to activation of VDAC2. Likewise, enhancing mitochondrial Ca^{2+} uptake by overexpression of the MCU restored rhythmic cardiac contractions in *tre* zebrafish. Presumably, both channels cohere as a transport unit to forward Ca^{2+} from the cytosol across both mitochondrial membranes into the organelle[181] and activation of this pathway through either of the two targets is effective to enhance mitochondrial Ca^{2+} uptake and to suppress arrhythmia in the zebrafish model. The MCU is activated by natural plant flavonoids with kaempferol (3,4′,5,7-Tetrahydroxyflavone, 3,5,7-H-1-benzopyran-4-one, Robigenin) being the most active compound to enhance Ca^{2+} uptake into mitochondria[183]. Work from our group indeed demonstrated that the MCU agonist kaempferol dose-dependently increased the rapid transfer of Ca^{2+} from the SR into mitochondria akin to efsevin[184]. Albeit kaempferol was demonstrated to reduce arrhythmogenic Ca^{2+} waves arising from dissipation of the mitochondrial membrane potential[180] and cardioprotective biological activities of the flavonoid have been assumed[185,186], potential antiarrhythmic effects of the MCU agonist in mammalian models of Ca^{2+} induced arrhythmia are still lacking. To close this major gap, I evaluated a potential antiarrhythmic effect of enhanced mitochondrial Ca^{2+} uptake in a murine cardiac disease model of CPVT harboring a mutation in the SR Ca^{2+} release

channel RyR2 and two human CPVT models with a RyR2 as well as a yet unknown mutation, with the following aims being adressed:

(1) Is there an antiarrhythmic effect of VDAC agonization with efsevin in cardiomyocytes from RyR2$^{R4496C/WT}$ mice in the various events underlying CPVT arrhythmia progression?

(a) Does Efsevin intervene as early as during Ca^{2+} signals during diastole (sparks, waves) and systole (SSCEs)?

(b) Does Efsevin's effect recur throughout the more expansive electrophysiological signals during diastole (DADs, APs) and systole (EADs)?

(2) Does enhanced mitochondrial Ca^{2+} uptake represent a general and standalone antiarrhythmic principle?

(a) Is enhanced mitochondrial Ca^{2+} uptake indeed the sole mechanism underlying the antiarrhythmic activity of efsevin?

(b) Is MCU agonization with Kaempferol equally effective as VDAC2 agonization with efsevin with regard to Ca^{2+} sparks?

(3) Could an antiarrhythmic effect of both efsevin and kaempferol be translated to RyR2$^{R4496C/WT}$ mice *in vivo*?

(a) Is there an antiarrhythmic effect of both substances also on full-blown CPVT arrhythmia concerning cardiac tissue as a whole in RyR2$^{R4496C/WT}$ mice over a course of 3 or even over a course of 8 days?

(b) Are there adverse effects observable in any of the aforementioned arrhythmogenic signals *in vitro* or in mice *in vivo*?

(4) Could an antiarrhythmic effect of both efsevin and kaempferol be translated to human induced pluripotent stem cell (iPSC)-derived cardiomyocytes from CPVT patients carrying a RyR2 or a yet unknown CPVT mutation, respectively?

2. MATERIALS

2.1 Consumables

Product	Name and Company
Cation exchanger dowex columns	packed by Dr. A. Breit with anion exchange resin, Bio Rad
Ceramic beads 2.8 mm (tissue homogenization)	CK28L Precellys Peqlab, Darmstadt, Germany, #91-PCS-CK28P
Filter mesh 200 µm (cardiomyocyte isolation)	Polyester Siebgewebe, Bartelt, Graz, Austria, #9068227
Glass bottom culture dishes	MatTek Corporation, Ashland, MA, USA, (for mouse cells) # P35G-0-0.170-14-C or (for human iPSCs) # P35G-0-0.170-10-C
Glass capillaries with filaments (patch clamp)	1.05x1.50x80 mm, Sutter Instruments HEKA Elektronik Dr. Schulze GmbH, Lamprecht, Germany, #GB150TF-8P
Millex-GV filter	Millipore Merck KGaA, Darmstadt, Germany, #SLGV004SL
Cell culture dish (patch clamp)	Nunclon™ Delta Surface, Thermo Fisher Scientific GmbH, Dreieich, Germany, #150318
Neutral alumina columns	packed by Dr. A. Breit with anion exchange resin, Bio Rad
Osmotic minipumps	ALZET DURECT Corporation, Charles River Laboratories GmbH, Sulzheim, Germany, (model 1003D) #0000289 or (model 1007D) #0000290
Suture (heart cannulation and fixation)	4/0 USP, white-braided polyester, non-absorbable, silicone coated, Medipac, Kilkis, Greece, #542
Suture with round bodied 3/8 circle needle (wound closure)	5/0 USP, blue monofilament, non-absorbable, polypropylen, Medipac, Kilkis, Greece, #6211
Syringe with 29G needle (epi/caff injection), 1mL	Terumo Myjector U100, Terumo, Eschborn, Germany
Syringe (filling of osmotic minipumps), 1 mL	Luer-Lok™ Tip, BD Biosciences VWR, Darmstadt, Germany, #BD-309628
Syringe (heart cannulation), 1 mL	Injekt®-F Solo, B. Braun, Melsungen, Germany, #9166017V

Syringe (iPSC explantation), 1 mL	Omnican®F, 0,30 x 12 mm / G 30 x 1/2", B. Braun, Melsungen, Germany, #9161502
Three-way valve Luer-Lock (cardiac perfusion)	Discofix®, B. Braun, Melsungen, Germany, # 4095111
Tissue homogenization tubes , 2 mL	Precellys Peqlab VWR, Darmstadt, Germany, #BERTKT03961-1-4052
Li-Heparin LH/1.3 coated vials (plasma extraction)	Sarstedt, Nümbrecht, Germany, #41.1393.005

2.2 Chemicals and reagents

Solutions of chemicals and reagents listed below were prepared with ultrapure Milli-Q water prepared from an ultrapure water system (Merck Millipore) unless otherwise stated in the Methods section.

Chemical/reagent.	**Company and order-no.**
2,3-Butanedione monoxime (BDM)	Sigma-Aldrich, Steinheim, Germany, #B0753-100G
2-Mercaptoethanol, ≥99.0 %	Sigma-Aldrich, Steinheim, Germany, #M6250-10ML
2-Methyl-2-butanol (tert-amyl alcohol), ReagentPlus®, 99.0 %	Sigma-Aldrich, Vienna, Austria, # 152463-250ML
2,2,2-Tribromoethanol, 97 %	Sigma-Aldrich, Vienna, Austria, #T48402-25G
[2,8-^{3}H]-adenine, 1mCi (37 MBa)	PerkinElmer, Rodgau, Germany, #NET063001MC
3-Isobutyl-1-methylxanthin (IBMX)	Sigma-Aldrich, Steinheim, Germany, #I5879-100MG
Acetonitrile LC-MS Chromasolv®	Fluka Analytical Sigma-Aldrich, Seelze, Germany, #3467-1L
L-adrenaline (Suprarenin®) ampulla 2MG/20mL	Fresenius Kabi, Graz, Austria #1-21272
Agarose Roti®garose	Carl Roth, Karlsruhe, Germany, #3810.3
Amphotericin B, solubilized, from *Streptomyces sp.*	Sigma-Aldrich, Steinheim, Germany # A9528-50MG
Anion exchange resin, analytical grade, 100-200 µm mesh, chloride form	AG®1-X8 , BioRad VWR, Darmstadt, Germany #1401441
K-aspartate (L-aspartic acid potassium salt) puriss. p.a., ≥99 %	Fluka Analytical Sigma-Aldrich, Seelze, Germany, #11230-100G-F

Caffeine	Sigma-Aldrich, Vienna, Austria, #C0750-100G
$CaCl_2*2H_2O$	Carl Roth, Karlsruhe, Germany, #5239.1
Creatine	Sigma-Aldrich, Steinheim, Germany, #C0780-50G
Diethyl pyrocarbonate (DEPC) water	Sigma-Aldrich, Steinheim, Germany, #40718
Dimethylsulfoxid (DMSO)	Carl Roth, Karlsruhe, Germany, #4720.2
Dulbecco's Modified Eagle's Medium (DMEM), serum-free	Sigma-Aldrich, Steinheim, Germany, #D6546
DNA ladder	Gene ruler 1 kb, Thermo Fisher Scientific GmbH, Dreieich, Deutschland, #SM0311
DNA loading dye, 6x	Thermo Fisher Scientific GmbH, Dreieich, Deutschland, #R0192
dNTPs (10 mM each)	dNTP mix, Thermo Fisher Scientific GmbH, Dreieich, Deutschland, #R0611
DPBS $+CaCl_2$ $+MgCl_2$ (for iPSC culture)	Sigma-Aldrich, Steinheim, Germany, #D8537-500ML
EB2	media provided by Klinikum Rechts der Isar TUM, Germany (for exact composition see Methods section)
EB20	media provided by Klinikum Rechts der Isar TUM, Germany (for exact composition see Methods section)
Ethylenediaminetetraacetic acid (EDTA)	Carl Roth, Karlsruhe, Germany, #8043.3
Efsevin	synthesized by Ohyun Kwon, Dept. of Chemistry and Biochemistry, UCLA, Los Angeles, USA
EGTA (≥99 % p.a.)	Carl Roth, Karlsruhe, Germany, #3045.2
Fetal bovine serum (FBS)	Gibco® Thermo Fisher Scientific, Schwerte, Germany, # 10270
Fibronectin from bovine plasma	Sigma-Aldrich, Steinheim, Germany, #F1141-2MG
Fluo-4, AM ester	Life technologies, Thermo Fisher Scientific, Ober- Olm, Germany, #F14201
Forskolin (FSK)	Sigma-Aldrich, Steinheim, Germany, #F6886
(Glacial) acetic acid, 100 % Ph.Eur. reinst	Carl Roth, Karlsruhe, Germany, #6755.2
L-Glucose	Carl Roth, Karlsruhe, Germany, #X997.2
L-Glutamic acid potassium salt	Sigma-Aldrich, Steinheim, Germany, #118K0181
HBSS	Gibco® Thermo Fisher Scientific, Schwerte, Germany, #14170
HCl Rotipuran®, 37 %	Carl Roth, Karlsruhe, Germany, #4625.1

Heparin sodium salt	Carl Roth, Karlsruhe, Germany, #7692.2
HEPES	Carl Roth, Karlsruhe, Germany, #HN78.2
Imidazole	Sigma-Aldrich, Steinheim, Germany, #56750-100G
Isoflurane (anesthesia before cervical dislocation)	Baxter, Unterschleißheim, Germany, #12K/19435
Isoflurane (ECG anesthesia)	Baxter, Vienna, Austria, #12K/15B25H33
Isoprenaline hydrochloride	Sigma-Aldrich, Steinheim, Germany, #I5627-5G
Isopropyl alcohol, 70 %	provided by Anstaltsapotheke Landeskrankenhaus Graz, Graz, Austria
Kaempferol (*in vitro* studies)	Sigma-Aldrich, Steinheim, Germany, #K0133-10MG
Kaempferol (*in vivo* studies) ≥99.0 %, analytical standard	Sigma-Aldrich, Steinheim, Germany, #96353-10MG
KCl	Carl Roth, Karlsruhe, Germany, #6781.1
KH_2PO_4	Carl Roth, Karlsruhe, Germany, #3904.2
KOH	Sigma-Aldrich, Steinheim, Germany, #60377
D-Mannitol	Sigma-Aldrich, Steinheim, Germany, #63559
$MgCl_2$	Carl Roth, Karlsruhe, Germany, #KK36.2
$MgCl_2$*$6H_2O$ ≥99.0 %	Sigma-Aldrich, Steinheim, Germany, #M2670-1KG
$MgSO_4$*$7H_2O$, EMSURE®	Merck, Darmstadt, Germany, #105886
NaCl	Carl Roth, Karlsruhe, Germany, #3957.1
Na_2HPO_4*$7H_2O$	Riedel-de Haën AG, Seelze, Germany, #04274
NaOH, pellets	Carl Roth, Karlsruhe, Germany, #6771.1
Nuclease-free H_2O	Qiagen, Hilden, Germany, #129114
Polyethylen glykol 400	Carl Roth, Karlsruhe, Germany, #0144.1
Pluronic® F-127	Sigma-Aldrich, Steinheim, Germany, #P2443-250G
(±)-propranolol hydrochloride	Sigma-Aldrich, Steinheim, Germany #P0884-5G
RotiSafe® DNA staining reagent	Carl Roth, Karlsruhe, Germany, #3865.1
Rotiszint® eco plus	Carl Roth, Karlsruhe, Germany, #0016.4
Ru_{360}	Calbiochem, Merck Millipore, Darmstadt, Germany, #557440
Saline 0.9 % ("Fresenius-Infusionslösung")	Fresenius Kabi, Graz, Austria #PKO3XEO10D6
Sodium metabisulfite, Reag. ACS	Sigma-Aldrich, Steinheim, Germany #31448
Taurine	Carl Roth, Karlsruhe, Germany #4721.2

Trichloroacetic acid (TCA), ACS reagent, ≥99.0 %	Sigma-Aldrich, Steinheim, Germany, #T6399
TRIS Pufferan® ≥99.0 %, p.a.	Carl Roth, Karlsruhe, Germany #4855.2

2.3 Enzymes

Chemical/reagent	**Company and order-no.**
Accumax™ cell detachment solution	Chemicon® Millipore Merck KGaA, Darmstadt, Germany, #SCR006
Collagenase II, 298 U/mg	Worthington, Troisdorf, Germany, #40N12244
DirectPCR® Lysis Reagent Tail	Peqlab VWR, Darmstadt, Germany, #31-101-T
GoTaq G2 HotStart Green Master Mix	Promega, Mannheim, Germany, #M7423
Liberase™	Roche Diagnostics Sigma-Aldrich, Steinheim, Germany, # 05401151001
Phusion High-fidelity DNA polymerase, 2U/mL	Thermo Fisher Scientific GmbH, Dreieich, Germany, #F530L
Proteinase K, recombinant, PCR grade, >600 U/mL	Thermo Fisher Scientific GmbH, Dreieich, Germany, #EO0491

2.4 Oligonucleotides

Primers	**sequence 5‘ – 3‘**
mRyR2 fwd	GAA-TGC-TGG-CCT-TGT-TTG-TT
mRyR2 rev	TAG-GCA-GCT-CCT-TTC-CTT-CA

2.5 Kits

Kit	**Company and order-no.**
NucleoSpin® gel and PCR clean-up	Macherey-Nagel, Düren, Germany, #740609.25
RevertAid First Strand cDNA Synthesis Kit	Thermo Fisher Scientific GmbH, Dreieich, Germany, #K1621

2.6 Instruments and devices

Instrument	Name and company
Agarose gel chambers	PerfectBlue™ horizontal mini gel systems, VWR, Darmstadt, Germany
Amplifier EPC10 (patch clamp)	HEKA Elektronik Dr.Schulze, Lamprecht, Germany
Analytical scale (chemicals)	Mettler Toledo XS205 Dual Range, Gießen, Germany
Anesthesia vaporizer (part of ECG setup)	Combi-vet® Base Anesthesia System Digital Flowmeter 0.3 - 16 lpm 02, Rothacher Medical GmbH, Heitenried, Switzerland
Blunt needle 19G (heart cannulation)	Custom-made from 19Gx1 ½ intramuscular needle, B. Braun, Melsungen, Germany #4657799
Body temperature controller and rectal probe (part of ECG setup)	TC-1000 mouse, Cwe incorporated, Ardmore, PA, USA, #08-13000
Centrifuge	Heraeus Megafuge 16R, Thermo Fisher Scientific GmbH, Dreieich, Germany
CO_2 incubator	HeraCell 150i, Thermo Fisher Scientific GmbH, Dreieich, Germany
Confocal microscope	TCS SP5, Leica, Wetzlar, Germany
Electronic pipettor	BD Falcon Express Pipet-Aid, BD Biosciences, Heidelberg, Germany
Electrophoresis Power Supply	EPS301, GE Healthcare, Munich, Germany
Fine Scissors	ToughCut® Scissors, Fine Science Tools, Heidelberg, Germany, #14558-11
Fine Scissors	Fine Iris Scissors, Fine Science Tool, Heidelberg, Germany, #14094-11
Forceps	Standard pattern forceps, Fine Science Tools, Heidelberg, Germany, #11000-14
Forceps	Angled forceps, S&T JFA-5b, Fine Science Tools, Heidelberg, Germany
Forceps	Hooked forceps, Hauptner & Herberholz, Solingen, Germany, #07700.000
Gel documentation darkhood	BioDocAnalyze, Biometra, Göttingen, Germany
Glass cylinder (part of cardiac perfusion setup)	Custom-made by Peter Mann, Walther Straub Institute of Pharmacology and Toxicology, Munich, Germany
Hydraulic pump	Minipuls 2, Gilson, Limburg an der Lahn, Germany

Hypodermic needle, 1 mL	Omnican®F, B Braun, Melsungen, Germany, #9161502S
Ice machine	Scotsman AT100, Sprockhövel, Germany
Isolated input amplifier (part of ECG setup)	Animal Bio Amp FE136, AD instruments, Oxford, UK
Stereo-Microscope (heart cannulation)	Stereo-Zoom Expert-Boom-B, Müller Optronic, Erfurt, Germany
Microscope (cell culture)	Nikon Eclipse TS100, Düsseldorf, Germany
Microscope (patch clamp)	IX70 Olympus, Hamburg, Germany
Magnet stirrer	MR Hei-Standard, Heidolph, Schwabach, Germany
Objective (patch clamp)	LCPlanFl, 40x/0.60 Ph.2, Olympus, Tokyo, Japan, # 1-UB347
Oil immersion objective (confocal microscope)	HCX PL APO CS 63x/1.40 Oil CS2, LEICA, Wetzlar, Germany, # 15506372
Osmometer	Vapro® vapor pressure osmometer 5520, Wescor Kreienbaum Wissenschaftliche Meßsysteme e. K., Langenfeld, Germany
pH meter	FiveEasy™ FE20, Mettler Toledo, Gießen, Germany
Pacing electrodes (attached to stimulator)	Custom-made by Peter Mann, Walther Straub Institute of Pharmacology and Toxicology, Munich, Germany
Patch pipette puller	DMZ Universal electrode puller WZ, Zeitz-Instruments Vertriebs GmbH, Martinsried, Germany
Reference electrode (patch clamp)	Custom-made
Scale (mouse, hearts)	Kern SB, Kern & Sohn GmbH, Balingen, Germany
Scintillation counter	WS1414, PerkinElmer, Rodgau, Germany
Spectrophotometer	Nanodrop 200C, Thermo Fisher Scientific, Dreieich, Germany
Steam sterilizer	Varioclav, H+P, Oberschleissheim, Germany
Sterile-working bench	Herasafe™, Heraeus Thermo Fisher Scientific, Dreieich, Germany
Shearing machine (depilation of mice)	Aesculap® Isis GT-608, B.Braun VetCare, Suhl, Germany
Stimulator	S48 square pulse stimulator, Grass Technologies, Warwick, RI, USA
Syringe (heart cannulation), 1 mL	Injekt®-F Solo syringe, B. Braun, Melsungen, Germany, #9166017V

Table centrifuge	Heraeus Fresco 17, Thermo Fisher Scientific, Dreieich, Germany
Thermal cycler	C1000 Touch™ cycler, BioRad, Darmstadt, Germany
Temperature controller with rodent rectal temperature probe (control of murine body temperature)	TC-1000 Mouse, Cwe incorporated, Ardmore, PA, USA, #08- 13
Thermomixer	JS1 Thermo Shaker, Biometra, Göttingen, Germany
Thermostatically regulated heating pad (mouse ECG)	Heat therapy temperature pad, Harvard Apparatus, Boston, MA, USA, #60-3420
Tissue homogenizer	Precellys® 24, Peqlab VWR, Darmstadt, Germany
Ultrapure water system	Milli-Q Gradient with Q-guard® 2 purification pack, Merck Millipore, Darmstadt, Germany
Vortex mixer	Corning LSE, Sigma-Aldrich, Taufkirchen, Germany
Water Bath (cell culture)	Lauda AL12, Lauda Dr. R. Wobser GmbH & Co. KG, Lauda-Königshofen, Germany
Water Bath equipped with circulation thermostat (part of cardiac perfusion setup)	MP-5, Julabo, Seelbach, Germany

2.7 Software

Software	**Name and company**
BioDoc Analyze	Biometra, Göttingen, Germany
GENtle, version 1.9.4	open source, Magnus Manske, University of Cologne, Germany, downloaded from: http://gentle.magnusmanske.de
Graph Pad prism, version 7.0	GraphPad Software Inc., San Diego CA, USA
Image J, version 1.49b	open source, Wayne Rasband, NIH, Bethesda, MD, USA, downloaded from: https://imagej.nih.gov/ij/download.html
LAS AF version 2.7.3.9723	Leica, Wetzlar, Germany
Lab Chart version 7.0	AD instruments, Oxford, UK
PatchMaster v2x80	HEKA Elektronik Dr. Schulze, Lamprecht, Germany
pClamp 10.4	Molecular Devices LLC, CA, USA

3. METHODS

3.1 Arrhythmia models

3.1.1 Murine RyR2$^{R4496C/WT}$ CPVT model

Mice harboring the RyR2-R4496C mutation which is analogous to the human CPVT-associated RyR2-R4497C mutation[125,129], were kindly provided by Silvia G. Priori (IRCCS Salvatore Maugeri Foundation, Pavia, Italy) and continuously bred in the animal facility of the Walther Straub Institute of Pharmacology and Toxicology of the Ludwig Maximilians University of Munich for *in vitro* experiments or the Zentrum für medizinische Grundlagenforschung of the Medical University of Graz for *in vivo* experiments. Heterozygous mice were crossbred with C57BL/6N WT mice (either purchased from Charles River Laboratories GmbH, Sulzheim, Germany or bred in our own facility) to obtain an equal ratio of heterozygous RyR2$^{R4496C/WT}$ mice and RyR2$^{WT/WT}$ control animals. Breeding in an air- and humidity-controlled animal husbandry under 12 hours (h) light-dark cycles with access to food and water ad libitum was performed in accordance with national and European ethical regulations (Directive 2010/63/EU) and both breeding facilities are approved by the responsible government agency.

3.1.2 Human iPSC-derived CPVT models

Induced pluripotent stem cells (iPSCs) carrying a RyR2$^{S406L/WT}$ mutation were obtained from a 24-year-old caucasian female CPVT patient and have been characterized before[187]. In contrast, CPVT^{unknown} iPSCs were procured from a 60-year-old male donor carrying a yet unidentified

mutation that could not be identified by screening of common CPVT-related genes. Cells generated from a 32-year-old female caucasian without history of cardiac disease undergoing plastic surgery served as a healthy control. Human iPSC generation via reprogramming of primary skin fibroblasts and cardiomyocyte differentiation was done by Dr. Lisa Dreizehnter in the laboratory of our collaboration partners Prof. Alessandra Moretti and Prof. Karl-Ludwig Laugwitz at Klinikum Rechts der Isar as described previously[188,189]. In brief, dermal-biopsy specimens were morcellated and applied to culture dishes. Fibroblasts having migrated out of the explants were passaged twice and transduced with retroviruses to transfer a construct encoding human transcription factors OCT4, SOX2, KLF4 and c-MYC and cultured on murine embryonic feeder cells until iPSC colonies were pickable. The cells were cultured on low-attachment plates in order to differentiate and aggregate into embryonic bodies which were plated on gelatin-coated dishes at day 7. Between days 20 and 30, areas exhibiting spontaneous contraction indicating cardiac differentiation, were microdissected, plated on fibronectin-coated dishes and maintained in culture in EB2 differentiation medium (DMEM-F12 supplemented with 50 U/mL penicillin, 50 mg/mL streptomycin, 2 mM L-Glutamin, 0.1 mM MEM non-essential amino acids solution, 0.1 mM β-mercaptoethanol) containing 2 % FBS for 3-12 months. For Ca^{2+} signaling experiments, cell culture dishes with beating explants were transferred to our laboratory, further cultured at 37°C and 5 % CO_2 and medium was exchanged once per week. To obtain single cells, cell clumps were dissected using the sharp tip of a hypodermic needle and up to 10 explants were pipetted into a reaction tube containing 800 µL EB2 medium. Afterwards, microdissected areas were washed twice with 500 µL HBSS. For enzymatic dissociation, collagenase II was dissolved in HBSS at 1.5 mg/mL just prior to the procedure and 250 µL of the enzyme solution was added to the explants. The enzymatic

digestion was performed for 1 h at 37°C and 700 rpm. Depending on the degree of dissociation, up to 4 further digestion steps with collagenase, for a maximum of 30 min each, were performed. Subsequently, remaining cell clumps were subjected to a 5 min digestion step with Accumax™ in DPBS. During all dissociation steps, the supernatant containing single iPS cells was transferred into a falcon tube containing 5 mL of EB20 differentiation medium containing 20 % FBS. Afterwards, cells in EB20 medium were centrifuged for 5 min at 200 g at room temperature (RT). Single cells were resuspended in 200 µL EB2 medium per dish and plated on glass bottom dishes coated with a 10 % fibronectin solution in DPBS supplemented with 0.90 mM $CaCl_2$ and 0.49 mM $MgCl_2$ at 200 µL per cm^2 for at least 16 h. After a minimum incubation time of 8 h, EB2 medium was aspirated, 2 mL of EB20 medium were added and cells were used for further experiments after incubation at 37°C and 5 % CO_2 for approx. 7 days.

3.2 Molecular Biology procedures

3.2.1 Genotyping of RyR2-R4496C mice

Tail clips of mice were taken between day 18 and 21 after birth and stored at -20°C until genotyping. 150 µL DirectPCR® Lysis Reagent Tail with 0.3 mg/mL (w/v) proteinase K were added per tail biopsy specimen of $RyR2^{R4496C/WT}$ mice and samples were incubated in a thermomixer at 55°C and 700 rpm for 16 h. Afterwards, the temperature was increased to 85°C for 45 min for inactivation of the reaction. The samples were then spun in a table centrifuge for 1 min at 17000 g to remove debris and supernatants containing genomic DNA were subjected to polymerase chain reaction (PCR) for genotyping. PCR primers were diluted to 100 pmol/µL in nuclease-free H_2O upon reception. For genotyping of $RyR2^{R4496C/WT}$ mice, 1 µL of

tail lysis supernatant was added with 0.5 µM RyR2 fwd and rev primers and amplified by GoTaq® G2 Hot Start polymerase. Cycling conditions were 95°C for 5 min, 35x [95°C for 30 s, 55°C for 30 s and 72°C for 1 min 20 s] followed by 72°C for 7 min. Subsequently, PCR products were analyzed on a 1.5 % agarose gel by electrophoresis. WT RyR2 yields one band of 800 bp whereas the mutant allele yields two bands of 800 and 1000 bp for heterozygous mice. DNA fragments were separated electrophoretically on horizontal agarose gels. Therefore, agarose was dissolved in 1x TAE buffer (in mM): 0.8 TRIS, 0.4 acetic acid, 0.04 EDTA, pH=8.0 with NaOH containing 8 µL/100 mL RotiSafe® DNA staining reagent. No further treatment was necessary for loading RyR2-R4496C genotyping PCR reactions in GoTaq® G2 HotStart Green Master Mix. Samples were loaded into gel pockets and the gel was subsequently run at 10 V/cm electrode distance in 1x TAE buffer. The size of murine DNA samples was determined with 1 kb gene ruler and fragments were visualized and documented upon UV illumination.

3.3 Murine *in vitro* experiments

3.3.1 Isolation of ventricular cardiomyocytes

Heterozygous $RyR2^{R4496C/WT}$ mice and their WT littermates of either sex aged 8–16 weeks were used for the isolation of ventricular cardiomyocytes. Ventricular cardiomyocytes were obtained by retrograde perfusion through the aorta using a modified enzymatic digestion protocol after O'Connel[190] which I introduced to our laboratory. Following cervical dislocation, the chest was opened and the heart was quickly excised by cutting the aorta behind the aortic arch. The heart was arrested in ice-cold cannulation solution (in mM): 135 NaCl, 4.7 KCl, 0.6 KH_2PO_4, 0.6 Na_2HPO_4*$7H_2O$, 1.2 $MgSO_4$ *$7H_2O$, 10 HEPES, 30 taurine, 10 BDM, 10 glucose, pH=7.46 with

NaOH supplemented with 1 mM $CaCl_2$ and 10 IU/mL heparin and weighed before being cannulated. Since the isolation of cardiomyocytes leads to a depletion of taurine, the substance was added to improve Ca^{2+} tolerance of isolated cardiomyocytes[191] whereas BDM was used to inhibit spontaneous myocyte contracture[192] and to protect cardiac tissue from damage by terminal contracture during dissection[193]. The heart was attached to a 1 mL syringe with a suture (Fig. 11a), submersed in and retrogradely flushed with cannulation solution through a blunted needle inserted into the aorta to remove blood from the coronary vessels. To surely tie the heart during perfusion, a small groove was milled into the blunted 19G cannula for the suture 1 mm away from the blunt tip. Afterwards, the heart was placed on a Langendorff mode perfusion system (Fig. 11b). A hydraulic pump was used to define the flow rate by which tissue was retrogradely perfused. Perfusion took place at constant 37°C which was achieved by a recirculating water bath equipped with a circulation thermostat with 3 mL/min of oxygenated cannulation solution containing 20 mM creatine for 5 minutes. The addition of creatine is beneficial for the viability and performance of ventricular cardiomyocytes since creatine is lost during the isolation procedure[191]. Afterwards, cardiac tissue was digested for 0.7 s/mg heart weight by perfusion with Liberase™ dissolved to a final concentration of 0.0375 µg/mL in creatine-containing cannulation solution added with 12.5 µM $CaCl_2$.

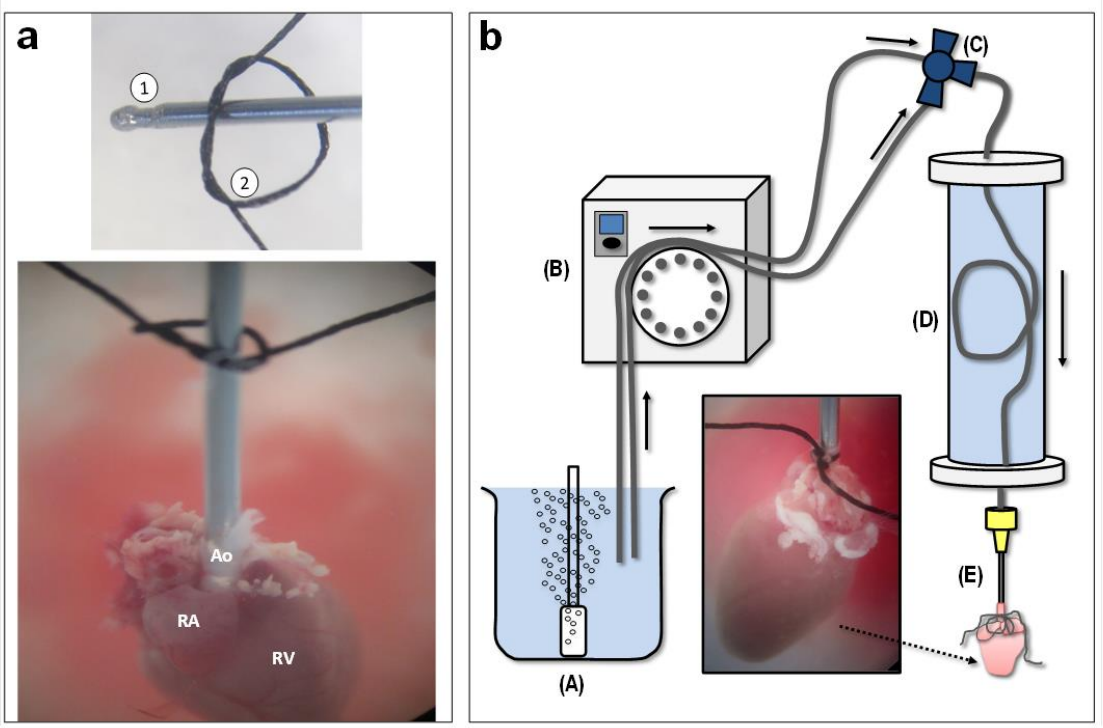

Fig. 10: Heart cannulation and retrograde perfusion of the aorta on a Langendorff mode cardiac perfusion setup.

(a) The heart was cannulated with the upper image illustrating the blunted 19G cannula with the small groove (1) for the suture (2) to fix the heart; the lower image shows a murine heart attached to cannula and syringe shortly before the aorta (Ao) is fixed by the suture. Abbreviations: RA= right atrium, RV= right ventricle. (b) Schematic overview of the Langendorff mode perfusion setup consisting of a recirculating water bath to keep the solutions at constant 37°C (A), a hydraulic pump to define the flow rate by which tissue is perfused and digested (B), a three-way valve to switch from perfusion to digestion solution (C), a glass cylinder containing 37°C warm water (D) to ensure the correct temperature of the solutions once they reach cardiac tissue. Part (E) illustrates the murine heart which is tied to the blunted cannula with an inlay showing an enlarged image of the heart after successful perfusion.

Following a transversal cut under the atria (Fig. 11 (1)), the ventricles were transferred to cannulation solution containing 12.5 µM $CaCl_2$ and 10 % FCS to stop digestion (Fig. 11 (2)) and tissue was carefully dissected into small pieces (Fig. 11 (3)). After mechanical separation by trituration, the suspension was filtered through a 200 µm polyester mesh (Fig. 11 (4)) and myocytes were allowed to sediment by gravity for 10 min. This procedure ensures fibroblasts

to remain in the supernatant with concentration of cardiomyocytes mainly in the pellet. Cells were then transferred into cannulation solution containing 1.5 mM $CaCl_2$ to reintroduce physiological Ca^{2+} concentrations. After an incubation time of 15 min, cardiomyocytes from the pellet were inspected on an inverted microscope and were only subjected to experiments if a minimum of 60 % viable cells without excessive spontaneous activity were present after Ca^{2+} reintroduction.

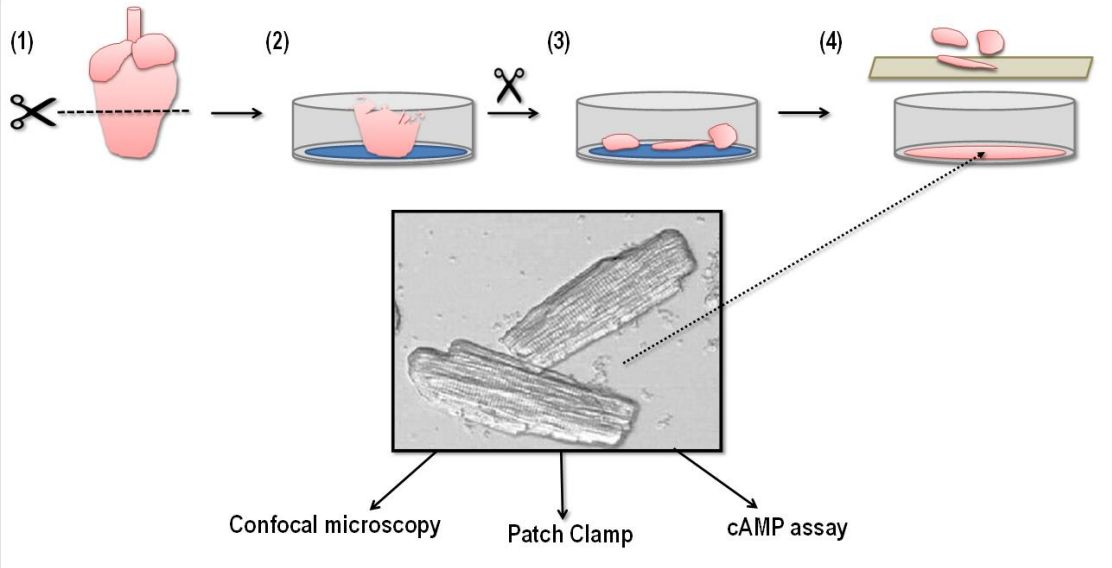

Fig. 11: Isolation of murine ventricular cardiomyocytes from the perfused heart.

Following a transversal cut under the atria of the perfused heart (1), cardiomyocytes were being isolated from the dissected ventricles. Therefore, ventricular tissue was transferred to cannulation solution containing FCS to stop digestion (2). Subsequently, the tissue was dissected into small pieces, mechanically separated by trituration (3) and filtered through a polyester mesh (4). Physiological Ca^{2+} concentrations of 1.5 mM $CaCl_2$ were reintroduced to the isolated cardiomyocytes before rod-shaped cells (see lower image) were subjected to confocal microscopy, patch clamp measurements or cAMP assays.

3.3.1.1 Confocal Ca^{2+} imaging

Confocal Ca^{2+} imaging experiments were conducted in murine and iPSC-derived cardiomyocytes, both of which I introduced to our laboratory. Cardiomyocytes were loaded with the Ca^{2+} indicator Fluo-4, AM (stored as 1 mM stock in DMSO) at 3 µM in external solution containing 0.06 % (w/v) Pluronic® F-127 (stored as 20 % stock in DMSO) under protection from light for 40 minutes at RT. The external solution consisted of (in mM) 140 NaCl, 4 KCl, 1 $MgCl_2$, 10 glucose, 5 HEPES, 10 BDM, pH 7.4 with NaOH supplemented with 1 mM $CaCl_2$ for murine ventricular cardiomyocytes or 1.8 $CaCl_2$ for human iPSC-derived cardiomyocytes respectively. Staining was followed by incubation in fluo-4 free external solution for 20 minutes to allow de-esterification of the dye. Treatment substances or DMSO as a vehicle were added to both staining and de-esterification solutions. For β-adrenergic stimulation, a subset of cardiomyocytes was treated with 1 µM Isoproterenol (Iso) during de-esterification. Blockade of mitochondrial Ca^{2+} uptake via MCU was achieved by treatment of myocytes with 8 µM Ruthenium 360 (Ru_{360}) for 20 min during de-esterification. Field stimulation was performed using a S48 square pulse stimulator with 5 ms test pulses at 0.5 Hz with 30 V/cm electrode distance for murine cells or 80V/cm for iPSC-derived cardiomyocytes (approx. 25 % above threshold level), respectively, to elicit Ca^{2+} transients in fluo-4 loaded cardiomyocytes. Only excitable cells, quiescent when unstimulated were considered for experiments.

Ca^{2+} signals were visualized by confocal microscopy on a TCS SP5 inverted confocal microscope equipped with a HCX PL APO CS 63x/1.4 oil immersion objective. Fluorescence was excited with the 488 nm line of an Argon laser at 20 % laser power restricted to 8 % laser intensity using an acousto-optical transmission filter and emission was collected between 498 and 627 nm. The pinhole diameter was set to 1 Airy Unit. Laser and spectral settings were kept constant

throughout all experiments with only slight adjustments to the photomultiplier gain to ensure a dark background and avoid overexposure of the respective image. Line scan series were generated by continuously recording fluorescence along a line spanning the entire myocyte longitudinally to record triggered Ca^{2+} transients, propagating spontaneous Ca^{2+} waves and spontaneous Ca^{2+} sparks. Recordings lasted for 2 min at a sampling rate of 400 Hz with a resolution of 512 pixels. Images were analyzed in Leica Application Suite Advanced Fluorescence. For further analysis of kinetics of murine systolic Ca^{2+} transients, average fluorescence of every single line was extracted and plotted against time in a csv file and imported into pClamp 10.4 software. The amplitude of the Ca^{2+} transient was expressed as ΔF/F0, the activation time as time to peak (ttp) and Ca^{2+} clearance from the cytosol was analyzed by calculating the inactivation constant tau (tau_{inact}) of a monoexponential fit of the decay phase of the Ca^{2+} transient.

Spontaneous Ca^{2+} sparks were measured under identical conditions as Ca^{2+} waves albeit in unstimulated cardiomyocytes at a scanning speed of 200 Hz and analyzed using the SparkMaster plugin in ImageJ[194]. SparkMaster was run with a value of 5 for background fluorescence [Fl.U.] and 3.8 as the hypothetical value "criteria" determining the threshold factor for the detection of sparks above the noise level of the image. Parameters were kept constant for all images. The extended kinetics mode was enabled. For the output image, the number of intervals was set to 3 and the option raw + sparks was chosen whereby the input image remained unchanged and detected spark regions were automatically marked and numbered. Pixelsize [µm] was calculated as follows: image width [µm] / 512. Each detected spark was analyzed for amplitude expressed as ΔF/F0, full width at half-maximum amplitude (FWHM), full duration at half-maximum amplitude (FDHM), full width, full duration, ttp and exponential time

constant of the spark decay (tau_{decay}). If more than one spark per observed area (one below or in juxtaposition to the other) were suggested as one single spark by SparkMaster, all output values were excluded from further analysis. Since all investigated conditions were equally affected by the misinterpretation of spatially narrow clustered sparks as one single spark, these Ca^{2+} events were not listed in the evaluation as one or the counted number of real sparks. In case an observation window to wide for the spark was generated, parameters of length (full duration and FDHM) were still collected if applicable. Sparks with the amplitude as their only usable parameter were not incorporated into the kinetics analysis but counted to determine spark frequency.

3.3.1.2 cAMP accumulation assay

For evaluation of intracellular cAMP levels as a measure of changes in β-adrenergic signaling, ventricular myocytes of $RyR2^{R4496C/WT}$ mice were isolated as described above and stored in serum-free DMEM until just before the assay. cAMP assays were performed by Dr. Andreas Breit at the Walther Straub Institute of Pharmacology and Toxicology, Ludwig Maximilians University of Munich (LMU). $RyR2^{R4496C/WT}$ cardiomyocytes were labeled with 2 µCi/mL of [^{3}H]adenine for 4 h in DMEM at 37°C, washed and treated with 10 µM efsevin, 100 nM Iso or 1 µM propranolol respectively for 30 min at 37°C. To block degradation of cAMP by phosphodiesterase, 1 mM 3-Isobutyl-1-methylxanthin (IBMX) was concurrently added to the aforementioned mixtures. 5 µM Forskolin (FSK) increasing intracellular cAMP levels served as a positive control. The reaction was stopped by aspiration of the medium and addition of 500 µL ice cold 10 % TCA. Subsequently, [^{3}H]cAMP and [^{3}H]ATP were separated by sequential chromatography on cation exchanger dowex and neutral alumina columns which were pre-

packed with different amounts of AG®1-X8 anion exchange resin. Dowex columns were activated with 10 mL 1M HCl, washed with 10 mL H_2O thereafter and alumina columns were washed with 10 mL 0.1M imidazole. Cell extracts were loaded onto dowex columns, washed with 4 mL H_2O, placed onto alumina columns and eluted with 10 mL H_2O. Alumina columns were washed with 1 mL imidazole, placed onto scintillation vials and eluted with 5 mL imidazole. Afterwards, scintillation vials containing the eluates were filled with 12 mL scintillation fluid. [^{3}H]ATP and ^{3}[H]cAMP were quantified in a scintillation counter and the accumulation of [^{3}H]cAMP was expressed as the ratio of [^{3}H]cAMP/ ([^{3}H]cAMP + [^{3}H]ATP).

3.3.1.3 Electrophysiology

Spontaneous arrhythmogenic APs, EADs and DADs were examined in RyR2$^{R4496C/WT}$ cardiomyocytes by patch-clamp recordings in the current clamp mode using an EPC10. Together with Prof. Michael Mederos y Schnitzler, I established these measurements in RyR2$^{R4496C/WT}$ cardiomyocytes at Walther Straub Institute. After isolation, cardiomyocytes were immediately placed in "Kraftbrühe" (KB) medium modified from Isenberg & Klöckner containing (in mM): 65 K-glutamate, 45 KCl, 30 KH_2PO_4, 3 $MgSO_4x7H_2O$, 0.5 EGTA, 20 taurine, 10 glucose, pH=7.4 with NaOH to improve Ca^{2+} tolerance[195]. Depending on yield and quality of the preparation, 5-10 µL of cell solution were pipetted into the recording chamber filled with external solution composed of (in mM): 135 NaCl, 5 KCl, 1 $CaCl_2*2H_2O$, 1 $MgCl_2*6H_2O$, 10 HEPES, 10 glucose, pH=7.4 with NaOH. The solution was adjusted to 290 mOsmol/L with Mannitol. A temperature-controlled superfusion was used to maintain the temperature of the bath solution at 35 ± 2°C. Cells were viewed on an inverted Olympus IX70 microscope equipped with a LCPlanFl, 40x/0.60 Ph.2 objective. Patch pipettes had a resistance of 2-8 MΩ when filled

with the pipette solution composed of (in mM): 30 KCl, 110 K-aspartate, 1 $MgCl_2$, 10 HEPES, 0.1 EGTA, pH=7.2 with KOH, adjusted to 300 mOsmol/L with Mannitol. An average of 5 min exposure to 900 µg/µL Amphotericin B was sufficient to achieve a perforated patch clamp configuration. Only cardiomyocytes with a membrane potential lower than -60 mV and where series resistance was ≤20 MΩ were further analyzed. Prior to recordings, a single stimulus of 1 nA amplitude and 2-4 ms duration was applied and only cells reacting to that test stimulus with a physiological AP were considered for the experiment. Membrane potential was sampled at 20 kHz, low-pass filtered at 2 kHz and corrected for the liquid junction potential of +13.8 mV. APs were evoked by depolarizing intracellular current injections of 1 nA amplitude and 2-4 ms duration with repetitive trains of 10 stimuli at a frequency of 0.5 Hz followed by a 60 s pause to detect potentially arrhythmogenic APs or DADs during this diastolic phase. Iso and Iso + efsevin-containing external solutions were washed in through continuous perfusion during the experiment. Conditions of catecholamine stress and efsevin administration under Iso were each washed in 5 s before the end of the preceding sweep. Each solution reached the bathing chamber after a 15 s passage through the perfusion setup. The residual 50 s remaining of the subsequent sweep following wash-in served as a reaction time for cells to every new condition and was excluded from analysis. During all three conditions, cardiomyocytes stayed attached to the patch pipette under continuous perfusion for a minimum of 15 min up to over 1 h. Only recordings from cells being properly attached to the pipette during all three conditions with at least one sweep per condition were considered for analysis. Analysis comprised only sweeps where a minimum of 8 of 10 stimuli led to a systolic AP and only depolarizations of an amplitude equal to or above +100 mV were counted as APs. Patch clamp recordings were displayed as voltage changes [mV] over time [ms]. APs as well as spontaneous

diastolic DADs of amplitudes greater than or equal to 5 mV as well as EADs during phase 2 or 3 of the AP were analyzed with PatchMaster v2x80 software. For further evaluation of resting membrane potential (RMP), AP amplitude, AP duration of triggered APs at 50 % (APD_{50}) or 90 % (APD_{90}) of repolarization, respectively, single sweeps were exported as ASCII files and analyzed in pClamp 10.4 software.

3.4 Murine *in vivo* experiments

3.4.1 Drug administration via osmotic minipumps

$RyR2^{R4496C/WT}$ mice of either sex at an age of 8-12 weeks were treated with MiCUps through 1003D or 1007D osmotic minipumps. *In vivo* drug administration experiments including murine ECG evaluation were conducted together with Prof. Simon Sedej at Medical University of Graz, Austria. Pump implantation was carried out analogously for all substances administered. MiCUps were dissolved in 50 % DMSO and 50 % PEG-400 before filling of the pump. Pumps containing only DMSO/PEG-400 served as a vehicle control. Filling of pumps was accomplished with a small Luer-Lok™ syringe attached to a blunt-tipped 27G filling tube. To achieve sterility of the respective solutions, a 0.22 µm Millex-GV filter was interposed between syringe and filling tube. Implantation surgery was performed under general anesthesia with 0.025 mg/kg bodyweight (BW) tribromoethanol. For a 1.25 % (w/v) Avertin solution, 1.5 g of tribromoethanol was added to 0.93 mL 2-methyl-2-butanol and dissolved by stirring under protection from light. After addition of 118.5 mL PBS, stirring was continued until complete dispersion and the solution was filtered through a 0.2 µm filter. pH of the solution was adjusted to 7.4 and the solution was stored at -20°C until just before surgery. For determination of the filling volume and verification of correct filling, pumps were weighed before and after addition of the drug

solution and a weight difference thereby gives the net volume of the solution loaded. At any time, the implanteur was blinded to the content administered by the mini-osmotic pumps. Before implantation, pumps were disinfected with 70 % isopropyl alcohol and primed in 0.9 % NaCl solution until subcutaneous implantation between scapulae. For the mid-scapular incision, the animals were positioned on their stomach and subcutaneous tissue was spread by carefully opening and closing an inserted forceps in order to create a subcutaneous skin pocket. Pumps were then placed into the pocket (Fig. 12b) with a caudal orientation of the flow moderator and the wound was closed with non-absorbable suture. Following implantation, interstitial fluid enters the pump via the semipermeable outer membrane thereby swelling the osmotic layer (Fig. 12a). This swelling results in a defined compression of the impermeable inner drug reservoir leading to a strictly rate-controlled drug release of 1 µL/h for 1003D and 0.5 µL/h for 1007D into the local subcutaneous space from where absorption of the compounds by local capillaries led to systemic administration. Mice were constantly monitored for signs of pain and distress during and after surgery (Fig. 12c) and none of the animals died during the treatment period. Procedures were performed in accordance with national and European ethical regulations (Directive 2010/63/EU) and approved by the Austrian Federal Ministry of Science, Research and Economy (BMWFW-66.010/0012-WF/V/3b/2015).

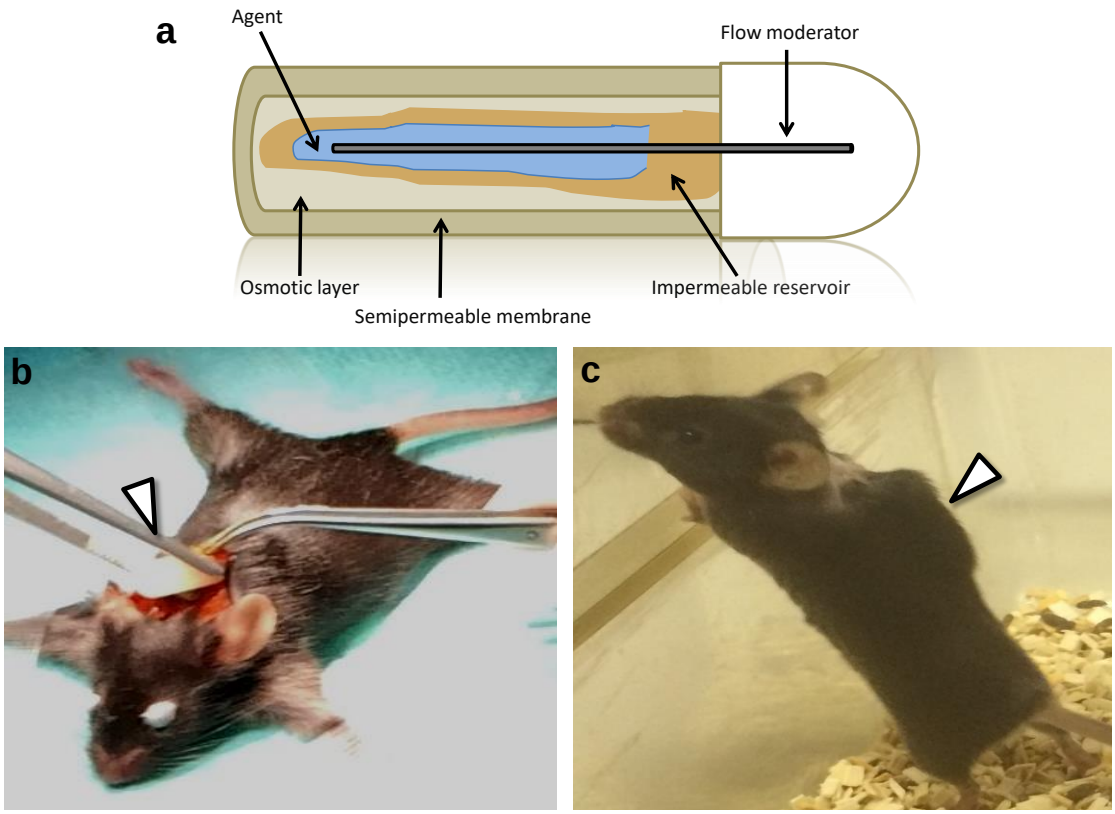

Fig. 12 Osmotic minipump implantation.

(a) Structure of an Alzet osmotic minipump (drawn after [196]): once the pump is implanted, the semipermeable membrane allows fluid from the surrounding murine tissue to enter the osmotic layer. This influx results in a compression of the impermeable reservoir which displaces the agent from the pump in a controlled and predetermined rate through the flow moderator. (b) Pump implantation surgery with a pump (indicated by white arrowhead) being placed subcutaneously between scapulae of a $RyR2^{R4496C/WT}$ mouse. (c) Example of a $RyR2^{R4496C/WT}$ mouse post-surgery while being monitored for any signs of pain or distress (white arrowhead indicates location of the pump).

3.4.2 ECG recordings and tissue isolation

To screen for arrhythmia, a single lead ECG was recorded through needle electrodes inserted subcutaneously into left forelimb and hindlimb (Fig. 13). A third electrode placed on the right hindlimb served as a grounding. Following induction of anesthesia in a chamber containing 5 % isoflurane, animals were sedated by inhalation anesthesia with 0.5 mL/h isoflurane provided

by a vaporizer during ECG recordings. Body temperature was maintained at 37°C by a thermostatically regulated heating pad and was continuously controlled by a rectal thermometer. At day 8 of drug administration for 1007D and at day 3 for 1003D pumps, a baseline ECG was recorded until steady-state was reached for an average of 8 min, after which mice were injected intraperitoneally (IP) with 2 mg/kg BW L-adrenaline and 120 mg/kg BW caffeine. Thereafter, animals were continuously monitored for episodes of ventricular tachycardia to occur for up to 23 min before mice were sacrificed at the end of the experiment. Immediately thereafter, blood was collected post-mortem from murine heart and total blood was separated by centrifugation for 20 min at 4°C and 6000 g for extraction of blood plasma which was stored at -80°C. Heart and liver tissue were excised, snap-frozen in liquid nitrogen and stored at -80°C until tissue lysis. Tissue harvesting was amended by removal of adipose tissue in the run with 1003D pumps. The tissue distribution and concentration of efsevin in different murine tissues and blood plasma was examined by Nathan Dupper and Dr. Oyun Kwon (Department of Chemistry and Biochemistry, UCLA, Los Angeles, USA). For determination of efsevin in heart, liver and adipose tissue, the respective tissue was lysed and added with 4 mL DEPC water per g of frozen tissue, transferred into tissue homogenization tubes containing 6 ceramic beads each and placed into a Precellys homogenizer. Lysates and blood plasma samples were then diluted 1:4 with acetonitrile for deproteinization, vortexed for 10 min, spun down for 5 min at 10°C and 5000 rpm and the supernatant was transferred to UCLA on dry ice. The concentration of efsevin was obtained by liquid chromatography-mass spectrometry, namely with an Applied Biosystems-MDS Sciex 4000 Q Trap equipped with a Shiseido C18 column coupled with a triple quadrupole Waters TQD mass spectrometer. Previous tests with efsevin at UCLA showed a mean 90 % recovery rate of the analyte, with a good reproducibility

(CV % = 2.9 %, n = 6, at 500 µg/L). The limit of detection at a signal-to-noise ratio of 3 amounted to 30 ng/L.

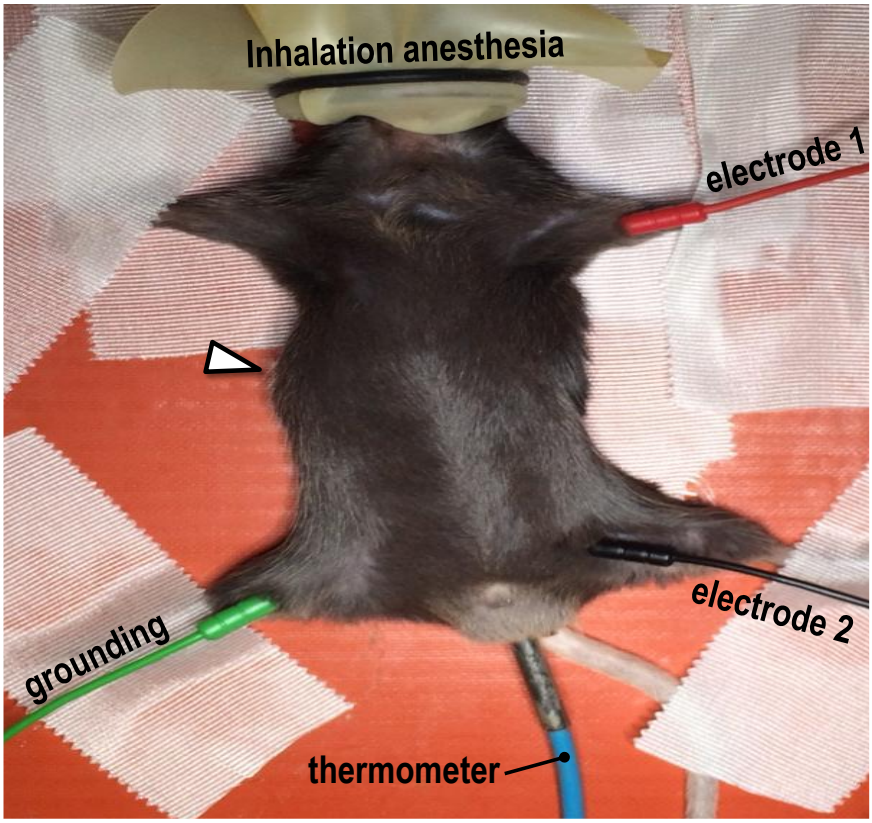

Fig. 13 Single lead ECG setup in anesthesized mouse for the detection of arrhythmia.

A single lead ECG was recorded through needle electrodes inserted subcutaneously into left forelimb (electrode 1, red) and hindlimb (electrode 2, black). A third electrode placed on the right hindlimb served as a grounding (green). During ECG recordings, animals were sedated by inhalation anesthesia with 0.5 mL/h isoflurane provided by a vaporizer. Body temperature was maintained at 37°C by a thermostatically regulated heating pad and was continuously controlled by a rectal thermometer (blue). The white arrowhead indicates the location of the osmotic minipump. A baseline ECG was recorded until steady-state was reached, after which mice were injected intraperitoneally with 2 mg/kg BW L-adrenaline and 120 mg/kg BW caffeine and continuously monitored for episodes of ventricular tachycardia.

3.5 Statistical analysis

Data are presented as mean ± SEM. Normality was assessed by Shapiro-Wilk test and the significance of differences between treatment groups was statistically evaluated with the respective test in GraphPad as outlined below. In case of a normal distribution of data, more than two unpaired treatment groups with equal variance were analyzed with two-way analysis of variance (ANOVA) combined with Tukey's multiple comparisons test. For more than two groups with unpaired, normally distributed data with unequal variance or for data which are not normally distributed, Kruskal-Wallis test was employed in combination with Dunn's post hoc test. In case of paired data, statistical analysis was performed with Friedman test. Fisher's exact test was used for comparison of difference between two treatment conditions in 2x2 contingency tables. Unless otherwise stated, * represents $p<0.05$, ** $p<0.01$, and *** $p<0.001$.

4. RESULTS

4.1 Effects of efsevin on diastolic proarrhythmic events in RyR2$^{R4496C/WT}$ myocytes

4.1.1 Efsevin suppresses spontaneous Ca^{2+} sparks in RyR2$^{R4496C/WT}$ cardiomyocytes

Our goal was to investigate the therapeutic potential of enhancing mitochondrial Ca^{2+} uptake in Ca^{2+} overload-induced arrhythmia. To this aim, we used efsevin in a murine model of CPVT1 caused by a mutation in RyR2, exemplary of a Ca^{2+} induced arrhythmia. Arrhythmias originating from imbalanced cellular Ca^{2+} homeostasis such as CPVT are triggered by an enhanced RyR2-mediated Ca^{2+} leak[126,160,197]. The most fundamental event of diastolic Ca^{2+} leak underlying arrhythmogenesis are spontaneous Ca^{2+} sparks. To visualize arrhythmogenic Ca^{2+} sparks, fluo-4 stained murine RyR2$^{R4496C/WT}$ cardiomyocytes (n=3 mice) were subjected to confocal microscopy (Fig. 14a). As a hallmark of CPVT, β-adrenergic stimulation resulting from stress situations enhances potentially arrhythmogenic Ca^{2+} release events during diastole such as spontaneous sparks. Consistent with the CPVT phenotype, arrhythmic events rarely occurred at baseline, but drastically increased after β-adrenergic stimulation with Iso (Fig. 14b). We observed an augmentation from 1.85±0.26 Ca^{2+} sparks x 100 μm^{-1} x s^{-1} (n=50 cells) in vehicle control to 2.36±0.23 sparks x 100 μm^{-1} x s^{-1} in Iso-administered myocytes (n=72 cells; Kruskal-Wallis test, p=0.067). $\Delta F/F_0$ was 0.56±0.01 under vehicle administration (n= 1934 sparks) and was significantly increased by Iso to 0.66±0.01 (n= 4383 sparks; Kruskal-Wallis test, p<0.0001). In contrast, the activation time of Ca^{2+} release (ttp) at 31.96±0.71 ms in vehicle-treated cells (n= 1307 sparks) was unaltered by Iso at 29.78±0.50 ms (n= 1761 sparks; Kruskal-Wallis test,

p=0.151). Further, Iso administration resulted in a tau_{decay} of 53.86±1.12 ms (n= 1774 sparks) which was significantly accelerated compared to 63.28±1.59 ms in vehicle-treated cells (n= 1332 sparks; Kruskal-Wallis test, p<0.0001). This led to a spatial and temporal restriction of sparks. Iso limited spatial expansion of sparks to a full width of 3.56±0.04 µm (n= 2306 sparks) as compared to 3.93±0.05 µm in vehicle-treated myocytes (n= 1450 sparks; Kruskal-Wallis test, p<0.0001). The same effect could be observed for FWHM starting at 2.45±0.02 µm under vehicle treatment (n= 1452 sparks) which was significantly reduced to 2.22±0.02 µm by Iso (n= 2319 sparks; Kruskal-Wallis test, p<0.0001). Local expansion was similarly reduced: whereas full duration amounted to 103.86±1.58 ms (n=1335 sparks) in vehicle-treated cardiomyocytes, an administration of Iso restricted the temporal expansion of Ca^{2+} sparks to 88.36±1.16 ms (n=1757 sparks; Kruskal-Wallis test, p<0.0001) Analogously, FDHM was reduced by Iso from 61.44±0.92 ms (n= 1336 sparks) to 55.51±0.71 ms (n=1755 sparks; Kruskal-Wallis test, p<0.0001).

Interestingly, efsevin significantly reduced the frequency of Ca^{2+} sparks to 1.59±0.20 sparks x 100 μm^{-1} x s^{-1} (n=47 cells; Kruskal-Wallis test, p=0.049 as compared to Iso) and additionally diminished the amplitude of sparks to 0.47±0.01 (n= 1511 sparks; Kruskal-Wallis test, p<0.0001 as compared to Iso). Ttp remained unaltered as compared to Iso at 29.73±0.80 ms with efsevin (n= 778 sparks; Kruskal-Wallis test, p=0.481) whereas tau_{decay} was further reduced by efsevin to 48.67±1.68 ms (n= 779 sparks; Kruskal-Wallis test, p<0.0001). Interestingly, the pharmacological activation of mitochondrial Ca^{2+} uptake led to an additional significant spatial restriction of sparks. Following application of efsevin, full width of sparks was limited to 3.25±0.05 µm (n= 929 sparks; Kruskal-Wallis test, p<0.0001 as compared to Iso). Analogously, FWHM was further drastically shortened to 2.08±0.03 µm by efsevin (n= 936 sparks; Kruskal-

Wallis test, $p<0.0001$ as compared to Iso). Also, efsevin produced a remarkable temporal restriction of sparks: it further reduced full duration to 82.08±1.56 ms (n= 789 sparks; Kruskal-Wallis test, $p<0.0001$ as compared to Iso) and FDHM was further diminished by efsevin to a value of 51.38±1.02 ms (n= 789 sparks, Kruskal-Wallis test, $p<0.0001$ as compared to Iso). In summary, the application of efsevin led to a reduced number of spontaneous Ca^{2+} release events and the spatial and temporal restriction of sparks.

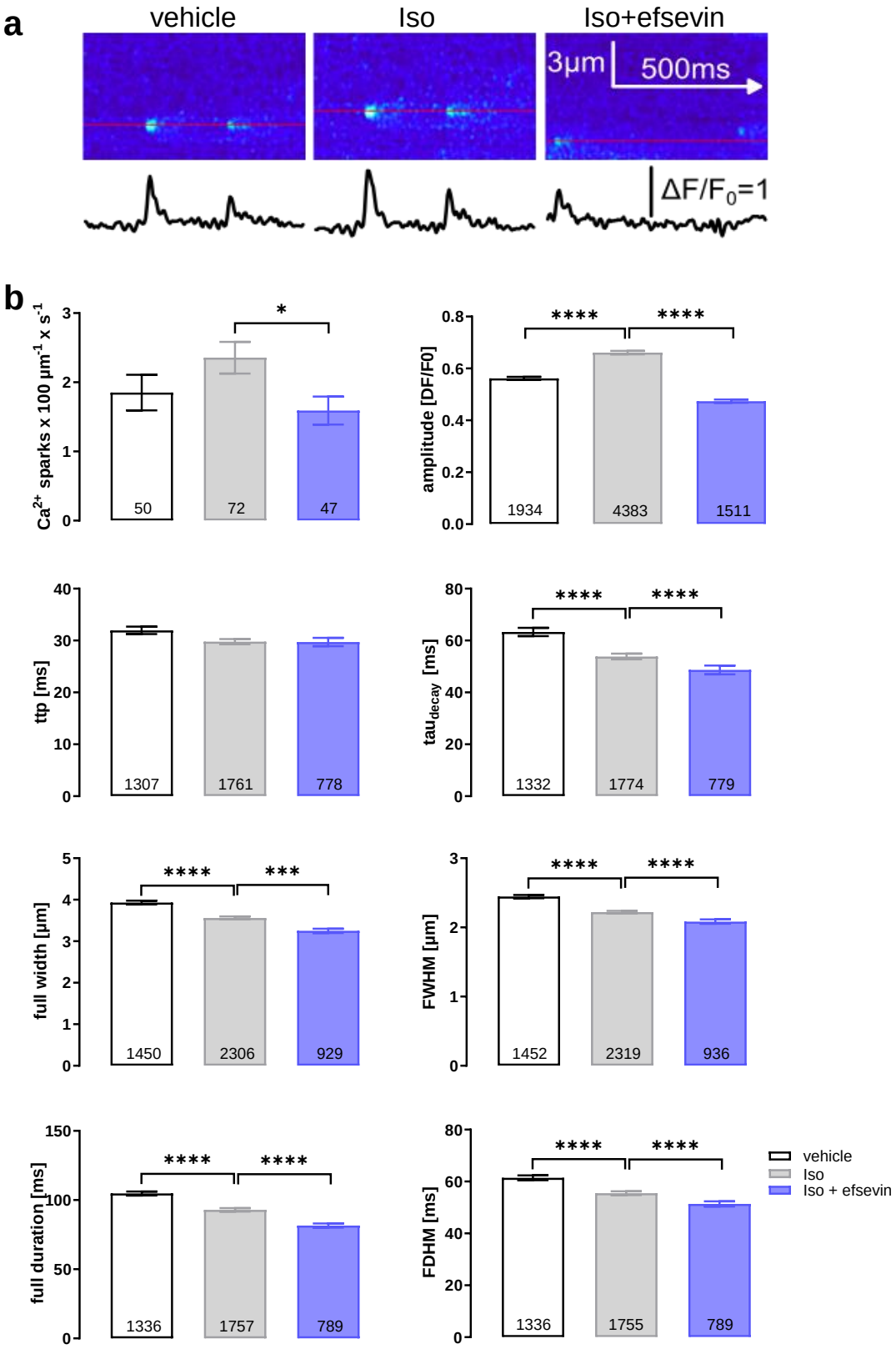

Fig. 14 Efsevin reduces spontaneous Ca^{2+} spark frequency in $RyR2^{R4496C/WT}$ cardiomyocytes and accelerates decay resulting in a spatial and temporal restriction of individual sparks.

(a) Representative confocal line scan images including their intensity profiles along the red line from RyR2$^{R4496C/WT}$ cardiomyocytes treated with vehicle, Iso or Iso + efsevin showing spontaneous Ca^{2+} sparks. (b) β-adrenergic stimulation with Iso induces a slightly higher spark frequency, a significantly higher amplitude (Kruskal-Wallis test, ****p<0.0001) and drastically accelerates cytosolic Ca^{2+} removal (tau_{decay}; Kruskal-Wallis test, ****p<0.0001) leading to narrower (full width; Kruskal-Wallis test, ****p<0.0001) and shorter (full duration; Kruskal-Wallis test, ****p<0.0001) sparks. The same applied to FDHM (Kruskal-Wallis test, ****p<0.0001) and FWHM (Kruskal-Wallis test, ****p<0.0001). Application of efsevin drastically reduced spark frequency (Kruskal-Wallis test, *p<0.05) and amplitude (Kruskal-Wallis test, ****p<0.0001). Following administration of efsevin, full duration (Kruskal-Wallis test, ****p<0.0001), FDHM (Kruskal-Wallis test, ****p<0.0001), width (Kruskal-Wallis test, ****p<0.0001) and FWHM (Kruskal-Wallis test, ****p<0.0001) were significantly reduced as compared to treatment with Iso alone. Whereas Iso slightly accelerated Ca^{2+} sparks (ttp), efsevin exerted no further effect on ttp but significantly accelerated tau_{decay} (Kruskal-Wallis test, ****p<0.0001) leading to a limited spatial and temporal expansion of sparks. Numbers in bars indicate the amount of cells or sparks examined, respectively (see text for details).

4.1.2 Efsevin suppresses spontaneously propagating Ca^{2+} waves

Spontaneous Ca^{2+} release events that propagate throughout the entire cardiomyocyte are termed Ca^{2+} waves[198]**.** Consistent with the CPVT phenotype, potentially arrhythmogenic Ca^{2+} waves occur particularly under β-adrenergic stimulation resulting from stress situations and rarely occurred at baseline, but drastically increased after β-adrenergic stimulation with Iso. We performed Ca^{2+} wave experiments in fluo-4 loaded RyR2$^{R4496C/WT}$ myocytes. Repetitive trains of 5 ms test pulses at 0.5 Hz for 30 s were followed by a 90 s pause mimicking diastole (Fig. 15a). While DMSO-administered RyR2$^{R4496C/WT}$ cardiomyocytes (n=8 mice), serving as a vehicle control, displayed no waves (n=37 cells), Iso application lead to a drastic increase to 0.46±0.09 diastolic Ca^{2+} waves x min^{-1} (n=68 cells; Kruskal-Wallis test, p<0.0001). Strikingly, application of 15 µM efsevin could diminish spontaneous waves to 0.07±0.05 waves x min^{-1} in myocytes (n=45 cells; Kruskal-Wallis test, p<0.001) (Fig. 15b). Thus, efsevin reduced waves to an amount

indistinguishable from vehicle (Kruskal-Wallis test, p=0.587). In addition to a reduction of Ca^{2+} waves x min^{-1}, administration of efsevin could further decrease the number of cardiomyocytes presenting with waves (Fig. 15c). In the absence of β-adrenergic stimulation, vehicle-treated $RyR2^{R4496C/WT}$ cardiomyocytes showed no arrhythmogenic Ca^{2+} signals (0/37). Iso induced waves in 36.77 % (25/68) of the cells (Fisher's exact test, p=0.0001). Promisingly, efsevin could confine the occurrence of Ca^{2+} waves to a subpopulation of only 4.44 % (2/45) of $RyR2^{R4496C/WT}$ cardiomyocytes (Fisher's exact test, p<0.0001).

Cardiomyocytes from WT littermates (n=7 mice) not prone to adrenergically-mediated arrhythmogenesis, served as a healthy control in this experiment and vehicle-treated $RyR2^{WT/WT}$ myocytes (n=39) displayed no waves. Iso could not induce Ca^{2+} waves standing at 0.12±0.12 waves x min^{-1} in WT cardiomyocytes (n=38 cells; Kruskal-Wallis test, p=0.691). The number of spontaneous waves was unchanged to 0.022±0.022 waves x min^{-1} by administration of efsevin (n=43 cells; Kruskal-Wallis test, p=0.706). In absence of the CPVT-causing mutation, $RyR2^{WT/WT}$ cardiomyocytes did not show Ca^{2+} waves under baseline conditions (0/39). Accordingly, Iso-treatment could not induce waves (2.63 % (1/38); Fisher's exact test, p=0.494) and efsevin completely abolished waves (0/32, Fisher's exact test, p=1.000).

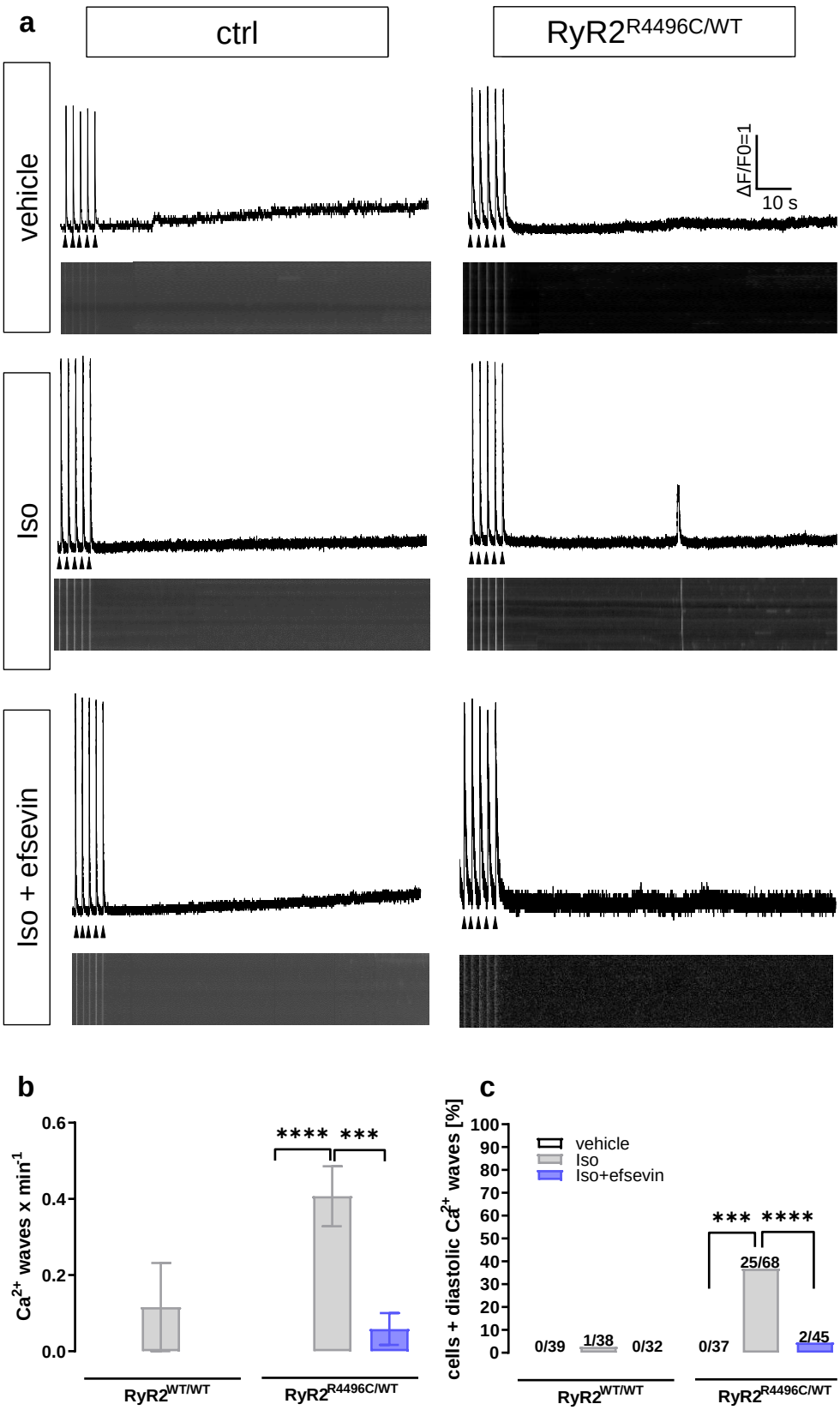

Fig. 15 Efsevin significantly reduces arrhythmogenic Ca^{2+} waves in $RyR2^{R4496C/WT}$ cardiomyocytes.

(a) Confocal linescan images and respective intensity plots of murine CPVT and WT cardiomyocytes. The last five triggered Ca^{2+} transients are shown (black arrowheads). (b) $RyR2^{WT/WT}$ myocytes displayed only a negligible number of waves under Iso application. In contrast, Iso treatment triggered significantly more waves in $RyR2^{R4496C/WT}$ cardiomyocytes (Kruskal-Wallis test, ****$p<0.0001$) whereas efsevin drastically abolished waves in these cells (Kruskal-Wallis test, ***$p<0.001$). (c) Bar graphs illustrate the percentage of cells presenting with diastolic Ca^{2+} waves. Numbers above the bars represent wave-positive cardiomyocytes of all myocytes examined. $RyR2^{WT/WT}$ cardiomyocytes showed almost no waves under any tested condition. Whereas Iso drastically increased the amount of wave-positive myocytes (Fisher's exact test, ***$p<0.001$), efsevin treatment could significantly restrict diastolic waves to a small subset of $RyR2^{R4496C/WT}$ cells (Fisher's exact test, ****$p<0.0001$).

4.1.3 Efsevin reduces spontaneous APs

Provided that a proarrhythmic wave propagates along the cardiomyocyte and activates NCX, leading to a transient inward current, resulting voltage oscillations have to reach an amplitude sufficiently large to trigger spontaneous APs[199]. Arrhythmogenic electrophysiological events, namely spontaneous APs, were measured by perforated patch clamp experiments in the current clamp mode. Analogous to triggered Ca^{2+} transients pictured above (Fig. 15a), 10 systolic APs per sweep were evoked by depolarizing current injection followed by a diastolic phase where spontaneous arrhythmogenic APs were recorded in $RyR2^{R4496C/WT}$ cardiomyocytes (n =15 cardiomyocytes, n=8 mice) which were sequentially superfused with vehicle, Iso and Iso + efsevin. One exemplary sweep for every condition is shown in Fig. 16a. Under vehicle treatment, cardiomyocytes presented with 1.12±0.62 diastolic APs x min^{-1}. The enhanced propensity for Ca^{2+} waves under β-adrenergic stimulation indeed reflected in an increase in diastolic APs to 5.76±2.45 x min^{-1} (Friedman test, $p=0.018$) after superfusion with Iso (Fig. 16b). Introduction of 15 µM efsevin to the Iso-containing bath solution did effectively reduce arrhythmogenic events to 0.58±0.34 APs x min^{-1} (Friedman test, $p=0.011$). Thus, the amount of

APs under efsevin was comparable to vehicle-treated cardiomyocytes (Friedman test, p=0.855). Although not statistically significant, a similar trend was observed for the total number of cells presenting APs (Fig. 16c). Under control conditions, 40.00 % (6/15) of cardiomyocytes exhibited diastolic APs. Superfusion with Iso increased this number to 73.33 % (11/15) of cells with APs (Fisher's exact test, p=0.1394) while administration of efsevin again reduced the occurrence of APs to 40.00 % (6/15) of myocytes (Fisher's exact test, p=0.1394), comparable to vehicle treatment. Summarizing the above, efsevin reduced the amount of AP-positive RyR2$^{R4496C/WT}$ cardiomyocytes with a major reduction of APs x min^{-1}.

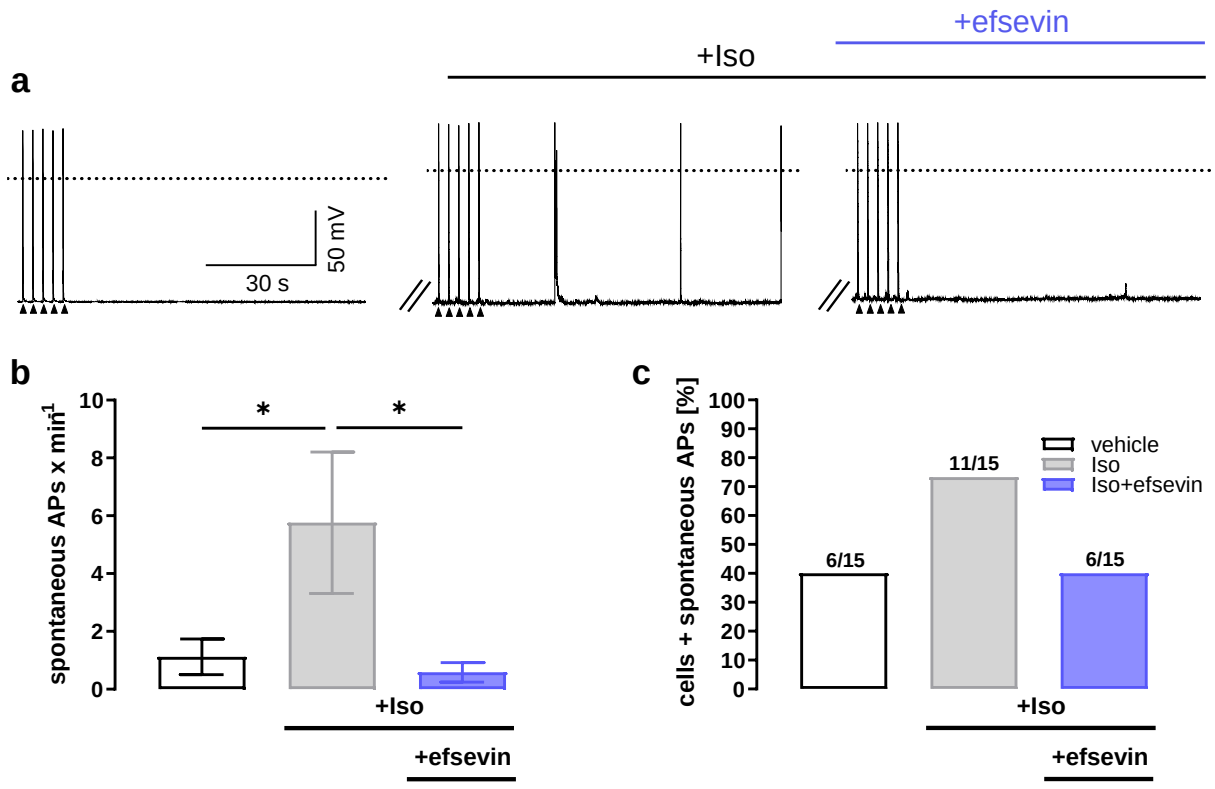

Fig. 16 Efsevin drastically reduces spontaneous APs in RyR2$^{R4496C/WT}$ cardiomyocytes.

(a) A single cell was consecutively treated with the following three conditions: After initial administration of vehicle, Iso was washed in followed by an additional wash-in of 15 µM efsevin. One sweep of every condition is depicted, representative of all 15 cells examined. The last five triggered APs are shown (black arrowheads). (b) Columns represent the quantification of averaged measurements from 8 mice. Whereas Iso significantly increased APs x min^{-1} as compared to vehicle (Friedman test, *p<0.05), efsevin wash-in

resulted in a significant reduction of arrhythmogenic APs x min^{-1} (Friedman test, *$p<0.05$). (c) Bar graphs illustrate the percentage of cardiomyocytes presenting with spontaneous APs as part of all myocytes examined. Numbers above the bars indicate AP-positive myocytes of all cells evaluated. An insignificantly enhanced number of Iso-treated $RyR2^{R4496C/WT}$ myocytes displayed spontaneous APs. Administration of efsevin reduces APs to a subset of cells according exactly with vehicle treatment.

4.1.3.1 Efsevin had no effect on delayed afterdepolarizations

Propagating Ca^{2+} waves triggered by Ca^{2+} sparks can activate NCX and Ca^{2+} efflux via NCX during diastole leading to transient inward currents resulting in delayed afterdepolarizations (DADs)[199]. DADs are defined as low amplitude depolarizations that occur after repolarization is complete, triggering spontaneous APs that ultimately represent the basis of arrhythmia. DADs as a potentially arrhythmogenic precursor to arrhythmogenic spontaneous APs, were evaluated from patch clamp experiments mentioned above. Diastolic DADs of amplitudes above or identical to 5mV during the diastolic phase were examined. Under vehicle conditions, cardiomyocytes displayed 0.10±0.04 DADs≥5mV x min^{-1}. Iso did not alter the frequency of DADs with 0.22±0.09 DADs x min^{-1} (Friedman test, $p=0.648$) and accordingly, efsevin left DADs greater than or equal to 5mV x min^{-1} unaltered at 0.54±0.30 (Friedman test, $p=0.855$), an amount also similar to vehicle (Friedman test, $p=0.523$). Only a small proportion of DADs ≥5 mV was present in all treatment groups since a depolarization of this amplitude seems to rather elicit a spontaneous AP. Hence, only 33.33 % (5/15) of cardiomyocytes exhibited DADs ≥5 mV as well as 40 % (6/15) of Iso and 40 % (6/15) of Iso + efsevin-treated cells (Fisher's exact test, $p=1.000$).

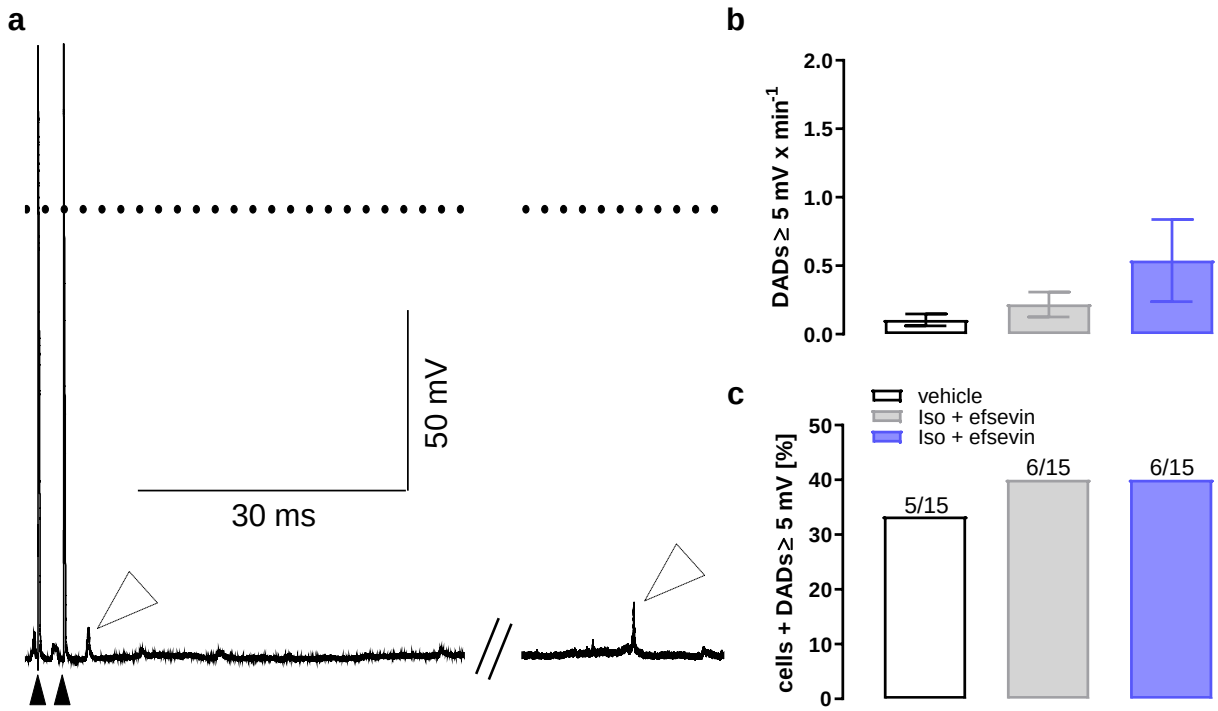

Fig. 17 Efsevin leaves DADs ≥ 5 mV unaltered in RyR2$^{R4496C/WT}$ myocytes.

(a) A single cell was consecutively treated with the following three conditions: After initial administration of vehicle, Iso was washed in followed by an additional wash-in of 15 µM efsevin. One sweep is depicted with white arrows indicating DADs. The last two triggered APs are shown (black arrowheads). (b) Columns represent the quantification of averaged measurements from 8 mice. Neither Iso (Friedman test, p=0.648) nor Iso+efsevin (Friedman test, p=0.855) significantly altered DADs≥ 5 mV x min^{-1} as compared to vehicle (c) Bar graphs illustrate the percentage of cardiomyocytes presenting with spontaneous DADs≥ 5 mV x min^{-1} as part of all myocytes examined. Numbers above the bars indicate AP-positive myocytes of all cells examined. The subset of cells presenting with DADs≥ 5 mV x min^{-1} did not significantly differ between the treatment groups.

4.1.4 Effects of efsevin on systolic proarrhythmic events in RyR2$^{R4496C/WT}$ myocytes

4.1.4.1 Efsevin suppresses secondary systolic Ca^{2+} elevations

Aside from spontaneous diastolic waves and APs, proarrhythmic events with the potential to trigger ventricular tachycardia (VT) also exist during systole. Spontaneous systolic Ca^{2+}

elevations (SSCEs) are arrhythmogenic Ca^{2+} signals that immediately follow a triggered systolic Ca^{2+} transient[200]**.** We examined triggered Ca^{2+} transients from our Ca^{2+} wave experiments shown above for the presence of SSCEs as well as the amount of SSCE-positive cardiomyocytes (Fig. 18a). Hence, the number of mice and cells subjected to the experiment are identical to 4.1.2. The amount of $RyR2^{R4496C/WT}$ cardiomyocytes with SSCEs (Fig. 18c) were comparable between vehicle-treatment with 18.91 % (7/37) and Iso-treatment with 28.38 % (21/74; Fisher's exact test, p=0.181). In Iso-stressed cells, efsevin was able to significantly reduce the percentage of SSCE-positive cells to 5.26 % (3/57; Fisher's exact test, p=0.0001 compared to Iso and p=0.0039 compared to vehicle). In contrast, a considerable number of $RyR2^{R4496C/WT}$ cells showed SSCEs already under vehicle treatment where efsevin exerted a promising antiarrhythmic effect. In $RyR2^{R4496C/WT}$ cardiomyocytes, 7.15 % (1.22/17) of all transients presented with a subsequent SSCE under control conditions (vehicle). Catecholaminergic stimulation (Iso) did not induce a significant increase in the number of transients with SSCEs, which amounted to 10.05 % (1.61/16; Fisher's exact test, p=0.613). Interestingly however, treatment of Iso-stressed $RyR2^{R4496C/WT}$ cardiomyocytes with 15 µM efsevin significantly reduced the number of transients with SSCEs to 1.56 % (0.25/16; Fisher's exact test, p=0.033). In summary, efsevin not only restricts the number of cardiomyocytes, but also the number of systolic transients presenting with SSCEs thus exerting an additional, inhibiting effect on systolic arrhythmogenic events *in vitro*.

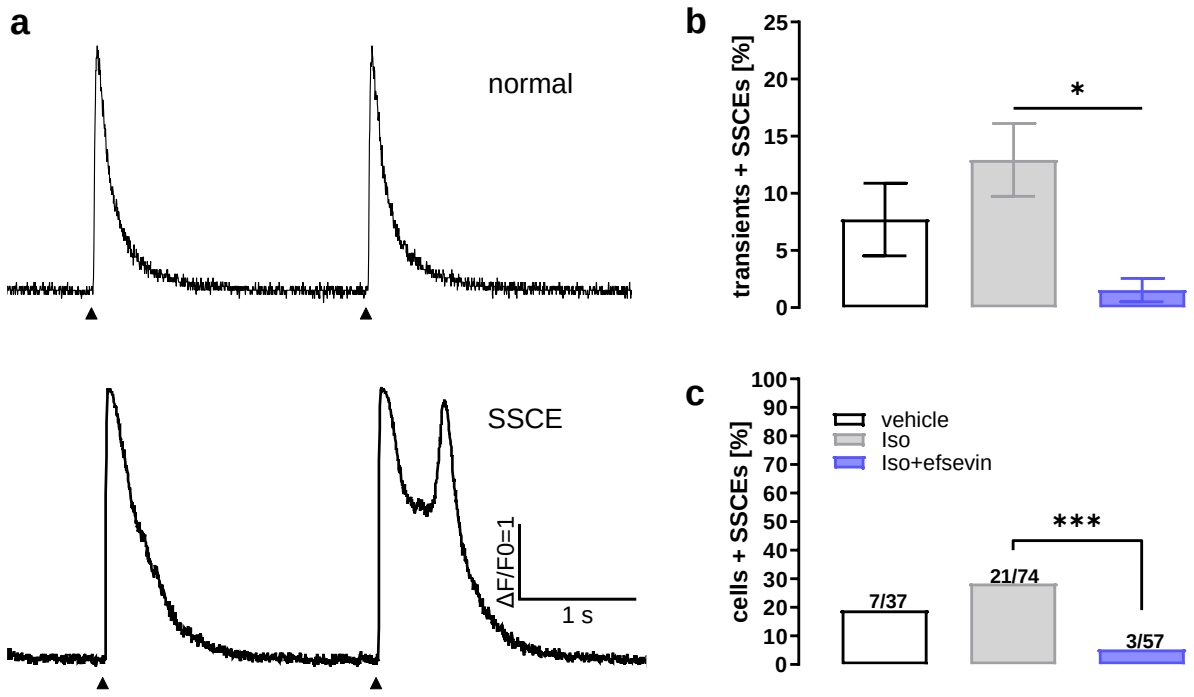

Fig. 18 Efsevin reduces spontaneous systolic SSCEs in RyR2$^{R4496C/WT}$ cardiomyocytes.

(a) Triggered systolic Ca^{2+} transients (marked by black arrowheads) are shown (normal) some of which are followed by subsequent SSCEs (lower trace). (b) Columns represent the amount of Ca^{2+} transients followed by arrhythmogenic SSCEs in [%]. The quantity of transients followed by SCCEs in RyR2$^{R4496C/WT}$ cardiomyocytes were reduced by treatment with efsevin (Fisher's exact test, *p<0.05). (c) Bar graphs illustrate the percentage of cardiomyocytes presenting with spontaneous SSCEs of all myocytes examined. Numbers above the bars represent SSCE-positive cells of all cells examined. Efsevin exerts a significant antiarrhythmic effect in RyR2$^{R4496C/WT}$ cardiomyocytes (Fisher's exact test, ***p<0.001).

4.1.4.2 Efsevin had no effect on early afterdepolarizations

A similar, but not significant tendency was observed for early afterdepolarizations (EADs) in patch clamp experiments. EADs are spontaneous afterdepolarizations occurring during phase 2 or 3 of repolarization[156]. Controversial theories exist about the genesis of EADs. Whereas the canonical theory states that EADs arise from a Ca^{2+} dependent reactivation of LTCCs[201,202], current studies indicate that SR Ca^{2+} overload might trigger these systolic events[203]. Regardless of the underlying mechanism or whether both versions hold partly true, EADs are known to be

elicited by Ca^{2+} abnormalities and represent a recently added event underlying arrhythmogenesis in CPVT[157]. Further, it is recognized that SSCEs, arrhythmogenic events on the Ca^{2+} level, have the ability to trigger EADs[204,205]. As can be appreciated from Fig. 18, we could demonstrate an antiarrhythmic effect of efsevin on SSCEs. As a consequence, we investigated whether efsevin reflects its potency to reduce arrhythmogenic Ca^{2+} events on the electrophysiological level. We examined triggered APs in $RyR2^{R4496C/WT}$ mice (n=8) from patch clamp experiments mentioned above for the occurrence of EADs. In accordance to what was observed for SSCE-positive Ca^{2+} transients, Iso treatment did not significantly increase the number of EAD-positive APs. Under vehicle treatment, 22.26 % (2.48/10) of all APs presented with EADs comparable to a fraction of EAD-positive APs at 23.34 % (3.00/10) after catecholaminergic stress (Fisher's exact test, p=1.000). Treatment of Iso-stressed $RyR2^{R4496C/WT}$ cardiomyocytes with 15 µM efsevin did not alter the number of APs + EADs with 13.35 % (2.00/10) (Fisher's exact test, p=0.097), a number indifferent from that in vehicle-administered cells (Fisher's exact test, p=0.1358). Likewise, the number of cardiomyocytes presenting with EADs was not affected by Iso or efsevin. The amount of EAD-positive cells under application of vehicle with 60 % (9/15) was indistinguishable from a value of 80 % (12/15) under Iso treatment (Fisher's exact test, p=0.427). Although not statistically significant, there is a clear trend towards a reduction of cells presenting with EADs following the additional wash-in of 15 µM efsevin: The percentage of EAD-positive $RyR2^{R4496C/WT}$ cardiomyocytes stressed with Iso amounted to 40 % (6/15; Fisher's exact test, p=0.060), a value indifferent from that in vehicle-treated cells (Fisher's exact test, p=0.466).

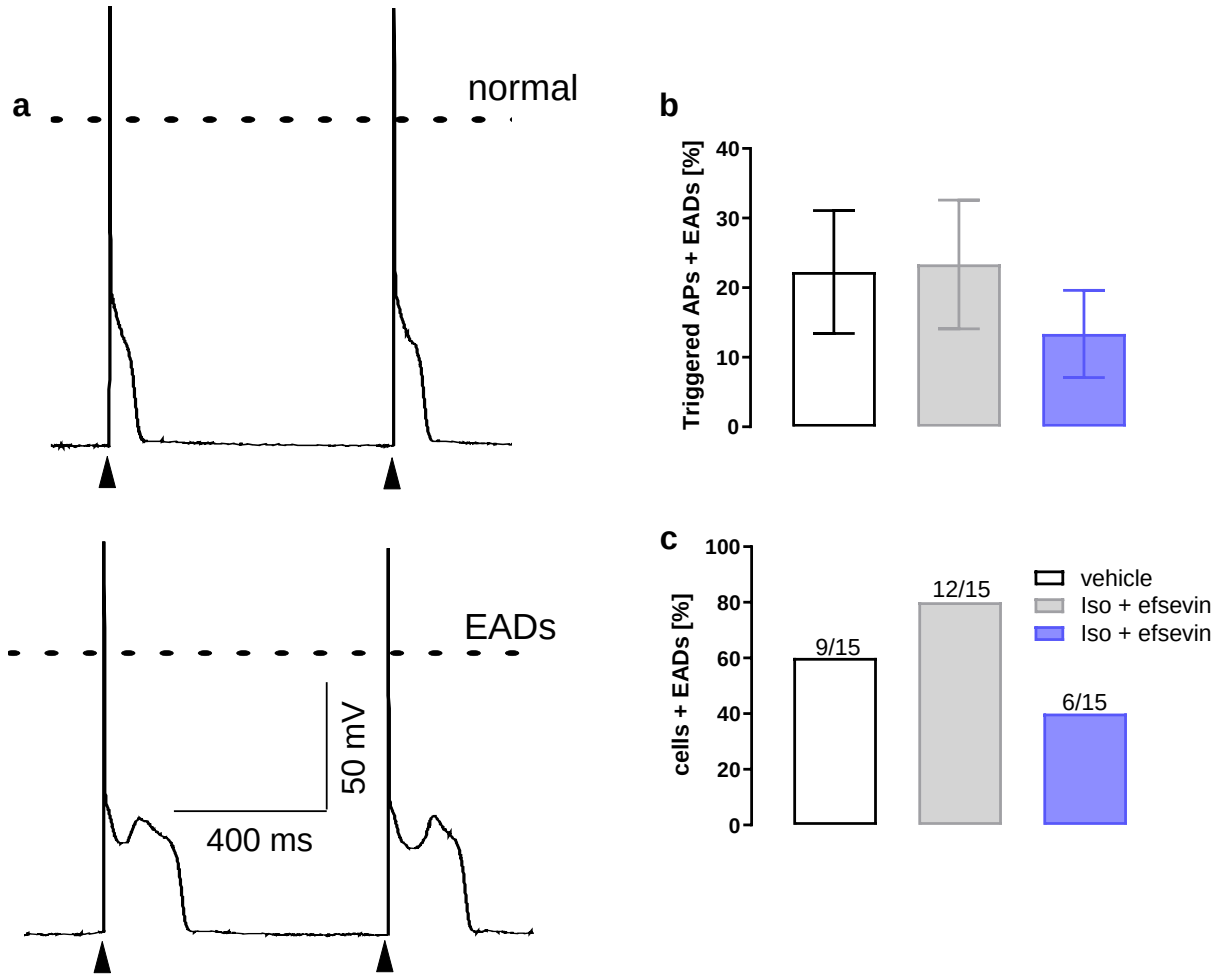

Fig. 19 Administration of efsevin had no effect on EADs.

(a) Triggered systolic APs (marked by black arrowheads) are shown (normal, upper trace) some of which are followed by subsequent EADs (lower trace). (b) A single cell was consecutively treated with vehicle and Iso followed by an additional wash-in of 15 µM efsevin. Columns represent the quantification of averaged measurements from 8 mice. Neither Iso (Fisher's exact test, p=1.000) nor Iso+efsevin (Fisher's exact test, p=0.097) significantly altered the amount of triggered APs presenting with EADs. (c) Bar graphs illustrate the percentage of cardiomyocytes presenting with EADs as part of all myocytes examined. Numbers above the bars indicate AP-positive myocytes of all cells examined. The subset of cells presenting with EADs did not significantly differ between $RyR2^{R4496C/WT}$ myocytes treated with vehicle and Iso (Fisher's exact test, p=0.427). Although not statistically significant, there is a clear trend towards a reduction of EAD-positive cardiomyocytes following the additional wash-in of 15 µM efsevin (Fisher's exact test, p=0.060).

4.2 Effects of efsevin on triggered systolic events

4.2.1 Impact of efsevin on systolic Ca^{2+} transients in $RyR2^{R4496C/WT}$ myocytes

In light of a future clinical application of efsevin it is of utmost importance that antiarrhythmic properties are not accompanied by any adverse effects on physiological contractions. We therefore assessed effects of efsevin on systolic Ca^{2+} transients in vehicle- (n=37), Iso- (n= 67) and Iso + efsevin-treated (n= 50) cardiomyocytes. Whilst suppressing diastolic Ca^{2+} waves, efsevin did not provoke any severe effects on electrically evoked Ca^{2+} transients of $RyR2^{R4496C/WT}$ cardiomyocytes (Fig. 20). The amount of Ca^{2+} released from the SR, expressed as $\Delta F/F_0$, was substantially increased by Iso from 3.18±0.12 in vehicle-treated myocytes to 3.99±0.10 (Kruskal-Wallis test, $p<0.001$) and retained unaltered at 3.78±0.11 under efsevin treatment (Kruskal-Wallis test, p=0.157). Ttp, representing the activation time of Ca^{2+} release, amounted to 32.85±1.26 ms in vehicle-treated cells and was significantly accelerated to 26.93±0.62 ms by Iso (Kruskal-Wallis test, p=0.0001). Application of efsevin led to a moderate deceleration of ttp to 30.70±1.13 ms (Kruskal-Wallis test, p=0.020). In contrast, no efsevin effect was observed for Ca^{2+} clearance from the cytosol. $Tau_{inactivation}$ was significantly reduced from 302.66±15.90 ms at baseline to 170.18±7.17 ms by Iso (Kruskal-Wallis test, $p<0.001$) and remained unaltered after administration of efsevin with a $tau_{inactivation}$ value of 198.24.42±1.63 ms (Kruskal-Wallis test, p=0.295). We additionally determined the aforementioned parameters in systolic transients from WT cells. Systolic transients from vehicle-treated cardiomyocytes (n= 30) were analyzed, whereas transients from cells administered Iso (n= 32) and from cardiomyocytes treated with Iso + efsevin (n= 31) were included in the analysis. $\Delta F/F_0$ in vehicle-treated cells amounted to 2.84±0.27 and was again significantly increased by Iso to 3.79±0.23 (Kruskal-

Wallis test, $p<0.001$). Concordant with data from CPVT cardiomyocytes, efsevin administration did not influence $\Delta F/F_0$ (3.74±0.35; Kruskal-Wallis test, $p=0.805$). Further, the activation time of Ca^{2+} release standing at 37.42±2.14 ms in vehicle-treated cells was significantly accelerated by Iso to 28.08±1.63 ms (Kruskal-Wallis test, $p<0.001$). Application of efsevin in Iso-treated cells decelerated ttp to 33.74±3.13 ms (Kruskal-Wallis test, $p=0.005$). Whereas $tau_{inactivation}$ in WT myocytes was 307.83±34.18 ms it was accelerated to 170.28±15.90 ms under catecholaminergic stress (Kruskal-Wallis test, $p<0.001$). Application of efsevin did not further influence $tau_{inactivation}$ (189.63±20.88 ms; Kruskal-Wallis test, $p=0.215$).

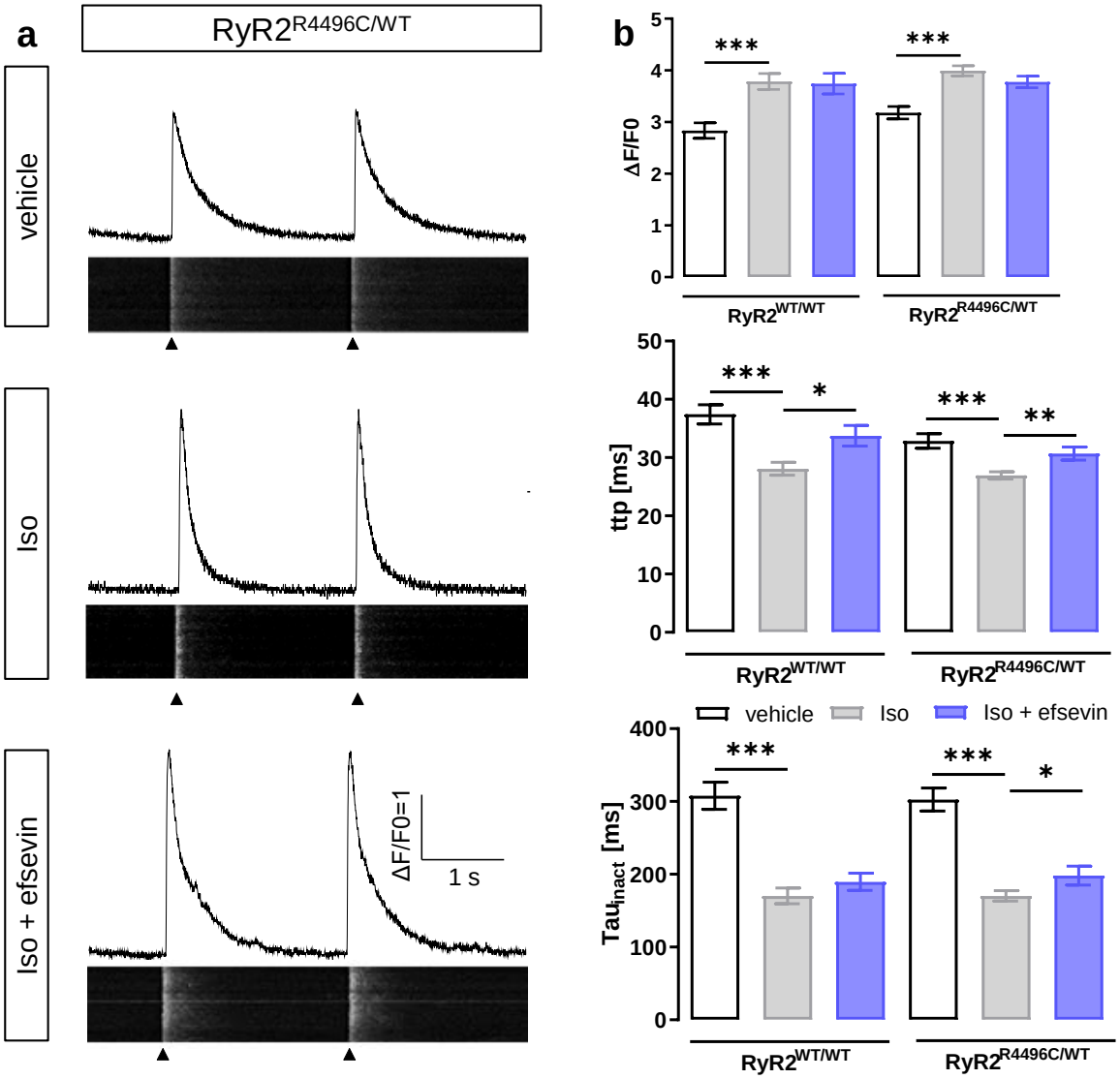

Fig. 20 Effect of efsevin on systolic Ca^{2+} transients in CPVT cardiomyocytes.

(a) Confocal line scan images and respective intensity plots of two triggered transients are shown (black arrowheads). (b) Iso significantly affects systolic Ca^{2+} transients in $RyR2^{R4496C/WT}$ myocytes by increasing their amplitude ($\Delta F/F_0$; Kruskal-Wallis test, ***p<0.001) and significantly accelerating Ca^{2+} activation (ttp; Kruskal-Wallis test, ***p=0.001) and inactivation (Tau_{inact}; Kruskal-Wallis test, ***p<0.001). In contrast, efsevin exerts no further effects on these Ca^{2+} transient parameters under Iso. Whereas transient amplitude and Ca^{2+} clearance in CPVT cells were not significantly altered following treatment with efsevin, ttp was slightly increased (Kruskal-Wallis test, **p<0.05). Similar trends were apparent in WT cardiomyocytes (see text for details).

4.2.2 Effects on triggered APs in RyR2$^{R4496C/WT}$ cardiomyocytes

Common antiarrhythmic drugs frequently intervene in the systolic AP causing proarrhythmic side effects. Therefore we investigated potential effects of efsevin on triggered APs, where we examined the duration of systolic APs at 50 % (APD_{50}) and 90 % (APD_{90}) of repolarization, respectively. Whereas efsevin prolonged APD_{50} 2.6-fold, it did not exert a significant effect on APD_{90} (Fig. 21). APD_{50} amounted to 11.12±2.17 ms under vehicle-perfusion and remained constant after Iso wash-in (15.32±4.90 ms; Friedman test, p=0.345). Perfusion of cardiomyocytes with efsevin-containing solution drastically prolonged APD_{50} to 39.56±7.05 ms (Friedman test, p=0.038). By contrast, following efsevin wash-in no prolongation of the AP was observed at 90 % of repolarization. Untreated myocytes showed an APD_{90} of 94.51±10.79 ms and of 75.14±9.17 ms after perfusion with Iso (one-way ANOVA, p=0.1453). Addition of efsevin to Iso-treated myocytes resulted in an APD_{90} of 95.35±10.80 ms (one-way ANOVA, p=0.090), a value comparable to the baseline value (one-way ANOVA, p=0.836). Furthermore, efsevin had no effect on the resting membrane potential (RMP) of cardiomyocytes. RyR2$^{R4496C/WT}$ myocytes exhibited a physiological RMP of 75.39±2.17 mV which became significantly more negative under Iso treatment standing at -77.79±2.17 mV (one-way ANOVA, p=0.020). After wash-in of efsevin, RMP amounted to -78.24±2.10 mV, pointing out that efsevin had no further effect (one way ANOVA, p=0.312). AP amplitude standing at 116.25±1.42 mV remained unaffected by Iso (116.47±1.48 mV; Friedman test, p=0.239) and was only slightly reduced to 111.22±2.17 by efsevin (Friedman test, p=0.019).

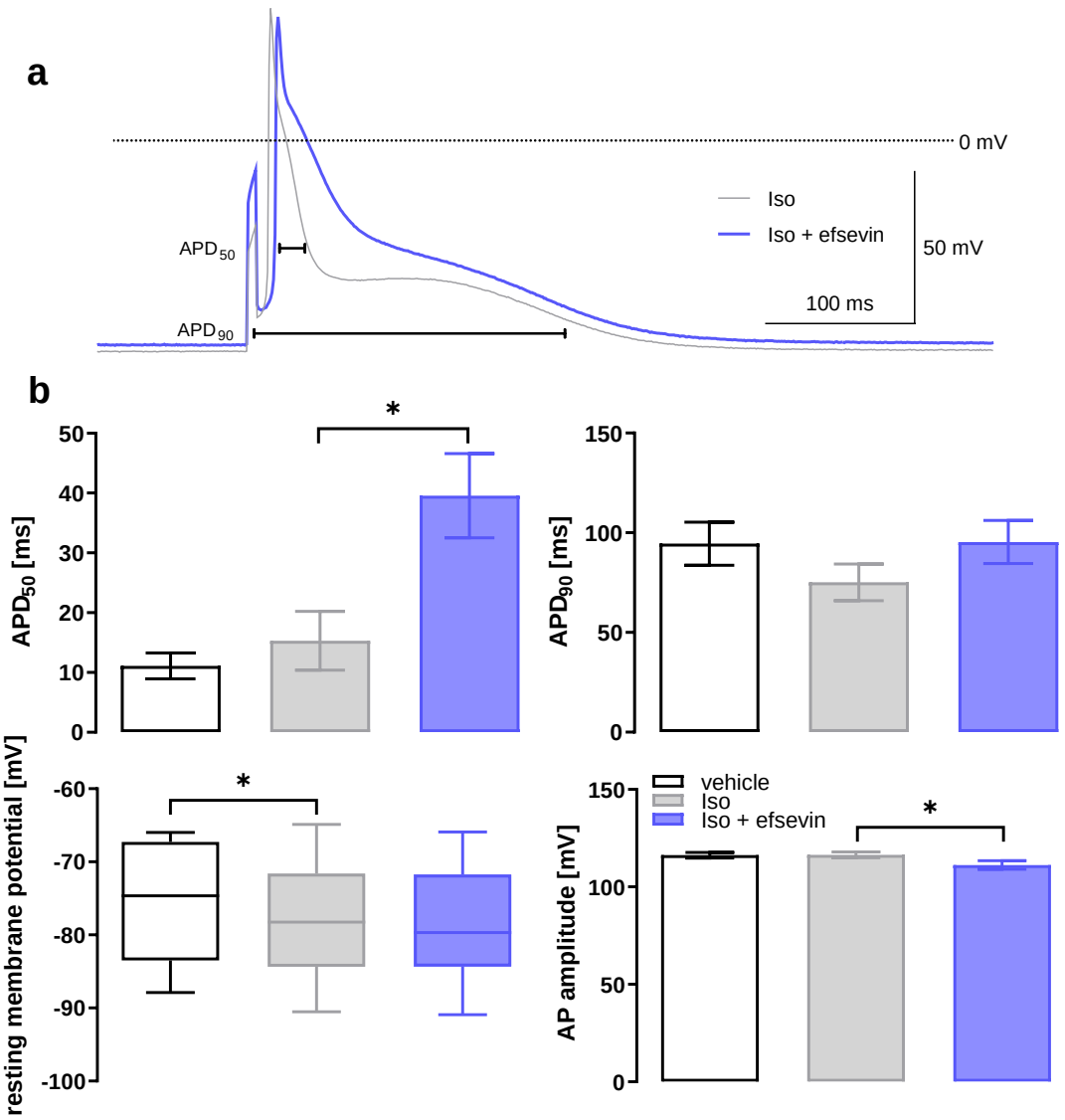

Fig. 21 Efsevin modulates triggered systolic APs in mouse cardiomyocytes.

(a) The characteristic shape of a triggered AP is shown for administration of Iso (grey) and for treatment with Iso + efsevin (blue), respectively. The duration of systolic APs at 50 % (APD_{50}) and 90 % of repolarization (APD_{90}) is exemplified. (b) Iso exerted no major effect on both parameters. Whereas efsevin also had no impact on APD_{90}, it significantly prolonged APD_{50} (Friedman test, *p<0.05). (c) The resting membrane potential (RMP) became significantly more negative following Iso wash-in (one-way ANOVA, *p<0.05) and remained unchanged after addition of efsevin. AP amplitude was not altered by Iso and was only marginally decreased by the addition of 15 µM efsevin (Friedman test, *p<0.05).

4.3 Mechanism of action

4.3.1 Efsevin does not intervene in β-adrenergic signaling

We next sought to investigate the mechanism of action of efsevin's antiarrhythmic effects. Efsevin was previously shown to act through VDAC2[181] and work from our lab demonstrates that it enhances Ca^{2+} uptake in cultured HL-1 cardiomyocytes[184]. We wanted to test whether the antiarrhythmic potency of efsevin is solely attributable to its action on VDAC2 since a suppression of Iso-mediated effects made an additional modulation of β-adrenergic signaling quite conceivable. We therefore measured cellular cAMP accumulation in $RyR2^{R4496C/WT}$ cardiomyocytes. β-AR agonists activate stimulatory G proteins and thereby trigger adenylate cyclase which in turn leads to enhanced cAMP production. Forskolin (FSK), a known activator of adenylate cyclases was employed as a positive control. Indeed, treatment with 5 µM FSK significantly increased the amount of cAMP generated in cardiomyocytes from 29.57±1.26 cAMP x $cAMP+ATP^{-1}$ under basal conditions to 47.62±2.16 cAMP x $cAMP+ATP^{-1}$ (Kruskal-Wallis test, $p<0.001$) (Fig. 22). We next applied Iso at a concentration of 100 nM: the catecholamine significantly increased cAMP levels to 43.11±2.36 cAMP x $cAMP+ATP^{-1}$ (Kruskal-Wallis test, $p<0.001$ basal vs. Iso), a value comparable to the positive control FSK (Kruskal-Wallis test, $p=0.546$). Conversely, cAMP accumulation after treatment with 10 µM efsevin alone closely resembled that of untreated cells with a value of 29.35±2.18 cAMP x $cAMP+ATP^{-1}$ (Kruskal-Wallis test, $p=0.999$). Taken together, this led us to conclude that efsevin is not a β-AR agonist. To investigate a putative β-blocking activity of the substance, we compared cAMP levels under efsevin to the ones in myocytes under β-blockade. In cells pretreated with Iso, 1 µM of the common β-blocker propranolol markedly diminished the amount of generated cAMP to

35.47±1.26 cAMP x cAMP+ATP^{-1} (Kruskal-Wallis test, p=0.036). By contrast, cellular cAMP in Iso-treated cells remains unaffected by the additional administration of 10 µM efsevin at 44.51±2.73 cAMP x cAMP+ATP^{-1} (Kruskal-Wallis test, p=0.999). Conclusively, our data show that a modulation of β-adrenergic signaling could not be allocated as the antiarrhythmic mechanism of efsevin. Indeed, efsevin seemingly exerts its effects on diastolic and systolic Ca^{2+} events by means of β-AR independent pathways.

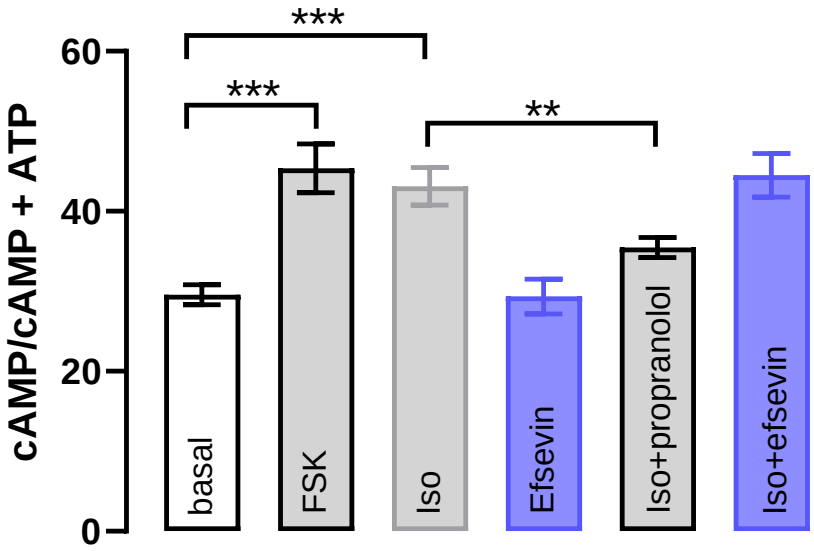

Fig. 22 Efsevin does not directly affect β-adrenergic signaling in RyR2$^{R4496C/WT}$ cardiomyocytes.

Columns represent the average cellular cAMP level expressed as cAMP x cAMP+ATP^{-1}±SEM. Administration of efsevin alone does not exert an effect on cellular cAMP accumulation compared to basal conditions (Kruskal-Wallis test, p=0.919), whereas adenylate cyclase activator FSK (Kruskal-Wallis test, ***p<0.001) and β-AR agonist Iso (Kruskal-Wallis test, ***p<0.001) drastically elevated cAMP accumulation. Also, efsevin has no negative effect on cellular cAMP in Iso-treated cardiomyocytes (Kruskal-Wallis test, p=0.999) as opposed to the common β-blocker propranolol (Kruskal-Wallis test, **p=0.036). This indicates that efsevin is neither an agonist nor a blocker of the β-AR.

4.3.2 Efsevin acts through enhanced mitochondrial Ca^{2+} uptake

4.3.2.1 Inhibition of Ca^{2+} uptake into mitochondria blocks efsevin's antiarrhythmic effect

In HL-1 cardiomyocytes, efsevin dose-dependently enhanced the mitochondrial uptake of Ca^{2+} released from the SR induced by addition of 10 mM caffeine. This effect was antagonized by addition of ruthenium red (RuR), a blocker of mitochondrial Ca^{2+} uptake. RuR blocks the MCU and thereby inhibits Ca^{2+} flux via the IMM, so that Ca^{2+} can still pass the OMM through VDAC2 but further transport into the mitochondrial matrix is blocked. We next investigated whether the enhanced Ca^{2+} uptake into mitochondria via VDAC2 represents the mechanism directly underlying efsevin's antiarrhythmic effect in $RyR2^{R4496C/WT}$ cardiomyocytes. Therefore, we assessed whether a block of Ca^{2+} influx into mitochondria would abolish the antiarrhythmic effect of efsevin on catecholamine-induced Ca^{2+} waves in $RyR2^{R4496C/WT}$ myocytes. Whereas no waves occurred under control conditions in cardiomyocytes (n=3 mice), Iso increased waves to 0.36±0.16 waves x min^{-1} (n=2 mice; Kruskal-Wallis test, p=0.032). Efsevin completely eliminated waves (n=3 mice; Kruskal-Wallis test, p=0.035) comparable to the data presented in chapter 4.1.2. Subsequently, Ca^{2+} uptake into mitochondria was inhibited by Ru_{360}. Addition of the blocker resulted in a minor insignificant increase in spontaneously propagating waves to 0.07±0.04 waves x min^{-1} (n=3 mice) already in vehicle-treated cardiomyocytes compared to the complete absence of arrhythmogenic events in untreated cells under vehicle conditions (Kruskal-Wallis test, p=0.476). Again, Iso caused a significant increase of waves in Ru_{360}-treated cardiomyocytes (n=4 mice) to 0.63±0.16 min^{-1} (Kruskal-Wallis test, p<0.001) compared to vehicle-treatment. Of note, the concurrent treatment with Iso and Ru_{360} caused a drastic increase in cardiomyocytes not suitable for analysis due to excessive spontaneous activity

without a reaction to systolic stimuli. In analyzable cells the number of Ca^{2+} waves x min^{-1} was indistinguishable between Iso-treated groups with and without application of Ru_{360}. Most strikingly, inhibition of mitochondrial Ca^{2+} uptake with Ru_{360} abrogated the suppressive effect of efsevin on spontaneous Ca^{2+} waves. The number of waves amounted to 0.62±0.12 waves x min^{-1} (n=6 mice) in cardiomyocytes treated with efsevin and was indifferent from the amount of waves in myocytes treated with Iso alone (Kruskal-Wallis test, p=0.354). Thus, efsevin lacks its antiarrhythmic potency under blockade of mitochondrial Ca^{2+} uptake. This can further be appreciated by the amount of wave-positive cardiomyocytes (Fig. 23b). No vehicle-treated $RyR2^{R4496C/WT}$ cells (0/23) showed Ca^{2+} waves under control conditions, whereas Iso induced waves in 33.33 % (5/15) of myocytes (Fisher's exact test, p=0.006). Administration of efsevin completely abolished waves (0/21; Fisher's exact test, p=0.0001). Application of Ru_{360} generated significantly more waves in vehicle control with 10.35 % (3/29) of wave-positive cardiomyocytes as compared to vehicle alone (Fisher's exact test, p=0.002). Concurrent treatment with Iso and Ru_{360} even extended Ca^{2+} waves to 52.38 % (11/21) of myocytes (Fisher's exact test, p=0.0001). Noteworthy, in the presence of Ru_{360}, addition of efsevin to Iso-treated cells no longer suppressed arrhythmogenic waves resulting in 40.32 % (25/62) of wave-positive cardiomyocytes (Fisher's exact test, p=0.118). Conclusively, a blockade of mitochondrial Ca^{2+} uptake counteracts efsevin's antiarrhythmic activity in isolated murine $RyR2^{R4496C/WT}$ cardiomyocytes, clearly linking enhanced mitochondrial Ca^{2+} uptake to the suppression of arrhythmogenic events in these cells.

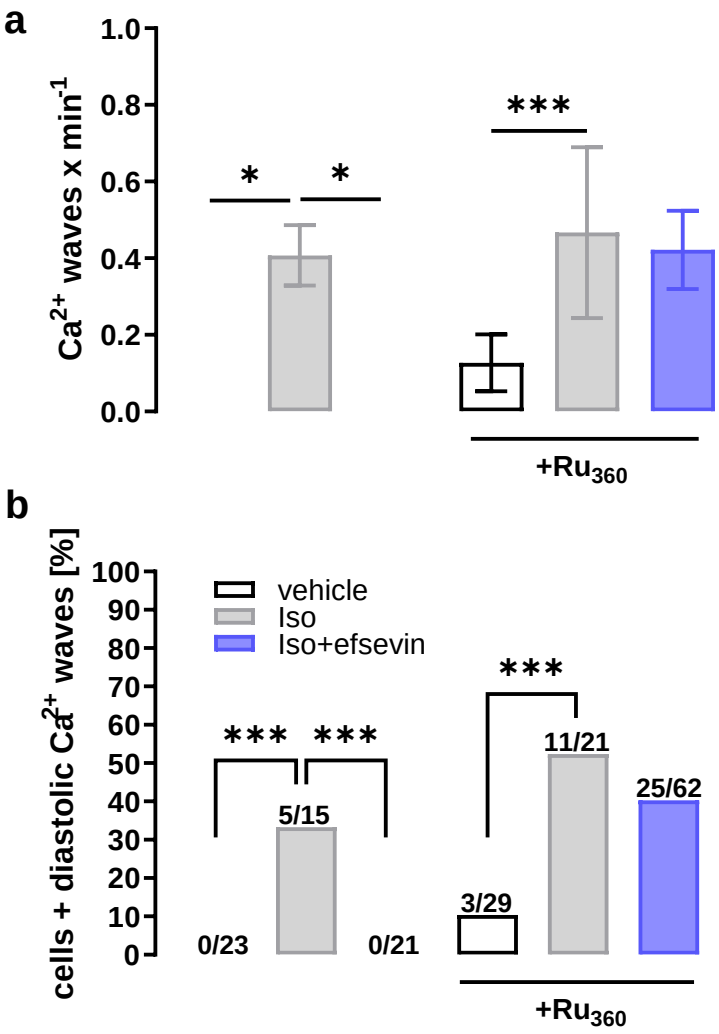

Fig. 23 Blockade of mitochondrial Ca^{2+} uptake abolishes the antiarrhythmic activity of efsevin in $RyR2^{R4496C/WT}$ cardiomyocytes.

(a) Average waves x min^{-1}±SEM are displayed for different treatment conditions. Whereas efsevin significantly reduces the number of spontaneous diastolic Ca^{2+} waves in untreated $RyR2^{R4496C/WT}$ cardiomyocytes (Kruskal-Wallis test, *$p<0.05$), the amount of waves after addition of Ru_{360} is similar in cells with or without efsevin. (b) Bar graph diagram illustrating the percentage of cardiomyocytes with diastolic Ca^{2+} waves. Numbers above the bars represent wave-positive cardiomyocytes of all myocytes examined. Whereas Iso drastically increased the amount of cells presenting with spontaneous Ca^{2+} waves x min^{-1} (Fisher's exact test, **$p<0.05$), no wave-positive myocytes were observed under efsevin treatment (Fisher's exact test,***$p<0.001$). Inhibition of mitochondrial Ca^{2+} uptake with Ru_{360} induced waves already under vehicle conditions. Iso significantly increased the amount of wave-positive cells (Fisher's exact test, ***$p<0.001$). However, efsevin was no longer able to reduce arrhythmogenic waves following treatment with Ru_{360}.

4.3.2.2 Mitochondrial Ca^{2+} uptake enhancers – the MCU activator kaempferol

The experiment above (4.3.2.1) has demonstrated that enhanced mitochondrial Ca^{2+} uptake is directly causative for the antiarrhythmic potency of efsevin. We next wanted to reveal if this specific effect is restricted to the enhancement of mitochondrial Ca^{2+} uptake through VDAC2 or would rather represent a more widely applicable prevailing principle for substances that enhance mitochondrial Ca^{2+} uptake in general. The MCU residing in the IMM is activated by natural plant flavonoids with kaempferol being the most active agent[183]. Research from our group demonstrated that kaempferol dose-dependently increased the rapid transfer of Ca^{2+} from the SR into mitochondria with a comparable profile to efsevin (experiment performed by Fabiola Wilting)[184]. To investigate the applicability of kaempferol as an additional antiarrhythmic agent acting through mitochondrial Ca^{2+} uptake, we sought to reproduce the effects observed in efsevin-treated $RyR2^{R4496C/WT}$ cardiomyocytes on Ca^{2+} sparks by application of 10 µM kaempferol (n=6 mice). The analysis of Ca^{2+} spark parameters was performed analogously to experiments with efsevin using the same vehicle- and Iso-treated myocytes as in 4.1.1 as controls (Fig. 24). Comparable to efsevin treatment, application of kaempferol led to a significantly reduced spark frequency of 0.49±0.09 sparks x 100 μm^{-1} x s^{-1} (n=18 cells; Kruskal-Wallis test, $p<0.0001$ compared to Iso). Kaempferol induced an analogous effect on amplitudes to efsevin: $\Delta F/F_0$ was decreased to 0.40±0.01 compared to 0.66±0.01 under Iso (n=577 sparks; Kruskal-Wallis test, $p<0.0001$) and 0.47±0.01 under Iso + efsevin (Kruskal-Wallis test, $p<0.0001$ as compared to Iso). In line with efsevin, kaempferol significantly accelerated Ca^{2+} clearance to a tau_{decay} of 40.46±0.96 ms (n=577 sparks; Kruskal-Wallis test, $p<0.0001$) thereby spatially and temporally restricting Ca^{2+} sparks. Sparks exhibited a full width of 2.60±0.05 µm (n=356;

Kruskal-Wallis test, $p<0.0001$ compared to Iso) with kaempferol and a FWHM of 2.08±0.04 µm (n=355 sparks; Kruskal-Wallis test, p=0.0004 compared to Iso). Ca^{2+} sparks obtained with kaempferol were spatially narrowed, a pattern already evident in efsevin-treated myocytes. This resulted in a full duration of 58.63±0.95 ms (n=314 sparks; Kruskal-Wallis test, $p<0.0001$ compared to Iso) and a FDHM of 46.51±0.76 ms (n=314 sparks; Kruskal-Wallis test, $p<0.0001$ compared to Iso), respectively. Furthermore, the activation time of Ca^{2+} release, ttp, was significantly accelerated to 24.97±0.69 ms by kaempferol application in Iso-treated myocytes (n=314; Kruskal-Wallis test, p=0.0084 compared to Iso). Additionally, kaempferol induced an acceleration of Ca^{2+} release flux ((F/F_0)/tmax) from the SR to 15.94±0.37 (n=356 sparks; Kruskal-Wallis test, $p<0.0001$). Our results further underpin that not only the reduced frequency of potentially arrhythmogenic Ca^{2+} sparks but also their spatial and temporal restriction all seem to be part of a general antiarrhythmic principle not solely restricted to efsevin. To further strengthen the mechanistical connection between enhanced mitochondrial Ca^{2+} uptake and the reduction of arrhythmogenic events, the effect of kaempferol on spontaneous Ca^{2+} waves in isolated $RyR2^{R4496C/WT}$ cardiomyocytes was assessed by Fabiola Wilting in our lab. Concordant with data for efsevin (4.1.1), the number of arrhythmogenic Ca^{2+} waves was significantly reduced by treatment of the cells with 10 µM kaempferol. These data led us to postulate that enhancing mitochondrial Ca^{2+} uptake indeed represents a general and novel antiarrhythmic principle and substances acting by this mechanism of action are referred to hereinafter as mitochondrial Ca^{2+} uptake enhancers (MiCUps).

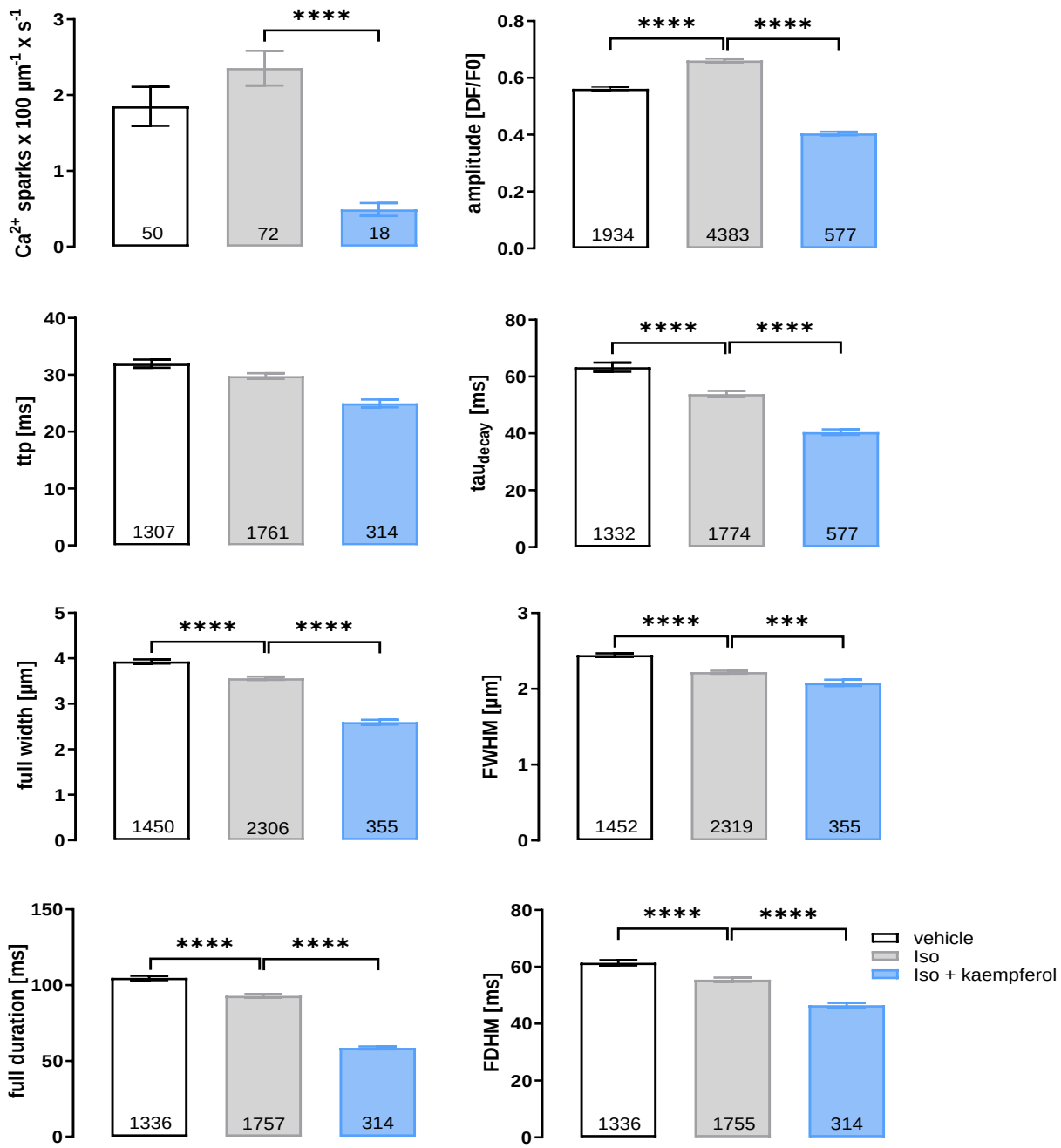

Fig. 24 Kaempferol reduces spontaneous Ca^{2+} spark frequency in $RyR2^{R4496C/WT}$ cardiomyocytes and accelerates Ca^{2+} decay resulting in a spatial and temporal restriction of individual sparks.

Vehicle- and Iso-treated cardiomyocytes were the same as used for comparison in 4.1.1 (Fig. 14). Columns represent the average of consecutive experiments for the different treatment conditions and numbers in bars indicate the amount of cells (for frequency) or sparks examined, respectively. β-adrenergic stimulation with Iso induces a slightly higher spark frequency, a significantly higher amplitude (Kruskal-Wallis test, ****p<0.0001) and drastically accelerates cytosolic tau_{decay} (Kruskal-Wallis test, ****p<0.0001) leading to significantly narrower (full width; Kruskal-Wallis test, ****p<0.0001) and shorter (full duration; Kruskal-Wallis test, ****p<0.0001) sparks. The same applied to FDHM (Kruskal-Wallis test, ****p<0.0001) and FWHM (Kruskal-Wallis test, ****p<0.0001). Application of kaempferol drastically

reduced spark frequency (Kruskal-Wallis test, ****p<0.0001) and amplitude (Kruskal-Wallis test, ****p<0.0001) and further limits spatial and temporal expansion of sparks: Following administration of kaempferol, full duration (Kruskal-Wallis test, ****p<0.0001), FDHM (Kruskal-Wallis test, ****p<0.0001), width (Kruskal-Wallis test, ****p<0.0001) and FWHM (Kruskal-Wallis test, ***p<0.001) were significantly reduced as compared to treatment with Iso alone. Whereas Iso alone had no effect on ttp, kaempferol significantly accelerated ttp (Kruskal-Wallis test, **p<0.01) and tau_{decay} (Kruskal-Wallis test, ****p<0.0001).

4.3.3 Antiarrhythmic effect of MiCUps in $RyR2^{R4496C/WT}$ mice *in vivo*

The highly promising antiarrhythmic effects of MiCUps *in vitro* combined with the absence of severe side effects on systolic events under efsevin treatment formed a solid base for consecutive *in vivo* experiments. In order to investigate the antiarrhythmic potential of MiCUps to suppress VT and to identify yet unforeseen side effects *in vivo*, we administered efsevin and kaempferol to $RyR2^{R4496C/WT}$ mice. Since this thesis represents the very first *in vivo* application of efsevin in mammals, we administered the novel antiarrhythmic compound to $RyR2^{WT/WT}$ littermates (n=2 mice) of either sex with a weight of 33,05 g and 23,60 g to exclude potential lethal or fatal side effects prior to a large scale experiment. None of the two WT mice, treated with 15 mg/kg BW efsevin per day at a pump rate of 0.5 µL/h died or showed any side effects during the 8 day treatment period. Under inhalation anaesthesia with isoflurane, a baseline ECG was performed until steady state was reached (Fig. 25a) before mice were β-adrenergically stressed by injection of a bolus of 2 mg/kg BW L-adrenaline and 120 mg/kg BW caffeine (epi/caff): Basal HR in efsevin-treated animals was 496.22±71.17 bpm and was in line with physiological values previously obtained from anesthesized mice[206]. Epi/caff injection accelerated the HR in mice to 560.05±60.61 bpm (Fig. 25b). Further, PR and QT intervals were evaluated as a measure of maintained systolic sinus rhythm (Fig. 25c). PR interval representing

the conduction of excitation from atria to ventricles amounted to 38.10±2.57 ms under baseline. PR remained constant after epi/caff stimulation with a value of 38.19±1.04 ms. QT characterizes the interval from depolarization to repolarization of the ventricles. Likewise, no difference existed between QT interval at baseline with 31.76±1.23 ms and QT after the epi/caff bolus with 31.31±1.62 ms. Thus, PR and QT intervals were within the physiological range under resting conditions and after epi/caff challenge, respectively. As expected, RyR2$^{WT/WT}$ mice did not display arrhythmia in response to β-adrenergic stress.

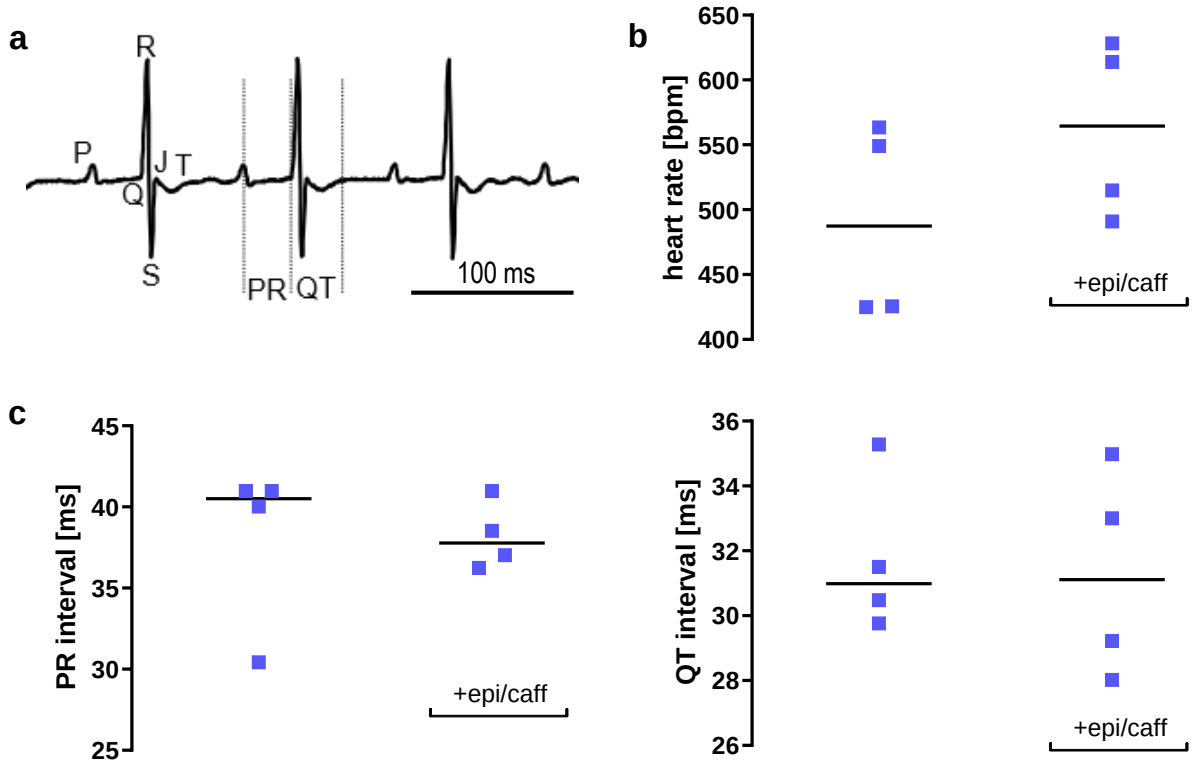

Fig. 25 Efsevin exerts no adverse effects in RyR2$^{WT/WT}$ mice *in vivo*.

(a) ECG recording in RyR2$^{WT/WT}$ mice (n=2) depicting the consecutive phases of conduction throughout the murine heart. The PR interval represents the conduction of excitation from atria to ventricles and QT characterizes the interval from depolarization to repolarization of the ventricles. (b) Under administration of efsevin, HR (in bpm) was maintained at a physiological level described for untreated anaesthesized mice. (c) PR and QT intervals were also within the physiological range under resting conditions and after epi/caff challenge, respectively.

Since application of efsevin did not provoke any perilous side effects in WT animals and ECG recordings were comparable to published values, efsevin was tested for its antiarrhythmic potential in CPVT mice. Therefore, $RyR2^{R4496C/WT}$ mice (n=10) of either sex were treated with 62 mg efsevin/kg BW per day at a pump rate of 1 µL/h over a course of 3 days. Mice (n=11) of either sex were equipped with vehicle-loaded pumps and served as a control. Baseline ECG was performed until steady-state was reached (Fig. 26a, normal) followed by a catecholaminergic stress phase. Epi/caff injection evoked VT (Fig. 26a, VT) in all vehicle-treated animals (11/11). Strikingly, application of efsevin resulted in a significant reduction of arrhythmia with only 60 % (6/10) of mice presenting with VT (Fisher's exact test, p=0.0351) (Fig. 26b).

To substantiate the antiarrhythmic potency of enhancing mitochondrial Ca^{2+} uptake *in vivo*, application of kaempferol was carried out as outlined above for efsevin. $RyR2^{R4496C/WT}$ mice (n=11) of either sex were administered with 12 mg/kg BW per day of the MCU agonist kaempferol at a pumping rate of 1 µL/h for 3 days. Notably, the administration of kaempferol could also significantly reduce VTs to 54.5 % (6/11) of $RyR2^{R4496C/WT}$ mice (Fisher's exact test, p=0.0351) (Fig. 26b).

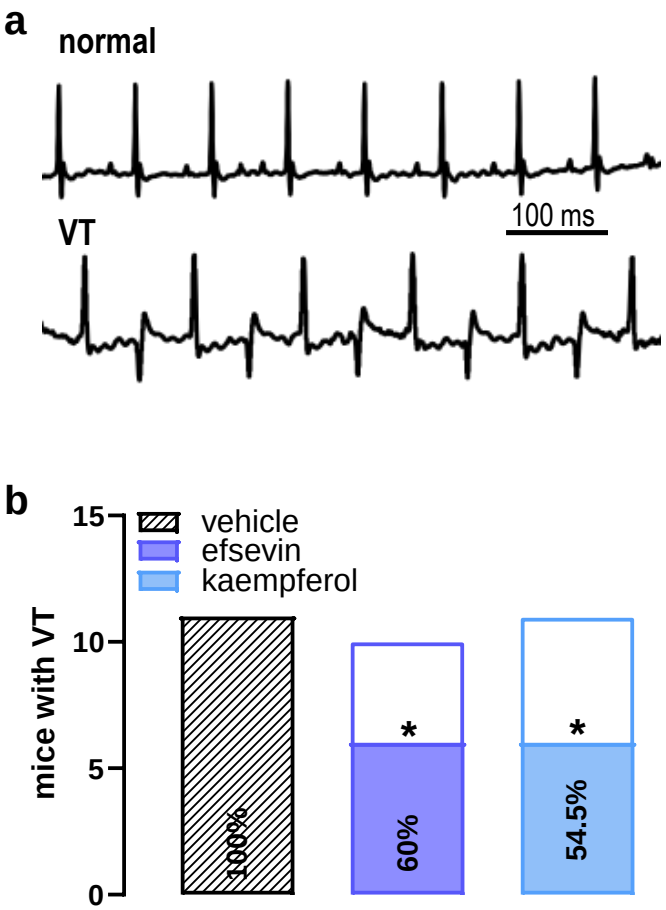

Fig. 26 Administration of MiCUps led to the significant reduction of VT episodes in RyR2$^{R4496C/WT}$ mice.

(a) Representative ECG trace with a physiological sinus rhythm (normal) and bidirectional VT as a hallmark of CPVT (VT). (b) Mice were treated with vehicle (n=11), 62 mg/kg BW per day efsevin (n=10) or 12 mg/kg BW per day kaempferol (n=11) over a course of 3 days. Whereas 100 % (11/11) of vehicle-treated animals presented with VT, the administration of MiCUps could significantly minimize the occurrence of ventricular tachycardia. Under efsevin, only 60 % (6/10) of mice presented with VT and only 54.5 % (6/11) of mice administered with kaempferol were arrhythmic (Fisher's exact test, *$p<0.05$ as compared to vehicle).

4.3.3.1 MiCUps shorten the duration of individual VT episodes

In addition to the occurrence of VT-type arrhythmia, single arrhythmic episodes were further analyzed. ECG traces were evaluated for episode duration, number of VT episodes and episode-free time. The number of single VT episodes was indifferent between the three groups. Whereas

$RyR2^{R4496C/WT}$ mice presented with 2.18±0.44 episodes when treated with vehicle, efsevin-treated animals displayed 4.17±1.30 episodes (Kruskal-Wallis test, p=0.116) and kaempferol-treated mice 3.17±0.87 episodes (Kruskal-Wallis test, p=0.305). In contrast, single VT episodes under MiCUps were of shorter duration resulting in extended periods of normal sinus rhythm which ensure adequate cardiac blood pumping throughout the body. Whereas episodes persisted for 74.69±19.75 s under vehicle-treatment, episode duration was significantly reduced to 25.00±5.85 s by efsevin (Kruskal-Wallis test, p=0.015). A similar, but not significant trend was observed for kaempferol with a mean episode length of 44.28±10.65 s (Kruskal-Wallis test, p=0.656 compared to vehicle) (Fig. 27a). The interval of episode-free time was unchanged by efsevin or kaempferol and closely resembled the VT episode-free time in vehicle-treated animals (Fig. 27b). Whereas in vehicle-treated mice, 46.21 % of the recording were episode-free, no VT episodes occurred in 56.16 % of the recording under efsevin (Fisher's exact test, p=1.000). With kaempferol, 50.85 % of the recording were devoid of VT episodes (Fisher's exact test, p=0.5708). Summarizing the above, application of efsevin and kaempferol led to a reduced number of mice manifesting VT-like arrhythmia. Furthermore, administration of both MiCUps diminished the length of single episodes. Even though a trend towards a longer episode-free time can be seen under MiCUp treatment, the difference was not significant.

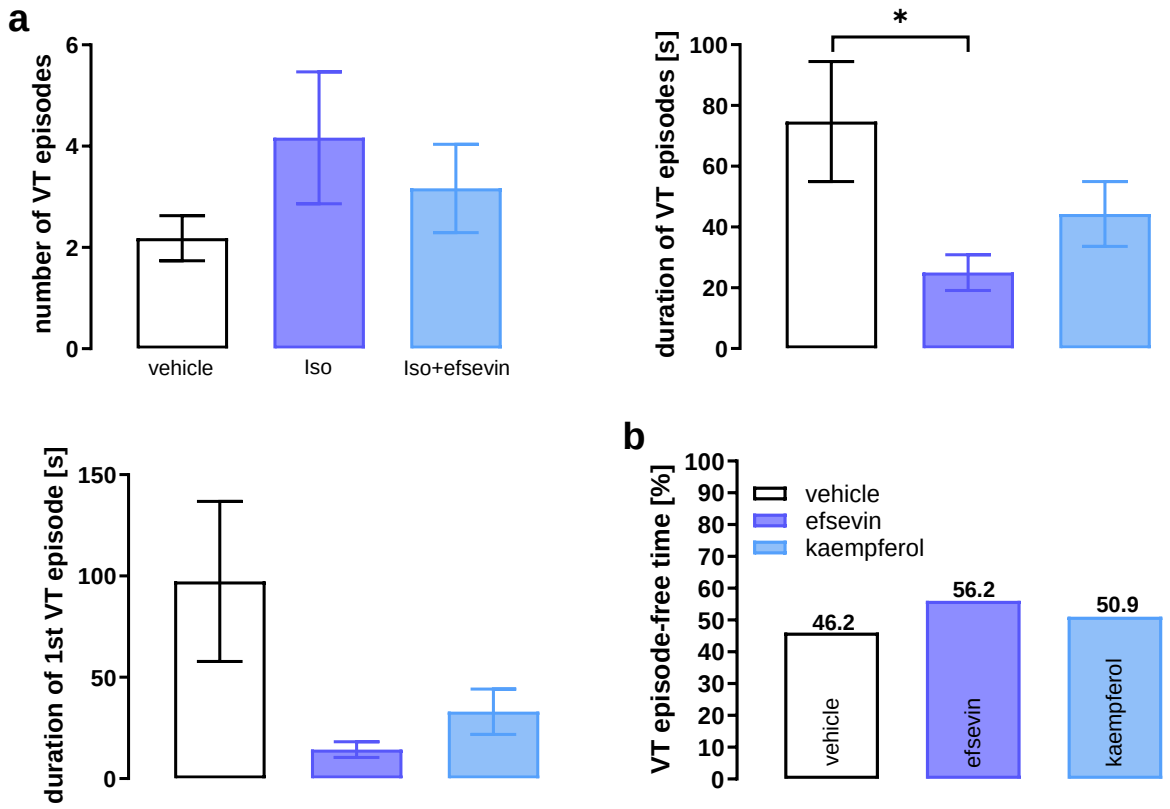

Fig. 27 Administration of MiCUps did not alter the amount of VT episodes but reduced their duration in RyR2$^{R4496C/WT}$ mice.

(a) No significant change in the number of single VT episodes was observed. Yet, both MiCUps shortened the duration of individual episodes with a more pronounced effect exerted by efsevin (Kruskal- Wallis test, *p<0.05). Analogously, under MiCUp treatment there was a clear trend towards a shortened first VT episode. (b) The interval of VT episode-free time was unaltered by MiCUPs.

4.3.3.2 Physiological sinus rhythm is unaffected by MiCUps

In light of a future human application, even minor side effects on normal sinus rhythm *in vivo* could be detrimental. Therefore, we examined ECGs of efsevin- and kaempferol-treated mice for a potential impact of MiCUps on HR (Fig. 28a) and conduction parameters (Fig. 28b) at rest and under catecholaminergic stress. Both, efsevin and kaempferol did not influence HR at rest: vehicle-treated mice (n=11) had a HR of 485.32±24.70 bpm at baseline, while HR amounted to

454.39±21.02 bpm in animals treated with efsevin (n=10; one-way ANOVA, p=0.338 compared to vehicle) and to 455.38±13.80 bpm in kaempferol-treated animals (n=11, one-way ANOVA, p=0.337 compared to vehicle). The same was observed for HR following β-AR stimulation. HR stood at 605.92±24.86 bpm in vehicle-administered control animals after epi/caff challenge. HR in MiCUp-treated animals did not significantly deviate from this value with 637.96±24.94 bpm for efsevin treated animals (one-way ANOVA, p=0.316) and 640.62±22.04 bpm for kaempferol-treated mice (one-way ANOVA, p=0.267), respectively. We further quantified parameters of cardiac conduction and found no significant changes in the conduction of excitation from atria to ventricles (PR) or the interval from excitation to repolarization of the ventricles (QT) in animals treated with MiCUps. The PR interval was 32.14±2.12 ms in vehicle-treated animals, 34.10±0.88 ms in the efsevin group (Kruskal-Wallis test, p=0.871) and 32.66±2.22 ms in animals treated with kaempferol (Kruskal-Wallis test, p=0.596). Also, there was no impact of MiCUps on PR under catecholaminergic stress. PR interval was 30.01±2.02 ms in the vehicle-treated group, 32.20±0.79 ms under efsevin (Kruskal-Wallis test, p=0.919) and 31.22±2.50 ms in the kaempferol-treated mice (Kruskal-Wallis test, p=0.187). At baseline, QT interval was 48.55±3.18 ms in vehicle-treated animals, 51.72±2.55 ms under efsevin (Kruskal-Wallis test, p=0.377) and 46.81±3.21 ms in mice receiving kaempferol (Kruskal-Wallis test, p=0.234). Also after epi/caff challenge, MiCUps did not influence the QT interval standing at 46.48±3.77 ms under vehicle conditions, at 53.08±0.71 ms in efsevin-treated mice (Kruskal-Wallis test, p=0.264) and at 50.99±3.55 ms under kaempferol (Kruskal-Wallis test, p=0.188). Thus, both MiCUps did not exert significant effects on normal sinus rhythm in $RyR2^{R4496C/WT}$ mice.

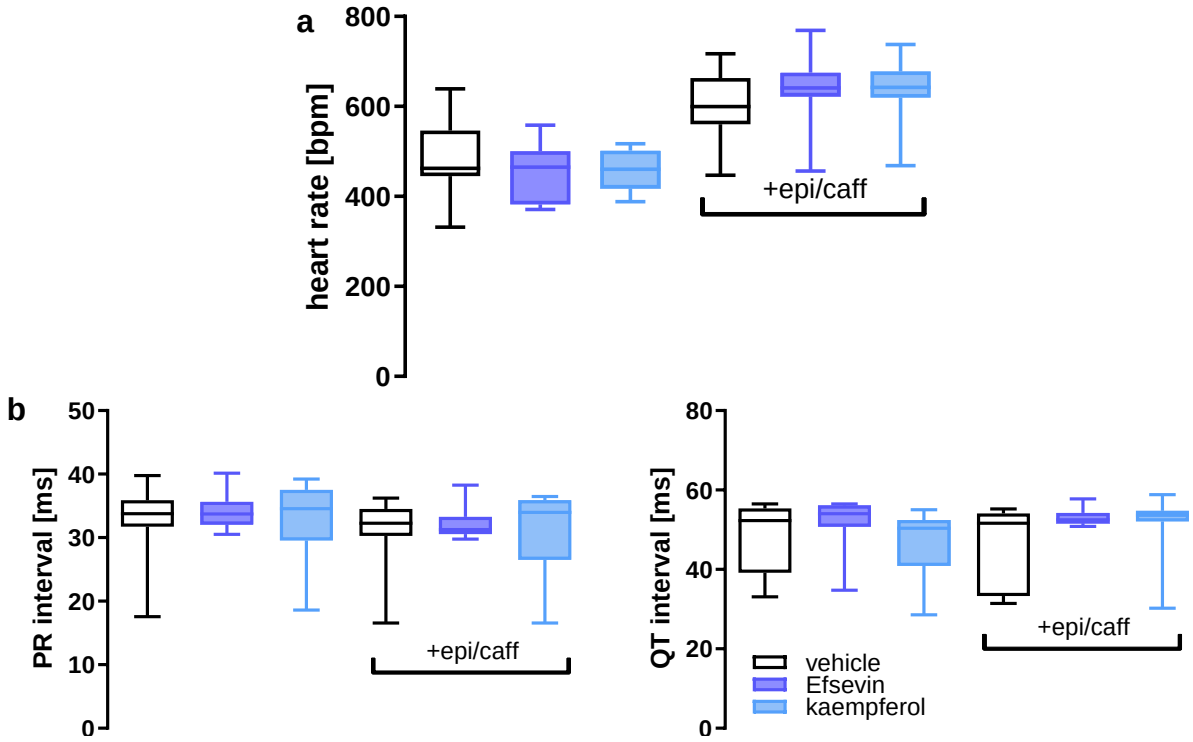

Fig. 28 MiCUps maintained a physiological sinus rhythm and cardiac conduction *in vivo* at baseline and under stress conditions.

Box-plot diagrams represent minimum, first quartile, median, third quartile and maximum of data obtained from RyR2$^{R4496C/WT}$ mice treated with vehicle (n=11), kaempferol (n=11) or efsevin (n=10), respectively. (a) Administration of 62 mg/kg BW efsevin or 12 mg/kg BW kaempferol had no effect on HR (in bpm). (b) Also, both MiCUps did not alter murine PR and QT intervals (both in ms).

4.3.4 Long-term application of efsevin causes no side effects in RyR2$^{R4496C/WT}$ mice

In the aforementioned *in vivo* experiments, MiCUps were delivered to RyR2$^{R4496C/WT}$ mice over a course of 3 days. Whereas kaempferol has been proven to be safe for the use in different animal models also in long-term experiments[207–209], no *in vivo* study existed for the novel substance efsevin prior to the present experiments. Hence, we employed a different minipump model to administer efsevin for a period of 8 days to identify potential side effects occurring

during long-term treatment. Administration of 15 mg/kg BW per day efsevin for 8 days in WT mice revealed no harmful side effects on systolic parameters (Fig. 25). Long-term treatment was performed with 15 mg/kg BW per day of efsevin in $RyR2^{R4496C/WT}$ mice (n=10) of either sex with an average weight of 22.84±0.61 g. $RyR2^{R4496C/WT}$ mice (n=10) with an average weight of 21.98±0.57 g were administered with vehicle and served as a control. Baseline ECG in vehicle- and efsevin-treated mice was performed until steady-state was reached. Afterwards, mice were injected with epi/caff as a stress bolus. Basal HR in vehicle-treated animals amounted to 445.96±22.36 bpm and to 513.97±26.79 bpm in efsevin-treated animals (one-way ANOVA, p=0.078). Under β-AR stimulation one can clearly appreciate a significantly faster HR. HR standing at 622.04±12.46 bpm in vehicle-treated mice was unaltered with 637.35±37.87 bpm in efsevin-treated mice (one-way ANOVA, p=0.685) (Fig. 29a). Also, efsevin showed no impact on PR or QT intervals here (Fig. 29b). Whilst under basal conditions in efsevin-treated mice, PR amounted to 37.16±0.49 ms, this value remained relatively stable at 35.92±0.96 ms after β-AR stimulation. Both values were highly comparable to 38.70±1.20 ms (one-way ANOVA, p=0.394) in vehicle-treated animals under baseline and to 35.46±0.87 ms after epi/caff injection (one-way ANOVA, p=0.800). In accordance with this, QT with and without catecholaminergic stress was not significantly altered by efsevin. QT under resting conditions amounted to 32.67±0.80 ms in vehicle-treated animals and to 31.30±0.93 ms with efsevin, respectively (one-way ANOVA, p=0.445). Likewise, QT intervals were comparable in both treatment groups after epi/caff administration with a value of 32.18±1.43 ms in vehicle-treated and of 32.17±1.65 ms in efsevin-administered mice, respectively (one-way ANOVA, p=0.996). Conclusively, administration of efsevin also for 8 days induced no significant side effects on ECG parameters in WT and CPVT mice. As an important vital parameter, body weight was not affected over the

whole period of efsevin-treatment and mice showed normal behavior and activity (Fig. 12c). Also, post-mortem examination of liver or heart weight yielded no difference between vehicle- and efsevin-treated animals. Interestingly, the treatment of mice with efsevin for 8 days revealed an antiarrhythmic trend similar to what was obtained after application of efsevin for 3 days (Fig. 29c). Stress boli with epi/caff evoked VT in 80 % (8/10) of vehicle-treated animals. Again, application of efsevin led to only 50 % (5/10) of RyR2$^{R4496C/WT}$ mice presenting with arrhythmia, which is, although not statistically significant, consistent with previous results (Fisher's exact test, p=0.350).

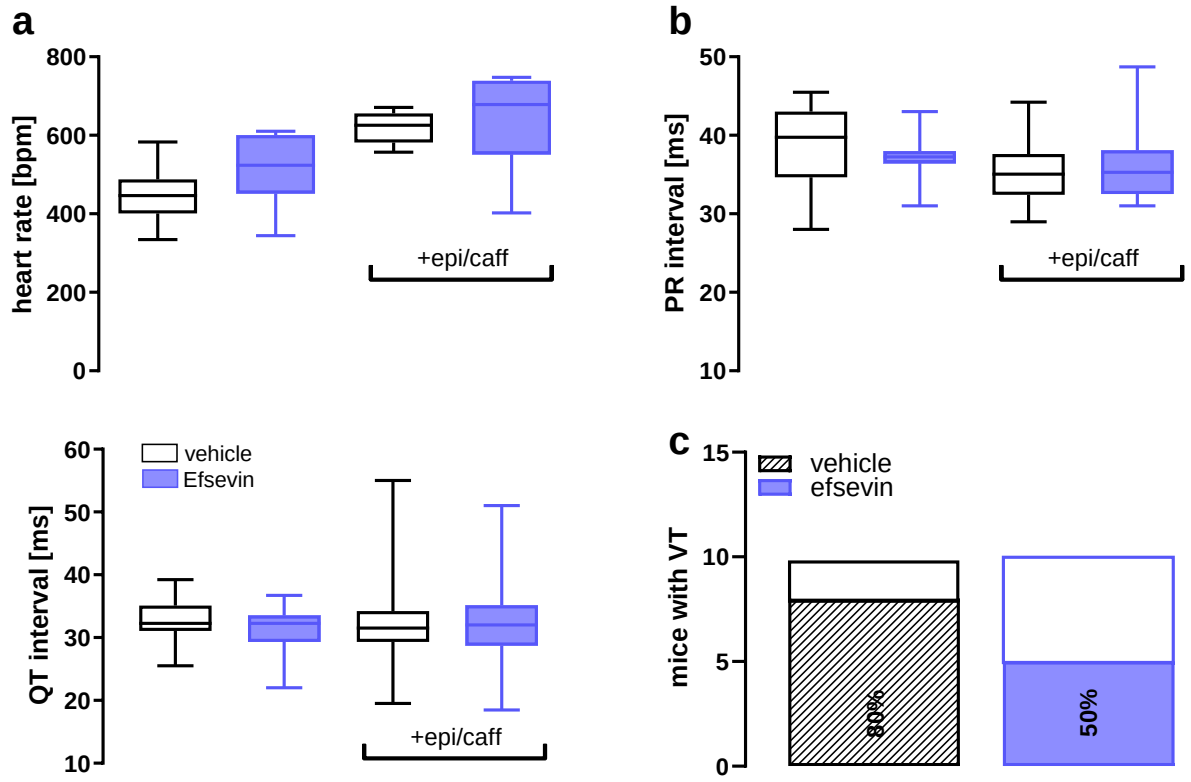

Fig. 29 Long-term treatment with efsevin at a concentration of 15 mg/kg BW per day revealed no adverse effects on ECG parameters and showed a trend towards reduction of VT *in vivo* in RyR2$^{R4496C/WT}$ mice.

(a) Treatment with efsevin for 7 consecutive days did not alter HR (bpm) in RyR2$^{R4496C/WT}$ mice. (b) Analogously, efsevin had no effects on PR and QT intervals of vehicle- (n=10) and efsevin-treated animals (n=10; both in ms). (c) Whereas 80 % of untreated animals exhibited VT, arrhythmia was only observed in 50 % of MiCUp-treated mice (Fisher's exact test, p=0.350).

4.4 MiCUps also suppress spontaneous Ca^{2+} waves in human iPSC-derived CPVT cardiomyocytes *in vitro*

The antiarrhythmic potency of MiCUps in mice not only *in vitro* but also *in vivo* makes the enhancement of mitochondrial Ca^{2+} uptake a highly promising candidate strategy for a future use in human arrhythmia patients. Therefore it is of paramount importance to confirm the efficacy of MiCUps in a human arrhythmia model. We used iPSC-derived cardiomyocytes from two CPVT patients who have been treated at Klinikum Rechts der Isar, Munich and investigated arrhythmogenic Ca^{2+} signals in these cells. First, cardiomyocytes were differentiated from iPSCs derived from a skin biopsy from a 24-year old patient with a familial history of CPVT[187]. The CPVT-causing mutation was mapped to the RyR locus. Hence, $RyR2^{S406L/WT}$ cardiomyocytes served as a model for RyR2-linked CPVT, comparable to the $RyR2^{R4496C/WT}$ mouse used previously in this thesis. Despite the S406L mutation being located in a different region of RyR2, the dysfunctional channel is likewise causative for spontaneous Ca^{2+} waves and APs. Cells from a 32-year old healthy donor served as a control. Analogous to the experiments in 4.1.2, we analyzed spontaneous diastolic Ca^{2+} waves in iPSC-derived cardiomyocytes (Fig. 30a). In line with the manifestation of VT in human patients only under catecholaminergic stimulation, $RyR2^{S406L/WT}$ cardiomyocytes (n=10 cells, N=15 preparations) exhibited only 0.37±0.37 waves x min^{-1} under vehicle conditions, while treatment with the β-adrenergic receptor agonist Iso evoked an increased number of 3.78±0.72 waves x min^{-1} (Kruskal-Wallis test, $p<0.0001$) in CPVT cardiomyocytes (n=18, N=5). Remarkably, β-adrenergically stressed cells administered with 15 µM efsevin (n=18, N=14) displayed a significant reduction of potentially arrhythmogenic Ca^{2+} waves to only 0.15±0.15 x min^{-1} (Kruskal-Wallis test, $p<0.0001$). The amount of waves was indistinguishable from vehicle (Kruskal-Wallis test, $p=0.888$). Similarly, treatment of stressed

cells with kaempferol (n=19, N=9) drastically diminished diastolic waves to 0.21±0.15 waves x min^{-1} as compared to Iso alone (Kruskal-Wallis test, $p<0.0001$), a value again undistinguishable from that under vehicle treatment (Kruskal-Wallis test, p=0.982) (Fig. 30b). In $RyR2^{S406L/WT}$ cardiomyocytes MiCUp treatment also restricted the occurrence of arrhythmogenic Ca^{2+} events to a smaller subpopulation of cells (Fig. 30c). In the vehicle control, diastolic waves occurred in only 9.10 % (1/11) of the cardiomyocytes. Whereas 77.78 % (14/18; Fisher's exact test, p=0.001) of Iso-stressed cells showed diastolic waves, only 7.69 % (1/13) of cardiomyocytes concurrently administered with Iso and efsevin exhibited waves (Fisher's exact test, p=0.0002). Likewise, treatment of stressed cells with kaempferol drastically reduced waves to only 10.53 % (2/19) of cardiomyocytes (Fisher's exact test, p=0.0001), a value comparable to the vehicle control. Cardiomyocytes from the healthy donor showed only a negligible amount of diastolic arrhythmogenic events under all observed conditions. The cells displayed no Ca^{2+} waves under control conditions (n=8, N=5) and after application of efsevin (n=7, N=5) or kaempferol (n=7, N=6). Iso-treated cardiomyocytes (n=20, N=7) also exhibited only 0.05±0.05 waves x min^{-1}, an amount statistically indifferent from vehicle (Kruskal-Wallis test, p=0.801). In control cells, Iso did not evoke Ca^{2+} waves evident by a fraction of only 5.00 % (1/20) of Iso-treated wave-positive cardiomyocytes and no waves (0/8) were evident in the vehicle control (Fisher's exact test, p=1.000). Likewise, no waves were observed under treatment with efsevin (0/7; Fisher's exact test, p=1.000) and kaempferol (0/7; Fisher's exact test, p=1.000).

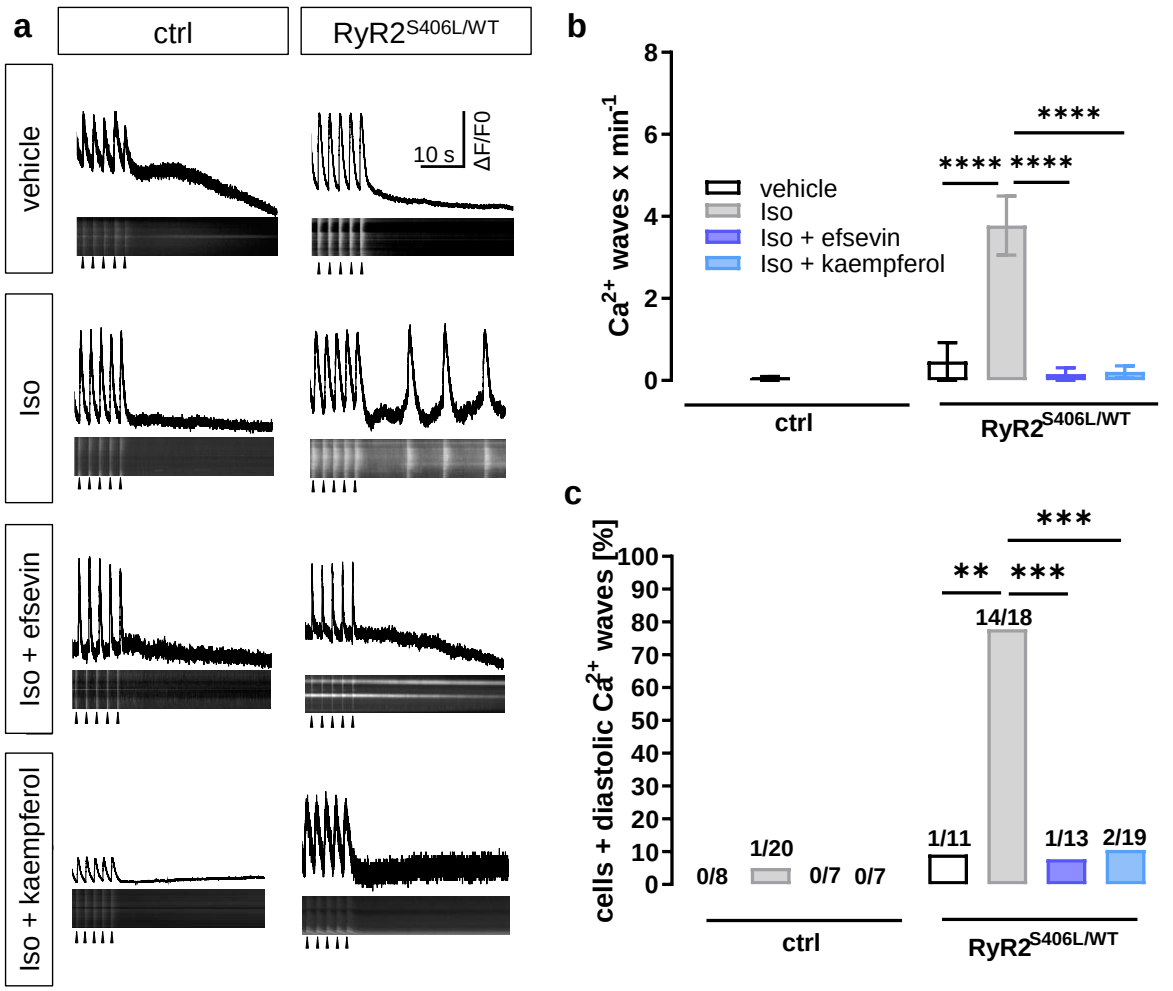

Fig. 30 MiCUps reduce spontaneous Ca^{2+} waves in $RyR2^{S406L/WT}$ cardiomyocytes.

(a) Confocal linescan images and fluorescence intensity plots of an entire cardiomyocyte are presented under the three different treatment conditions. The last five triggered Ca^{2+} transients are shown (black arrowheads). (b) The average of waves x min^{-1}±SEM is displayed for the different treatment conditions. Ctrl myocytes obtained from a healthy donor not susceptible to β-AR mediated arrhythmogenesis displayed only a negligible number of waves under Iso application. In contrast, Iso treatment triggered significantly more waves in $RyR2^{S406L/WT}$ cells (Kruskal-Wallis test, ****p<0.0001). Efsevin (Kruskal-Wallis test, ****p<0.0001) and kaempferol (Kruskal-Wallis test, ****p<0.0001) drastically abolished waves in CPVT cells. (c) Bar graphs illustrate the proportion of cells presenting with diastolic Ca^{2+} waves among all cells examined. Numbers above the bars represent wave-positive cardiomyocytes in relation to all myocytes examined. Whereas ctrl cardiomyocytes showed almost no waves under any tested condition, MiCUp treatment could significantly restrict diastolic waves to a small subset of $RyR2^{S406L/WT}$ cells. As compared to 77.78 % of CPVT cardiomyocytes displaying Ca^{2+} waves following application of Iso, efsevin restricted waves to 7.69 % (Fisher's exact test, ***p<0.001) and kaempferol to 10.53 % of myocytes (Fisher's exact test, ***p<0.001).

Similarly, we also tested iPSC-derived cardiomyocytes from a 60-year-old male patient presenting with severe arrhythmia phenotypically consistent with clinical signs of CPVT. However, despite being subjected to screens of loci of the canonical mutational hotspots in CaM, RyR and Casq, the underlying mutation remains elusive. These cells are hereinafter described as $CPVT^{unknown}$. We investigated spontaneous diastolic Ca^{2+} waves analogously to experiments stated above for $RyR2^{S406L/WT}$ cardiomyocytes (Fig. 31a). The identical healthy donor cardiomyocytes as in Fig. 30 served as a healthy control. $CPVT^{unknown}$ cardiomyocytes (n=11, N=2) displayed no spontaneous Ca^{2+} waves under vehicle and in accordance with the patients' phenotype, myocytes (n=15, N=13) revealed a significant increase in diastolic Ca^{2+} events to 5.87±1.80 waves x min^{-1} under Iso (Kruskal-Wallis test, $p<0.0001$). Strikingly, MiCUps could reduce waves also in cardiomyocytes of this CPVT model. While efsevin significantly reduced waves in CPVT cells (n=17, N=2) to 0.12±0.12 x min^{-1} (Kruskal-Wallis test, $p<0.0001$), the administration of kaempferol completely blocked waves in $CPVT^{unknown}$ myocytes (n=18, N=11; Kruskal-Wallis test, $p<0.0001$) (Fig. 31b). In $CPVT^{unknown}$ cardiomyocytes MiCUp treatment also restricted the occurrence of arrhythmogenic Ca^{2+} events to a smaller subpopulation of cells. 9.10 % (1/11) of vehicle-treated $CPVT^{unknown}$ cardiomyocytes displayed spontaneous Ca^{2+} waves. Administration of Iso induced waves in a significantly enlarged subset of 53.30 % (8/15) of myocytes (Fisher's exact test, $p=0.036$). Again, efsevin was able to restrict diastolic waves to only 5.90 % (1/17) of myocytes (Fisher's exact test, $p=0.005$) and kaempferol even completely suppressed these proarrhythmic events (0/18; Fisher's exact test, $p=0.0005$) (Fig. 31c). In summary, MiCUps not only limited the number of wave-positive $CPVT^{unknown}$ cardiomyocytes to a value indifferent from vehicle. Additionally, both substances significantly suppressed or even completely abolished the amount of waves x min^{-1} in these cells.

Conclusively, both MiCUps were able to reset the number of wave-positive cells as well as the amount of waves x min^{-1} to values comparable to the control level in cardiomyocytes derived from two different CPVT-patients. These findings undermine that MiCUps indeed exert their antiarrhythmic effect also in a human CPVT model

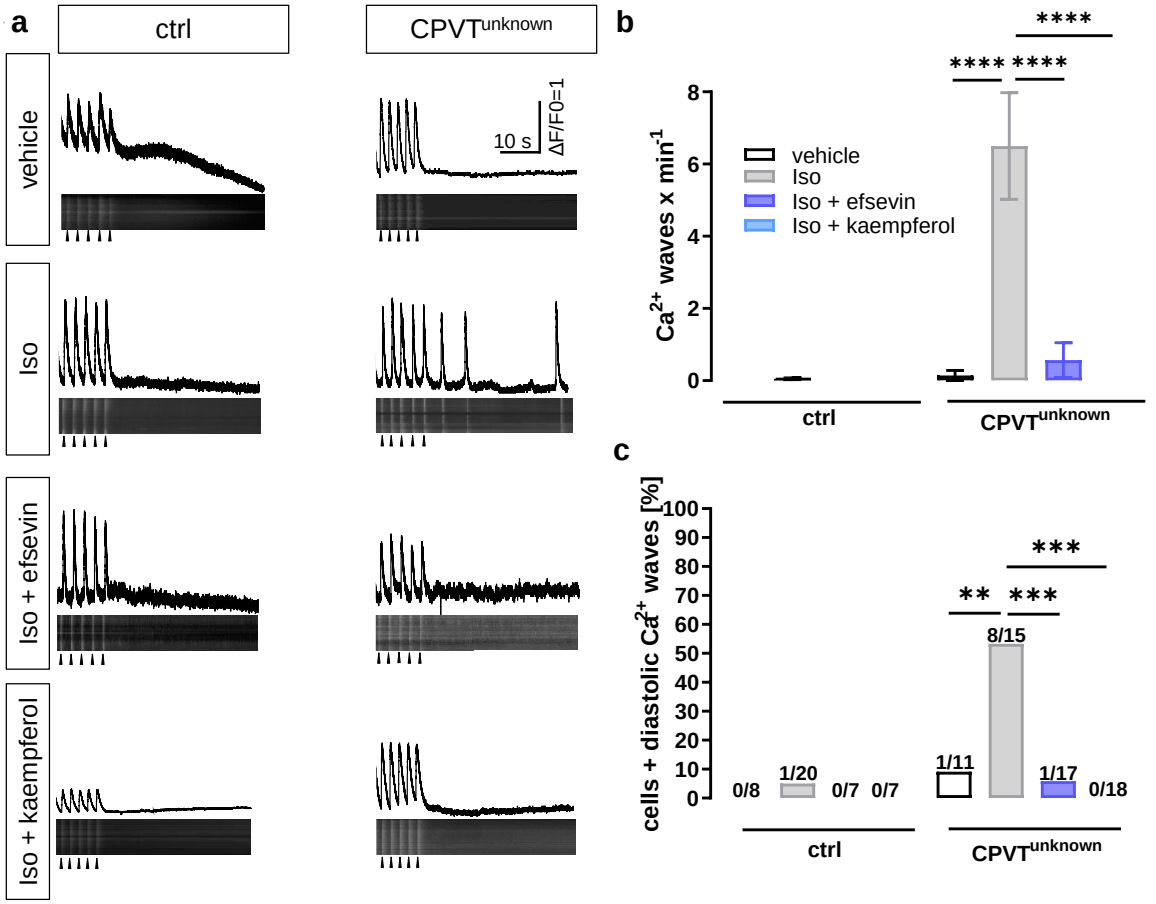

Fig. 31 MiCUps abolish spontaneous Ca^{2+} waves in $CPVT^{unknown}$ cardiomyocytes.

(a) Confocal linescan images and fluorescence intensity plots of entire cardiomyocytes are presented under the three different treatment conditions. The last five triggered Ca^{2+} transients are shown (black arrowheads). (b) The average of waves x min^{-1}±SEM is displayed for the different treatment conditions. Whereas only a negligible amount of waves occurred under vehicle treatment, application of Iso significantly increased the amount of waves in $CPVT^{unknown}$ cardiomyocytes, susceptible to β-AR mediated arrhythmogenesis (Kruskal-Wallis test, ****$p<0.0001$). Efsevin (Kruskal-Wallis test, ****$p<0.0001$) and kaempferol (Kruskal-Wallis test, ****$p<0.0001$) drastically reduced waves in $CPVT^{unknown}$ cells. (c) Bar graphs illustrate the proportion of cells presenting with diastolic Ca^{2+} waves among all cells examined. Numbers above the bars represent wave-positive cardiomyocytes in relation to all myocytes examined. Whereas ctrl cardiomyocytes showed almost no waves under any tested

condition, MiCUp treatment could significantly restrict diastolic waves to a small subset of $CPVT^{unknown}$ myocytes. Whereas under application of efsevin, only 5.90 % of cells exhibit spontaneous waves as compared to 53.30 % of Iso-treated cardiomyocytes (Fisher's exact test, $^{**}p<0.01$), kaempferol completely suppressed waves (Fisher's exact test, $^{***}p<0.001$).

5. DISCUSSION

5.1 Mitochondria as "fire extinguishers" in the arrhythmogenic setting

In contrast to the well-established β-AR agonist Iso and the adenylate cyclase activator FSK, efsevin did not alter cellular cAMP levels. These findings unequivocally demonstrated that a modulation of β-adrenergic signaling could not be allocated as a mechanism of the antiarrhythmic effect of efsevin. In addition, an effect of efsevin on adrenergic receptors can be reliably precluded by the evaluation of murine ECG traces. The RR interval was unchanged by efsevin whereas the commonly used antiadrenergic propranolol significantly slowed RR in a previous study[125]. Additionally, RMP is unchanged in patch-clamped cardiomyocytes under administration of efsevin which led us to conclude that a RMP-decrease can also be precluded as an antiarrhythmic mechanism. Taken together, we infer that the antiarrhythmic effect of efsevin could indeed be ascribed solely to its binding to VDAC2 and thus to enhanced Ca^{2+} uptake into mitochondria. Due to their ability to employ Ca^{2+} concentrations greatly exceeding those that mitochondria are generally facing in a healthy cell, the removal of excess Ca^{2+} from the cytosol was concluded to be a major role of these organelles[67]. Consistent with this, Zhao et al. suggest that the local Ca^{2+} level in the microdomain close to the RyRs is controlled by mitochondrial Ca^{2+} release and uptake[180] whereby an increase of $[Ca^{2+}]$ in the vicinity of mitochondria leads to a reversible accumulation of Ca^{2+} [72]. However, the roles of mitochondria and Ca^{2+} in arrhythmia are still controversially discussed in literature: Do mitochondria exert a preventive role or do they act as a proarrhythmic sink? To further complicate matters, different studies found both an enhanced and a reduced $[Ca^{2+}]_m$ to be effective therapeutic strategies

for the elimination of arrhythmia in CVDs[210]. We observed a cardioprotective role of pharmacologically increased mitochondrial Ca^{2+} uptake, which is to our knowledge the first time this was shown in arrhythmia *in vivo*. Our results clearly argue in favor of a preventive role of mitochondria as "fire extinguishers" in the arrhythmogenic setting of CPVT and establish pharmacological activation of rapid mitochondrial Ca^{2+} uptake as a novel therapeutic strategy. This hypothesis is further substantiated by the fact that the inhibition of mitochondrial Ca^{2+} uptake with Ru_{360} abrogated the suppressive effect of efsevin on spontaneous Ca^{2+} waves. The number of waves in R4496C cardiomyocytes treated with efsevin was indifferent from the amount of waves in myocytes treated with Iso alone indicating that efsevin lacks its antiarrhythmic potency under blockade of mitochondrial Ca^{2+} uptake. Consistent with this, Seguchi et al. observed an increase in spontaneously propagating Ca^{2+} waves induced by blocking mitochondrial Ca^{2+} uptake with Ru_{360}[181]. Over the course of our Ru_{360}-experiments, numerous $RyR2^{R4496C/WT}$ cardiomyocytes showed very excessive spontaneous activity when treated with Iso and Ru_{360}. This means that in the setting of CPVT, a non-functioning Ca^{2+} buffering into mitochondria under catecholaminergic stress causes extreme harm to the cells which react with excessive arrhythmia. Thus, enhanced Ca^{2+} uptake into mitochondria might ensure that excess Ca^{2+} from the cytosol that would otherwise favor arrhythmogenic signals propagating throughout the cell, is buffered into mitochondria. The fact that in our study under Iso, the amount of waves is indistinguishable with and without Ru_{360}, could lead to the distorted picture that the addition of the MCU-blocker exerts no effect. Yet, the addition of Ru_{360} triggers a mere burst of arrhythmic Ca^{2+} events in cardiomyocytes pretreated with Iso so that these cells did not meet our pre-defined criteria for evaluability: Only myocytes that develop systolic Ca^{2+} transients in reaction to stimulation, but concomitantly are quiescent when unstimulated,

were included in the analysis. Hence, cardiomyocytes meeting these criteria seem to have a rather low arrhythmic "preload" thus exhibiting less waves. Further, the fact that Ru_{360}-treated myocytes showed an increased amount of waves per min already under vehicle conditions substantiates the notion that indeed a blockade of Ca^{2+} uptake into mitochondria by Ru_{360} could cause serious damage to cardiomyocytes and that reduced mitochondrial Ca^{2+} uptake is proarrhythmic. Further studies clearly substantiate the role of mitochondria as "high-capacity sinks that are placed on the way of a propagating Ca^{2+} wave" and that clear Ca^{2+} in restricted microdomains[211]: kaempferol reduced FCCP-induced waves and spontaneos APs in murine cardiomyocytes and an increase of mitochondrial Ca^{2+} release was sufficient to elicit APs thus increasing arrhythmogenicity. Consistently, the Peuchen group observed that in astrocytes the rate of propagation of cytosolic Ca^{2+} waves was limited by mitochondrial Ca^{2+} uptake[212]. Further, the propagation of cytosolic Ca^{2+} was restricted by a „firewall" of mitochondria located in the center of pancreatic acinar cells[213]. In line with this, an inhibition of mitochondrial Ca^{2+} uptake by carbonyl cyanide m-chlorophenyl hydrazone augmented Ca^{2+} waves[214]. A study by Liu and O'Rourke in a HF model demonstrated that MCU overexpression inhibited arrhythmia *in vivo* as well as substantially reduced the amount of PVCs[215]. Another study even demonstrated that a restored mitochondrial Ca^{2+} accumulation prevented from SCD[215], all clearly arguing in favor of a preventive role of mitochondrial Ca^{2+} uptake in the arrhythmogenic setting.

5.2 The fate of Ca^{2+} after enhanced mitochondrial uptake

Mitochondrial Ca^{2+} is a pleiotropic signal with a delicate balance existing between its positive and negative effects. Whereas insufficient mitochondrial Ca^{2+} uptake in the heart can compromise the matching between energy supply and demand and the scavenging capacity of ROS, Ca^{2+} overloaded mitochondria might react with excessive ROS production triggering mPTP opening[215], a collapse of the mitochondrial membrane potential and apoptosis[216,217]. Mitochondria with an excessive and persistent Ca^{2+} overload react with apoptosis. For instance, kaempferol was shown to exert its beneficial effect via an induction of apoptosis as an anti-cancer drug[218,219] albeit it seemingly preserves normal cell viability in some cases exerting a protective effect[216]. Intriguingly, cardiomyocytes seem not to suffer from an increase in apoptosis under enhanced mitochondrial Ca^{2+} uptake mediated by MiCUPs, even though we cannot completely preclude this possibility by experiments in adult murine cardiomyocytes due to their transitory nature. Although few studies demonstrate a long-term culture[217], freshly isolated adult murine cardiomyocytes are known to degenerate and cannot be kept overnight in contrast to rat myocytes. Thus, we discarded myocytes immediately after each experiment, making it impossible to observe apoptotic events that might occur afterwards. However, previous experiments from our lab suggest that apoptosis is not the method of choice for mitochondria to deal with enhanced Ca^{2+} concentrations induced by MiCUp treatment: Neither the treatment of zebrafish embryos with efsevin for 26 hours nor an overexpression of VDAC2 did increase apoptosis as analyzed by TUNEL assays as well as acridine orange staining[181]. Further, HL-1 cells did not show any adverse effects by long-term treatment with efsevin (Fabiola Wilting, unpublished).

Likewise, we can exclude mPTP formation resulting from MiCUp treatment with great certainty. Although persistent mitochondrial Ca^{2+} overload is a prerequisite for an opening of the mPTP, ROS and Ca^{2+} both are essential for this process[220]. This is in line with the "two-hit" hypothesis developed by Brookes et al. in which it takes two concurrent stimuli to turn Ca^{2+} from a physiological to a pathological effector to bring about mitochondrial dysfunction and mPTP opening is exclusively triggered by a combination of high Ca^{2+} and ROS instead of excess Ca^{2+} alone[221]. In fact, a vicious cycle exists where sustained mitochondrial Ca^{2+} uptake leads to an increase in ROS levels triggering mitochondrial Ca^{2+} overload, mPTP and cell death[222]. Thus, the switch of mitochondrial Ca^{2+} uptake from a "useful" physiological mechanism to the pathophysiological state of mPTP opening and cell death seems to require oxidative stress as a prerequisite and a major part of data pointing to a negative role of increased mitochondrial Ca^{2+} were entirely collected in the setting of a simultaneous increase in ROS. In contrast, results from our group demonstrated that efsevin enhanced mitochondrial Ca^{2+} uptake without an increase in global ROS in HL-1 cells (Eliane Klein, unpublished) whereby the absolute prerequisite for mPTP and cell death is not met.

Apart from the scenario that another harmful stimulus is missing in our case of MiCUp treatment in CPVT, we reasonably believe that the Ca^{2+} equilibrium is not severely or only transiently perturbed. It is thus logical to assume that under MiCUp treatment, enhanced Ca^{2+} uptake is not sustained long enough to cause a "real", persistent Ca^{2+} overload situation that would mean harm to mitochondria or even lead to apoptosis, mPTP opening or a depolarization of $\Delta\Psi_m$. Thus, another strategy is seemingly existent to dispose of the excess Ca^{2+} from mitochondria so that physiological Ca^{2+} concentrations are sustained for proper cellular functions. For maintained physiological sinus rhythm, Ca^{2+} that enters mitochondria

following each Ca^{2+} transient, has to be extruded before the subsequent transient to prevent mitochondria from the perilous state of Ca^{2+} overload. Following this logic, Ca^{2+} influx must equal its extrusion. Therefore, it seems very likely that Ca^{2+} is dissipated by concomitant increase of mitochondrial Ca^{2+} export, meaning the avoidance of mitochondrial Ca^{2+} overload and/or vicious Ca^{2+} cycling across the mitochondrial membrane. In other words, mitochondria only work as a transient buffer with the enhanced Ca^{2+} only temporarily retained inside the organelle in our setting. Alternatively, a reverse transport of Ca^{2+} inside the microdomain (from mitochondria back into the SR) is also quite conceivable. The existence of such a shuttling mechanism of Ca^{2+} from mitochondria back into the SR was previously demonstrated with an implication of NCLX in the Ca^{2+} communication between both organelles[115]. This might suggest that Ca^{2+} is immediately shuttled back from mitochondria into the SR under MiCUp treatment. The assumption of a shuttling from mitochondria back into the SR may also explain why we observe an antiarrhythmic effect without harmful side effects. Previous work from our group (Eliane Klein, unpublished) showed that increased Ca^{2+} uptake under efsevin in HL-1 cells stimulates oxidative phosphorylation. This in turn leads to an augmented ATP production that enhances SERCA activity. This state could further contribute to the antiarrhythmic potential of efsevin since recent work by Fernandez-Tenorio et al. showed that SERCA stimulation reduces the frequency of spontaneous Ca^{2+} waves in murine ventricular myocytes[223]. Another interesting fact is that the A4860G RyR2 mutation causative for an altered Ca^{2+} homeostasis and in turn for CPVT leads to an induction of so-called nanotunneling between mitochondria[224]. While the increase in these long-distance intermitochondrial communications in the setting of cytosolic Ca^{2+} imbalances is unknown, a transport of ions between mitochondria was reported which would allow for an intermitochondrial shifting of Ca^{2+} ions[225]. Work from our group

demonstrated that the increasedly leaked Ca^{2+} by mutated RyR2 is being taken up by mitochondria under MiCUp treatment. We may therefore speculate that the aggrandized amount of nanotunnels formed by mitochondria in the setting of CPVT could serve as a means to distribute the increased amount of uptaken Ca^{2+}. This implies that mitochondria adopt a „problem shared is a problem halved"-strategy to prevent Ca^{2+} overload of individual mitochondria. In line with this, Vincent et al. proposed that nanotunnels were a means of communication for mitochondria to "reach out for help" under stress conditions[225]. Future experiments are thus needed to finally elucidate the whereabouts of Ca^{2+} after enhanced mitochondrial uptake by live cell imaging with concomitant staining and tracing of mitochondrial Ca^{2+}.

5.3 MiCUPs successfully recrute the "firewall" of mitochondria in the arrhythmogenic setting of CPVT

5.3.1 MiCUPs restrict spontaneous Ca^{2+} sparks by modulating multiple parameters in $RyR2^{R4496C/WT}$ cardiomyocytes

In this thesis we have measured spontaneous Ca^{2+} sparks and waves as well as spontaneous APs as a measure of the arrhythmogenic potential of cardiomyocytes from the $RyR2^{R4496C/WT}$ CPVT mouse model. Strikingly, we could demonstrate a suppressive effect of efsevin on all of the aforementioned arrhythmogenic events. As a consequence of altered properties of RyR2 including RyR2 mutations such as the CPVT causing R4496C mutation, cardiomyocytes are prone to spontaneous leak of Ca^{2+} from the SR in the form of Ca^{2+} sparks. This leakage already exists under basal conditions but is drastically aggravated under stress conditions mimicked

by Iso. An increase in spark frequency is associated with an increased risk for arrhythmia. Previous reports demonstrated that downregulation of VDAC2 spatially and temporally extends Ca^{2+} sparks in cultured HL-1 cells as quantified by an increased width and duration of sparks[101,102]. Vice-versa, upregulation of the channel would be expected to narrow sparks. Indeed pharmacological activation of VDAC2 by efsevin was previously shown to induce this effect. Hence, it was postulated that the enhanced Ca^{2+} uptake into mitochondria induced by efsevin leads to an accelerated cytosolic Ca^{2+} clearance and thus a reduced width and duration of Ca^{2+} sparks[181]. Thereby the diffusion of Ca^{2+} inside the cytosol is restricted thus halting the propagation of cytosolic Ca^{2+} signals under Ca^{2+} overload (Fig. 32). Our data clearly support this concept. Also in the present study, treatment with efsevin entailed the spatial and temporal restriction of sparks in the CPVT mouse model. Shimizu et al. concluded that by the acceleration of Ca^{2+} removal from the cytosol in cardiomyocytes, efsevin narrows and temporally shortens local Ca^{2+} sparks with no influence on SR Ca^{2+} load or RyR Ca^{2+} release. However, in our experiments these effects were accompanied by a reduction of spark frequency and spark amplitude in Iso-treated $RyR2^{R4496C/WT}$ cardiomyocytes.

RyR channels in adult ventricular as well as in hIPSC-cardiomyocytes show Ca^{2+} sensitivity[226] and the open probability of a channel is critically dependent on the local $[Ca^{2+}]_c$[227] meaning that the probability to trigger a Ca^{2+} spark is oftentimes not due to increases in either bulk cytoplasmic Ca^{2+} concentration or SR Ca^{2+} content but rather to changes in microdomain Ca^{2+} [228]. Hence any process increasing the local $[Ca^{2+}]$ near the cytoplasmic domain of a RyR increases its open probability and thereby the probability of spark production reflected by a high spark frequency. However, to really trigger a full-blown Ca^{2+} spark, a single RyR first has to recruit multiple near neighbors[229]. Under high microdomain Ca^{2+}, spontaneous Ca^{2+} from

one spark can in turn recruit nearby RyR clusters thereby triggering additional saltatory sparks from the second firing site, RyR2 clusters that are active and fire Ca^{2+} sparks (Fig. 32(A) untreated). This spark-induced spark activation can in turn provoke multiple sparks, called a macrospark[226] by near-synchronous activation of multiple adjacent CRUs[230]. Of note, the channel activity of WT-RyR2 greatly differs from that of RyR2-R4496C in the setting of CPVT [126,231]: RyR2-R4496C is characterized by a hypersensitization to activation by cytosolic Ca^{2+}. Further, RyR2-R4496C is hyperactive meaning $RyR2^{R4496C/WT}$ cardiomyocytes present more firing sites and a greater probability of these clusters to repetitively open. As a result, the spark frequency is doubled in $RyR2^{R4496C/WT}$ cells[126].

A reduction of both Ca^{2+} spark frequency and amplitude underlies the antiarrhythmic principle of several compounds whose mechanism of action is oftentimes based on a direct modulation of RyR2. Flecainide blocks RyR2 in its open state which is reflected in a reduced spark amplitude and spark width[232] whereas tetracaine blocks the open probability[233] and decreases spark frequency[234]. Yet, the fact that kaempferol reduces both spark frequency and amplitude analogously to efsevin makes it rather unlikely that MiCUps directly target RyR2. In this case, two chemically distinct substances at the same time targeting different mitochondrial channels, would both additionally show an off-target effect particularly on RyR2. Yet, since efsevin and kaempferol both target the mitochondrial Ca^{2+} uptake complex, we assume that the effect seen on spark frequency and amplitude is rather caused by their common mechanism of action, enhanced mitochondrial Ca^{2+} uptake. Ca^{2+} overload as in CPVT acts as a constant driving force of RyR's hyperactivity and thereby of arrhythmogenic firing (characterized by an increased frequency of sparks). And this is precisely where MiCUps intervene as game changers (as described in depth in 5.1): Following MiCUp treatment, Ca^{2+} is increasingly aspirated from the

microdomain by mitochondria and as a consequence, less Ca^{2+} would be available in the close vicinity of RyR2-R4496Cs to trigger spark-induced spark activation (Fig. 32(B) MiCUp treatment) explaining the decrease in spark frequency. By resetting the high diastolic Ca^{2+} level in the microdomain back to a more physiological [Ca^{2+}] in the immediate vicinity of hyperactive R4496C-RyR2s, MiCUps cut off these mutated channels from their excess Ca^{2+} supply. In addition to Ca^{2+} spark frequency, the amplitude of a Ca^{2+} spark increases with elevated $[Ca^{2+}]_c$, where rogue Ca^{2+} sparks can activate neighboring CRUs to form higher amplitude macrosparks[230,235]. Vice versa, MiCUp application and mitochondrial Ca^{2+} buffering is followed by a reduced microdomain [Ca^{2+}] where the majority of sparks are of smaller amplitudes as can be appreciated from our experiments. The reduction in amplitude points to a local restriction of sparks then incapable to recruit enough further sparks to eventually trigger a cell-wide propagating Ca^{2+} wave. Apart from an increased spark frequency and amplitude, spark width and duration are important factors that act synergistically to promote spark propagation[40]. As anticipated from our data in Iso-treated $RyR2^{R4496C/WT}$ cardiomyocytes, MiCUps also modulate these factors: less and shorter as well as narrower sparks whirl about in the cytosol. These sparks are being buffered into mitochondria, before they even stand a chance to activate neighboring RyR clusters and thereby to form diastolic Ca^{2+} waves. The reduction of spark frequency and spark amplitude might further contribute to this suppressive effect of efsevin on propagating Ca^{2+} waves and indeed, we could demonstrate an antiarrhythmic effect of efsevin on spontaneous waves. This is in line with findings from Hüser et al. where a narrower spread of Ca^{2+} in PLN-knockout myocytes reduced the capability of one site of SR Ca^{2+} release to activate a neighboring site meaning a "reduced degree of cooperativity" among adjacent SR Ca^{2+} release units which resulted in a reduction of Ca^{2+} waves[227].

In contrast to Shimizu et al. where efsevin had no effect on spark frequency and amplitude, we treated cells with 15 µM efsevin, a concentration that greatly exceeds the 1 µM applied by Shimizu et al.[181]. Thus, a dose-dependent effect on sparks only apparent under the higher concentration in our setting might be quite conceivable. Following this logic, a reduced Ca^{2+} spark frequency as well as a diminished spark amplitude would only become apparent at concentrations somewhere above 1 µM efsevin. As a mechanistic explanation, 15 µM efsevin in our experiments lead to a further enhancement of mitochondrial Ca^{2+} uptake automatically meaning a more drastic reduction of cytosolic Ca^{2+}. Hence, only a few RyR2-R4496C clusters can fire whereby spark frequency is reduced**.** In line with this notion, Shimizu et al. observed that 10 µM of efsevin more effectively reduced spontaneous Ca^{2+} waves than 1 µM.

5.3.2 Efsevin has no effect on spontaneous DADs, the immediate trigger of arrhythmogenic APs

Propagating Ca^{2+} waves triggered by sparks can activate NCX and the electrogenic exchange of one Ca^{2+} ion for 3 Na^{+} ions results in a transient inward current during diastole creating low voltage oscillations[199]. These can trigger APs that ultimately induce ectopic excitations and finally arrhythmia. We analyzed diastolic DADs of amplitudes above or identical to 5 mV during the diastolic phase in patch-clamped $RyR2^{R4496C/WT}$ cardiomyocytes (Fig. 17). The administration of Iso revealed no increase in DADs as compared to vehicle conditions. Interestingly, treatment with 15 µM efsevin did also not alter the amount of DADs ≥5 mV. It is important to note that only suprathreshold DADs are arryhthmogenic to the extent that they might occasionally trigger APs whereas APs themselves represent the severe arrhythmogenic event and are the

final step towards arrhythmia. This becomes particularly obvious by the fact that DADs by themselves are not capable of causing CPVT arrhythmia[158]. In our experiments, efsevin had no effect on low amplitude oscillations of ≥5 mV but significantly reduced spontaneous APs. This suggests that under treatment with efsevin, arrhythmogenic suprathreshold voltage oscillations above a certain threshold (somewhere above 5 mV) that might eventually fire an AP are blocked whereas DADs beneath that threshold (subthreshold DADs) that "cause no further harm" can still fire and erupt. Our hypothesis is further substantiated by the fact that other compounds reliably suppressing APs also show no effect on DADs in the $RyR2^{R4496C/WT}$ mouse model. K201 had no effect on the frequency of DADs[158] and also flecainide completely abolished arrhythmogenic APs but did not suppress DADs[236]. Unfortunately, the authors do not give an indication as to why their substances only affect APs and not DADs. This is presumably due to the fact that subthreshold DADs per se are not arrhythmogenic and that the only important antiarrhythmic measure of a respective substance is a reduction of spontaneous APs.

An APD prolongation promotes DADs by increasing intracellular Ca^{2+} loading[237]. The APD prolongation attributable to efsevin observed in our murine experiments might therefore lead to a slight increase of Ca^{2+} loading. $RyR2^{R4496C/WT}$ cardiomyoycytes already present with a tremendous cytosolic Ca^{2+} overload which can be rescued by efsevin application. However, in a „doubled" Ca^{2+} overload situation as hypothesized in patch-clamped $RyR2^{R4496C/WT}$ cardiomyoycytes, efsevin in the applied concentration might encounter its limits of antiarrhythmic efficacy. Therefore, we observe that efsevin is not able to reduce DADs. More importantly, the amount of DADs is also not increased and a DAD under efsevin application is seemingly less severe which explains the reduced amount of APs. Another possible explanation

for the different impact of efsevin on DADs and APs might lie in efsevin's blocking effect on Ca^{2+} spark propagation (as discussed in 5.3.1). Ca^{2+} spark propagation differs between sub- and suprathreshold DADs with subthreshold DADs appearing as a burst of Ca^{2+} sparks that form a Ca^{2+} ring around the cardiomyocyte periphery but do not trigger CICR in deeper cytosolic layers. Contrastingly, in the case of suprathreshold DADs, the Ca^{2+} ring causes CICR in deeper layers of the cytosol meaning the synchronized activation of a large number of sparks which ultimately trigger an AP[238]. Hence, the reduced amount of sparks under efsevin treatment (reduced frequency) trigger a Ca^{2+} ring that can only locally propagate (as indicated by a reduction of propagating Ca^{2+} waves) and promote subthreshold DADs. In contrast, a synchronized activation of many sparks as seen under Iso treatment rather causes APs. These principles are reflected in a significant reduction of APs with no effect of efsevin on subthreshold DADs.

5.4 Efsevin's suppressive effect suggests SR Ca^{2+} overload as causative for systolic arrhythmogenic events

SSCEs and EADs during systole were added to the repertoire of arrhythmogenesis in CPVT only in the 2010s[157,205] and EADs were more commonly accepted as causative for arrhythmias associated with LQTS. SSCEs have the ability to trigger EADs with the rise of the Ca^{2+} elevation always preceding the onset of the afterdepolarization[204]. Until now there is an ongoing debate whether SSCEs result from a window current where LTCCs are neither activated nor completely inactivated or from spontaneous Ca^{2+} release from the SR. While before, EADs were assumed to arise from I_{CaL} reactivation during the late phase of an AP, recent evidence suggests SSCEs

to also originate from SR Ca^{2+} overload. Interestingly, in the same study SSCE-positive myocytes concomitantly displayed asynchronous diastolic waves indicative of SR Ca^{2+} overload and analogously DADs and EADs were present in the same ventricular regions during VT[200]. Hence, epicardial regions exhibiting systolic and diastolic arrhythmogenic events are well correlated pointing to SR Ca^{2+} overload as their common underlying mechanism. DADs on the opposite are canonically caused by SR Ca^{2+} release and resulting I_{ti} is associated with cellular Ca^{2+} overload[239]. DADs are more common at normal to high HR and especially under β-AR activation. Yet, Iso is known to facilitate both EADs and DADs[240] pointing to the possibility that both pathological voltage oscillations might share the same mechanism[241]. Indeed, an increase in cytosolic Ca^{2+} accompanies EADs and DADs[240]. The work reported in this thesis contributes to answer this unsolved dispute: as an important finding in this context, efsevin is able to also suppress arrhythmic events during systole in addition to its antiarrhythmic effect on diastolic events. Clear evidence is given of a suppressive effect of efsevin on SSCEs and a trend towards a suppression of EADs which extends the previous finding that both arrhythmogenic events might indeed result from Ca^{2+} overload. This is in line with the finding from Horvath et al. that EADs occur at positive voltages above the Ca^{2+} window current voltage range meaning the window current is not responsible for EAD generation[242]. Further, results from Kujala et al. also support the emerging consensus on the role of NCX-mediated generation of EADs[157]. Indeed, NCX-mediated EADs and SSCEs would best explain the effect of efsevin not only on diastolic but also on systolic arrhythmogenesis: in the setting of CPVT, cytosolic Ca^{2+} overload drives the NCX in its reverse mode thereby driving arrhythmogenesis. Efsevin reduces the frequency of Ca^{2+} sparks and waves and thereby limits the amount of Ca^{2+} available for reverse NCX. As a result pathologic NCX activation is minimized and the amount of arrhythmogenic APs is

decreased. Assuming that SR Ca^{2+} overload is also the trigger of SSCEs, the overload subsequently results in Ca^{2+} leaking from the SR. This situation corresponds to our setting in $RyR2^{R4496C/WT}$ mice where Ca^{2+} spontaneously leaks from the SR due to the defective RyR2. Regardless of the cause, both situations lead to spontaneous Ca^{2+} release acting arrhythmogenic: in the first case SSCEs occur, in the latter waves. Under efsevin-treatment, Ca^{2+} from the SR is increasedly taken up by mitochondria (as described in detail in 5.1) leading to a reduced occurrence of both Ca^{2+} abnormalities. We therefore propose that efsevin reduces both, diastolic waves and systolic SSCEs, by the same mechanism. Diastolic waves can trigger DADs and SSCEs can trigger EADs. Assuming that SSCEs arise from Ca^{2+} overload, the same would apply to EADs. In fact, we observed a trend towards a reduction of EADs (Fig. 19). Conclusively, our results with SSCEs and EADs clearly substantiate the hypothesis that systolic and diastolic arrhythmogenic events indeed share SR Ca^{2+} overload as their underlying mechanism. The finding that CPVT patients harbouring mutations in RyR2 also present with EADs indicates that these patients might be susceptible to both DADs and EADs[157]. This makes EADs another proarrhythmogenic event of interest in Ca^{2+} overload induced arrhythmia. In contrast to efsevin, Verapamil only suppressed waves and not SSCEs termed "early release events"[243] which further strengthens the highly promising effect of efsevin in Ca^{2+} triggered arrhythmia. Since EADs favored by catecholaminergic stimulation are believed to underlie torsade des Pointes (TdP) and LQTS[240], an expansion of efsevin treatment to these and other arrhythmia syndromes seems conceivable.

5.5 Translation to the clinic – Antiarrhythmic effect of MiCUps in patient-derived CPVT cardiomyocytes

The antiarrhythmic effect of MiCUps on different Ca^{2+} abnormalities *in vitro* and in our $RyR2^{R4496C/WT}$ CPVT model *in vivo* is very auspicious. Yet, promising antiarrhythmic agents are frequently not effective when translated from preclinical mouse models to human patients owed to interspecies differences. Striking differences exist between small animal models and human cardiac physiology in particular with regard to beating rates, energetics, myofilament composition, expression of key ion channels, cellular electrophysiology and Ca^{2+} cycling[244]. Therefore, human-based models are of particular interest in cardiovascular research. Unfortunately, there is almost no opportunity to obtain healthy cardiac tissue or primary human cardiomyocytes which are coincidentally derived from a CPVT patient. To partly bypass these difficulties, we took recourse to a human iPSC-based CPVT model and administered MiCUPs to cardiomyocytes from two CPVT patients. Unlike nonhuman animal models, iPSC cardiomyocytes are of human origin and as such show Ca^{2+} handling properties and electrophysiological behavior according to the disease pathophysiology of human CPVT patients[245]. Strikingly, MiCUPs significantly reduced the frequency of Ca^{2+} waves also in human cardiomyocytes from both the $RyR2^{S406L/WT}$ and $CPVT^{unknown}$ background. In comparison to $RyR2^{S406L/WT}$ cells, wave-positive $CPVT^{unknown}$ cardiomyocytes generated more Ca^{2+} waves per minute, indicative of the aggressive phenotype that ultimately caused the death of this patient. The majority of patients presenting with a CPVT phenotype have a long history of arrhythmia and sometimes of failed treatment options. Nevertheless, efsevin was shown to effectively reduce spontaneous Ca^{2+} waves in these cardiomyocytes comparable to those from RyR2-mutant cells described above. We therefore propose enhanced mitochondrial Ca^{2+} uptake to

rescue cells regardless of the respective mutation causing cytosolic Ca^{2+} overload leading to CPVT.

As a major drawback, iPSCs remain largely immature resembling fetal myocytes[246] as compared to adult cardiomyocytes[247] which show a mature Ca^{2+} handling apparatus, T tubuli and enlarged SR cisternae[246]. Moreover, they represent a mixed population of atrial, nodal-, ventricular-like cells[248] and even cells with an intermediate phenotype[246]. Even though they represent a heterogenous population of cardiac cell types, stem-cell derived cardiomyocytes are unable to reproduce the complexity and functionality of an adult heart syncytium[246] meaning that our iPSC-experiments do not compensate for clinical drug testing in humans. Rather, we sought to evaluate our antiarrhythmic agents on cardiac cells as similar as possible to primary human ventricular CPVT cardiomyocytes. Collectively, we clearly demonstrated that MiCUps are potent antiarrhythmic substances also in cells from human CPVT patients. As such, our experiments are not meant to supersede a direct application of MiCUps in human tissue and individuals but as a perfect translational bridge paving the way to further preclinical (in further animal species) and also to clinical drug testing (in human individuals).

5.6 MiCUps as a promising alternative to common antiarrhythmics?

5.6.1 A safe(r) way to fight arrhythmia in the absence of severe side effects

Due to the fact that mitochondrial Ca^{2+} uptake proteins such as VDAC2 and MCU are ubiquitously expressed, it could be assumed that the administration of MiCUps might be accompanied by off-target effects which would hinder the further development towards a

medical application in human patients already at this stage. However, beyond the highly promising antiarrhythmic effects of MiCUps, both applied substances were devoid of obvious side effects which we could exclude *in vitro* and *in vivo* at different levels in analogy to arrhythmogenic events. We monitored triggered systolic Ca^{2+} transients and APs as well as different electrophysiological parameters from patch-clamped cardiomyocytes as well as murine ECG parameters for possible adverse effects. Treatment with efsevin caused if any only minor additional effects on myocytes of either genotype. In Shimizu et al., efsevin had no effect on the amplitude and time to peak of paced Ca^{2+} transients[181]. This fits the notion that VDAC2 controls duration and diffusion of cytosolic Ca^{2+} in vicinity to Ca^{2+} release sites to assure rhythmic cardiac contractions. It therefore seems reasonable that the observed Ca^{2+} uptake is a local phenomenon between SR and mitochondria leaving global, cell-wide Ca^{2+} signaling unaffected. Correspondingly, previous studies stated that a blockade of mitochondrial Ca^{2+} uptake has little impact on cytosolic transients[249,250]. Although no changes in cytosolic Ca^{2+} due to enhanced mitochondrial Ca^{2+} uptake were apparent in our experiments, long-term effects on a potential cardiac redistribution of Ca^{2+} and also a redistribution in other organs needs to be evaluated.

Our experiments represent the very first *in vivo* application of efsevin in a murine arrhythmia model and therefore, its antiarrhythmic effect as well as an assessment of potentially harmful effects of the synthetic substance on the living organism were of particular interest. Beforehand, zebrafish embryos were incubated in 10 µM efsevin for 26 hours in our working group without any undesired effects. Prior to the large scale experiment, we also excluded potentially lethal or fatal side effects by *in vivo* application of efsevin to $RyR2^{WT/WT}$ littermates.

Strikingly, none of the two WT mice, treated with 15 mg/kg BW efsevin per day showed any side effects during the 8 day treatment period.

5.6.2 A safe(r) way to fight arrhythmia – Efsevin does not prolong human APD and murine QT interval

Common antiarrhythmic drugs such as Na^+, K^+ or Ca^{2+} channel blockers act on plasmalemma ion channels thereby directly intervening in and modulating the cellular AP. This leads to common side effects of these therapeutics including changes in cardiac electrophysiology like an acceleration or slowing of the cardiac depolarization and repolarization. These changes underlie the positive antiarrhythmic mechanism of these drugs making them a double-edged sword and sometimes not safe to use. Our results clearly demonstrate that efsevin significantly reduces spontaneous APs, a highly promising outcome for the inhibition of diastolic arrhythmogenic events. Thereby, efsevin does not change APD_{90}. However, efsevin prolonged triggered APs by slowing "early" repolarization covered by APD_{50}. This prolongation might be caused by a direct interaction of efsevin with a channel active during repolarization in murine cardiomyocytes. Repolarization in murine cardiac tissue is mediated by several different K^+ currents ($I_{Kto,f}$, $I_{Kto,s}$, $I_{K,slow1}$, $I_{K,slow2}$ and I_{Kss})[5–8] and we therefore consider one or several of these murine K^+ channels as very plausible candidate targets of efsevin leading to the observed prolongation of APD_{50}.

In the light of a future therapeutic application of efsevin in human arrhythmia, it was of paramount importance to preclude the aforeseen effects of efsevin on human APs. Since human repolarization is predominantly carried by the delayed K^+ currents I_{Kr} and I_{Ks}, it would

be preferable that the putative effect of efsevin on murine K^+ channels would not reflect in an analogous modulation of I_{Kr} or I_{Ks} and human APD. Indeed, a previous study by Kim et al. indicates that efsevin might not target I_{Kr}. Whereas a complete I_{Kr} block initially prolongs APD to a sufficient degree to increase myocyte Ca^{2+} load and SSCEs[200], SSCEs were even significantly reduced by efsevin in our case. The major proarrhythmic correlate of prolonged repolarization such as in bradycardia are EADs. We do not only see no proarrhythmic effect of this sort induced by efsevin in $RyR2^{R4496C/WT}$ mice but the substance even showed a trend towards reduction of the amount of $RyR2^{R4496C/WT}$ cardiomyoctes presenting with EADs. In fact, efsevin did not alter AP kinetics in our experiments on human iPSC-derived cardiomyocytes as performed by Prof. Michael Mederos y Schnitzler in[184]. Moreover, we precluded an effect of efsevin on the delayed K^+ current I_{Kr} which is carried by hERG channels, in a heterologous hERG inhibition assay in HEK293 human embryonic kidney cells that stably express hERG channels. Efsevin did not block hERG activity at a concentration of 15 µM[184]. The FDA criterion for hERG-positive drugs is defined as a half maximal inhibitory concentration (IC_{50}) < 1 µM and the known hERG inhibitor dofetilide already displays hERG inhibition with an IC_{50} of 0.01 µM, while efsevin showed an IC_{50} of 40.36 µM which is clearly above the criteria for inhibition. Besides, an evaluation of a potential effect on human hERG channel precedes the application procedure of every compound. This so-called hERG safety assay serves as a measure of side effects for every future therapeutic and various actually effective substances are withdrawn from late stage clinical trials due to perilous side effects caused by an action of the drug on hERG channels[251]. An inhibition of the associated I_{Kr} current results in QT prolongation leading to a potentially fatal TdP tachycardia. The fact that efsevin did not inhibit hERG is very promising

regarding its further development towards a human therapeutic whose development would not be discontinued at an early stage due to hERG block.

Though efsevin seems to directly or indirectly interfere with K^+ channels in isolated cardiomyocytes thereby slightly delaying repolarization, the QT interval in ECG measurements remains unaffected by efsevin treatment in $RyR2^{R4496C/WT}$ mice *in vivo*. Yet, major effects as induced by many common antiarrhythmics seen on the electrophysiological level would entail measurable effects *in vivo*. These include for example a prolongation of the QT interval induced by an inhibition of hERG channels. Accordingly, class III antiarrhythmics not only prolong the AP by their K^+ channel blocking properties, but also tend to lengthen the QT interval. Interestingly enough, QT lengthening is absent under efsevin meaning that the observed effect on the prolongation of APD_{50} does not spread out further and is not accompanied by any alteration on ECG parameters *in vivo*. Experimental conditions might come into consideration to explain that the effect observed on the single cell level in cardiomyocytes *in vitro* somehow does not reflect in ECG parameters in the intact animal *in vivo*. For example, the conscious visual selection of cardiomyocytes of only ventricular origin before each patch clamp experiment very likely resulted in a homogenous cell population for APD assessment, whereas ECG measurements represent the QT data selection from the ventricular syncytium. This assumption is supported by the notion from Babij et al. stating that the syncytial nature of the ventricular wall can alleviate APD prolongation seen at the single cell level[252]. It is also possible that non-physiological experimental conditions add to an APD prolongation and thereby to the discrepancy between *in vitro* and *in vivo* data in mice. Owed to our experimental setting, murine cardiomyocytes stayed attached to the patch pipette under continuous perfusion alltogether for up to over 1 hour. Thereby, efsevin was always washed in at the end of the

recording following vehicle- and Iso+vehicle-treatment to eliminate falsification. A change of this order is unfortunately not feasible since otherwise, artefacts of efsevin could eventually contaminate the patch pipette while measuring cells that had actually not yet been treated with efsevin. In contrast, human myocytes underwent only the two conditions of vehicle- and efsevin-application and APs were measured with a fluorescence approach using Di-8-ANEPPS which definitely represents a more gentle method.

Conclusively, if at all a channel is modulated by efsevin in murine $RyR2^{R4496C/WT}$ cardiomyocytes, this effect seems to either be restricted to mouse hearts or does if any play a minor role in human repolarization so that APD-prolongation is not reflected in iPSC-derived cardiomyocytes. Promisingly, the observed APD prolongation does not cause QT prolongation in mice *in vivo*. To draw a very promising conclusion from both findings, MiCUp treatment could indeed represent a safe or safer way, strongly contrasting common antiarrhythmic drugs that often bear proarrhythmic side effects due to APD and/or QT-prolongation.

5.7 Suitability of kaempferol as an antiarrhythmic therapy

We postulate that the enhanced Ca^{2+} uptake into mitochondria induced by efsevin leads to an accelerated cytosolic Ca^{2+} clearance[181]. Thereby the diffusion of Ca^{2+} inside the cytosol is restricted which averts propagation of cytosolic Ca^{2+} signals under Ca^{2+} overload. Our data with kaempferol clearly support this concept with the MCU agonist seemingly exerting its antiarrhythmic properties by the same mechanism. Treatment of cardiomyocytes with both MiCUps led to a comparable spatial and temporal restriction of Ca^{2+} sparks. Moreover, kaempferol showed an antiarrhythmic effect in our *in vivo* experiments. As a first step towards

kaempferol as a treatment in human arrhythmia, we show convincing evidence here that kaempferol drastically reduced or even completely abolished arrhythmogenic diastolic waves in human-derived iPS cardiomyocytes from two different models of CPVT. The naturally occurring substance kaempferol has many advantages as compared to efsevin, in particular related to the fact that it is already characterized more precisely. Albeit kaempferol showed highly promising effects in a plethora of diseases such as cancer[186,253–255], diabetes[256,257], allergic asthma[258], brain injury[259] and inflammation[260] or dementia[261] and Alzheimer's[262,263], applications in the cardiovascular field remain scarce[185,186]. Generally, the amount of polyphenols present in the diet is associated with a reduction in the risk for CVDs[207,263,264]. For example, a meta-analysis suggested that the consumption of polyphenol-rich foods and beverages can reduce the risk of myocardial infarction and further studies confirmed these protective effects against cardiovascular risk[265]. Yet, clinical trials were only carried out with foods and beverages comprising of distinct polyphenols, where the exact nature of the contained active substances remains largely elusive[265,266]. Hence, studies with pure polyphenols to establish their role in the prevention of CVDs are still elusive. To our best knowledge, our study represents the very first application of kaempferol in an arrhythmia model where its antiarrhythmic effect is attributed to the MCU agonizing effect. Mice administered with kaempferol for 3 days in our study showed normal behavior and were devoid of significant changes of ECG parameters. In contrast to efsevin, kaempferol is a naturally occurring substance and its *in vivo* administration was previously performed in numerous studies in mice and rats with no to only moderate observable side effects. Various preclinical studies already proved the safety of kaempferol *in vivo*[207–209,267]. In these studies, kaempferol was administered intravenously, intraperitoneally or orally to mice as well as rats with doses of up to 10 g/kg BW[208] and for as long as 21 months[207]

with no safety concerns existing. During the treatment of mice with 20 mg/kg BW kaempferol for 3 weeks, vital parameters such as body, spleen or liver weight were not markedly affected[219]. Since high-dose kaempferol did not result in any clinical symptoms, Shih et al. propose kaempferol to be non-toxic, safe and applicable for clinical studies[208]. We ourselves were also able to preclude potential side effects of kaempferol even though the evaluation of kaempferol plasma concentration is still pending. Yet, as a key issue, the pharmacodynamic and pharmacokinetic profiles of kaempferol were successfully investigated in various studies in different species[268]. Whereas the substance is characterized by a rapid clearance, an extremely short half-life and a poor oral bioavailability after intravenous administration[269], its bioavailability could already be improved by different approaches: Co-administration with ethanol enhanced its oral bioavailability in rats[270] and packing of the flavonoid into phospholipid complexes drastically improved its poor absorption and its pharmacological activity[271,272]. These efforts clearly demonstrate that kaempferol has already made significant steps regarding the improval of its bioavailability and thereby towards a therapeutic use as compared to efsevin. Thus, an accordingly modified version of kaempferol might be established as a cardiac therapeutic much earlier. However, for an improved efficacy of kaempferol or at best to completely abolish arrhythmia in our experiments, the first step would not necessarily be to radically modify the applied substance per se. Rather, modifications should be made regarding application and dosage of the kaempferol applied in this study. Firstly, kaempferol is not to the same extent susceptible to precipitation as efsevin. Hence, there is not a corresponding limitation to increase its concentration *in vivo*. Even without taking into account efsevin's precipitation in the applied concentration, its dosage was further complicated by the fact that it is only soluble in PEG-DMSO. As a further advantage, kaempferol is at least

slightly soluble in water[273], whereby the administered amount of kaempferol can be further increased without considering constraints of the solvent (i.e. the maximum amount of DMSO tolerable by the organism). In our 3 days *in vivo* experiments, efsevin was already applied in higher concentrations for a comparable antiarrhythmic effect as that observed with kaempferol. A modification of the flavonoid or a different formulation (in analogy to[270–272]) might further boost its antiarrhythmic effect in a new set of *in vivo* experiments in RyR2$^{R4496C/WT}$ mice, at best towards a complete prevention of arrhythmia such as shown for flecainide[167]. A further distinct benefit of the flavonoid in light of a prospective approval in human arrhythmia is the fact that it has been extensively studied regarding its pharmacokinetics and pharmacodynamics in different species. This would greatly accelerate the admission procedure since some of the required examinations would become redundant just as it happened previously with flecainide. Summarizing these aforementioned benefits and promising data from our study, kaempferol clearly attracts greater hope regarding an earlier use in clinical trials with human patients thereby implemented as an antiarrhythmic therapeutic with faster success.

5.8 Optimization of efsevin towards clinical applicability

The primary substance used in this study is the newly identified VDAC2 modifier efsevin with previously unknown pharmacokinetic and pharmacodynamic properties. Thus, efsevin does not only have to undergo a series of tests in human patients for the development as a human therapeutic, but before that also needs to be chemically improved. Thereby, a high bioavailability and a long plasma half-life time are critical parameters for efsevin to eventually

become druggable. To get a first impression about metabolism, tissue distribution and absorption of efsevin, we analyzed blood plasma and urine as well as lyzed liver and heart tissue from $RyR2^{R4496C/WT}$ mice treated with efsevin via a liquid chromatography-mass spectrometry (LC/MS-MS) approach. Despite the extremely high sensitivity of the device, efsevin was not traceable in any of the samples neither from mice treated with 15 nor from mice treated with 62 mg/kg BW implying that the tissue concentration in heart and liver was somewhat below the detection limit of 30 ng/L. During the process of metabolization, efsevin undergoes a biotransformation into its metabolites which are unidentified to date and thereby likely not detectable by the LC/MS-MS analysis tracking efsevin. Metabolization ensures that a substance is made more readily water-soluble to improve its elimination via urine. Efsevin was not detected in urine possibly indicating that efsevin can only be eliminated in very small quantities and instead is accumulated somewhere inside the organism. Yet, a potential deposition of efsevin in adipose tissue was excluded by the extraction of gonadal adipose tissue from the abdominal cavity. A possible scenario to explain the absence of efsevin in urine was a modification of the drug *in vivo* before its elimination. A rapid conversion of the parent compound into yet unknown metabolites after its successful administration would also explain the disappearance of efsevin in blood, liver and heart. Preliminary results from our lab indeed showed a rapid hydrolyzation of efsevin (within 10 minutes) in human liver microsomes[274], pointing towards the rapid „disassembly" of efsevin yielding a metabolite or metabolites that are still active causing the antiarrhythmic effect clearly observable in our experiments. The same applies to kaempferol with an extensive first-pass metabolism in gut and liver after oral and intravenous administration[268]. Thus, an important matter will be the identification and verification of efsevin's metabolites, particularly with regard to possible early originating

metabolites still existing in plasma. Another possibility might lie in the fact that efsevin is only poorly soluble at RT. Hence, we may speculate that the majority or even a large part of the substance is insolubly retained inside the pump during the experiment and never even gets close to murine plasma. In this case, the actual concentration of efsevin in murine plasma might indeed range below 30 ng/L. According to the manufacturer, a precipitation of the substance inside the pump cannot be ascertained retrospectively. In defiance of this, we cut open minipumps from both treatment groups and encountered whitish clots and crumbs. Since there were apparently more crumbs in efsevin-containing pumps, we consider a premature precipitation of the substance to be an entirely probable scenario to explain why efsevin was not detectable in blood plasma even at high concentrations. Further, efsevin might accumulate in an organ or in organs other than the tissues we collected. In either case, the small amount of efsevin that actually reaches the organism or tissue in the latter case was already efficient pointing to an unbelievably good performance already below 30 ng/L. Even though we were not able to detect efsevin following our successful *in vivo* studies, its antiarrhythmic effect was still clearly present. However, also in previous studies on this model a clear link between plasma concentrations and the antiarrhythmic effects was never established: While several authors present an antiarhythmic effect but do not present plasma levels[234,236,275], other studies did not find an antiarrhythmic effect, though plasma concentrations were high enough to reach effective *in vivo* concentrations[158]. In one of the studies dealing with the clear efficacy of an undetectable substance, the authors specifically note this problem: Kaempferol is so rapidly eliminated that effective concentrations at the site of action are apparently not reached making it unclear how the anxiolytic-like effects that definitely are proven for the compound do occur[269].

Taken together, the actually used version of efsevin has a low stability and a relatively low potency which is evident from its high EC_{50} of 2.2 µM in HL-1 cardiomyocytes[274]. Following a successful optimization after appropriate chemical modification of efsevin, a higher affinity and bioavailability might both increase its antiarrhythmic potency. If the modified efsevin might then reach a similar concentration in the heart as its target organ as for example flecainide or Carvedilol (in[164,167]), it is plausible to assume that its potency might even increase towards a complete suppression of arrhythmia.

5.9 Applicability of MiCUps in other Ca^{2+} induced arrhythmias as an advantage compared to other explorative approaches

Despite the discovery of promising novel treatment approaches acting intracellularly at the side of arrhythmia origin, the substances in large part present with considerable off-target effects and to date only flecainide has recently emerged as a novel therapeutic for the routine application in CPVT patients. The most researched explorative strategy to fight arrhythmia through intracellular targets is a blockade of RyR to prevent excessive Ca^{2+} spark activity. Dantrolene was shown to significantly reduce spontaneous sparks and APs in iPSCs from a CPVT patient with an underlying RyR2 mutation[187]. The substance suppressed arrhythmogenic Ca^{2+} leak by stabilizing interdomain interactions and its antiarrhythmic effect depends on a distinct conformational state of the channel only present in disease conditions[276]. Another Rycal, the RyR2 blocker K201 (analog. JTV-519) showed inconsistent antiarrhythmic effects in $RyR2^{R4496C/WT}$ mice. K201 could neither abolish β-AR-induced spontaneous APs in R4496C cardiomyocytes *in vitro* nor prevent VT *in vivo*[158]. Higher doses prompt proarrhythmic effects

and the use in clinical trials for the treatment of AF did not achieve satisfactory outcomes[13]. Since K201 is a multichannel modulator that exerts a blocking effect on SERCA on resting $[Ca^{2+}]_c$ and affects further ion channels such as the LTCC[277], Na^+ and K^+ channels[278], another Rycal with more specific stabilizing properties was developed[279]. The newly established agent S107 enhanced the binding of FKBP to leaky RyR2s thereby inhibiting the Ca^{2+} leak and was demonstrated to protect against fatal arrhythmias in $RyR2^{R2474S/WT}$ mice[280]. Accordingly, yet in a Casq2-model of CPVT, an unnatural verticilide enantiomer was most recently shown to inhibit RyR2 and attenuated arrhythmia *in vivo*[275]. Therapeutic approaches with a less equivocal action on RyR2 channels are the β-blocker Carvedilol and the minimally β-blocking carvedilol analogue VK-II-86. Both significantly reduced the duration of single RyR2 openings, abolished occurrence and frequency of Ca^{2+} waves and were found to prevent stress-induced VT in the R4496C mouse model of CPVT *in vivo*[164]. By directly modifying gating properties of RyR2, both substances uniquely combine β-blockade and anti-SOICR activity. Analogous to flecainide, the carvedilol analogue VK-II-86 proved more effective as a combined therapy with β-blockers metoprolol or bisoprolol. Although a subject of controversial debate[281], the aforementioned Na^+ channel blocker flecainide beyond its action on Na^+ channels might represent another blocker of RyR2 in the open state[232,282,283]. In summary, a therapeutic potential of RyR2 block by Rycals remains controversial as antiarrhythmic action is counteracted by negative results.

In contrast to Rycals, MiCUps do not operate by stabilizing RyR in the SR (even though they seemingly exert an additional effect on mutated RyR2 and Ca^{2+} sparks) but by increasing mitochondrial Ca^{2+} uptake. Consequently, MiCUps circumvent directly fixing disease-causing mutations on RyR2 but activate cellular Ca^{2+} sinks in close proximity to the SR to buffer Ca^{2+}, thereby not being restricted to the treatment of arrhythmia solely caused by mutations in RyR2

or its associated proteins. Accordingly, efsevin was shown to rescue equally well from cytosolic Ca^{2+} overload caused by a NCX mutation in zebrafish or by exposure of murine WT cardiomyocytes to high extracellular Ca^{2+} [181]. Furthermore, efsevin as well as kaempferol demonstrated their antiarrhythmic potential in murine and human cardiomyocytes with RyR2 mutations where overload is caused by a leaky channel and in cardiomyocytes derived from a CPVT patient with a yet unknown mutation causing excessive Ca^{2+} waves. Even though we lack results from further arrhythmia models, the latter suggests that the antiarrhythmic effect of MiCUps might indeed be mutation-independent which could be particularly useful in the case of cardiac diseases of unknown etiology with currently no approved treatment. This is what happened with flecainide, which was recently shown to act mutation-independent[284] and which was successfully implemented in genotype-negative patients where conventional therapy was ineffective against VT[168]. Yet, as a major drawback, the efficacy of flecainide is lowered by Ca^{2+} overload. Hence, flecainide no longer reduced Ca^{2+} waves *in vitro* already at 4 mM Ca^{2+} in $Casq2^{-/-}$ and $RyR2^{R4496C/WT}$ cardiomyocytes[284]. As a highly promising benefit in this context, Shimizu et al. could demonstrate that efsevin was still able to inhibit Ca^{2+} waves in WT cardiomyocytes treated with an external Ca^{2+} concentration of as much as 10 mM[181]. Moreover, MiCUps exerted a highly promising antiarrhythmic effect *in vivo* in R4496C mice treated with a stress challenge of 2 mg/kg adrenaline and 120 mg/kg caffeine. As a major disadvantage of flecainide, its efficacy is reduced by an exposure of mice to an analogous catecholamine challenge. It is thus quite conceivable that in the future MiCUps might be applied in forms of CPVT where flecainide is not as effective due to its dependency on the concentration of extracellular Ca^{2+} and other substances.

Even though CPVT is not very widespread in the population with an estimated 1 person in 10.000 affected, data from Shimizu et al.[181] combined with previous work from our group and especially the results obtained in this thesis strongly suggest the beneficial action of MiCUps to be a more general principle. It is likely that efsevin and kaempferol are effective for the treatment of cardiac arrhythmia associated with cytosolic Ca^{2+} overload regardless of the underlying mutation or if the condition is hereditary or acquired. To further underline the mechanism of action to be universally applicable in Ca^{2+} induced arrhythmia, the two aforementioned MiCUps could initially be tested in different CPVT „forms" other than CPVT1 with different affected proteins such as for example Casq2. Following this, it is quite conceivable to further expand the therapeutic paradigm of enhancing mitochondrial Ca^{2+} uptake to other types of arrhythmia associated with disturbances in intracellular Ca^{2+} signaling such as AF as a very common condition. Mortality associated with AF was doubled from 1990 to 2010[285] clearly indicating that there is an urgent need for effective therapeutic interventions. A beneficial effect of enhanced mitochondrial Ca^{2+} uptake in the treatment of AF could be anticipated not only since efsevin was previously shown to restore cardiac contractions in *tre* zebrafish suffering from cardiac fibrillation of the atria[181]. Just as CPVT, AF is accompanied by elevated cytosolic Ca^{2+} levels following an increase in SR Ca^{2+} leak. The elevated intracellular Ca^{2+} levels and increased RyR2 activity result in increased EADs[286,287]. Certain RyR mutations associated with CPVT also predispose to AF[288,289] and so, future research will be directed towards an application of MiCUps in these and further disease entities.

5.10 Conclusion

It was previously shown that efsevin exerts an antiarrhythmic effect in *tre* zebrafish, where aberrant intracellular Ca^{2+} handling leads to cardiac arrhythmia due to a mutation in NCX. This was further endorsed by the effect of efsevin on spontaneous Ca^{2+} waves in murine WT cardiomyocytes exposed to high extracellular Ca^{2+} as an arrhythmic stimulus. Our experiments in murine $RyR2^{R4496C/WT}$ cardiomyocytes in particular serve as a proof of principle that activation of mitochondrial Ca^{2+} uptake with MiCUPs represents a highly promising therapeutic approach to treat arrhythmias in an animal model of CPVT. In the arrhythmic setting of CPVT, mutated RyR2 channels spontaneously leak Ca^{2+} in form of Ca^{2+} sparks into the cytosol leading to spark-induced spark activation and cytosolic Ca^{2+} overload (Fig. 32 (A) Untreated) which initiate CPVT arrhythmogenesis ultimately resulting in arrhythmia. We demonstrated that the antiarrhythmic effect of enhanced mitochondrial Ca^{2+} uptake already intervenes at the early, most fundamental Ca^{2+} release events of sparks. Efsevin as well as kaempferol blocked spark-induced spark activation and reset the high diastolic [Ca^{2+}] in the microdomain back to a more physiological level (Fig. 32 (B) MiCUp treatment) whereby less mutated RyR2s were at all able to trigger neighboring RyR channels. As a consequence, less Ca^{2+} was available for spontaneous waves to propagate through cardiomyocytes. This antiarrhythmic principle recurs throughout more expansive arrhythmogenic events from spontaneous APs up to VT arrhythmia concerning cardiac tissue as a whole. However, efsevin not only proved effective to reduce spontaneous diastolic events but also exerted a suppressive effect on systolic arrhythmogenic Ca^{2+} elevations that only recently accrued to the repertoire of disease-causing events in CPVT. In a translational approach, MiCUps could also proof their highly promising antiarrhythmic potency in human iPSC-based cardiomoyctes from two different CPVT patients ($RyR2^{S406L/WT}$

and CPVT^{unknown}). As another highly promising finding strongly contrasting common antiarrhythmics, MiCUp treatment *in vitro* and *in vivo* revealed no severe side effects. Summarizing the above, our findings with efsevin and kaempferol prepare the ground for the introduction of MiCUps as a new class of antiarrhythmics for the prospective treatment of human, Ca^{2+} induced arrhythmia regardless of its molecular origin. With efsevin and kaempferol, we applied substances targeting only two proteins out of an entire protein complex in mitochondrial membranes implicated in Ca^{2+} uptake. Therefore, future research should be aimed at testing an antiarrhythmic effect of compounds with the highest possible efficiency targeting the auxiliary MCU regulators MICU1 and 2, MCUb, EMRE or MCUR1 as promising further candidate proteins.

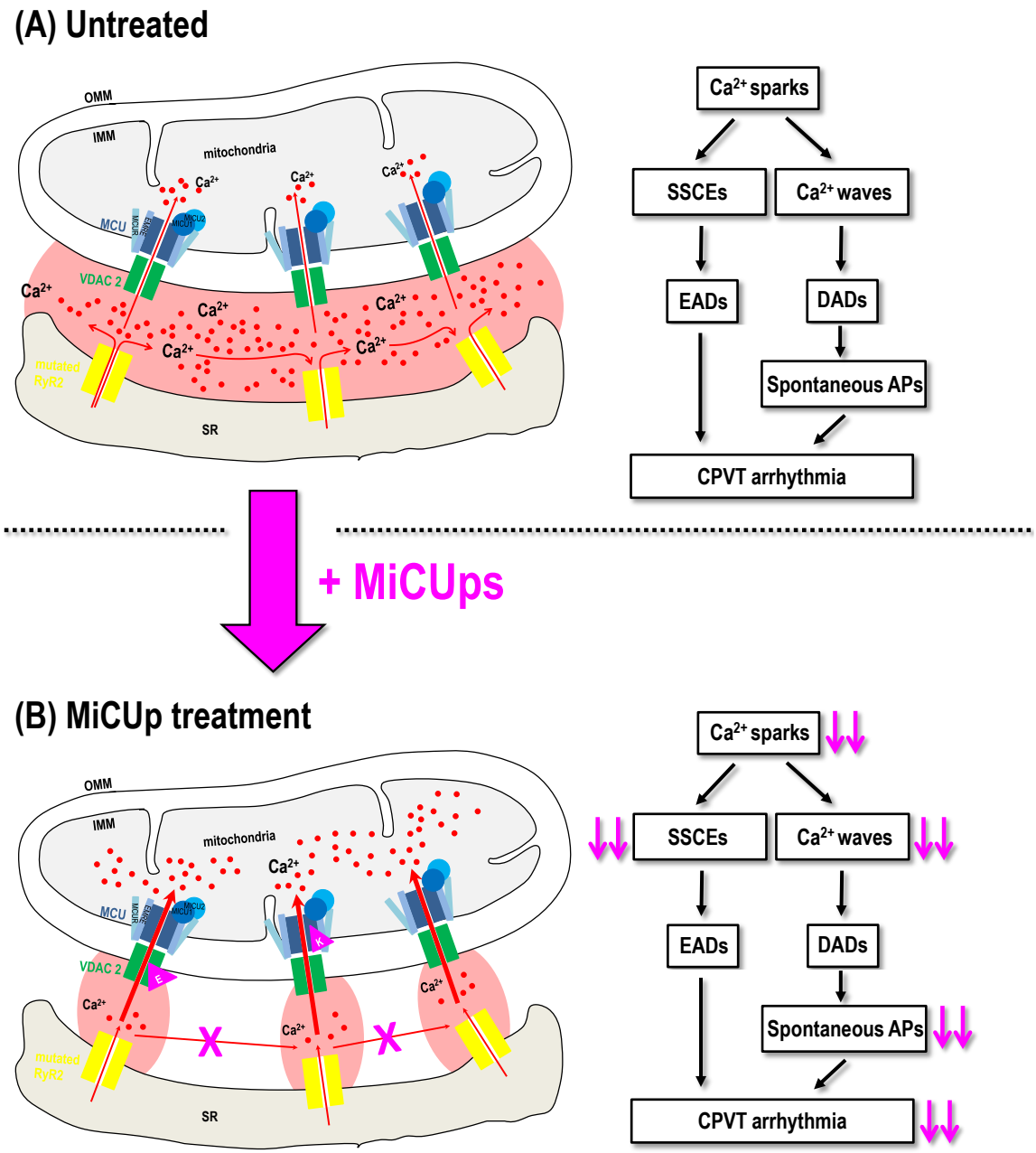

Fig. 32 Mechanism of action underlying the antiarrhythmic effect of MiCUps.

(A) In the untreated CPVT cardiomyocyte, mutated RyR2s spontaneously leak Ca^{2+} from the SR leading to a saltatory activation of adjacent RyR2s. The Ca^{2+} builds up as a Ca^{2+} wave which propagates through the entire cell and eventually triggers NCX resulting in EADs or DADs. Suprathreshold DADs can trigger spontaneous APs which are causative for full-blown CPVT arrhythmia. (B) MiCUps enhance the mitochondrial uptake of Ca^{2+} that would otherwise favor arrhythmogenic signals. As demonstrated herein, MiCUps exerted antiarrhythmic effects on almost every single step of CPVT pathogenesis (pink arrows indicate significant reduction of arrhythmogenic or arrhythmic event), but can already intervene as early as in the most fundamental event of Ca^{2+} sparks, representing the very basis of CPVT pathogenesis.

Author contributions

Original Articles

Sander P, Arduino D, **Schweitzer MK**, Wilting F, Gutenthaler S, Dreizehnter L, Nicke A, Moretti A, Gudermann T, Perocchi F, Schredelseker J (2020) Approved drugs ezetimibe and disulfiram enhance mitochondrial Ca^{2+} uptake and suppress cardiac arrhythmogenesis. Under review *Br J Pharmacol*

Schweitzer MK, Wilting F, Sedej S, Dreizehnter L, Dupper NJ, Tian Q, Moretti A, My I, Kwon O, Priori SG, Laugwitz KL, Storch U, Lipp P, Breit A Mederos y Schnitzler M, Gudermann T, Schredelseker J (2017) Suppression of arrhythmia by enhancing mitochondrial Ca^{2+} uptake in catecholaminergic ventricular tachycardia models. *JACC Basic Transl Sci:* doi: 10.1016/j.jacbts.2017.06.008

Schweitzer MK, Wilting F, Sedej S, Dreizehnter L, Dupper NJ, Moretti A, Kwon O, Priori SG, Laugwitz KL, Mederos y Schnitzler M, Gudermann T, Schredelseker J (2017) Suppression of Arrhythmia by Enhancing Mitochondrial Calcium Uptake in Experimental Models of Catecholaminergic Ventricular Tachycardia. Conference Paper *Biophys J.* doi: 10.1016/j.bpj.2016.11.552

Schredelseker J, Paz A, López CJ, Altenbach C, Leung CS, **Drexler MK**, Chen JN, Hubbell WL, Abramson J (2014) High-resolution structure and double electron-electron resonance of the zebrafish voltage-dependent anion channel 2 reveal an oligomeric population. *J Biol Chem*. doi:10.1074/jbc.M113.497438

Drexler MK, Wilting F, Dreizehnter L, Sedej S, Moretti A, Priori SG, Kwon O, Gudermann T, Schredelsker J (2015) Pharmacological activation of mitochondrial Ca^{2+} uptake suppresses arrhythmogenic events in CPVT cardiomyocytes. Conference Paper in Archiv für Experimentelle Pathologie und Pharmakologie Vol 388

Poster presentations (presenting author underlined)

Schweitzer MK, Wilting F, Sedej S, Dreizehnter L, Dupper NJ, Moretti A, Kwon O, Priori SG, Laugwitz KL, Mederos y Schnitzler M, Gudermann T, Schredelseker J (2017) Suppression of

Arrhythmia by Enhancing Mitochondrial Calcium Uptake in Experimental Models of Catecholaminergic Ventricular Tachycardia. 61th Biophysics 2017, New Orleans, USA

Drexler MK, Wilting F, Dreizehnter L, Sedej S, Kwon O, Moretti A, Priori SG, Gudermann T, Schredelseker J. Pharmacological activation of voltage-dependent anion channel 2 suppresses arrhythmogenic events in CPVT cardiomyocytes. 60th Annual Meeting of the Biophysical Society (03/2016), Los Angeles California, USA

Drexler MK, Wilting F, Dreizehnter L, Sedej S, Kwon O, Moretti A, Priori SG, Gudermann T, Schredelseker J. Pharmacological activation of mitochondrial calcium uptake suppresses arrhythmogenic events in CPVT cardiomyocytes. Deutsches Zentrum für Herz-Kreislauf-Forschung International Symposium on Receptors, G proteins and integration of calcium signaling in the cardiovascular system (11/2014), Max-Delbrück Center Berlin Buch, Germany

Drexler MK, Wilting F, Dreizehnter L, Sedej S, Kwon O, Moretti A, Priori SG, Gudermann T, Schredelseker J. Pharmacological activation of mitochondrial calcium uptake suppresses arrhythmogenic events in CPVT cardiomyocytes. Munich Heart Alliance Winter Meeting (02/2015), Schloss Nymphenburg Munich Germany

Drexler MK, Wilting F, Dreizehnter L, Sedej S, Kwon O, Moretti A, Priori SG, Gudermann T, Schredelseker J. Pharmacological activation of mitochondrial calcium uptake suppresses arrhythmogenic events in CPVT cardiomyocytes. 81st Annual Meeting of the German Society for Experimental and Clinical Pharmacology and Toxicology (DGPT) Meeting (03/2015), CAU Kiel, Germany

Drexler MK, Huang J, Wilting F, Sedej S, Kwon O, Gudermann T, Chen JN, Schredelseker J. Activation of VDAC2 enhances mitochondrial Ca^{2+} uptake and suppresses arrhythmogenic Ca^{2+} waves. 2nd European Calcium Channel Conference (05/2015) Alpbach, Austria

Mittermeier L, **Drexler MK**, Sedej S, Grönke S, Gudermann T, Schredelseker J. Expression profiling of VDAC isoforms 1-3. Munich Heart Alliance Winter Meeting (02/2014), Schloss Nymphenburg Munich Germany

Patents

Schredelseker J, Wilting F, **Drexler M** (2017) Kaempferol for the treatment of cardiac diseases. Patent application WIPO (PCT) WO2017211780A1.

Acknowledgements

A lot of people were involved directly or indirectly in the successful completion of this work and it would not have been possible for me to write this thesis without the help and continuous support of the wonderful people around me. I could not possibly leave the institute without expressing my sincere gratitude. First of all, I would like to thank my supervisor Prof. Thomas Gudermann for offering me the possibility to perform my Ph.D. studies in his institute and for providing me with funding for this project. I cannot put in words how much I appreciated the active support at all stages of the project. I am grateful for assistance in selecting collaborators, valuable advice and the outstanding freedom I was able to enjoy in the laboratory. Everything I know about cardiomyocytes and cardiac Ca^{2+} signaling and how successful yet funny and easygoing experimental science is done, I learned through my direct supervisor Dr. Johann Schredelseker. I most highly appreciate all the significant contributions in time, ideas, and in reviewing data, that were necessary to make my PhD experience productive and successful. His joy and enthusiasm for research was contagious and motivational for me, even during tough times in the Ph.D. pursuit. I am thankful for him always having a sympathetic ear as well as for critical input and fruitful discussions but also for the freedom to follow up and constantly restructure my own priorities. None of this present work would have been possible without my Doktorvater Prof. Michael Mederos y Schnitzler. Thank you so much for taking the time to teach me all this theoretical and practical knowledge of the patch clamp technique as well as hitherto unknown facts about cardiomyocyte well-being while always being open to questions. During the experimental work of this Ph.D. study a number of other excellent scientists were involved in different aspects of the projects. These were mainly Prof. Dr. Michael Mederos and Dr. Ursula Storch from Walther Straub Institute. A big thank you is owed to the people involved in our

collaborations for their invaluable help with performing experiments relative to the CPVT *in vivo* and the human CPVT project. I would like to especially thank Prof. Dr. Simon Sedej at Medical University Graz for his every-year help: namely teaching me the mouse cardiomyocyte isolation procedure in 2013 and performing *in vivo* experiments in 2014 and 2015. Thanks for your practical help with all this and thanks for also scientifically discussing all the theoretical aspects. Speaking of mouse stuff, I would like to express my thanks to Petra Eigner and her colleagues working in the animal facility. Many thanks to Lisa Dreizehnter for dissting tons of human CPVT explants and for teaching me all aspects about iPSC dissociation for this project to be successful. Moreover I appreciate the valuable cooperation with Dr. Andreas Breit from Walther Straub Institute who performed cAMP-assays on murine cardiomyocytes. I would like to thank Brigitte Mayerhofer for technical and any other type of support. Moreover, I am very grateful for the scientifc help as well as the good distraction of all of my lab mates, Kira Steinhorst, Eliane Klein, Fabiola Wilting, Simon Huber, Paulina Sander, Brigitte Mayerhofer and Eva Vetter. I would like to thank ### for reading and evaluating this thesis and for agreeing to be part of my thesis defense committee.

Finally, but definitely not least, I want to thank my family: Thank you, Mama and Papa for providing me with strong roots, resilience and an inquiring mind and for constantly encouraging me on my path. Most of all, I want to thank my husband and my children for their constant support, funny distractions and confidence. None of this would have been possible without you!

Affidavit

Eidesstattliche Versicherung

Maria Katharina Schweitzer, geb. Drexler

Ich erkläre hiermit an Eides statt, dass ich die vorliegende Dissertation mit dem Thema

Therapeutic potential of enhancing mitochondrial Ca^{2+} uptake in experimental cardiac arrhythmia models

selbständig verfasst, mich außer der angegebenen keiner weiteren Hilfsmittel bedient und alle Erkenntnisse, die aus dem Schrifttum ganz oder annähernd übernommen sind, als solche kenntlich gemacht und nach ihrer Herkunft unter Bezeichnung der Fundstelle einzeln nachgewiesen habe.

Ich erkläre des Weiteren, dass die hier vorgelegte Dissertation nicht in gleicher oder in ähnlicher Form bei einer anderen Stelle zur Erlangung eines akademischen Grades eingereicht wurde.

München, den 07.05.2022	Maria Katharina Schweitzer
Ort, Datum	Unterschrift Doktorandin

References

1. Klabunde RE. *Cardiovascular physiology concepts*. 2nd ed. Philadelphia: Wolters Kluwer Health/Lippincott Williams & Wilkins, 2012.
2. Ramrakha P, Hill J. *Oxford Handbook of Cardiology*. 2nd ed. Oxford: OUP Oxford, 2012.
3. Sidebotham D. *Cardiothoracic critical care.* Philadelphia: Butterworth-Heinemann, 2007.
4. Nerbonne JM, Kass RS. Molecular physiology of cardiac repolarization. *Physiol Rev* 2005;**85**:1205–1253.
5. Guo W, Xu H, London B, Nerbonne JM. Molecular basis of transient outward K+ current diversity in mouse ventricular myocytes. *The Journal of Physiology* 1999;**521**:587–599.
6. Brouillette J, Clark RB, Giles WR, Fiset C. Functional properties of K+ currents in adult mouse ventricular myocytes. *The Journal of Physiology* 2004;**559**:777–798.
7. Sabir IN, Killeen MJ, Grace AA, Huang CL-H. Ventricular arrhythmogenesis: insights from murine models. *Prog Biophys Mol Biol* 2008;**98**:208–218.
8. Zhou J, Kodirov S, Murata M, Buckett PD, Nerbonne JM, Koren G. Regional upregulation of Kv2.1-encoded current, IK,slow2, in Kv1DN mice is abolished by crossbreeding with Kv2DN mice. *Am J Physiol Heart Circ Physiol* 2003;**284**:H491-500.
9. Bignolais O, Le Quang K, Naud P, El Harchi A, Briec F, Piron J, Bourge A, Leoni A-L, Charpentier F, Demolombe S. Early ion-channel remodeling and arrhythmias precede hypertrophy in a mouse model of complete atrioventricular block. *J Mol Cell Cardiol* 2011;**51**:713–721.
10. Kaese S, Verheule S. Cardiac electrophysiology in mice: a matter of size. *Front. Physiol.* 2012;**3**:345.
11. Qu Z, Chung D. Mechanisms and determinants of ultralong action potential duration and slow rate-dependence in cardiac myocytes. *PLoS One* 2012;**7**:e43587.
12. Edvardsson N, Hirsch I, Olsson SB. Right ventricular monophasic action potentials in healthy young men. *Pacing Clin Electrophysiol* 1984;**7**:813–821.
13. Driessen HE, Bourgonje VJA, van Veen TAB, Vos MA. New antiarrhythmic targets to control intracellular calcium handling. *Netherlands Heart Journal* 2014;**22**:198–213.
14. Avram R, Tison GH, Aschbacher K, Kuhar P, Vittinghoff E, Butzner M, Runge R, Wu N, Pletcher MJ, Marcus GM, Olgin J. Real-world heart rate norms in the Health eHeart study. *NPJ Digit Med* 2019;**2**:58.

15. Milani-Nejad N, Janssen PML. Small and large animal models in cardiac contraction research: advantages and disadvantages. *Pharmacol Ther* 2014;**141**:235–249.

16. Janssen PML, Biesiadecki BJ, Ziolo MT, Davis JP. The Need for Speed: Mice, Men, and Myocardial Kinetic Reserve. *Circ Res* 2016;**119**:418–421.

17. Tanner MR, Beeton C. DIFFERENCES IN ION CHANNEL PHENOTYPE AND FUNCTION BETWEEN HUMANS AND ANIMAL MODELS. *Front Biosci (Landmark Ed)* 2018;**23**:43–64.

18. Rosenthal N, Brown S. The mouse ascending: perspectives for human-disease models. *Nat Cell Biol* 2007;**9**:993–999.

19. Endo M. Calcium release from the sarcoplasmic reticulum. *Physiol Rev* 1977;**57**:71–108.

20. Laitinen PJ, Brown KM, Piippo K, Swan H, Devaney JM, Brahmbhatt B, Donarum EA, Marino M, Tiso N, Viitasalo M, Toivonen L, Stephan DA, Kontula K. Mutations of the cardiac ryanodine receptor (RyR2) gene in familial polymorphic ventricular tachycardia. *Circulation* 2001;**103**:485–490.

21. Zipes DP, Jalife J, eds. *Cardiac electrophysiology: From cell to bedside*. Sixth edition. Philadelphia, PA: Elsevier/Saunders, 2014.

22. Tada M, Kirchberger MA, Katz AM. Phosphorylation of a 22,000-dalton component of the cardiac sarcoplasmic reticulum by adenosine 3':5'-monophosphate-dependent protein kinase. *J. Biol. Chem.* 1975;**250**:2640–2647.

23. Andrienko TN, Picht E, Bers DM. Mitochondrial free calcium regulation during sarcoplasmic reticulum calcium release in rat cardiac myocytes. *J Mol Cell Cardiol* 2009;**46**:1027–1036.

24. Luo M, Anderson ME. Mechanisms of altered Ca^{2+} handling in heart failure. *Circ Res* 2013;**113**:690–708.

25. Lanner JT, Georgiou DK, Joshi AD, Hamilton SL. Ryanodine receptors: structure, expression, molecular details, and function in calcium release. *Cold Spring Harb Perspect Biol* 2010;**2**:a003996.

26. Nakai J, Imagawa T, Hakamata Y, Shigekawa M, Takeshima H, Numa S. Primary structure and functional expression from cDN A of the cardiac ryanodine receptor/calcium release channel. *FEBS Letters* 1990;**271**:169–177.

27. Györke S, Terentyev D. Modulation of ryanodine receptor by luminal calcium and accessory proteins in health and cardiac disease. *Cardiovasc Res* 2008;**77**:245–255.

28. Ottolia M, Torres N, Bridge JHB, Philipson KD, Goldhaber JI. Na/Ca exchange and contraction of the heart. *J Mol Cell Cardiol* 2013;**61**:28–33.

29. Terentyev D, Viatchenko-Karpinski S, Valdivia HH, Escobar AL, Gyorke S. Luminal Ca2+ controls termination and refractory behavior of Ca2+-induced Ca2+ release in cardiac myocytes. *Circ Res* 2002;**91**:414–420.

30. Priori SG, Napolitano C. Cardiac and skeletal muscle disorders caused by mutations in the intracellular Ca2+ release channels. *J Clin Invest* 2005;**115**:2033–2038.

31. Blayney LM, Lai FA. Ryanodine receptor-mediated arrhythmias and sudden cardiac death. *Pharmacol Ther* 2009;**123**:151–177.

32. van Petegem F. Ryanodine receptors: allosteric ion channel giants. *J Mol Biol* 2015;**427**:31–53.

33. Xiao B, Zhong G, Obayashi M, Yang D, Chen K, Walsh MP, Shimoni Y, Cheng H, Ter Keurs H, Chen SRW. Ser-2030, but not Ser-2808, is the major phosphorylation site in cardiac ryanodine receptors responding to protein kinase A activation upon beta-adrenergic stimulation in normal and failing hearts. *Biochem J* 2006;**396**:7–16.

34. Wehrens XHT, Lehnart SE, Reiken SR, Marks AR. Ca2+/calmodulin-dependent protein kinase II phosphorylation regulates the cardiac ryanodine receptor. *Circ Res* 2004;**94**:e61-70.

35. Rodriguez P, Bhogal MS, Colyer J. Stoichiometric phosphorylation of cardiac ryanodine receptor on serine 2809 by calmodulin-dependent kinase II and protein kinase A. *J. Biol. Chem.* 2003;**278**:38593–38600.

36. Marx SO, Reiken S, Hisamatsu Y, Jayaraman T, Burkhoff D, Rosemblit N, Marks AR. PKA phosphorylation dissociates FKBP12.6 from the calcium release channel (ryanodine receptor): defective regulation in failing hearts. *Cell* 2000;**101**:365–376.

37. Lehnart SE, Wehrens XHT, Marks AR. Calstabin deficiency, ryanodine receptors, and sudden cardiac death. *Biochem Biophys Res Commun* 2004;**322**:1267–1279.

38. Györke I, Hester N, Jones LR, Györke S. The role of calsequestrin, triadin, and junctin in conferring cardiac ryanodine receptor responsiveness to luminal calcium. *Biophys J* 2004;**86**:2121–2128.

39. Hoang-Trong TM, Ullah A, Jafri MS. Calcium Sparks in the Heart: Dynamics and Regulation. *Res Rep Biol* 2015;**6**:203–214.

40. Cheng H, Lederer WJ, Cannell MB. Calcium sparks: elementary events underlying excitation-contraction coupling in heart muscle. *Science* 1993;**262**:740–744.

41. Wang SQ, Song LS, Lakatta EG, Cheng H. Ca2+ signalling between single L-type Ca2+ channels and ryanodine receptors in heart cells. *Nature* 2001;**410**:592–596.

42. Cheng H, Lederer MR, Lederer WJ, Cannell MB. Calcium sparks and Ca2+i waves in cardiac myocytes. *Am J Physiol* 1996;**270**:C148-59.

43. Guatimosim S, Dilly K, Santana LF, Saleet Jafri M, Sobie EA, Lederer WJ. Local Ca(2+) signaling and EC coupling in heart: Ca(2+) sparks and the regulation of the Ca(2+)(i) transient. *J Mol Cell Cardiol* 2002;**34**:941–950.

44. Sobie EA, Dilly KW, dos Santos Cruz J, Lederer WJ, Jafri MS. Termination of cardiac Ca(2+) sparks: an investigative mathematical model of calcium-induced calcium release. *Biophys J* 2002;**83**:59–78.

45. Sham JS, Song LS, Chen Y, Deng LH, Stern MD, Lakatta EG, Cheng H. Termination of Ca2+ release by a local inactivation of ryanodine receptors in cardiac myocytes. *Proc Natl Acad Sci U S A* 1998;**95**:15096–15101.

46. Gillespie D, Fill M. Pernicious attrition and inter-RyR2 CICR current control in cardiac muscle. *J Mol Cell Cardiol* 2013;**58**:53–58.

47. Williams GSB, Chikando AC, Tuan H-TM, Sobie EA, Lederer WJ, Jafri MS. Dynamics of calcium sparks and calcium leak in the heart. *Biophys J* 2011;**101**:1287–1296.

48. Litwin SE, Zhang D, Bridge JH. Dyssynchronous Ca(2+) sparks in myocytes from infarcted hearts. *Circ Res* 2000;**87**:1040–1047.

49. Lytton J. Na+/Ca2+ exchangers: three mammalian gene families control Ca2+ transport. *Biochem J* 2007;**406**:365–382.

50. Nakai J, Sekiguchi N, Rando TA, Allen PD, Beam KG. Two Regions of the Ryanodine Receptor Involved in Coupling withl-Type Ca 2+ Channels. *J. Biol. Chem.* 1998;**273**:13403–13406.

51. Fill M, Copello JA. Ryanodine receptor calcium release channels. *Physiol Rev* 2002;**82**:893–922.

52. Raeymaekers L, Vandecaetsbeek I, Wuytack F, Vangheluwe P. Modeling Ca2+ dynamics of mouse cardiac cells points to a critical role of SERCA's affinity for Ca2+. *Biophys J* 2011;**100**:1216–1225.

53. Vandecaetsbeek I, Vangheluwe P, Raeymaekers L, Wuytack F, Vanoevelen J. The Ca2+ pumps of the endoplasmic reticulum and Golgi apparatus. *Cold Spring Harb Perspect Biol* 2011;**3**.

54. Xiang YK. Compartmentalization of beta-adrenergic signals in cardiomyocytes. *Circ Res* 2011;**109**:231–244.

55. Ho D, Yan L, Iwatsubo K, Vatner DE, Vatner SF. Modulation of beta-adrenergic receptor signaling in heart failure and longevity: targeting adenylyl cyclase type 5. *Heart Fail Rev* 2010;**15**:495–512.

56. Grimm M, Brown JH. Beta-adrenergic receptor signaling in the heart: role of CaMKII. *J Mol Cell Cardiol* 2010;**48**:322–330.

57. Briston SJ, Dibb KM, Solaro RJ, Eisner DA, Trafford AW. Balanced changes in Ca buffering by SERCA and troponin contribute to Ca handling during β-adrenergic stimulation in cardiac myocytes. *Cardiovasc Res* 2014;**104**:347–354.

58. Lukyanenko V, Chikando A, Lederer WJ. Mitochondria in cardiomyocyte Ca2+ signaling. *Int J Biochem Cell Biol* 2009;**41**:1957–1971.

59. Pilchova I, Klacanova K, Tatarkova Z, Kaplan P, Racay P. The Involvement of Mg2+ in Regulation of Cellular and Mitochondrial Functions. *Oxidative Medicine and Cellular Longevity* 2017;**2017**:8.

60. Hajnóczky G, Robb-Gaspers LD, Seitz MB, Thomas AP. Decoding of cytosolic calcium oscillations in the mitochondria. *Cell* 1995;**82**:415–424.

61. Carafoli E. The fateful encounter of mitochondria with calcium: how did it happen? *Biochim Biophys Acta* 2010;**1797**:595–606.

62. Contreras L, Drago I, Zampese E, Pozzan T. Mitochondria: the calcium connection. *Biochim Biophys Acta* 2010;**1797**:607–618.

63. Rapizzi E, Pinton P, Szabadkai G, Wieckowski MR, Vandecasteele G, Baird G, Tuft RA, Fogarty KE, Rizzuto R. Recombinant expression of the voltage-dependent anion channel enhances the transfer of Ca2+ microdomains to mitochondria. *J Cell Biol* 2002;**159**:613–624.

64. Rizzuto R, Duchen MR, Pozzan T. Flirting in little space: the ER/mitochondria Ca2+ liaison. *Sci STKE* 2004;**2004**:re1.

65. Szabadkai G, Duchen MR. Mitochondria: the hub of cellular Ca2+ signaling. *Physiology (Bethesda)* 2008;**23**:84–94.

66. Pozzan T, Rizzuto R. The renaissance of mitochondrial calcium transport. *Eur J Biochem* 2000;**267**:5269–5273.

67. Halestrap AP. Mitochondrial calcium in health and disease. *Biochim Biophys Acta* 2009;**1787**:1289–1290.

68. Denton RM. Regulation of mitochondrial dehydrogenases by calcium ions. *Biochim Biophys Acta* 2009;**1787**:1309–1316.

69. Patron M, Raffaello A, Granatiero V, Tosatto A, Merli G, Stefani D de, Wright L, Pallafacchina G, Terrin A, Mammucari C, Rizzuto R. The mitochondrial calcium uniporter (MCU): molecular identity and physiological roles. *J Biol Chem* 2013;**288**:10750–10758.

70. Jouaville LS, Pinton P, Bastianutto C, Rutter GA, Rizzuto R. Regulation of mitochondrial ATP synthesis by calcium: evidence for a long-term metabolic priming. *Proc Natl Acad Sci U S A* 1999;**96**:13807–13812.

71. Raffaello A, Stefani D de, Rizzuto R. The mitochondrial Ca(2+) uniporter. *Cell Calcium* 2012;**52**:16–21.

72. Nicholls DG. Mitochondrial calcium function and dysfunction in the central nervous system. *Biochim Biophys Acta* 2009;**1787**:1416–1424.

73. Rizzuto R, Marchi S, Bonora M, Aguiari P, Bononi A, Stefani D de, Giorgi C, Leo S, Rimessi A, Siviero R, Zecchini E, Pinton P. Ca(2+) transfer from the ER to mitochondria: when, how and why. *Biochim Biophys Acta* 2009;**1787**:1342–1351.

74. Herrera-Cruz MS, Simmen T. Over Six Decades of Discovery and Characterization of the Architecture at Mitochondria-Associated Membranes (MAMs). *Adv Exp Med Biol* 2017;**997**:13–31.

75. Gerencser AA, Adam-Vizi V. Mitochondrial Ca2+ dynamics reveals limited intramitochondrial Ca2+ diffusion. *Biophys J* 2005;**88**:698–714.

76. Rizzuto R, Pinton P, Carrington W, Fay FS, Fogarty KE, Lifshitz LM, Tuft RA, Pozzan T. Close contacts with the endoplasmic reticulum as determinants of mitochondrial Ca2+ responses. *Science* 1998;**280**:1763–1766.

77. Hayashi M, Denjoy I, Extramiana F, Maltret A, Buisson NR, Lupoglazoff J-M, Klug D, Hayashi M, Takatsuki S, Villain E, Kamblock J, Messali A, Guicheney P, Lunardi J, Leenhardt A. Incidence and risk factors of arrhythmic events in catecholaminergic polymorphic ventricular tachycardia. *Circulation* 2009;**119**:2426–2434.

78. RAMESH V, SHARMA VK, SHEU S-S, FRANZINI-ARMSTRONG C. Structural Proximity of Mitochondria to Calcium Release Units in Rat Ventricular Myocardium May Suggest a Role in Ca2+ Sequestration. *Annals NY Acad Sci* 1998;**853**:341–344.

79. Williams GSB, Boyman L, Chikando AC, Khairallah RJ, Lederer WJ. Mitochondrial calcium uptake. *Proc Natl Acad Sci U S A* 2013;**110**:10479–10486.

80. García-Pérez C, Hajnóczky G, Csordás G. Physical coupling supports the local Ca2+ transfer between sarcoplasmic reticulum subdomains and the mitochondria in heart muscle. *J Biol Chem* 2008;**283**:32771–32780.

81. Dorn GW, Song M, Walsh K. Functional implications of mitofusin 2-mediated mitochondrial-SR tethering. *J Mol Cell Cardiol* 2015;**78**:123–128.

82. Chen Y, Csordás G, Jowdy C, Schneider TG, Csordás N, Wang W, Liu Y, Kohlhaas M, Meiser M, Bergem S, Nerbonne JM, Dorn GW, Maack C. Mitofusin 2-containing mitochondrial-

reticular microdomains direct rapid cardiomyocyte bioenergetic responses via interorganelle Ca(2+) crosstalk. *Circ Res* 2012;**111**:863–875.

83. Brito OM de, Scorrano L. Mitofusin 2 tethers endoplasmic reticulum to mitochondria. *Nature* 2008;**456**:605–610.

84. Csordás G, Várnai P, Golenár T, Roy S, Purkins G, Schneider TG, Balla T, Hajnóczky G. Imaging interorganelle contacts and local calcium dynamics at the ER-mitochondrial interface. *Mol Cell* 2010;**39**:121–132.

85. Giacomello M, Drago I, Bortolozzi M, Scorzeto M, Gianelle A, Pizzo P, Pozzan T. Ca2+ hot spots on the mitochondrial surface are generated by Ca2+ mobilization from stores, but not by activation of store-operated Ca2+ channels. *Mol Cell* 2010;**38**:280–290.

86. Qi H, Li L, Shuai J. Optimal microdomain crosstalk between endoplasmic reticulum and mitochondria for Ca 2+ oscillations. *Sci Rep*;**5**:1–11.

87. Csordás G, Thomas AP, Hajnóczky G. Quasi-synaptic calcium signal transmission between endoplasmic reticulum and mitochondria. *EMBO J* 1999;**18**:96–108.

88. Shkryl VM, Shirokova N. Transfer and tunneling of Ca2+ from sarcoplasmic reticulum to mitochondria in skeletal muscle. *J. Biol. Chem.* 2006;**281**:1547–1554.

89. Báthori G, Csordás G, Garcia-Perez C, Davies E, Hajnóczky G. Ca2+-dependent control of the permeability properties of the mitochondrial outer membrane and voltage-dependent anion-selective channel (VDAC). *J. Biol. Chem.* 2006;**281**:17347–17358.

90. Shoshan-Barmatz V, Gincel D. The Voltage-Dependent Anion Channel: Characterization, Modulation, and Role in Mitochondrial Function in Cell Life and Death. *CBB* 2003;**39**:279–292.

91. Lemeshko VV. Electrical control of the cell energy metabolism at the level of mitochondrial outer membrane. *Biochim Biophys Acta Biomembr* 2021;**1863**:183493.

92. Roston TM, Guo W, Krahn AD, Wang R, van Petegem F, Sanatani S, Chen SRW, Lehman A. A novel RYR2 loss-of-function mutation (I4855M) is associated with left ventricular non-compaction and atypical catecholaminergic polymorphic ventricular tachycardia. *J Electrocardiol* 2017;**50**:227–233.

93. Gattin Z, Schneider R, Laukat Y, Giller K, Maier E, Zweckstetter M, Griesinger C, Benz R, Becker S, Lange A. Solid-state NMR, electrophysiology and molecular dynamics characterization of human VDAC2. *J Biomol NMR* 2015;**61**:311–320.

94. Naghdi S, Hajnóczky G. VDAC2-specific cellular functions and the underlying structure. *Biochim Biophys Acta* 2016;**1863**:2503–2514.

95. Colombini M, Blachly-Dyson E, Forte M. VDAC, a channel in the outer mitochondrial membrane. *Ion Channels* 1996;**4**:169–202.

96. Sander P, Gudermann T, Schredelseker J. A Calcium Guard in the Outer Membrane: Is VDAC a Regulated Gatekeeper of Mitochondrial Calcium Uptake? *Int J Mol Sci* 2021;**22**.

97. Simson P, Jepihhina N, Laasmaa M, Peterson P, Birkedal R, Vendelin M. Restricted ADP movement in cardiomyocytes: Cytosolic diffusion obstacles are complemented with a small number of open mitochondrial voltage-dependent anion channels. *J Mol Cell Cardiol* 2016;**97**:197–203.

98. Böhm R, Amodeo GF, Murlidaran S, Chavali S, Wagner G, Winterhalter M, Brannigan G, Hiller S. The Structural Basis for Low Conductance in the Membrane Protein VDAC upon β-NADH Binding and Voltage Gating. *Structure* 2020;**28**:206-214.e4.

99. Tan W, Colombini M. VDAC closure increases calcium ion flux. *Biochim Biophys Acta* 2007;**1768**:2510–2515.

100. Gincel D, Zaid H, Shoshan-Barmatz V. Calcium binding and translocation by the voltage-dependent anion channel: a possible regulatory mechanism in mitochondrial function. *Biochem J* 2001;**358**:147–155.

101. Min CK, Yeom DR, Lee K-E, Kwon H-K, Kang M, Kim Y-S, Park ZY, Jeon H, Kim DH. Coupling of ryanodine receptor 2 and voltage-dependent anion channel 2 is essential for Ca^2+ transfer from the sarcoplasmic reticulum to the mitochondria in the heart. *Biochem J* 2012;**447**:371–379.

102. Subedi KP, Kim J-C, Kang M, Son M-J, Kim Y-S, Woo S-H. Voltage-dependent anion channel 2 modulates resting Ca^2+ sparks, but not action potential-induced Ca^2+ signaling in cardiac myocytes. *Cell Calcium* 2011;**49**:136–143.

103. Liao Y, Hao Y, Chen H, He Q, Yuan Z, Cheng J. Mitochondrial calcium uniporter protein MCU is involved in oxidative stress-induced cell death. *Protein Cell* 2015;**6**:434–442.

104. Baughman JM, Perocchi F, Girgis HS, Plovanich M, Belcher-Timme CA, Sancak Y, Bao XR, Strittmatter L, Goldberger O, Bogorad RL, Koteliansky V, Mootha VK. Integrative genomics identifies MCU as an essential component of the mitochondrial calcium uniporter. *Nature* 2011;**476**:341–345.

105. Stefani D de, Raffaello A, Teardo E, Szabò I, Rizzuto R. A forty-kilodalton protein of the inner membrane is the mitochondrial calcium uniporter. *Nature* 2011;**476**:336–340.

106. Kirichok Y, Krapivinsky G, Clapham DE. The mitochondrial calcium uniporter is a highly selective ion channel. *Nature* 2004;**427**:360–364.

107. Szalai G, Csordás G, Hantash BM, Thomas AP, Hajnóczky G. Calcium Signal Transmission between Ryanodine Receptors and Mitochondria. *J. Biol. Chem.* 2000;**275**:15305–15313.

108. Mannella CA, Buttle K, Rath BK, Marko M. Electron microscopic tomography of rat-liver mitochondria and their interaction with the endoplasmic reticulum. *Biofactors* 1998;**8**:225–228.

109. Patergnani S, Suski JM, Agnoletto C, Bononi A, Bonora M, Marchi E de, Giorgi C, Marchi S, Missiroli S, Poletti F, Rimessi A, Duszynski J, Wieckowski MR, Pinton P. Calcium signaling around Mitochondria Associated Membranes (MAMs). *Cell Commun Signal* 2011;**9**:19.

110. Bondarenko AI, Parichatikanond W, Madreiter CT, Rost R, Waldeck-Weiermair M, Malli R, Graier WF. UCP2 modulates single-channel properties of a MCU-dependent Ca(2+) inward current in mitochondria. *Pflugers Arch* 2015;**467**:2509–2518.

111. Hajnóczky G, Csordás G. Calcium signalling: fishing out molecules of mitochondrial calcium transport. *Curr Biol* 2010;**20**:R888-91.

112. Gunter TE, Buntinas L, Sparagna G, Eliseev R, Gunter K. Mitochondrial calcium transport: mechanisms and functions. *Cell Calcium* 2000;**28**:285–296.

113. Takeuchi A, Kim B, Matsuoka S. The destiny of Ca(2+) released by mitochondria. *J Physiol Sci* 2015;**65**:11–24.

114. Cai X, Lytton J. Molecular cloning of a sixth member of the K+-dependent Na+/Ca2+ exchanger gene family, NCKX6. *J Biol Chem* 2004;**279**:5867–5876.

115. Takeuchi A, Kim B, Matsuoka S. The mitochondrial Na+-Ca2+ exchanger, NCLX, regulates automaticity of HL-1 cardiomyocytes. *Sci Rep* 2013;**3**:2766.

116. Mozaffarian D, Benjamin EJ, Go AS, Arnett DK, Blaha MJ, Cushman M, Das SR, Ferranti S de, Després J-P, Fullerton HJ, Howard VJ, Huffman MD, Isasi CR, Jiménez MC, Judd SE, Kissela BM, Lichtman JH, Lisabeth LD, Liu S, Mackey RH, Magid DJ, McGuire DK, Mohler ER, Moy CS, Muntner P, Mussolino ME, Nasir K, Neumar RW, Nichol G, Palaniappan L, Pandey DK, Reeves MJ, Rodriguez CJ, Rosamond W, Sorlie PD, Stein J, Towfighi A, Turan TN, Virani SS, Woo D, Yeh RW, Turner MB. Heart Disease and Stroke Statistics\textemdash2016 Update. *Circulation* 2016;**133**:e38-e360.

117. World Health Organization. Cardiovascular diseases (CVDs): Fact Sheet. https://www.who.int/news-room/fact-sheets/detail/cardiovascular-diseases-(cvds). Accessed March 13, 2021.

118. Shiferaw Y, Aistrup GL, Wasserstrom JA. Intracellular Ca(2+) waves, afterdepolarizations, and triggered arrhythmias. *Cardiovasc Res* 2012;**95**:265–268.

119. Jiang D, Wang R, Xiao B, Kong H, Hunt DJ, Choi P, Zhang L, Chen SRW. Enhanced store overload-induced Ca2+ release and channel sensitivity to luminal Ca2+ activation are common defects of RyR2 mutations linked to ventricular tachycardia and sudden death. *Circ Res* 2005;**97**:1173–1181.

120. Mehra R. Global public health problem of sudden cardiac death. *J Electrocardiol* 2007;**40**:S118-22.

121. Bagnall RD, Das K J, Duflou J, Semsarian C. Exome analysis-based molecular autopsy in cases of sudden unexplained death in the young. *Heart Rhythm* 2014;**11**:655–662.

122. Liu N, Ruan Y, Priori SG. Catecholaminergic polymorphic ventricular tachycardia. *Prog Cardiovasc Dis* 2008;**51**:23–30.

123. Liu N, Rizzi N, Boveri L, Priori SG. Ryanodine receptor and calsequestrin in arrhythmogenesis: what we have learnt from genetic diseases and transgenic mice. *J Mol Cell Cardiol* 2009;**46**:149–159.

124. Pérez-Riera AR, Barbosa-Barros R, Rezende Barbosa MPC de, Daminello-Raimundo R, Lucca AA de, Abreu LC de. Catecholaminergic polymorphic ventricular tachycardia, an update. *Ann Noninvasive Electrocardiol* 2018;**23**:e12512.

125. Cerrone M, Colombi B, Santoro M, Di Barletta MR, Scelsi M, Villani L, Napolitano C, Priori SG. Bidirectional ventricular tachycardia and fibrillation elicited in a knock-in mouse model carrier of a mutation in the cardiac ryanodine receptor. *Circ Res* 2005;**96**:e77-82.

126. Fernández-Velasco M, Rueda A, Rizzi N, Benitah J-P, Colombi B, Napolitano C, Priori SG, Richard S, Gómez AM. Increased Ca2+ sensitivity of the ryanodine receptor mutant RyR2R4496C underlies catecholaminergic polymorphic ventricular tachycardia. *Circ Res* 2009;**104**:201-9, 12p following 209.

127. COUMEL P. Catecholamine-induced severe ventricular arrhythmias with Adams-Stokes syndrome in children: Report of four cases. *Br Heart J* 1978;**40**:28–37.

128. Leenhardt A, Lucet V, Denjoy I, Grau F, Ngoc DD, COUMEL P. Catecholaminergic Polymorphic Ventricular Tachycardia in Children: A 7-Year Follow-up of 21 Patients. *Circulation* 1995;**91**:1512–1519.

129. Priori SG, Napolitano C, Tiso N, Memmi M, Vignati G, Bloise R, Sorrentino V, Danieli GA. Mutations in the cardiac ryanodine receptor gene (hRyR2) underlie catecholaminergic polymorphic ventricular tachycardia. *Circulation* 2001;**103**:196–200.

130. Priori SG, Napolitano C, Memmi M, Colombi B, Drago F, Gasparini M, DeSimone L, Coltorti F, Bloise R, Keegan R, Cruz Filho FE, Vignati G, Benatar A, DeLogu A. Clinical and Molecular Characterization of Patients With Catecholaminergic Polymorphic Ventricular Tachycardia. *Circulation* 2002;**106**:69–74.

131. Sumitomo N. Current topics in catecholaminergic polymorphic ventricular tachycardia. *Journal of Arrhythmia*;**32**:344–351.

132. Behere SP, Weindling SN. Catecholaminergic polymorphic ventricular tachycardia: An exciting new era. *Ann Pediatr Cardiol* 2016;**9**:137–146.

133. Liu N, Colombi B, Raytcheva-Buono EV, Bloise R, Priori SG. Catecholaminergic polymorphic ventricular tachycardia. *Herz* 2007;**32**:212–217.

134. Sumitomo N, Harada K, Nagashima M, Yasuda T, Nakamura Y, Aragaki Y, Saito A, Kurosaki K, Jouo K, Koujiro M, Konishi S, Matsuoka S, Oono T, Hayakawa S, Miura M, Ushinohama H, Shibata T, Niimura I. Catecholaminergic polymorphic ventricular tachycardia: electrocardiographic characteristics and optimal therapeutic strategies to prevent sudden death. *Heart* 2003;**89**:66–70.

135. Campos FO, Shiferaw Y, Prassl AJ, Boyle PM, Vigmond EJ, Plank G. Stochastic spontaneous calcium release events trigger premature ventricular complexes by overcoming electrotonic load. *Cardiovasc Res* 2015;**107**:175–183.

136. Cerrone M, Noujaim SF, Tolkacheva EG, Talkachou A, O'Connell R, Berenfeld O, Anumonwo J, Pandit SV, Vikstrom K, Napolitano C, Priori SG, Jalife J. Arrhythmogenic mechanisms in a mouse model of catecholaminergic polymorphic ventricular tachycardia. *Circ Res* 2007;**101**:1039–1048.

137. Wilde AAM, Bhuiyan ZA, Crotti L, Facchini M, Ferrari GM de, Paul T, Ferrandi C, Koolbergen DR, Odero A, Schwartz PJ. Left cardiac sympathetic denervation for catecholaminergic polymorphic ventricular tachycardia. *N Engl J Med* 2008;**358**:2024–2029.

138. Zhao Y-T, Valdivia CR, Gurrola GB, Hernandez JJ, Valdivia HH. Arrhythmogenic mechanisms in ryanodine receptor channelopathies. *Sci China Life Sci* 2015;**58**:54–58.

139. van der Werf C, Wilde AAM. Catecholaminergic polymorphic ventricular tachycardia: disease with different faces. *Circ Arrhythm Electrophysiol* 2015;**8**:523–525.

140. Gray B, Bagnall RD, Lam L, Ingles J, Turner C, Haan E, Davis A, Yang P-C, Clancy CE, Sy RW, Semsarian C. A novel heterozygous mutation in cardiac calsequestrin causes autosomal dominant catecholaminergic polymorphic ventricular tachycardia. *Heart Rhythm* 2016;**13**:1652–1660.

141. Bhuiyan ZA, Hamdan MA, Shamsi ETA, Postma AV, Mannens MMAM, Wilde AAM, Al-Gazali L. A novel early onset lethal form of catecholaminergic polymorphic ventricular tachycardia maps to chromosome 7p14-p22. *J Cardiovasc Electrophysiol* 2007;**18**:1060–1066.

142. Nyegaard M, Overgaard MT, Søndergaard MT, Vranas M, Behr ER, Hildebrandt LL, Lund J, Hedley PL, Camm AJ, Wettrell G, Fosdal I, Christiansen M, Børglum AD. Mutations in

calmodulin cause ventricular tachycardia and sudden cardiac death. *Am J Hum Genet* 2012;**91**:703–712.

143. Roux-Buisson N, Cacheux M, Fourest-Lieuvin A, Fauconnier J, Brocard J, Denjoy I, Durand P, Guicheney P, Kyndt F, Leenhardt A, Le Marec H, Lucet V, Mabo P, Probst V, Monnier N, Ray PF, Santoni E, Trémeaux P, Lacampagne A, Fauré J, Lunardi J, Marty I. Absence of triadin, a protein of the calcium release complex, is responsible for cardiac arrhythmia with sudden death in human. *Hum Mol Genet* 2012;**21**:2759–2767.

144. Rooryck C, Kyndt F, Bozon D, Roux-Buisson N, Sacher F, Probst V, Thambo J-B. New Family With Catecholaminergic Polymorphic Ventricular Tachycardia Linked to the Triadin Gene. *J Cardiovasc Electrophysiol* 2015;**26**:1146–1150.

145. Silvia G. Priori. The gene connection for the heart: genetic mutations and inherited arrhythmias. http://triad.fsm.it/cardmoc/. Accessed March 4, 2021.

146. Wehrens XHT, Lehnart SE, Huang F, Vest JA, Reiken SR, Mohler PJ, Sun J, Guatimosim S, Song LS, Rosemblit N, D'Armiento JM, Napolitano C, Memmi M, Priori SG, Lederer WJ, Marks AR. FKBP12.6 deficiency and defective calcium release channel (ryanodine receptor) function linked to exercise-induced sudden cardiac death. *Cell* 2003;**113**:829–840.

147. Jiang D, Xiao B, Yang D, Wang R, Choi P, Zhang L, Cheng H, Chen SRW. RyR2 mutations linked to ventricular tachycardia and sudden death reduce the threshold for store-overload-induced Ca2+ release (SOICR). *Proc Natl Acad Sci U S A* 2004;**101**:13062–13067.

148. Bers DM. Cardiac ryanodine receptor phosphorylation: target sites and functional consequences. *Biochem J* 2006;**396**:e1-3.

149. O'Neill SC, Miller L, Hinch R, Eisner DA. Interplay between SERCA and sarcolemmal Ca2+ efflux pathways controls spontaneous release of Ca2+ from the sarcoplasmic reticulum in rat ventricular myocytes. *The Journal of Physiology* 2004;**559**:121–128.

150. Chen X, Guo L, Kang J, Huo Y, Wang S, Tan W. Calcium waves initiating from the anomalous subdiffusive calcium sparks. *J R Soc Interface* 2014;**11**:20130934.

151. Kashimura T, Briston SJ, Trafford AW, Napolitano C, Priori SG, Eisner DA, Venetucci LA. In the RyR2(R4496C) mouse model of CPVT, beta-adrenergic stimulation induces Ca waves by increasing SR Ca content and not by decreasing the threshold for Ca waves. *Circ Res* 2010;**107**:1483–1489.

152. Dawson SP, Keizer J, Pearson JE. Fire–diffuse–fire model of dynamics of intracellular calcium waves. *Proc Natl Acad Sci U S A* 1999;**96**:6060–6063.

153. Berlin JR, Cannell MB, Lederer WJ. Cellular origins of the transient inward current in cardiac myocytes. Role of fluctuations and waves of elevated intracellular calcium. *Circ Res* 1989;**65**:115–126.

154. LAKATTA EG, GUARNIERI T. Spontaneous Myocardial Calcium Oscillations. *J Cardiovasc Electrophysiol* 1993;**4**:473–489.

155. Verkerk AO, Veldkamp MW, Baartscheer A, Schumacher CA, Klöpping C, van Ginneken AC, Ravesloot JH. Ionic Mechanism of Delayed Afterdepolarizations in Ventricular Cells Isolated From Human End-Stage Failing Hearts. *Circulation* 2001;**104**:2728–2733.

156. Burashnikov A, Antzelevitch C. Late-phase 3 EAD. A unique mechanism contributing to initiation of atrial fibrillation. *Pacing Clin Electrophysiol* 2006;**29**:290–295.

157. Kujala K, Paavola J, Lahti A, Larsson K, Pekkanen-Mattila M, Viitasalo M, Lahtinen AM, TOIVONEN L, KONTULA K, SWAN H, Laine M, Silvennoinen O, Aalto-Setälä K. Cell model of catecholaminergic polymorphic ventricular tachycardia reveals early and delayed afterdepolarizations. *PLoS One* 2012;**7**:e44660.

158. Liu N, Colombi B, Memmi M, Zissimopoulos S, Rizzi N, Negri S, Imbriani M, Napolitano C, Lai FA, Priori SG. Arrhythmogenesis in catecholaminergic polymorphic ventricular tachycardia: Insights from a RyR2 R4496C knock-in mouse model. *Circ Res* 2006;**99**:292–298.

159. Muir W, Hubbell JAE. *Equine anesthesia: Monitoring and emergency therapy*. 2nd ed. St. Louis, Mo: Saunders/Elsevier, 2009.

160. Sedej S, Heinzel FR, Walther S, Dybkova N, Wakula P, Groborz J, Gronau P, Maier LS, Vos MA, Lai FA, Napolitano C, Priori SG, Kockskamper J, Pieske B. Na+-dependent SR Ca2+ overload induces arrhythmogenic events in mouse cardiomyocytes with a human CPVT mutation. *Cardiovasc Res* 2010;**87**:50–59.

161. Schmitt N, Grunnet M, Olesen S-P. Cardiac potassium channel subtypes: new roles in repolarization and arrhythmia. *Physiol Rev* 2014;**94**:609–653.

162. Xie Y, Sato D, Garfinkel A, Qu Z, Weiss JN. So Little Source, So Much Sink: Requirements for Afterdepolarizations to Propagate in Tissue. *Biophys J* 2010;**99**:1408–1415.

163. Myles RC, Wang L, Kang C, Bers DM, Ripplinger CM. Local beta-adrenergic stimulation overcomes source-sink mismatch to generate focal arrhythmia. *Circ Res* 2012;**110**:1454–1464.

164. Zhou Q, Xiao J, Jiang D, Wang R, Vembaiyan K, Wang A, Smith CD, Xie C, Chen W, Zhang J, Tian X, Jones PP, Zhong X, Guo A, Chen H, Zhang L, Zhu W, Yang D, Li X, Chen J, Gillis AM, Duff HJ, Cheng H, Feldman AM, Song L-S, Fill M, Back TG, Chen SRW. Carvedilol and its new analogs suppress arrhythmogenic store overload-induced Ca2+ release. *Nat Med* 2011;**17**:1003–1009.

165. Nicolai MPJ, Liem SS, Both S, Pelger RCM, Putter H, Schalij MJ, Elzevier HW. A review of the positive and negative effects of cardiovascular drugs on sexual function: a proposed table for use in clinical practice. *Neth Heart J* 2014;**22**:11–19.

166. SWAN H, Laitinen P, KONTULA K, TOIVONEN L. Calcium channel antagonism reduces exercise-induced ventricular arrhythmias in catecholaminergic polymorphic ventricular tachycardia patients with RyR2 mutations. *J Cardiovasc Electrophysiol* 2005;**16**:162–166.

167. Watanabe H, Chopra N, Laver D, Hwang HS, Davies SS, Roach DE, Duff HJ, Roden DM, Wilde AAM, Knollmann BC. Flecainide prevents catecholaminergic polymorphic ventricular tachycardia in mice and humans. *Nat Med* 2009;**15**:380–383.

168. Watanabe H, van der Werf C, Roses-Noguer F, Adler A, Sumitomo N, Veltmann C, Rosso R, Bhuiyan ZA, Bikker H, Kannankeril PJ, Horie M, Minamino T, Viskin S, Knollmann BC, Till J, Wilde AAM. Effects of flecainide on exercise-induced ventricular arrhythmias and recurrences in genotype-negative patients with catecholaminergic polymorphic ventricular tachycardia. *Heart Rhythm* 2013;**10**:542–547.

169. Lieve KV, Wilde AA, van der Werf C. The Role of Flecainide in the Management of Catecholaminergic Polymorphic Ventricular Tachycardia. *Arrhythm Electrophysiol Rev* 2016;**5**:45–49.

170. Banerjee K, Ghosh RK, Kamatam S, Banerjee A, Gupta A. Role of Ranolazine in cardiovascular disease and diabetes: Exploring beyond angina. *Int J Cardiol* 2017;**227**:556–564.

171. Rosso R, Kalman JM, Rogowski O, Diamant S, Birger A, Biner S, Belhassen B, Viskin S. Calcium channel blockers and beta-blockers versus beta-blockers alone for preventing exercise-induced arrhythmias in catecholaminergic polymorphic ventricular tachycardia. *Heart Rhythm* 2007;**4**:1149–1154.

172. Priori SG, Wilde AA, Horie M, Cho Y, Behr ER, Berul C, Blom N, Brugada J, Chiang C-E, Huikuri H, Kannankeril P, Krahn A, Leenhardt A, Moss A, Schwartz PJ, Shimizu W, Tomaselli G, Tracy C. HRS/EHRA/APHRS expert consensus statement on the diagnosis and management of patients with inherited primary arrhythmia syndromes: document endorsed by HRS, EHRA, and APHRS in May 2013 and by ACCF, AHA, PACES, and AEPC in June 2013. *Heart Rhythm* 2013;**10**:1932–1963.

173. Priori SG, Blomstrom-Lundqvist C, Mazzanti A, Blom N, Borggrefe M, Camm J, Elliott PM, Fitzsimons D, Hatala R, Hindricks G, Kirchhof P, Kjeldsen K, Kuck K-H, Hernandez-Madrid A, Nikolaou N, Norekval TM, Spaulding C, van Veldhuisen DJ. 2015 ESC Guidelines for the management of patients with ventricular arrhythmias and the prevention of sudden cardiac death: The Task Force for the Management of Patients with Ventricular Arrhythmias and the Prevention of Sudden Cardiac Death of the European Society of Cardiology (ESC). Endorsed

by: Association for European Paediatric and Congenital Cardiology (AEPC). *Eur Heart J* 2015;**36**:2793–2867.

174. Gussak I, Antzelevitch C, Wilde AAM, Friedman PA, Ackerman MJ. *Electrical Diseases of the Heart: Genetics, Mechanisms, Treatment, Prevention*. 1. Aufl. s.l.: Springer Verlag London Limited, 2008.

175. Ozyilmaz I, Ozyilmaz S, Ergul Y, Akdeniz C, Tuzcu V. Catecholaminergic Polymorphic Ventricular Tachycardia: A Rare Cause of Cardiac Arrest Following Blunt Chest Trauma. *Acta Cardiol Sin* 2015;**31**:361–364.

176. Cho Y. Left cardiac sympathetic denervation: An important treatment option for patients with hereditary ventricular arrhythmias. *Journal of Arrhythmia*;**32**:340–343.

177. Makanjee B, Gollob MH, Klein GJ, Krahn AD. Ten-year follow-up of cardiac sympathectomy in a young woman with catecholaminergic polymorphic ventricular tachycardia and an implantable cardioverter defibrillator. *J Cardiovasc Electrophysiol* 2009;**20**:1167–1169.

178. Ferrari GM de, Dusi V, Spazzolini C, Bos JM, Abrams DJ, Berul CI, Crotti L, Davis AM, Eldar M, Kharlap M, Khoury A, Krahn AD, Leenhardt A, Moir CR, Odero A, Olde Nordkamp L, Paul T, Rosés I Noguer F, Shkolnikova M, Till J, Wilde AAM, Ackerman MJ, Schwartz PJ. Clinical Management of Catecholaminergic Polymorphic Ventricular Tachycardia: The Role of Left Cardiac Sympathetic Denervation. *Circulation* 2015;**131**:2185–2193.

179. Seguchi H, Ritter M, Shizukuishi M, Ishida H, Chokoh G, Nakazawa H, Spitzer KW, Barry WH. Propagation of Ca2+ release in cardiac myocytes: role of mitochondria. *Cell Calcium* 2005;**38**:1–9.

180. Zhao Z, Gordan R, Wen H, Fefelova N, Zang W-J, Xie L-H. Modulation of intracellular calcium waves and triggered activities by mitochondrial ca flux in mouse cardiomyocytes. *PLoS One* 2013;**8**:e80574.

181. Shimizu H, Schredelseker J, Huang J, Lu K, Naghdi S, Lu F, Franklin S, Fiji HD, Wang K, Zhu H, Tian C, Lin B, Nakano H, Ehrlich A, Nakai J, Stieg AZ, Gimzewski JK, Nakano A, Goldhaber JI, Vondriska TM, Hajnóczky G, Kwon O, Chen J-N. Mitochondrial Ca(2+) uptake by the voltage-dependent anion channel 2 regulates cardiac rhythmicity. *Elife* 2015;**4**.

182. Ebert AM, Hume GL, Warren KS, Cook NP, Burns CG, Mohideen MA, Siegal G, Yelon D, Fishman MC, Garrity DM. Calcium extrusion is critical for cardiac morphogenesis and rhythm in embryonic zebrafish hearts. *Proc Natl Acad Sci U S A* 2005;**102**:17705–17710.

183. Montero M, Lobaton CD, Hernandez-Sanmiguel E, Santodomingo J, Vay L, Moreno A, Alvarez J. Direct activation of the mitochondrial calcium uniporter by natural plant flavonoids. *Biochem J* 2004;**384**:19–24.

184. Schweitzer MK, Wilting F, Sedej S, Dreizehnter L, Dupper NJ, Tian Q, Moretti A, My I, Kwon O, Priori SG, Laugwitz K-L, Storch U, Lipp P, Breit A, Mederos y Schnitzler M, Gudermann T, Schredelseker J. Suppression of Arrhythmia by Enhancing Mitochondrial Ca2+ Uptake in Catecholaminergic Ventricular Tachycardia Models. *JACC: Basic to Translational Science* 2017.

185. Calderón-Montaño JM, Burgos-Morón E, Pérez-Guerrero C, López-Lázaro M. A review on the dietary flavonoid kaempferol. *Mini Rev Med Chem* 2011;**11**:298–344.

186. Imran M, Salehi B, Sharifi-Rad J, Aslam Gondal T, Saeed F, Imran A, Shahbaz M, Tsouh Fokou PV, Umair Arshad M, Khan H, Guerreiro SG, Martins N, Estevinho LM. Kaempferol: A Key Emphasis to Its Anticancer Potential. *Molecules* 2019;**24**.

187. Jung CB, Moretti A, Mederos y Schnitzler M, Iop L, Storch U, Bellin M, Dorn T, Ruppenthal S, Pfeiffer S, Goedel A, Dirschinger RJ, Seyfarth M, Lam JT, Sinnecker D, Gudermann T, Lipp P, Laugwitz K-L. Dantrolene rescues arrhythmogenic RYR2 defect in a patient-specific stem cell model of catecholaminergic polymorphic ventricular tachycardia. *EMBO Mol Med* 2012;**4**:180–191.

188. Moretti A, Bellin M, Jung CB, Thies T-M, Takashima Y, Bernshausen A, Schiemann M, Fischer S, Moosmang S, Smith AG, Lam JT, Laugwitz K-L. Mouse and human induced pluripotent stem cells as a source for multipotent Isl1+ cardiovascular progenitors. *FASEB J* 2010;**24**:700–711.

189. Moretti A, Bellin M, Welling A, Jung CB, Lam JT, Bott-Flügel L, Dorn T, Goedel A, Höhnke C, Hofmann F, Seyfarth M, Sinnecker D, Schömig A, Laugwitz K-L. Patient-specific induced pluripotent stem-cell models for long-QT syndrome. *N Engl J Med* 2010;**363**:1397–1409.

190. O'Connell TD, Rodrigo MC, Simpson PC. Isolation and Culture of Adult Mouse Cardiac Myocytes. In: Vivanco F. *Cardiovascular proteomics: Methods and protocols*. Totowa, NJ: Humana Press, 2007:271–296. Methods in molecular biology.

191. Voigt N, Pearman CM, Dobrev D, Dibb KM. Methods for isolating atrial cells from large mammals and humans. *J Mol Cell Cardiol* 2015;**86**:187–198.

192. Hall AR, Hausenloy DJ. Mitochondrial respiratory inhibition by 2,3-butanedione monoxime (BDM): implications for culturing isolated mouse ventricular cardiomyocytes. *Physiol Rep* 2016;**4**.

193. Louch WE, Sheehan KA, Wolska BM. Methods in cardiomyocyte isolation, culture, and gene transfer. *J Mol Cell Cardiol* 2011;**51**:288–298.

194. Picht E, Zima AV, Blatter LA, Bers DM. SparkMaster: automated calcium spark analysis with ImageJ. *Am J Physiol , Cell Physiol* 2007;**293**:C1073-81.

195. Isenberg G, Klockner U. Calcium tolerant ventricular myocytes prepared by preincubation in a "KB medium". *Pflugers Arch* 1982;**395**:6–18.

196. Durect Corporation. ALZET osmotic pumps - overview. (http://www.alzet.com/products/ALZET_Pumps/index.html).

197. Paavola J, Viitasalo M, Laitinen-Forsblom PJ, Pasternack M, SWAN H, Tikkanen I, TOIVONEN L, KONTULA K, Laine M. Mutant ryanodine receptors in catecholaminergic polymorphic ventricular tachycardia generate delayed afterdepolarizations due to increased propensity to Ca2+ waves. *Eur Heart J* 2007;**28**:1135–1142.

198. Shkryl VM, Blatter LA. Ca(2+) release events in cardiac myocytes up close: insights from fast confocal imaging. *PLoS One* 2013;**8**:e61525.

199. Allen DG, Eisner DA, Orchard CH. Characterization of oscillations of intracellular calcium concentration in ferret ventricular muscle. *The Journal of Physiology* 1984;**352**:113–128.

200. Kim JJ, Nemec J, Li Q, Salama G. Synchronous systolic subcellular Ca2+-elevations underlie ventricular arrhythmia in drug-induced long QT type 2. *Circ Arrhythm Electrophysiol* 2015;**8**:703–712.

201. January CT, Riddle JM. Early afterdepolarizations: mechanism of induction and block. A role for L-type Ca2+ current. *Circ Res* 1989;**64**:977–990.

202. January CT, Riddle JM, Salata JJ. A model for early afterdepolarizations: Induction with the Ca2+ channel agonist Bay K 8644. *Circ Res* 1988;**62**:563–571.

203. Morotti S, Grandi E, Summa A, Ginsburg KS, Bers DM. Theoretical study of L-type Ca(2+) current inactivation kinetics during action potential repolarization and early afterdepolarizations. *The Journal of Physiology* 2012;**590**:4465–4481.

204. Maruyama M, Lin S-F, Xie Y, Chua S-K, Joung B, Han S, Shinohara T, Shen MJ, Qu Z, Weiss JN, Chen P-S. Genesis of phase 3 early afterdepolarizations and triggered activity in acquired long-QT syndrome. *Circ Arrhythm Electrophysiol* 2011;**4**:103–111.

205. Němec J, Kim JJ, Salama G. The link between abnormal calcium handling and electrical instability in acquired long QT syndrome – does calcium precipitate arrhythmic storms? *Prog Biophys Mol Biol* 2015;**120**:210–221.

206. Ho D, Zhao X, Gao S, Hong C, Vatner DE, Vatner SF. Heart Rate and Electrocardiography Monitoring in Mice. *Curr Protoc Mouse Biol* 2011;**1**:123–139.

207. Montero M, La Fuente S de, Fonteriz RI, Moreno A, Alvarez J. Effects of long-term feeding of the polyphenols resveratrol and kaempferol in obese mice. *PLoS One* 2014;**9**:e112825.

208. Shih T-Y, Young T-H, Lee H-S, Hsieh C-B, Hu OY-P. Protective effects of kaempferol on isoniazid- and rifampicin-induced hepatotoxicity. *AAPS J* 2013;**15**:753–762.

209. Song H, Bao J, Wei Y, Chen Y, Mao X, Li J, Yang Z, Xue Y. Kaempferol inhibits gastric cancer tumor growth: An in vitro and in vivo study. *Oncol Rep* 2015;**33**:868–874.

210. Hamilton S, Terentyeva R, Kim TY, Bronk P, Clements RT, O-Uchi J, Csordás G, Choi B-R, Terentyev D. Pharmacological Modulation of Mitochondrial Ca2+ Content Regulates Sarcoplasmic Reticulum Ca2+ Release via Oxidation of the Ryanodine Receptor by Mitochondria-Derived Reactive Oxygen Species. *Front. Physiol.* 2018;**9**:1831.

211. Celsi F, Pizzo P, Brini M, Leo S, Fotino C, Pinton P, Rizzuto R. Mitochondria, calcium and cell death: a deadly triad in neurodegeneration. *Biochim Biophys Acta* 2009;**1787**:335–344.

212. Peuchen S, Clark JB, Duchen MR. Mechanisms of intracellular calcium regulation in adult astrocytes. *Neuroscience* 1996;**71**:871–883.

213. Duchen MR. Mitochondria and calcium: from cell signalling to cell death. *The Journal of Physiology* 2000;**529**:57–68.

214. Li S, Cheng H, Tomaselli GF, Li RA. Mechanistic basis of excitation-contraction coupling in human pluripotent stem cell-derived ventricular cardiomyocytes revealed by Ca2+ spark characteristics: direct evidence of functional Ca2+-induced Ca2+ release. *Heart Rhythm* 2014;**11**:133–140.

215. Liu T, O'Rourke B. Abstract 10579: Beneficial Effect of Mitochondrial Calcium Uniporter Overexpression in a Guinea Pig Heart Failure and Sudden Cardiac Death Model; Arteriosclerosis, Thrombosis, Vascular Biology. https://www.ahajournals.org/doi/10.1161/circ.138.suppl_1.10579. Accessed January 10, 2020.

216. Chen AY, Chen YC. A review of the dietary flavonoid, kaempferol on human health and cancer chemoprevention. *Food Chem* 2012;**138**:2099–2107.

217. Judd J, Lovas J, Huang GN. Isolation, Culture and Transduction of Adult Mouse Cardiomyocytes. *J Vis Exp* 2016.

218. Kim S-H, Choi K-C. Anti-cancer Effect and Underlying Mechanism(s) of Kaempferol, a Phytoestrogen, on the Regulation of Apoptosis in Diverse Cancer Cell Models. *Toxicol Res* 2013;**29**:229–234.

219. Song W, Dang Q, Xu D, Chen Y, Zhu G, Wu K, Zeng J, Long Q, Wang X, He D, Li L. Kaempferol induces cell cycle arrest and apoptosis in renal cell carcinoma through EGFR/p38 signaling. *Oncol Rep* 2014;**31**:1350–1356.

220. Duchen MR. Mitochondria and Ca(2+)in cell physiology and pathophysiology. *Cell Calcium* 2000;**28**:339–348.

221. Brookes PS, Yoon Y, Robotham JL, Anders MW, Sheu S-S. Calcium, ATP, and ROS: a mitochondrial love-hate triangle. *Am J Physiol , Cell Physiol* 2004;**287**:C817-33.

222. Demaurex N, Rosselin M. Redox Control of Mitochondrial Calcium Uptake. *Mol Cell* 2017;**65**:961–962.

223. Fernandez-Tenorio M, Niggli E. Stabilization of Ca2+ signaling in cardiac muscle by stimulation of SERCA. *J Mol Cell Cardiol* 2018;**119**:87–95.

224. Lavorato M, Iyer VR, Dewight W, Cupo RR, Debattisti V, Gomez L, La Fuente S de, Zhao Y-T, Valdivia HH, Hajnóczky G, Franzini-Armstrong C. Increased mitochondrial nanotunneling activity, induced by calcium imbalance, affects intermitochondrial matrix exchanges. *Proc Natl Acad Sci U S A* 2017;**114**:E849-58.

225. Vincent AE, Turnbull DM, Eisner V, Hajnóczky G, Picard M. Mitochondrial Nanotunnels. *Trends Cell Biol* 2017;**27**:787–799.

226. Zhang GQ, Wei H, Lu J, Wong P, Shim W. Identification and characterization of calcium sparks in cardiomyocytes derived from human induced pluripotent stem cells. *PLoS One* 2013;**8**:e55266.

227. Hüser J, Bers DM, Blatter LA. Subcellular properties of Ca2+i transients in phospholamban-deficient mouse ventricular cells. *Am J Physiol* 1998;**274**:H1800-11.

228. Goldhaber JI, Lamp ST, Walter DO, Garfinkel A, Fukumoto GH, Weiss JN. Local regulation of the threshold for calcium sparks in rat ventricular myocytes: Role of sodium-calcium exchange. *The Journal of Physiology* 1999;**520**:431–438.

229. Sato D, Bers DM. How does stochastic ryanodine receptor-mediated Ca leak fail to initiate a Ca spark? *Biophys J* 2011;**101**:2370–2379.

230. Cheng H, Lederer WJ. Calcium sparks. *Physiol Rev* 2008;**88**:1491–1545.

231. Uehara A, Murayama T, Yasukochi M, Fill M, Horie M, Okamoto T, Matsuura Y, Uehara K, Fujimoto T, Sakurai T, Kurebayashi N. Extensive Ca2+ leak through K4750Q cardiac ryanodine receptors caused by cytosolic and luminal Ca2+ hypersensitivity. *J Gen Physiol* 2017;**149**:199–218.

232. Hilliard FA, Steele DS, Laver D, Yang Z, Le Marchand SJ, Chopra N, Piston DW, Huke S, Knollmann BC. Flecainide inhibits arrhythmogenic Ca2+ waves by open state block of ryanodine receptor Ca2+ release channels and reduction of Ca2+ spark mass. *J Mol Cell Cardiol* 2010;**48**:293–301.

233. Liu N, Priori SG. Disruption of calcium homeostasis and arrhythmogenesis induced by mutations in the cardiac ryanodine receptor and calsequestrin. *Cardiovasc Res* 2008;**77**:293–301.

234. Liu N, Ruan Y, Denegri M, Bachetti T, Li Y, Colombi B, Napolitano C, Coetzee WA, Priori SG. Calmodulin kinase II inhibition prevents arrhythmias in RyR2(R4496C+/-) mice with catecholaminergic polymorphic ventricular tachycardia. *J Mol Cell Cardiol* 2011;**50**:214–222.

235. Sorrentino V. *Ryanodine receptors.* Boca Raton [etc.]: CRC Press, 1996.

236. Liu N, Denegri M, Ruan Y, Avelino-Cruz JE, Perissi A, Negri S, Napolitano C, Coetzee WA, Boyden PA, Priori SG. Short communication: Flecainide exerts an antiarrhythmic effect in a mouse model of catecholaminergic polymorphic ventricular tachycardia by increasing the threshold for triggered activity. *Circ Res* 2011;**109**:291–295.

237. Song Z, Ko CY, Nivala M, Weiss JN, Qu Z. Calcium-Voltage Coupling in the Genesis of Early and Delayed Afterdepolarizations in Cardiac Myocytes. *Biophys J* 2015;**108**:1908–1921.

238. Mackenzie L, Bootman MD, Laine M, Berridge MJ, Thuring J, Holmes A, Li W-H, Lipp P. The role of inositol 1,4,5-trisphosphate receptors in Ca(2+) signalling and the generation of arrhythmias in rat atrial myocytes. *The Journal of Physiology* 2002;**541**:395–409.

239. Bers DM. Cardiac excitation-contraction coupling. *Nature* 2002;**415**:198–205.

240. Ferrari GM de, Viola M, D'Amato E, Antolini R, Forti S. Distinct Patterns of Calcium Transients During Early and Delayed Afterdepolarizations Induced by Isoproterenol in Ventricular Myocytes. *Circulation* 1995;**91**:2510–2515.

241. Priori SG, Corr PB. Mechanisms underlying early and delayed afterdepolarizations induced by catecholamines. *Am J Physiol* 1990;**258**:H1796-805.

242. Horvath B, Banyasz T, Jian Z, Hegyi B, Kistamas K, Nanasi PP, Izu LT, Chen-Izu Y. Dynamics of the late Na(+) current during cardiac action potential and its contribution to afterdepolarizations. *J Mol Cell Cardiol* 2013;**64**:59–68.

243. Stokke MK, Tovsrud N, Louch WE, Oyehaug L, Hougen K, Sejersted OM, Swift F, Sjaastad I. I(CaL) inhibition prevents arrhythmogenic Ca(2+) waves caused by abnormal Ca(2+) sensitivity of RyR or SR Ca(2+) accumulation. *Cardiovasc Res* 2013;**98**:315–325.

244. Karakikes I, Ameen M, Termglinchan V, Wu JC. Human induced pluripotent stem cell-derived cardiomyocytes: insights into molecular, cellular, and functional phenotypes. *Circ Res* 2015;**117**:80–88.

245. Musunuru K, Sheikh F, Gupta RM, Houser SR, Maher KO, Milan DJ, Terzic A, Wu JC. Induced Pluripotent Stem Cells for Cardiovascular Disease Modeling and Precision Medicine: A Scientific Statement From the American Heart Association. *Circ Genom Precis Med* 2018;**11**:e000043.

246. Priori SG, Napolitano C, Di Pasquale E, Condorelli G. Induced pluripotent stem cell-derived cardiomyocytes in studies of inherited arrhythmias. *J Clin Invest* 2013;**123**:84–91.

247. Ahmed RE, Anzai T, Chanthra N, Uosaki H. A Brief Review of Current Maturation Methods for Human Induced Pluripotent Stem Cells-Derived Cardiomyocytes. *Front Cell Dev Biol* 2020;**8**:178.

248. Khan JM, Lyon AR, Harding SE. The case for induced pluripotent stem cell-derived cardiomyocytes in pharmacological screening. *British Journal of Pharmacology* 2013;**169**:304–317.

249. Kohlhaas M, Liu T, Knopp A, Zeller T, Ong MF, Böhm M, O'Rourke B, Maack C. Elevated Cytosolic Na+ Increases Mitochondrial Formation of Reactive Oxygen Species in Failing Cardiac Myocytes. *Circulation* 2010;**121**:1606–1613.

250. Maack C, Cortassa S, Aon MA, Ganesan AN, Liu T, O'Rourke B. Elevated Cytosolic Na+ Decreases Mitochondrial Ca2+ Uptake During Excitation–Contraction Coupling and Impairs Energetic Adaptation in Cardiac Myocytes. *Circ Res* 2006;**99**:172–182.

251. Haverkamp W, Breithardt G, Camm AJ, Janse MJ, Rosen MR, Antzelevitch C, Escande D, Franz M, Malik M, Moss A, Shah R. The potential for QT prolongation and pro-arrhythmia by non-anti-arrhythmic drugs: clinical and regulatory implications. Report on a Policy Conference of the European Society of Cardiology. *Cardiovasc Res* 2000;**47**:219–233.

252. Babij P, Askew GR, Nieuwenhuijsen B, Su CM, Bridal TR, Jow B, Argentieri TM, Kulik J, DeGennaro LJ, Spinelli W, Colatsky TJ. Inhibition of cardiac delayed rectifier K+ current by overexpression of the long-QT syndrome HERG G628S mutation in transgenic mice. *Circ Res* 1998;**83**:668–678.

253. Lee J, Kim JH. Kaempferol Inhibits Pancreatic Cancer Cell Growth and Migration through the Blockade of EGFR-Related Pathway In Vitro. *PLoS One* 2016;**11**:e0155264.

254. Kim TW, Lee SY, Kim M, Cheon C, Ko S-G. Kaempferol induces autophagic cell death via IRE1-JNK-CHOP pathway and inhibition of G9a in gastric cancer cells. *Cell Death Dis* 2018;**9**:875.

255. Wang X, Yang Y, An Y, Fang G. The mechanism of anticancer action and potential clinical use of kaempferol in the treatment of breast cancer. *Biomed Pharmacother* 2019;**117**:109086.

256. Alkhalidy H, Moore W, Wang Y, Luo J, McMillan RP, Zhen W, Zhou K, Liu D. The Flavonoid Kaempferol Ameliorates Streptozotocin-Induced Diabetes by Suppressing Hepatic Glucose Production. *Molecules* 2018;**23**.

257. Al-Numair KS, Chandramohan G, Veeramani C, Alsaif MA. Ameliorative effect of kaempferol, a flavonoid, on oxidative stress in streptozotocin-induced diabetic rats. *Redox Rep* 2015;**20**:198–209.

258. Gong J-H, Shin D, Han S-Y, Kim J-L, Kang Y-H. Kaempferol suppresses eosionphil infiltration and airway inflammation in airway epithelial cells and in mice with allergic asthma. *J Nutr* 2012;**142**:47–56.

259. Yu L, Chen C, Wang L-F, Kuang X, Liu K, Zhang H, Du J-R. Neuroprotective effect of kaempferol glycosides against brain injury and neuroinflammation by inhibiting the activation of NF-κB and STAT3 in transient focal stroke. *PLoS One* 2013;**8**:e55839.

260. Ren J, Lu Y, Qian Y, Chen B, Wu T, Ji G. Recent progress regarding kaempferol for the treatment of various diseases. *Exp Ther Med* 2019;**18**:2759–2776.

261. Kouhestani S, Jafari A, Babaei P. Kaempferol attenuates cognitive deficit via regulating oxidative stress and neuroinflammation in an ovariectomized rat model of sporadic dementia. *Neural Regen Res* 2018;**13**:1827–1832.

262. Beg T, Jyoti S, Naz F, Rahul, Ali F, Ali SK, Reyad AM, Siddique YH. Protective Effect of Kaempferol on the Transgenic Drosophila Model of Alzheimer's Disease. *CNS Neurol Disord Drug Targets* 2018;**17**:421–429.

263. Vries JH de, Hollman PC, Meyboom S, Buysman MN, Zock PL, van Staveren WA, Katan MB. Plasma concentrations and urinary excretion of the antioxidant flavonols quercetin and kaempferol as biomarkers for dietary intake. *Am J Clin Nutr* 1998;**68**:60–65.

264. Kim JK, Choi SJ, Cho HY, Hwang H-J, Kim YJ, Lim ST, Kim C-J, Kim HK, Peterson S, Shin D-H. Protective effects of kaempferol (3,4',5,7-tetrahydroxyflavone) against amyloid beta peptide (Abeta)-induced neurotoxicity in ICR mice. *Biosci Biotechnol Biochem* 2010;**74**:397–401.

265. Manach C, Mazur A, Scalbert A. Polyphenols and prevention of cardiovascular diseases. *Curr Opin Lipidol* 2005;**16**:77–84.

266. Hodgson JM. Tea flavonoids and cardiovascular disease. *Asia Pac J Clin Nutr* 2008;**17 Suppl 1**:288–290.

267. Qin Y, Cui W, Yang X, Tong B. Kaempferol inhibits the growth and metastasis of cholangiocarcinoma in vitro and in vivo. *Acta Biochim Biophys Sin (Shanghai)* 2016;**48**:238–245.

268. Barve A, Chen C, Hebbar V, Desiderio J, Saw CL-L, Kong A-N. Metabolism, oral bioavailability and pharmacokinetics of chemopreventive kaempferol in rats. *Biopharm Drug Dispos* 2009;**30**:356–365.

269. Zabela V, Sampath C, Oufir M, Moradi-Afrapoli F, Butterweck V, Hamburger M. Pharmacokinetics of dietary kaempferol and its metabolite 4-hydroxyphenylacetic acid in rats. *Fitoterapia* 2016;**115**:189–197.

270. Zhou Z, Wang M, Guo Z, Zhang X. Pharmacokinetic evaluation of the interaction between oral kaempferol and ethanol in rats. *Acta Pharm* 2016;**66**:563–568.

271. Zhang K, Gu L, Chen J, Zhang Y, Jiang Y, Zhao L, Bi K, Chen X. Preparation and evaluation of kaempferol-phospholipid complex for pharmacokinetics and bioavailability in SD rats. *J Pharm Biomed Anal* 2015;**114**:168–175.

272. Telange DR, Patil AT, Pethe AM, Tatode AA, Anand S, Dave VS. Kaempferol-Phospholipid Complex: Formulation, and Evaluation of Improved Solubility, In Vivo Bioavailability, and Antioxidant Potential of Kaempferol. *JEFC* 2016;**7**:1174.

273. Dar RA, Naikoo GA, Hassan IU, Shaikh AM. Electrochemical behavior of kaempferol and its determination in presence of quercetin employing multi-walled carbon nanotube modified carbon paste electrode. *Analytical Chemistry Research* 2016;**7**:1–8.

274. Wilting F, Kopp R, Gurnev PA, Schedel A, Dupper NJ, Kwon O, Nicke A, Gudermann T, Schredelseker J. The antiarrhythmic compound efsevin directly modulates voltage-dependent anion channel 2 by binding to its inner wall and enhancing mitochondrial Ca2+ uptake. *British Journal of Pharmacology* 2020;**177**:2947–2958.

275. Batiste SM, Blackwell DJ, Kim K, Kryshtal DO, Gomez-Hurtado N, Rebbeck RT, Cornea RL, Johnston JN, Knollmann BC. Unnatural verticilide enantiomer inhibits type 2 ryanodine receptor-mediated calcium leak and is antiarrhythmic. *Proc Natl Acad Sci U S A* 2019;**116**:4810–4815.

276. Paul-Pletzer K, Yamamoto T, Ikemoto N, Jimenez LS, Morimoto H, Williams PG, Ma J, Parness J. Probing a putative dantrolene-binding site on the cardiac ryanodine receptor. *Biochem J* 2005;**387**:905–909.

277. Sacherer M, Sedej S, Wakuła P, Wallner M, Vos MA, Kockskämper J, Stiegler P, Sereinigg M, Lewinski D von, Antoons G, Pieske BM, Heinzel FR, investigators oboC. JTV519 (K201) reduces sarcoplasmic reticulum Ca(2+) leak and improves diastolic function in vitro in murine and human non-failing myocardium. *British Journal of Pharmacology* 2012;**167**:493–504.

278. Darcy YL, Diaz-Sylvester PL, Copello JA. K201 (JTV519) is a Ca2+-Dependent Blocker of SERCA and a Partial Agonist of Ryanodine Receptors in Striated Muscle. *Mol Pharmacol* 2016;**90**:106–115.

279. Andersson DC, Marks AR. Fixing ryanodine receptor Ca leak - a novel therapeutic strategy for contractile failure in heart and skeletal muscle. *Drug Discov Today Dis Mech* 2010;**7**:e151-e157.

280. Lehnart SE, Mongillo M, Bellinger A, Lindegger N, Chen B-X, Hsueh W, Reiken S, Wronska A, Drew LJ, Ward CW, Lederer WJ, Kass RS, Morley G, Marks AR. Leaky Ca(2+) release

channel/ryanodine receptor 2 causes seizures and sudden cardiac death in mice. *J Clin Invest* 2008;**118**:2230–2245.

281. Williams AJ, Bannister ML, Thomas NL, Sikkel MB, Mukherjee S, Maxwell C, MacLeod KT, George CH. Questioning flecainide's mechanism of action in the treatment of catecholaminergic polymorphic ventricular tachycardia. *The Journal of Physiology* 2016;**594**:6431–6432.

282. Savio-Galimberti E, Knollmann BC. Channel Activity of Cardiac Ryanodine Receptors (RyR2) Determines Potency and Efficacy of Flecainide and R-Propafenone against Arrhythmogenic Calcium Waves in Ventricular Cardiomyocytes. *PLoS One* 2015;**10**:e0131179.

283. Yang P-C, Moreno JD, Miyake CY, Vaughn-Behrens SB, Jeng M-T, Grandi E, Wehrens XHT, Noskov SY, Clancy CE. In silico prediction of drug therapy in catecholaminergic polymorphic ventricular tachycardia. *The Journal of Physiology* 2016;**594**:567–593.

284. Hwang HS, Baldo MP, Rodriguez JP, Faggioni M, Knollmann BC. Efficacy of Flecainide in Catecholaminergic Polymorphic Ventricular Tachycardia Is Mutation-Independent but Reduced by Calcium Overload. *Front. Physiol.* 2019;**10**:992.

285. Morillo CA, Banerjee A, Perel P, Wood D, Jouven X. Atrial fibrillation: the current epidemic. *J Geriatr Cardiol* 2017;**14**:195–203.

286. Heijman J, Voigt N, Nattel S, Dobrev D. Cellular and molecular electrophysiology of atrial fibrillation initiation, maintenance, and progression. *Circ Res* 2014;**114**:1483–1499.

287. Neef S, Dybkova N, Sossalla S, Ort KR, Fluschnik N, Neumann K, Seipelt R, Schöndube FA, Hasenfuss G, Maier LS. CaMKII-dependent diastolic SR Ca2+ leak and elevated diastolic Ca2+ levels in right atrial myocardium of patients with atrial fibrillation. *Circ Res* 2010;**106**:1134–1144.

288. Shan J, Xie W, Betzenhauser M, Reiken S, Chen B-X, Wronska A, Marks AR. Calcium leak through ryanodine receptors leads to atrial fibrillation in 3 mouse models of catecholaminergic polymorphic ventricular tachycardia. *Circ Res* 2012;**111**:708–717.

289. Salvage SC, King JH, Chandrasekharan KH, Jafferji DIG, Guzadhur L, Matthews HR, Huang CL-H, Fraser JA. Flecainide exerts paradoxical effects on sodium currents and atrial arrhythmia in murine RyR2-P2328S hearts. *Acta Physiol (Oxf)* 2015;**214**:361–375.